Los Alamos
NATIONAL LABORATORY
EST. 1943

Associate Directorate for Environmental Management
P.O. Box 1663, MS M992
Los Alamos, New Mexico 87545
(505) 606-2337

Environmental Management
1900 Diamond Drive, MS M984
Los Alamos, New Mexico 87544
(505) 665-5658/FAX (505) 606-2132

RECEIVED
APR 07 2017
NMED
Hazardous Waste Bureau

Date: APR 07 2017
Refer To: ADEM-17-0070
LAUR: 17-22550
Locates Action No.: n/a

John Kieling, Bureau Chief
Hazardous Waste Bureau
New Mexico Environment Department
2905 Rodeo Park Drive East, Building 1
Santa Fe, NM 87505-6303

Subject: Summary Report for Intermediate Groundwater System Characterization Activities at Consolidated Unit 16-021(c)-99

Dear Mr. Kieling:

Enclosed please find two hard copies with electronic files of the Summary Report for Intermediate Groundwater System Characterization Activities at Consolidated Unit 16-021(c)-99. This report is being submitted to fulfill a milestone requirement in Appendix B of the Compliance Order on Consent, signed June 24, 2016. The report summarizes the results of pumping test activities conducted in 2016 at three monitoring wells, CdV-9-1(i), CdV-16-1(i), and CdV-16-4ip, in the vicinity of Consolidated Unit 16-021(c)-99 in Technical Areas 16 (TA-16) and TA-09 at Los Alamos National Laboratory (the Laboratory). These activities were conducted in accordance with the Work Plan for Intermediate Groundwater System Characterization at Consolidated Unit 16-021(c)-99, submitted to the New Mexico Environment Department (NMED) on August 7, 2015, and approved by NMED on October 13, 2015.

Appendix B of the June 2016 Consent Order refers to this deliverable as the "CdV-9-1(i) Aquifer Test Report" and requires the Laboratory to submit a summary report of the test results and relevant data. The original 90-d extended-duration pumping test was planned for only well CdV-9-1(i). However, when initial testing of CdV-9-1(i) screen 1 indicated the well is completed in a zone with relatively limited yield, the technical approach was revised from a 90-d test at CdV-9-1(i) to three 30-d tests in separate wells completed on both sides of and within Cañon de Valle. The pumping tests provided valuable information regarding vertical and horizontal connectivity within perched-intermediate groundwater at TA-16.

If you have any questions, please contact Stephani Swickley at (505) 606-1628 (sfuller@lanl.gov) or Cheryl Rodriguez at (505) 665-5330 (cheryl.rodriguez@em.doe.gov).

Sincerely,

Bruce Robinson, Program Director
Environmental Remediation Program
Los Alamos National Laboratory

Sincerely,

for

David S. Rhodes, Director
Office of Quality and Regulatory Compliance
Los Alamos Environmental Management
Field Office

BR/DR/SS/TG:sm

Enclosures: Two hard copies with electronic files – Summary Report for Intermediate Groundwater System Characterization Activities at Consolidated Unit 16-021(c)-99 (EP2017-0008)

Cy: (w/enc.)
Cheryl Rodriguez, DOE-EM-LA
Stephani Swickley, ADEM ER Program

Cy: (w/electronic enc.)
Laurie King, EPA Region 6, Dallas, TX
Raymond Martinez, San Ildefonso Pueblo
Dino Chavarria, Santa Clara Pueblo
Steve Yanicak, NMED-DOE-OB, MS M894
emla.docs@em.doe.gov
Tim Goering, ADEM ER Program
Velimir Vesselinov, EES-16
Public Reading Room (EPRR)
ADESH Records
PRS Database

Cy: (w/o enc./date-stamped letter emailed)
lasomailbox@nnsa.doe.gov
Peter Maggiore, DOE-NA-LA
Kimberly Davis Lebak, DOE-NA-LA
David Rhodes, DOE-EM-LA
Bruce Robinson, ADEM ER Program
Randy Erickson, ADEM ER Program
Mark Everett, ADEM ER Program
Danny Katzman, ADEM ER Program
Sachin Pandey, EES-16
Ted Ball, PM6-RCO
Jocelyn Buckley, ADESH-EPC-CP
Mike Saladen, ADESH-EPC-CP
John Bretzke, ADESH-EPC-DO
Michael Brandt, ADESH
William Mairson, PADOPS
Craig Leasure, PADOPS

LA-UR-17-22550
April 2017
EP2017-0008

Summary Report for Intermediate Groundwater System Characterization Activities at Consolidated Unit 16-021(c)-99

Prepared by the Associate Directorate for Environmental Management

EP2017-0008

Summary Report for Intermediate Groundwater System Characterization Activities at Consolidated Unit 16-021(c)-99

April 2017

Responsible project manager:

for Stephani Swickley		Project Manager	Environmental Remediation Program	3/30/2017
Printed Name	Signature	Title	Organization	Date

Responsible LANS representative:

for Randall Erickson		Associate Director	Associate Directorate for Environmental Management	3/30/17
Printed Name	Signature	Title	Organization	Date

Responsible DOE-EM-LA representative:

David S. Rhodes	for	Office Director	Quality and Regulatory Compliance	4/5/17
Printed Name	Signature	Title	Organization	Date

EXECUTIVE SUMMARY

Cross-well pumping tests were conducted at monitoring wells CdV-9-1(i), CdV-16-1(i), and CdV-16-4ip, completed in perched-intermediate groundwater at Los Alamos National Laboratory's Technical Area 16 (TA-16).

The primary objectives of the testing were to evaluate the degree of hydraulic connectivity within the perched groundwater system and to improve the understanding of contaminant transport pathways. Monitoring wells CdV-9-1(i), CdV-16-1(i), and CdV-16-4ip were pumped for approximately 30 d each, and potentiometric responses were monitored in nearby perched-intermediate and regional wells. To assess transient responses in hexahydro-1,3,5-trinitro-1,3,5-triazine (RDX) concentrations, samples were collected from test wells during pumping and recovery.

The pumping tests provided valuable information regarding vertical and horizontal connectivity within perched-intermediate groundwater at TA-16. Hydraulic communication was observed between screens relatively proximal to each other and completed in the upper Puye Formation. The primary area of hydraulic communication is a laterally continuous saturated zone within the upper Puye Formation that is at least as large as the triangle formed by CdV-9-1(i), CdV-16-4ip, and R-25 screen 2. The preferential communication across the upper Puye Formation is likely driven by stratification (i.e., high anisotropy) within Puye strata.

Pumping from wells within the upper Puye caused little or no response in monitored screens within the lower Puye Formation and Otowi Member, including monitoring points that are very close to the pumping locations. In one case, limited hydraulic communication may have been observed across the Otowi/Puye boundary, based on apparent water-level responses in CdV-9-1(i) PZ-2 as a result of pumping at CdV-16-1(i). These observations indicate apparent high lateral to vertical anisotropy and a potentially important hydrostratigraphic characteristic of the Otowi/Puye contact.

Because of the relatively low sustainable pumping rates at CdV-9-1(i), CdV-16-1(i), and CdV-16-4ip, the total mass of RDX removed during 90 d of pumping was an estimated 0.17 kg, representing approximately 0.02% to 0.08% of the estimated RDX inventory believed to be present in perched-intermediate groundwater beneath the TA-16/TA-09 area. These findings provide a basis for updating the conceptual model for the perched-intermediate zone in the RDX project area. Geologic cross-sections incorporating the revised understanding of perched-intermediate groundwater and the laterally continuous zone within the upper Puye Formation where hydraulic communication was observed are presented in this report.

CONTENTS

Figures

Tables

Appendixes

1.0 INTRODUCTION

This report summarizes the results of pumping test activities conducted in 2016 at three monitoring wells, CdV-9-1(i), CdV-16-1(i), and CdV-16-4ip, in the vicinity of Consolidated Unit 16-021(c)-99 in Technical Areas 16 (TA-16) and TA-09 at Los Alamos National Laboratory (LANL or the Laboratory). These activities were conducted in accordance with the "Work Plan for Intermediate Groundwater System Characterization at Consolidated Unit 16-021(c)-99" (LANL 2015, 600686), submitted to the New Mexico Environment Department (NMED) on August 7, 2015. NMED approved the work plan on October 13, 2015 (NMED 2015, 600957) and requested that the Laboratory submit a report summarizing the results and recommending characterization activities. The report was initially due on December 15, 2016, but the date was revised to April 7, 2017, in the June 2016 Compliance Order on Consent (the Consent Order).

Appendix B of the June 2016 Consent Order lists the "aquifer test report" as a milestone and requires the Laboratory to submit a summary report of the test results and relevant data. The original 90-d extended-duration pumping test was planned for only well CdV-9-1(i), and the Consent Order refers to this deliverable as the "CdV-9-1(i) Aquifer Test Report." However, when initial testing of CdV-9-1(i) screen 1 (S1) indicated the well is completed in a zone with relatively limited yield, the technical approach was revised from a 90-d test at CdV-9-1(i) to three 30-d tests in separate wells completed on both sides of and within Cañon de Valle. The alternate approach was selected in an effort to assess the hydraulic connection across Cañon de Valle among CdV-9-1(i), CdV-16-1(i), and CdV-16-4ip. In addition, water levels in CdV-9-1(i) and its two associated piezometers are at higher elevations than in other perched-intermediate wells near the 260 Outfall, and the upper piezometer [CdV-9-1(i) PZ-1] is completed in the Otowi Member. Well CdV-16-1(i) is also completed in the Otowi Member, and the revised testing approach of pumping CdV-16-1(i) for 30 d was expected to show water-level responses in the piezometer within the formation.

The activities described in this report supplement investigation and corrective actions underway to address contaminated groundwater related to Consolidated Unit 16-021(c)-99 (the 260 Outfall) in the vicinity of TA-16. Data collected from the activities described in this report will be used during the evaluation of potential remedial alternatives for high-explosives (HE) contamination in intermediate and regional groundwater at Consolidated Unit 16-021(c)-99.

Figure 1.0-1 shows the location of TA-16 with respect to other Laboratory TAs, Consolidated Unit 16-021(c)-99, and associated features. Figure 1.0-2 shows the current network of perched-intermediate and regional groundwater wells at TA-16. Figure 1.0-2 also shows the current understanding of the distribution of hexahydro-1,3,5-trinitro-1,3,5-triazine (RDX) contamination in perched-intermediate and regional groundwater.

1.1 Cross-Borehole Testing Overview

Cross-borehole extended duration pumping tests were conducted at three wells in accordance with the "Work Plan for Intermediate Groundwater System Characterization at Consolidated Unit 16-021(c)-99" (LANL 2015, 600686). The primary objectives of the testing were to evaluate the degree of hydraulic connectivity within the perched-groundwater system and to improve the understanding of contaminant transport pathways. Monitoring wells CdV-9-1(i), CdV-16-1(i), and CdV-16-4ip were pumped for ~30 d each, and potentiometric responses were monitored in nearby perched-intermediate wells, piezometers, and regional wells.

Water levels were monitored in the three primary pumping wells CdV-9-1(i) S1, CdV-16-1(i), and CdV-16-4ip and in nine additional screens completed in perched-intermediate groundwater [CdV-9-1(i) PZ-1; CdV-9-1(i) PZ-2; CdV-16-2ir; R-25 (S1, S2, and S4); R-25b; R-47i; R-63i] and regional groundwater [monitoring well R-63]. Figure 1.1-1 shows the locations of the pumping and observation wells, and Table 1.1-1 lists the lateral distances between pumping and observation wells, in feet.

1.2 Cross-Borehole Testing Objectives

Specific objectives of the pumping-test activities were to evaluate the degree of hydraulic connection horizontally and vertically in the perched groundwater zones beneath Cañon de Valle near the 260 Outfall to assess transport pathways for RDX and other contaminants. The pumping test was also used to evaluate the hydraulic connection between perched groundwater in the Puye Formation and in the Otowi Member of the Bandelier Tuff. A better understanding of the hydraulic connectivity across the Otowi/Puye Formation contact may provide insight into the volume of RDX-contaminated groundwater and the role of hydrogeologic features in controlling the distribution and flow direction in deep perched groundwater.

An additional objective was to evaluate contaminant characteristics in the perched zone and contaminant-transport properties by monitoring temporal variations in RDX during the extended pumping. Changes in contaminant concentrations during pumping may provide insight regarding possible secondary contaminant sources in the vadose zone and RDX distribution within the perched-intermediate groundwater.

2.0 BACKGROUND

Building 16-260, located on the north side of TA-16 (Figure 1.0-2), has been used for processing and machining HE since 1951. Because water was used to machine the HE (which is slightly water soluble), wastewater from machining operations contained dissolved and particulate HE. Historical wastewater treatment at building 16-260 consisted of routing the water to 13 settling sumps to recover any entrained HE cuttings. From 1951 to 1996, the water from these sumps was discharged to the 260 Outfall that drained into Cañon de Valle. In 1994, outfall discharge volumes were measured at several million gallons per year. The discharge volumes were probably higher during the 1950s when the HE production output from the 260 Outfall was substantially greater than it was in the 1990s (LANL 1994, 076858).

2.1 Previous Tests at CdV-9-1(i), CdV-16-1(i), and CdV-16-4ip

Pumping tests have been conducted in the past at CdV-9-1(i), CdV-16-1(i), and CdV-16-4ip. However, these tests were not specifically designed to assess the degree of lateral hydraulic connection in perched groundwater across Cañon de Valle because until CdV-9-1(i) was installed in 2015 (LANL 2015, 600503), no data regarding perched-intermediate groundwater north of Cañon de Valle were available. Data collected during the installation of CdV-9-1(i) showed the presence of a thick zone of RDX-contaminated perched-intermediate groundwater north of Cañon de Valle.

Earlier pumping tests conducted at CdV-9-1(i), CdV-16-1(i), and CdV-16-4ip include the following.

- A 72-h pumping test was conducted at CdV-9-1(i) and is discussed in the CdV-9-1(i) well completion report (LANL 2015, 600503). This test concluded that CdV-9-1(i) had a maximum sustainable yield of less than 2 gallons per minute (gpm).

- A 24-h pumping test was conducted at CdV-16-1(i) in March 2004 following well development. Details of this test are included in the CdV-16-1(i) well completion report (Kleinfelder 2004, 087844). CdV-16-1(i) was found to be fairly low-yielding, also producing a sustained pumping rate of less than 2 gpm.

- Two 10-d pumping tests were conducted on CdV-16-4ip S1 and S2 following well completion in 2011 to meet the requirements of the "Hydrologic Testing Work Plan for Consolidated Unit 16-021(c)-99" (LANL 2010, 108534). The pumping tests resulted in the removal of less than 0.18 kg (0.4 lb) of RDX from the deep perched groundwater at the site.

- CdV-16-4ip was subsequently reconfigured to a single-screen monitoring well (section 2.2.3), with the lower screen plugged, and in summer of 2014, the well was pumped for approximately 60 d to assess the potential for source removal. The test demonstrated that long-term pumping at CdV-16-4ip for the sole objective of removing mass from the deep perched groundwater is not cost-effective because of this well's relatively low yield and the limited mass of RDX that could be extracted. Based on the results, it was estimated that long-term pumping at CdV-16-4ip would remove RDX from the deep perched groundwater at a rate of approximately 1 kg/yr (2.2 lb/yr).

2.2 Well Completion Details

Table 2.2-1 presents the completion details for the pumping wells and observation wells monitored during the pumping tests. Table 2.2-1 also includes recent water table elevation data for each screen monitored, and the relative position of the water table above or below the top of the well screen. Fact sheets showing the well configuration and borehole stratigraphy for CdV-9-1(i), CdV-16-1(i), and CdV-16-4ip are included in Appendix A.

2.3 Data Collection

This section discusses the data collected during the cross-borehole pumping test activities. Section 2.3.1 summarizes the hydraulic data collected during testing, and section 2.3.2 summarizes the analytical data collected.

2.3.1 Hydraulic Data

Water levels were monitored in the three primary pumping wells: CdV-9-1(i) S1, CdV-16-1(i), and CdV-16-4ip and in nine additional screens completed in perched-intermediate groundwater [CdV-9-1(i) PZ-1; CdV-9-1(i) PZ-2; CdV-16-2ir; R-25 (S1, S2, and S4); R-25b; R-47; R-63i] and in regional groundwater [well R-63]. Figure 1.1-1 shows the locations of the pumping and observation wells, and Table 1.1-1 lists the lateral distances between pumping and observation wells, in feet. Appendix B (on CD) provides the water-level data for these wells for the period of the test.

2.3.2 Analytical Data

Table 2.3-1 lists sampling analytes, sample ports, analytical laboratory, and sampling frequency for samples collected during the pumping test activities and rebound sampling. Sampling analytical parameters were specified in the approved "Work Plan for Intermediate Groundwater System Characterization at Consolidated Unit 16-021(c)-99" (LANL 2015, 600686; NMED 2015 600957) and included metals, anions, alkalinity/pH, RDX, HE with degradation products, volatile organic compounds, and the tracers, including bromide and the naphthalene sulfonate compounds, employed at TA-16.

Samples for characterization were collected three times per week from the pumping wells and two times per week during rebound sampling. The characterization samples (untreated groundwater) were collected from ports designated VS-9-1i-1, VS-4ip-1, and VS-16-1i-1, plumbed directly to the wellhead.

Operational and compliance samples were collected three times per week during pumping for analysis at the Geochemistry and Geomaterials Research Laboratory (GGRL) and weekly for off-site analysis at GEL Laboratories, LLC. The samples were analyzed on-site for RDX and off-site for the full HE suite with degradation products (HEXMOD) (Table 2.3-1). The operational and compliance samples were used to confirm the granular activated carbon (GAC) treatment system was operating properly and to ensure land-application requirements for RDX were met.

Tables 2.3-2 through 2.3-4 present the samples taken, including both characterization and operational samples, during pumping and recovery at each of the three wells. The complete set of analytical data collected for characterization and for compliance with the land-application permit (section 2.4) during pumping and recovery are included in Appendix C (on CD).

Field water-quality parameters were measured at CdV-9-1(i) before sample collection to evaluate groundwater conditions and to provide insights into any changes in groundwater quality or conditions in the well. Parameters measured included pH, temperature, specific conductance, dissolved oxygen (DO), turbidity, and oxidation-reduction potential (ORP). The parameters were measured using an In Situ Aquatroll 400 probe installed inline ahead of the pumping treatment system. Field water-quality parameters are presented in Table 2.3-5. However, field parameters were not measured at CdV-16-1(i) and CdV-16-4ip because this requirement was inadvertently excluded from the sampling plan for the pumping test activities. As a result, no field parameter data were collected before sampling at CdV-16-1(i) and CdV-16-4ip.

2.4 Treatment and Disposal of Contaminated Groundwater

Before discharge (i.e., land application), GAC was used to treat groundwater produced during the pumping test at CdV-9-1(i), CdV-16-4ip, and CdV-16-1(i). Two GAC treatment systems, a large system and a small system, were used to remove the RDX during the pumping tests. The large system was used at CdV-9-1(i) and CdV-16-4ip, and the small system was used at CdV-16-1(i). Details on the treatment systems are included in the "Work Plan for Treatment and Land Application of Groundwater from Technical Areas 09 and 16, DP-1793, WP #4," submitted to the NMED Groundwater Quality Bureau (GWQB) on March 23, 2016, and approved by NMED-GWQB on May 27, 2016.

In accordance with the Work Plan #4 Sampling Plan, treated water was sampled and analyzed for RDX by the on-site analytical laboratory. In addition, during the pumping test period, duplicate confirmation samples were collected and submitted for analysis by GEL Laboratories, LLC, an off-site analytical laboratory.

No results for RDX exceeded the land-application limit of 6.3 µg/L. The Laboratory submitted a discharge report to NMED-GWQB on February 13, 2017 (LANL 2017, 602164) with details regarding the volume of water discharged, land-application rates, the analytical results from samples collected, and a map identifying the locations where water was discharged.

3.0 CHRONOLOGY AND DETAILS OF PUMPING TESTS

Cross-borehole extended pumping tests were conducted at three wells in accordance with the "Work Plan for Intermediate Groundwater System Characterization at Consolidated Unit 16-021(c)-99" (LANL 2015, 600686). During the period from June 7 to October 11, 2016, monitoring wells CdV-9-1(i), CdV-16-1(i), and CdV-16-4ip were pumped for approximately 30 d each, and potentiometric responses were monitored in nearby perched-intermediate wells and piezometers, and regional wells.

Water levels were monitored in the three primary pumping wells CdV-9-1(i) S1, CdV-16-1(i), and CdV-16-4ip and in nine additional screens completed in perched-intermediate groundwater [CdV-9-1(i) PZ-1; CdV-9-1(i) PZ-2; CdV-16-2ir; R-25 (S1, S2, and S4); R-25b; R-47; R-63i] and in regional groundwater [well R-63]. Figure 1.1-1 shows the locations of the pumping and observation wells. Well completion details for the pumping and observation wells are presented in Table 2.2-1, and fact sheets showing the well configuration and geology for the three wells are included in Appendix A.

Detailed analyses of the cross-borehole water-level responses and pumping test data are presented in Appendixes D through G and are summarized in section 4 of this report.

3.1 CdV-9-1(i) Slug Tests and Pumping Test

Cross-hole hydraulic testing at CdV-9-1(i) consisted of slug-injection tests performed in late 2015 during tracer deployment at CdV-9-1(i) (LANL 2015, 600535) and a 30-d cross-borehole pumping test conducted in June and July 2016 in conjunction with other cross-borehole pumping test activities in CdV-16-2(i) and CdV-16-4ip discussed in this report.

3.1.1 Slug Test Data from CdV-9-1(i)

The slug-injection tests at CdV-9-1(i) consisted of introducing 5-gal. water into the 1-in.-diameter CdV-9-1(i) piezometers, PZ-1 and PZ-2, and monitoring the water-level responses within the two piezometers and in the primary screen, S1. The tests were conducted in October 2015 before groundwater tracers were deployed in the two CdV-9-1(i) piezometers. The objectives of the slug tests were to better understand the hydraulic properties of the upper Puye Formation and the Otowi Member of the Bandelier Tuff and to provide data to evaluate the hydraulic connectivity between vertical strata in the vicinity of CdV-9-1(i).

In addition to introducing the relatively small volume of potable water into the two piezometers, the 10,632 gal. of tracer mixed with potable water introduced into CdV-9-1(i) S1 in November 2015 was also evaluated numerically as a slug-injection test. The evaluation of the slug-test data is included in Appendix D of this report.

3.1.2 CdV-9-1(i) Pumping Test

The primary pumping test at CdV-9-1(i) was conducted from June 7 to July 12, 2016, followed by recovery monitoring and rebound sampling through July 25. One month before the pumping test, a significant recharge event occurred, manifested in water levels increasing by approximately 12 ft in CdV-9-1(i) S1 starting in early May. Water levels were also observed to increase in CdV-9-1(i) PZ-2 but at a small magnitude. Water levels in CdV-9-1(i) S1 peaked on May 29 at a maximum elevation of 6617.34 ft and then began to decline as the recharge event moved through. Figure 3.1-1 shows water levels in pumping well CdV-9-1(i) S1 for the period of record from January 1 to November 3, including when the recharge event occurred and during the pumping test at CdV-9-1(i).

The rise in water levels likely reflects the influence of snowmelt runoff or a potential precipitation event. Similar recharge events have been observed at other wells completed in deep perched-intermediate groundwater in the past and are documented in the March 2011 groundwater level status report (Koch and Schmeer 2011, 201566) and in Appendix H of the Water Canyon/Cañon de Valle investigation report (LANL 2011, 207069). However, the large magnitude of water-level rise observed at CdV-9-1(i) S1 (~12 ft) is unusual and has not been observed at other wells completed in perched-intermediate groundwater at TA-16.

The pumping test activities at CdV-9-1(i) were initiated 9 d after the peak was observed on June 7, even while water levels were still declining from the recharge event. The potentiometric responses during the pumping test were significantly greater than the declines from the recharge event, allowing pumping test activities to continue; however, the large-scale recharge event added additional complexity to the analysis of the data.

Figure D-1A in Appendix D shows the water levels in pumping well CdV-9-1(i) S1 during the pumping test and recovery. Drawdown from the pumping test was significantly greater than the rate of drawdown from the snowmelt recharge event, allowing accurate analyses of the results.

Pumping at CdV-9-1(i) S1 started at 2:40 pm on June 7 and continued for approximately 2 d until 9:31 am on June 9. The pumping test was paused on June 9 at 9:31 am because of concerns about the piezometer water-level data, and the telemetry system used to remotely monitor water levels in the CdV-9-1(i) piezometers was not operating. Recovery was monitored for the next 5 d while the transducers were replaced in the piezometers and the telemetry system was repaired.

After a 5-d hiatus, pumping was resumed on June 14 at 9:40 am and continued until July 12 at 3:28 pm, when the active pumping was terminated and recovery was initiated. Pumping rates during the CdV-9-1(i) testing varied between 2.05 and 1.64 gpm.

During the recovery period, five 1-h rebound sampling events occurred on July 13, 15, 18, 20, and 25 with pumping rates ranging from 2.05 to 2.4 gpm. Potentiometric responses from these rebound pumping events, both in the pumping well and in observation wells, were evaluated as part of the analysis of the CdV-9-1(i) test data.

Figure D-1B shows daily pumping rates during the CdV-9-1(i) pumping test and the rebound sampling events. The pumping rate averaged 1.88 gpm during the 30-d duration of the pumping test.

During the final days of the pumping test, the daily pumping rate declined as a result of a plugged prefiltration bag filter in the GAC treatment unit. The filter could not be removed without shutting off the pump, so a decision was made to continue the pumping test to the end of the 30-d pumping period without shutting off the system. A subsequent design modification was made to the treatment unit to allow the bag filter to be replaced without shutting off the system.

Figure D-1C shows a cumulative pumping curve, with the total volume pumped and daily volume pumped during the pumping and recovery portions of the test. A total of 80,003 gal. was pumped from CdV-9-1(i) during the active 30-d pumping period of the test.

The results from the CdV-9-1(i) pumping test are summarized in section 4. In-depth analyses of the results from the CdV-9-1(i) pumping test data are presented in Appendixes D and G.

3.2 CdV-16-1(i) Pumping Test

Pumping at CdV-16-1(i) started on August 1, 2016, at 3:19 pm. The well was pumped for 30 d, with variable pumping rates ranging from 0.38 to 0.6 gpm, averaging 0.43 gpm over the 30-d duration of the test. The low pumping rate is from the low yield of the Otowi Member of the Bandelier Tuff in which the well is completed.

Electrical problems with the pump during the pumping test caused intermittent shutoffs, with the pump inadvertently shutting off seven times during the 30-d pumping test. The pump had to be manually restarted each time. These dynamic shutoff periods were considered in the pump-test analysis using analytical methods.

Recovery at CdV-16-1(i) was monitored for 23 d, with a total of seven rebound samples collected during this period. Typical recovery sampling events lasted approximately 3 h in duration, while purging at rates of 0.478 to 0.64 gpm.

Figure E-1A in Appendix E shows the water levels in CdV-16-1(i) during the pumping test and recovery, including dynamic pulse shutoff events and rebound sampling events. Because of the low yield of the formation, drawdown was observed to be nearly instantaneous. In each case when the pump was turned on, water levels stabilized at a relatively steady plateau at ~6781 ft, possibly indicating steady-state flow was achieved at this pumping rate. During periods where pumping ceased, the water quickly recovered to levels close to the background prepumping condition.

Figure E-1B shows daily measured pumping rates during the CdV-16-1(i) pumping test and rebound sampling events. Figure 3.2-1 shows cumulative volume pumped and daily pumping volume during the CdV-16-1(i) pumping test. A total of 16,227 gal. was pumped from CdV-16-4ip during the active 30-d pumping period of the test.

The results from the CdV-16-1(i) pumping test are summarized in section 4. In-depth analyses of the results from the CdV-9-1(i) pumping test are presented in Appendixes E and G.

3.3 CdV-16-4ip Pumping Test

Pumping at CdV-16-4ip S1, hereafter referred to as CdV-16-4ip, started on September 6, 2016, at 11:10 am. The well was pumped for a total of 30 d at variable pumping rates ranging from 3.88 to 7.8 gpm, with three restart periods to assess dynamic responses. The pump was turned off on October 11, and recovery monitoring was conducted to October 31. A total of seven rebound samples were collected during the recovery phase of the test.

Figure F-1A in Appendix F shows water levels measured in CdV-16-4ip during pumping test and recovery, including pump shutoff and rebound sampling events. Water levels declined at variable rates throughout the test, reflecting both changes in pumping rates and the influence of hydrostratigraphic contacts on groundwater flow into the borehole (Appendix F). The maximum drawdown over the duration of the test was approximately 51 ft (Figure F-1C).

Figure F-1B shows the daily measured pumping rates during the CdV-16-4ip pumping test and during rebound sampling events. Pumping rates were initially held steady at approximately 6 gpm for the first part of the test, which spanned from September 6 to 22. On September 22, pumping was terminated for a period of 4 d to evaluate transients in RDX concentrations during dynamic pumping conditions. Rebound samples were collected during the shutoff period from September 23 to 26 to assess transient pumping influences on RDX concentrations (section 4.3). Pumping then resumed at maximum pump capacity (starting at 7.8 gpm), and the pumping rate declined with increasing drawdown, ending at 3.88 gpm on the final full day of pumping (October 11). The average pumping rate during the test was 5.98 gpm, excluding pumping during recovery sampling.

Figure 3.3-1 shows a cumulative pumping curve, with total volume pumped and daily volume pumped during the pumping and recovery portions of the test. A total of 245,120 gal. was pumped from CdV-16-4ip during the active 30-d pumping period of the test.

The results from the CdV-16-4ip pumping test are summarized in section 4. In-depth analyses of the results from the CdV-9-1(i) pumping test are presented in Appendixes F and G.

4.0 INTERMEDIATE GROUNDWATER SYSTEM TESTING RESULTS

Appendixes D, E, and F describe the analyses of the pumping tests conducted at CdV-9-1(i), CdV-16-1(i), and CdV-16-4ip in the summer and fall of 2016. Appendix D also includes an analysis of the slug tests conducted on the piezometers and primary screen at CdV-9-1(i).

For each well, the software AQTESOLV (Duffield 2007, 601723) is used to interpret the pumping test data. Three models, Theis (1934-1935, 098241); Neuman (1974, 085421); and Cooper-Jacob (1946, 098236), which are built into the software AQTESOLV, were applied to interpret the pumping test data and estimate hydraulic (groundwater flow) parameters of the saturation zone, including hydraulic conductivity, storage coefficient, specific yield, and anisotropic factor. The results of the three models as well as previous estimates are compared. Appendix G provides an in-depth summary of the three pumping test results, with primary emphasis on analysis of water-level responses in the pumping wells and the observation screens.

4.1 Aquifer Parameters

Three numerical methods incorporating the Theis, Neuman, and Cooper-Jacob models were used to estimate aquifer parameters at each of the three pumping wells and between the pumping wells and observation screens (Appendixes D, E, and F). The results were compared with each other and to previous estimates for these parameters, when available. The results for each well are summarized below.

4.1.1 CdV-9-1(i) Aquifer Parameters

Table D-5 in Appendix D summarizes the estimated values of hydraulic conductivity, transmissivity, storage coefficient, and the horizontal to vertical anisotropy ratio for CdV-9-1(i). The previous estimates for aquifer parameters were based on a 3-d pumping test conducted shortly after well completion (LANL 2015, 600503). The estimated transmissivity based on the three-dimensional test conducted in 2015 ranged from 3.73 to 7.64 m^2/d. However, transmissivity values based on the 30-d test conducted in 2016 range from 0.66 to 0.987 m^2/d, roughly an order of magnitude lower. Similarly, hydraulic conductivities estimated based on the 30-d test in 2016 are approximately an order of magnitude lower than the value measured during the 3-d test (with an estimate of 0.023 m/d for the 30-d test [Appendix D], and 0.396 m/d for the three-dimensional test).

These apparent differences are believed to reflect scaling effects of the hydraulic properties, with the 30-d test in 2016 interrogating a considerably larger volume of porous media than the 3-d test. For this reason, the estimates of aquifer parameters based on the 30-d test are believed to be more reliable estimates of the pumped zone at a larger scale, while the estimates based on the 3-d test conducted in 2015 are more representative of the hydraulic properties in the vicinity of the CdV-9-1(i) well screen.

Attachment D-1 in Appendix D presents the analysis of the three slug tests conducted on PZ-1, PZ-2, and the primary screen, S1, at CdV-9-1(i). The Bouwer-Rice model was used to estimate the hydraulic conductivity of the saturated zone in the vicinity of the piezometer screens. The results for the slug tests are summarized in Table 4.1-1. The PZ-1 slug test yielded relatively high hydraulic conductivity and transmissivity compared with the PZ-2 slug test results. The slug test for CdV-9-1(i) S1 yielded a hydraulic conductivity and transmissivity estimate similar to that from the 30-d pumping test.

4.1.2 CdV-16-1(i) Aquifer Parameters

Table E-5 in Appendix E summarizes the estimated values of hydraulic conductivity, transmissivity, storage coefficient, and vertical to horizontal anisotropy ratio for CdV-16-1(i). The previous estimates for hydraulic conductivity and storage coefficient are included in this table and are based on a 24-h pumping test conducted following well completion at CdV-16-1(i) (Kleinfelder 2004, 087844). Previous estimates are generally consistent with the estimates provided in Table E-5.

4.1.3 CdV-16-4ip Aquifer Parameters

Table F-5 in Appendix F summarizes the estimated values of hydraulic conductivity, transmissivity, storage coefficient, and vertical to horizontal anisotropy ratio for CdV-16-4ip.

Overall, the Theis and Neuman models matched the observed drawdowns of the pumping period reasonably well but did not capture the recovery data and rebound sampling events very well. Nontheless, the estimated hydraulic conductivity is 0.035 m/d, based on the Neuman model, which is believed to provide the most representative value. However, all three models provided well-constrained estimates for hydraulic conductivity, with a range of 0.035 to 0.059 m/d. The hydraulic conductivity and transmissivity in the Puye Formation based on the 30-d pump test at CdV-16-4ip were measured to be approximately an order of magnitude lower than the hydraulic conductivity and transmissivity based on the 30-d day pump test at CdV-9-1(i).

4.2 Water-Level Responses

In-depth analyses of cross-borehole responses to the extended pumping at CdV-9-1(i), CdV-16-1(i), and CdV-16-4ip are presented in Appendix G, “Pumping Test Results for CdV-9-1(i), CdV-16-1(i), and CdV-16-4ip.” Thirty-day pumping tests were conducted consecutively on the three pumping wells, each followed by a recovery period ranging from one to several weeks in duration. Figure G-1 in Appendix G shows daily measured pumping rates during extended-duration testing conducted at CdV-9-1(i), CdV-16-1(i), and CdV-16-4ip.

Table 2.2-1 presents details of well completion for three pumping wells and all observation wells. All the wells, except R-63, are completed in perched-intermediate groundwater, while R-63 is completed in the regional aquifer. The water-level data were measured using vented pressure transducers and were corrected for barometric fluctuations based on data obtained from http://weather.lanl.gov for the meteorological station at TA-54.

Data analyses were conducted using the software AQTESOLV (Duffield 2007, 601723) to interpret the pumping test data. The Theis model (Theis 1934–1935, 098241) was used to interpret cross-well responses and to predict estimated potential maximum drawdown at each screen as a result of pumping at wells CdV-9-1(i), CdV-16-1(i), and CdV-16-4ip.

4.2.1 CdV-9-1(i) Responses

Water-level responses in CdV-9-1(i) PZ-1, PZ-2, and S1 during deployment of the tracers (section 3.1.1) were reviewed to better understand the basis for nearly identical water levels in CdV-9-1(i) PZ-1 and PZ-2 and to assess the vertical connectivity between the two piezometer screens. The results of the data showed nearly instantaneous responses in water levels within the two piezometers when tracers were introduced, suggesting possible vertical preferential flow between the two zones in which these piezometers are completed. Water-level responses were not observed in the CdV-9-1(i) primary screen (S1) when tracers were introduced in PZ-1 and PZ-2.

Figure G-2 shows water-level elevation (feet) and pumping rates (gpm) during the 2016 pumping test. CdV-9-1(i) S1 water levels exhibited drawdown-recovery behavior that may be more indicative of low complexity and less stratification (Figure G-2) when compared with data collected at CdV-16-4ip, for example (Figure G-4). The higher degree of stratification at CdV-16-4ip is reflected in the additional points of inflection or slope changes in the drawdown and recovery curve for CdV-16-4ip compared with CdV-9-1(i).

Before pumping began, a hydrologic event of unknown origin resulted in a surge in water level at CdV-9-1(i) (the water-level rise may have been caused by an infiltration event). This event was also potentially observed in CdV-9-1(i) PZ-2 and may indicate a hydrologic transient that cannot be represented using the analytical modeling tools applied here.

The moderate pumping rates (~2 gpm) at CdV-9-1(i) resulted in water-level decline of ~40 ft. The first stage of pumping was relatively short, resulting in a moderate decline in water elevation to ~6593 ft, followed by recovery after the pump was shut off and prolonged drawdown during the second (longest) stage of pumping, which occurred from June 14 to July 11, 2016, and resulted in a maximum decline in water elevation to ~6570 ft, followed by intermittent pumping at a slightly higher rate, which caused sharp declines in the water level. These declines did not drastically influence recovery to background water levels. The general rate of water-level declines during prolonged pumping (second stage) was initially rapid but decreased over time, potentially indicating an approach to steady-state drawdown for pumping rates of 1.8 to 2.0 gpm.

The absence of drastic declines in water level before the minimum water level was reached suggests dewatering of the borehole did not occur. No major inflection points are apparent in the water-level curves, suggesting major hydrostratigraphic contacts or boundaries may not exist in the vicinity of the pumped screen interval.

4.2.2 CdV-16-1(i) Responses

Figure G-3 shows water-level elevation (feet) and pumping rates (gpm) at CdV-16-1(i) during the 2016 pumping test. Changes in water levels of CdV-16-1(i) during the pump test are difficult to interpret because of the low pumping rates used during the test (Figure D-3). The maximum decline in water level observed at the pumping well was ~17 ft and corresponds to a water elevation of ~6778 ft. Extended-duration pumping at ~0.4 gpm resulted in an accelerated decrease in water level until a relatively steady plateau was reached at ~6781 ft, potentially indicating the achievement of a steady-state flow regime at this pumping rate. During periods where pumping ceased, the water level quickly recovered to levels close to the prepumping condition. The recovery data did not show inflection points in recovery temporal trends that could suggest hydraulic effects caused by hydrostratigraphic contacts or boundary effects. The absence of any substantial decreases in water level before the minimum water level was reached further suggests dewatering of the borehole did not occur at the applied pumping rates.

4.2.3 CdV-16-4ip Responses

Figure G-4 shows water-level elevation (feet) and pumping rates (gpm) at CdV-16-4ip during the 2016 pumping test. The water level at CdV-16-4ip S1 demonstrates complexity in the pumped zone of saturation and potential stratification in this area, as described below. A similar water-level profile was observed during both the 2011 and 2014 pump tests of the same screen (LANL 2011, 111608, Figure B-7.0-1; LANL 2014, 600004, Figure B-2).

Initially, pumping at ~6 gpm caused a rapid water-level decline to an elevation of ~6620 ft, followed by a decrease in the rate of water-level decline until the water-level elevation reached ~6605 ft when pumping stopped. Some recovery in water level occurred at ~6615 ft until pumping restarted.

Subsequent pump cycles resulted in accelerated decreases in water level, especially when pumping rates were highest (~7.8 gpm), although a plateau in the observed water level occurred during pumping from October 3 to 11, 2016, as a result of incremental decline in pumping rate. The minimum water level observed was ~6595 ft, resulting in a maximum decrease in water level of ~50 ft. However, below 6602 ft, the water level declined very rapidly, suggesting dewatering of the borehole.

During the final stage of the pump test, short-duration pumping occurred intermittently, causing sharp declines in water level that did not drastically interfere with recovery to background water levels. As with the 2014 pump test, inflection points in the water-level recovery curve at ~6615 and ~6620 ft suggest hydrostratigraphic contacts are affecting the flow towards the saturated zone pumped by the well; the elevations of the inflection points in the water-level recovery curve potentially identify the elevations of these hydrostratigraphic contacts. More permeable hydrostratigraphic zones are potentially located between ~6600 and ~6620 ft. However, the groundwater flow along these more permeable zones is not sufficient to provide sustainable pumping of CdV-16-4ip at a rate of 6 to 8 gpm.

4.3 Cross-Well Water-Level Responses between the Pumping Wells and Observation Screens

Cross-well water-level responses observed during the extended aquifer pumping at wells CdV-9-1(i), CdV-16-1(i), and CdV-16-4ip provide key information regarding the hydraulic interconnections between wells and the responses to pumping in adjacent geologic units. Water-level responses indicate the well screen in the observation well is hydrologically connected to the well screen in the pumping well. However, the lack of a water-level response may indicate (1) the observation and pumping well screens are not hydrologically connected or (2) the pump rate in the pumping well or the duration of the pumping period was insufficient to perturb water levels in the observation well.

During the pumping test in 2016, water levels were monitored at the following monitoring well locations: CdV-9-1(i) S1; CdV-9-1(i) PZ-1; CdV-9-1(i) PZ-2; CdV-16-1(i); CdV-16-2ir; CdV-16-4ip S1; R-25 S1, S2, and S4; R-25b; R-47i; R 63; and R-63i. The wells where the pumping tests occurred were also used as observation wells.

The water-level data were analyzed using the software AQTESOLV (Duffield 2007, 601723) to interpret the data. The Theis model (Theis 1934–1935, 098241) was used to interpret cross-well responses and to estimate potential maximum drawdown at each screen as a result of pumping at wells CdV-9-1(i), CdV-16-1(i), and CdV-16-4ip. Additional details regarding the methodology used for the cross-well analysis and the results are discussed in detail in Appendix G.

Figures G-5 to G-9 in Appendix G graphically show the results of this analytical approach. Each figure shows the model-based deconstruction of the water-level transients observed in each monitoring well. The upper panels in each figure show the observed and simulated water levels at the monitoring well, and the lowest panel shows the individual contributions of each pump test to drawdown at the observation well. Dashed lines in the lowest panel represent a general linear trend of water-level decline that is independent of responses and may be attributed to pumping associated with the pumping tests. The water-level decline trend is not explicitly represented in the model but may influence interpretation of water-level responses.

For all observation wells, the model was calibrated using water-level data from the 2016 pumping test. Because longer water-level records are available, CdV-16-4ip S1, R-25 S 2, R-25b, R-47i, and R-63 were also calibrated using the 2014 pump test along with the 2016 tests.

The model also simulated the maximum simulated drawdown contribution of each pumping well that occurs at each observation well in 2016. Table 4.2-1 shows the estimated maximum drawdown in 2016 at each screen as a result of pumping at wells CdV-9-1(i), CdV-16-1(i), and CdV-16-4ip. This table also summarizes hydraulic connections observed during the pumping tests. Impacts from each pumping well on water levels in the observation wells are categorized as certain, with drawdown responses shown in red, as potential (with estimated drawdowns shown in blue), and as unlikely (with simulated drawdowns shown in grey). Additional details regarding the interpretation of the modeling results are summarized in Appendix G (pp. G-3 to G-5).

Figures 4.3-1, 4.3-2, and 4.3-3 show the estimated potential maximum drawdown values in nearby monitoring wells, resulting from pumping at CdV-9-1(i), CdV-16-1(i), and CdV-16-4ip. Only values considered certain or potential are shown in these figures.

4.3.1 Estimated Aquifer Parameters between Observation Screens and Pumping Wells

Table G-2 in Appendix G presents estimates of the transmissivity (m^2/day) and storativity (-) between the observation screens and the pumping wells. In general, large storativity estimates reflect the low sensitivity of observation-well drawdowns to pumping transients, and large transmissivity estimates result from negligible influence of pumping on drawdown at the observation well. Exceedingly large transmissivities and small storativities do not represent real physical values but instead indicate the lack of hydraulic connectivity.

Table G-2 in Appendix G lists only effective transmissivity and storativity estimates, considered to be reasonable and representative of drawdowns and sufficiently well identified based on the available data. Estimated transmissivity and storativity values that resulted in drawdown contributions less than 1 cm were considered unrepresentative and were removed from the data set.

4.4 Pumping Test Geochemistry

4.4.1 Transient Concentrations of RDX and HMX

An additional objective of the extended pumping test at CdV-9-1(i), CdV-16-1(i), and CdV-16-4ip was to evaluate contaminant characteristics in the perched-intermediate zone by monitoring temporal variations in RDX during the 30-d pumping periods. Changes in contaminant concentrations during pumping provide insight regarding spatial variability and possible storage and distribution of contamination within unsaturated zones adjacent to perched zones.

Figures 4.4-1 through 4.4-3 show RDX concentrations measured during pumping and recovery at CdV-9-1(i), CdV-16-1(i), and CdV-16-4ip. The samples for analysis at the on-site laboratory GGRL (shown as EES on the plots) were collected 3 times per week. Samples were also collected weekly for off-site analysis at the GEL Laboratories.

Both data sets are shown on these plots and are comparable for samples from CdV-9-1(i) and CdV-16-1(i), where RDX concentrations ranged from approximately 20 µg/L to 35 µg/L. However, the RDX concentration values measured in samples from CdV-16-4ip, which has higher RDX levels on the order of approximately 150 µg/L, showed an apparent difference in concentration values in samples measured at GGRL versus at GEL Laboratories. The RDX concentrations measured at GEL Laboratories were approximately 20% to 25% lower than the concentration measured on-site; the reason for this difference is not known.

Figures 4.4-4 through 4.4-6 compare RDX concentrations with changes in groundwater elevation during pumping and recovery at each well. At monitoring wells CdV-9-1(i) and CdV-16-1(i), where RDX concentrations are relatively low, some correlation exists between groundwater levels during pumping and RDX concentrations. As groundwater levels declined during the pumping tests, a moderate decrease in RDX concentrations was observed in both CdV-9-1(i) and CdV-16-4ip. During recovery, RDX concentrations were observed to increase with increasing groundwater levels. However, this apparent correlation with groundwater levels is not observed at CdV-16-4ip, where RDX concentrations remain relatively consistent during both pumping and recovery (Figure 4.4-6).

Figures 4.4-7 through 4.4-9 show RDX and HMX (1,3,5,7-tetranitro-1,3,5,7-tetracyclo-octane) concentrations plotted on the same graph during pumping and recovery at CdV-9-1(i), CdV-16-1(i), and

CdV-16-4ip. HMX concentrations generally trend with RDX concentrations, particularly at wells CdV-16-1(i) and CdV-16-4ip. At CdV-9-1(i), RDX concentrations appear to decline during pumping, while HMX concentrations trend upward; the reason for this effect is not known.

4.4.2 Additional Geochemical Parameters

Additional plots of geochemical analytical data are presented in Appendix H but are not discussed here. These plots present data for following analytes sampled during pumping and recovery at the three wells:

- RDX degradation products MNX (hexahydro-1-nitroso-3,5-dinitro-1,3,5-triazine); DNX (hexahydro-1,3-dinitro-5-nitro-1,3,5-triazine); and TNX (hexahydro-1,3,5-trinitroso-1,3,5-triazine)
- RDX and HMX along with the RDX degradation products MNX, DNX, and TNX
- TNT [trinitrotoluene(2,4,6-)] and its degradation products
- Volatile organic compounds (VOCs) MTBE (methyl-t-butyl ether), PCE (tetrachloroethylene), and TCE (trichloroethene)
- Nitrate and chloride
- Barium and boron

4.5 Estimate of RDX Mass Removed during Pumping

The mass of RDX removed by GAC treatment during the pumping tests at CdV-9-1(i), CdV-16-1(i), and CdV-16-4ip was calculated to determine the percent of RDX mass removed during these pumping tests. The total RDX removed was determined by multiplying the average RDX concentration measured during pumping at each of the three wells by the total volume of water removed during each pumping test to estimate the total mass of RDX removed during each test. The results are summarized in Table 4.5-1.

Based on this approach, an estimated 0.17 kg of RDX was removed during the three 30-d pumping tests at CdV-9-1(i), CdV-16-1(i), and CdV-16-4ip.

For comparison, the total estimated mass of RDX in perched-intermediate groundwater at TA-16 ranges 219 to 887 kg based on a recent reevaluation of the RDX inventory at TA-16. Assuming a total inventory of RDX ranging from 219 to 887 kg, the 2016 pumping test activities removed 0.019% to 0.078% of the RDX currently estimated to be in perched-intermediate groundwater at TA-16.

5.0 KEY FINDINGS

Cross-well pumping tests at monitoring wells CdV-9-1(i), CdV-16-1(i), and CdV-16-4ip completed in perched-intermediate groundwater provided valuable information regarding vertical and horizontal connectivity within perched-intermediate groundwater at TA-16. Key findings include the following.

Hydraulic communication was observed between screens relatively proximal to each other and completed in the upper Puye Formation. The primary area of hydraulic communication is a laterally continuous saturated zone within the upper Puye Formation that is at least as large as the triangle formed by CdV-9-1(i), CdV-16-4ip, and R-25 S2. Figure 5.0-1 shows this primary area of hydraulic communication and the maximum predicted drawdowns observed in each well as a result of pumping in nearby wells. The preferential communication across the upper Puye Formation is likely driven by stratification (i.e., high anisotropy) within Puye strata.

Thirty days of pumping of CdV-9-1(i) S1 generated no water-level response in CdV-9-1(i) PZ-2, even though both screens are completed in the Puye Formation. Pumping from wells within the upper Puye caused little or no response in monitored screens within the lower Puye Formation and Otowi Member, including monitoring points that are very close to the pumping locations. In one case, limited hydraulic communication may have been observed across the Otowi/Puye boundary, based on an apparent water-level responses in CdV-9-1(i) PZ-2 as a result of pumping at CdV-16-1(i). These observations suggest a high lateral to vertical anisotropy ratio and a potentially important hydrostratigraphic characteristic of the Otowi/Puye contact.

The apparent boundary effect observed during pumping at CdV-16-4ip in 2014 (LANL 2014, 600004) is believed to reflect contrasts in aquifer properties rather than a spatially limited perched body based on the good hydraulic responses in nearby upper Puye wells during the pumping tests.

RDX concentrations showed some correlation with water levels at CdV-9-1(i) and CdV-16-1(i) but not at CdV-16-4ip. RDX concentrations in wells CdV-9-1(i) and CdV-16-1(i) declined during pumping as water levels dropped and then appeared to increase during recovery. Because of the relatively low sustainable pumping rates at CdV-16-1(i), CdV-9-1(i), and CdV-16-4ip, the total mass of RDX removed during 90 d of pumping was an estimated 0.17 kg, representing approximately 0.02% to 0.08% of the estimated RDX inventory believed to be present in perched-intermediate groundwater beneath the TA-16/TA-09 area.

These findings provide a basis for updating the conceptual model for the perched-intermediate zone in the RDX project area. Figures 5.0-2a–d present four geologic cross-sections reflecting the revised understanding of perched-intermediate groundwater and the laterally continuous zone within the upper Puye Formation where hydraulic communication was observed.

6.0 REFERENCES

The following list includes all documents cited in this report. Parenthetical information following each reference provides the author(s), publication date, and ERID or ESHID. This information is also included in text citations. ERIDs were assigned by the Environmental Programs Directorate's Records Processing Facility (IDs through 599999), and ESHIDs are assigned by the Environment, Safety, and Health (ESH) Directorate (IDs 600000 and above). IDs are used to locate documents in the Laboratory's Electronic Document Management System and, where applicable, in the master reference set.

Copies of the master reference set are maintained at the NMED Hazardous Waste Bureau and the ESH Directorate. The set was developed to ensure that the administrative authority has all material needed to review this document, and it is updated with every document submitted to the administrative authority. Documents previously submitted to the administrative authority are not included.

Cooper, H.H., Jr., and C.E. Jacob, August 1946. "A Generalized Graphical Method for Evaluating Formation Constants and Summarizing Well-Field History," *American Geophysical Union Transactions,* Vol. 27, No. 4, pp. 526-534. (Cooper and Jacob 1946, 098236)

Duffield, G.M., June 16, 2007. "AQTESOLV for Windows, Version 4.5, User's Guide," HydroSOLVE, Inc., Reston, Virginia. (Duffield 2007, 601723)

Kleinfelder, May 7, 2004. "Final Well CdV-16-1(i) Completion Report," report prepared for Los Alamos National Laboratory, Project No. 37151/9.12, Albuquerque, New Mexico. (Kleinfelder 2004, 087844)

Koch, R.J., and S. Schmeer, March 2011. “Groundwater Level Status Report for 2010, Los Alamos National Laboratory,” Los Alamos National Laboratory report LA-14437-PR, Los Alamos, New Mexico. (Koch and Schmeer 2011, 201566)

LANL (Los Alamos National Laboratory), May 9, 1994. “Process Flow Reductions from Waste Minimization for Value Engineering Study,” Los Alamos National Laboratory, Los Alamos, New Mexico. (LANL 1994, 076858)

LANL (Los Alamos National Laboratory), February 2010. “Hydrologic Testing Work Plan for Consolidated Unit 16-021(c)-99,” Los Alamos National Laboratory document LA-UR-10-0404, Los Alamos, New Mexico. (LANL 2010, 108534)

LANL (Los Alamos National Laboratory), January 2011. “Completion Report for Intermediate Well CdV-16-4ip,” Los Alamos National Laboratory document LA-UR-11-0187, Los Alamos, New Mexico. (LANL 2011, 111608)

LANL (Los Alamos National Laboratory), September 2011. “Investigation Report for Water Canyon/Cañon de Valle,” Los Alamos National Laboratory document LA-UR-11-5478, Los Alamos, New Mexico. (LANL 2011, 207069)

LANL (Los Alamos National Laboratory), March 2012. “Technical Area 16 Well Network Evaluation and Recommendations,” Los Alamos National Laboratory document LA-UR-12-1082, Los Alamos, New Mexico. (LANL 2012, 213573)

LANL (Los Alamos National Laboratory), November 2012. “Work Plan to Reconfigure Well CdV-16-4ip,” Los Alamos National Laboratory document LA-UR-12-26150, Los Alamos, New Mexico. (LANL 2012, 232222)

LANL (Los Alamos National Laboratory), September 2013. “Well Reconfiguration of CdV-16-4ip Field Summary Report,” Los Alamos National Laboratory document LA-UR-13-26926, Los Alamos, New Mexico. (LANL 2013, 249519)

LANL (Los Alamos National Laboratory), October 2014. “Interim Measures Report for Source-Removal Testing at Well CdV-16-4ip,” Los Alamos National Laboratory document LA-UR-14-27065, Los Alamos, New Mexico. (LANL 2014, 600004)

LANL (Los Alamos National Laboratory), June 2015. “Completion Report for Intermediate Aquifer Well CdV-9-1(i),” Los Alamos National Laboratory document LA-UR-15-23954, Los Alamos, New Mexico. (LANL 2015, 600503)

LANL (Los Alamos National Laboratory), July 2015. “Work Plan for a Tracer Test at Consolidated Unit 16-021(c)-99, Technical Area 16, Revision 1,” Los Alamos National Laboratory document LA-UR-15-24089, Los Alamos, New Mexico. (LANL 2015, 600535)

LANL (Los Alamos National Laboratory), August 2015. “Work Plan for Intermediate Groundwater System Characterization at Consolidated Unit 16-021(c)-99,” Los Alamos National Laboratory document LA-UR-15-24545, Los Alamos, New Mexico. (LANL 2015, 600686)

LANL (Los Alamos National Laboratory), February 2017. “Work Plan #4 Discharge Report, Land Application of Treated Groundwater from Technical Areas 9 and 16, DP-1793,” Los Alamos National Laboratory document LA-UR-17-20288, Los Alamos, New Mexico. (LANL 2017, 602164)

Neuman, S.P., April 1974. “Effect of Partial Penetration on Flow in Unconfined Aquifers Considering Delayed Gravity Response,” *Water Resources Research,* Vol. 10, No. 2, pp. 303-312. (Neuman 1974, 085421)

NMED (New Mexico Environment Department), December 21, 2012. “Approval with Modifications, Work Plan to Reconfigure Well CdV-16-4ip,” New Mexico Environment Department letter to P. Maggiore (DOE-LASO) and J.D. Mousseau (LANL) from J.E. Kieling (NMED-HWB), Santa Fe, New Mexico. (NMED 2012, 521747)

NMED (New Mexico Environment Department), October 13, 2015. “Approval, Work Plan for Intermediate Groundwater System Characterization at Consolidated Unit 16-021(c)-99,” New Mexico Environment Department letter to C. Gelles (DOE-NA-LA) and M.T. Brandt (LANL) from J.E. Kieling (NMED-HWB), Santa Fe, New Mexico. (NMED 2015, 600957)

Theis, C.V., 1934-1935. “The Relation Between the Lowering of the Piezometric Surface and the Rate and Duration of Discharge of a Well Using Ground-Water Storage,” *American Geophysical Union Transactions,* Vol. 15-16, pp. 519-524. (Theis 1934-1935, 098241)

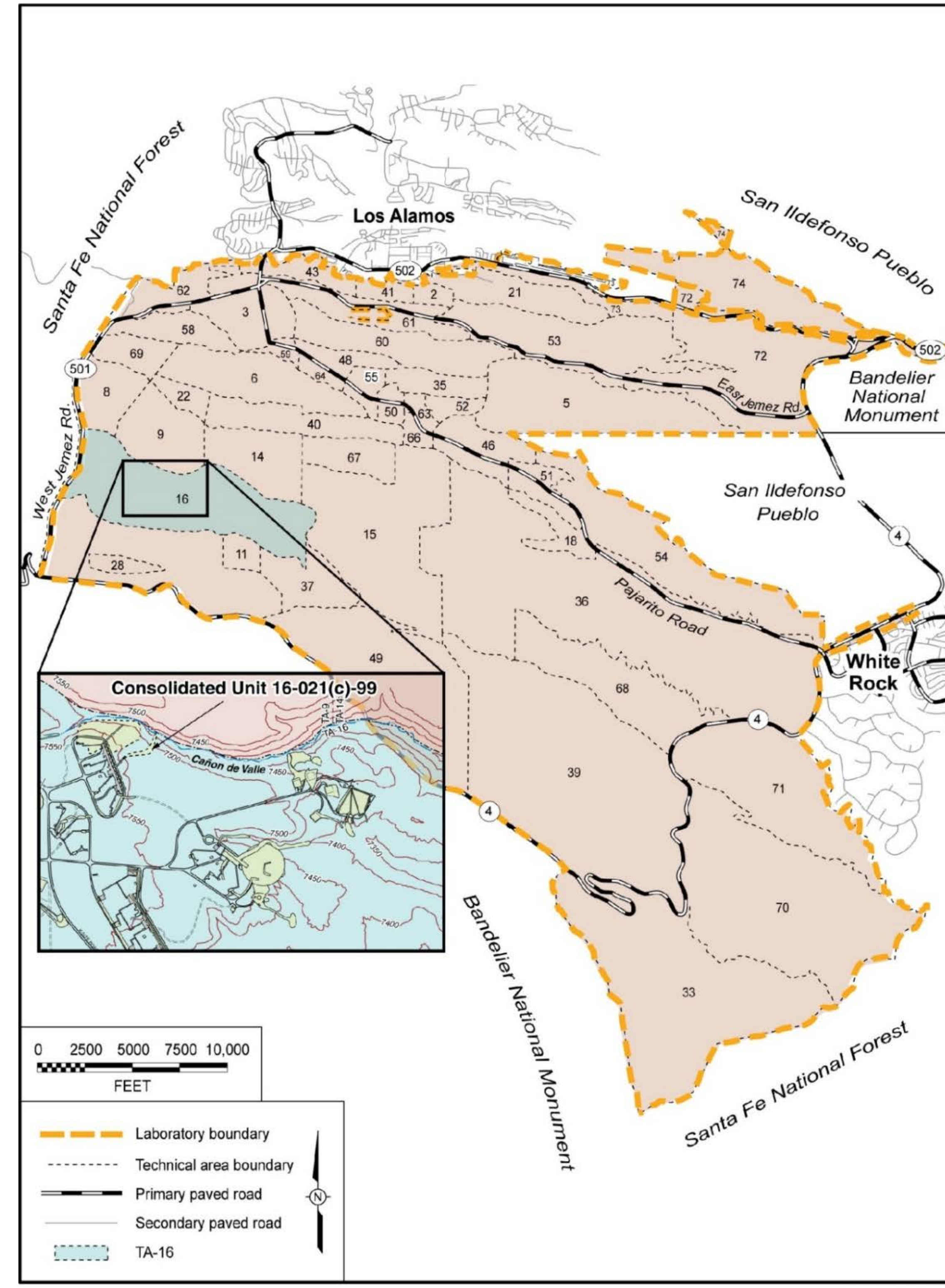

Figure 1.0-1 Location of TA-16 and other TAs at the Laboratory

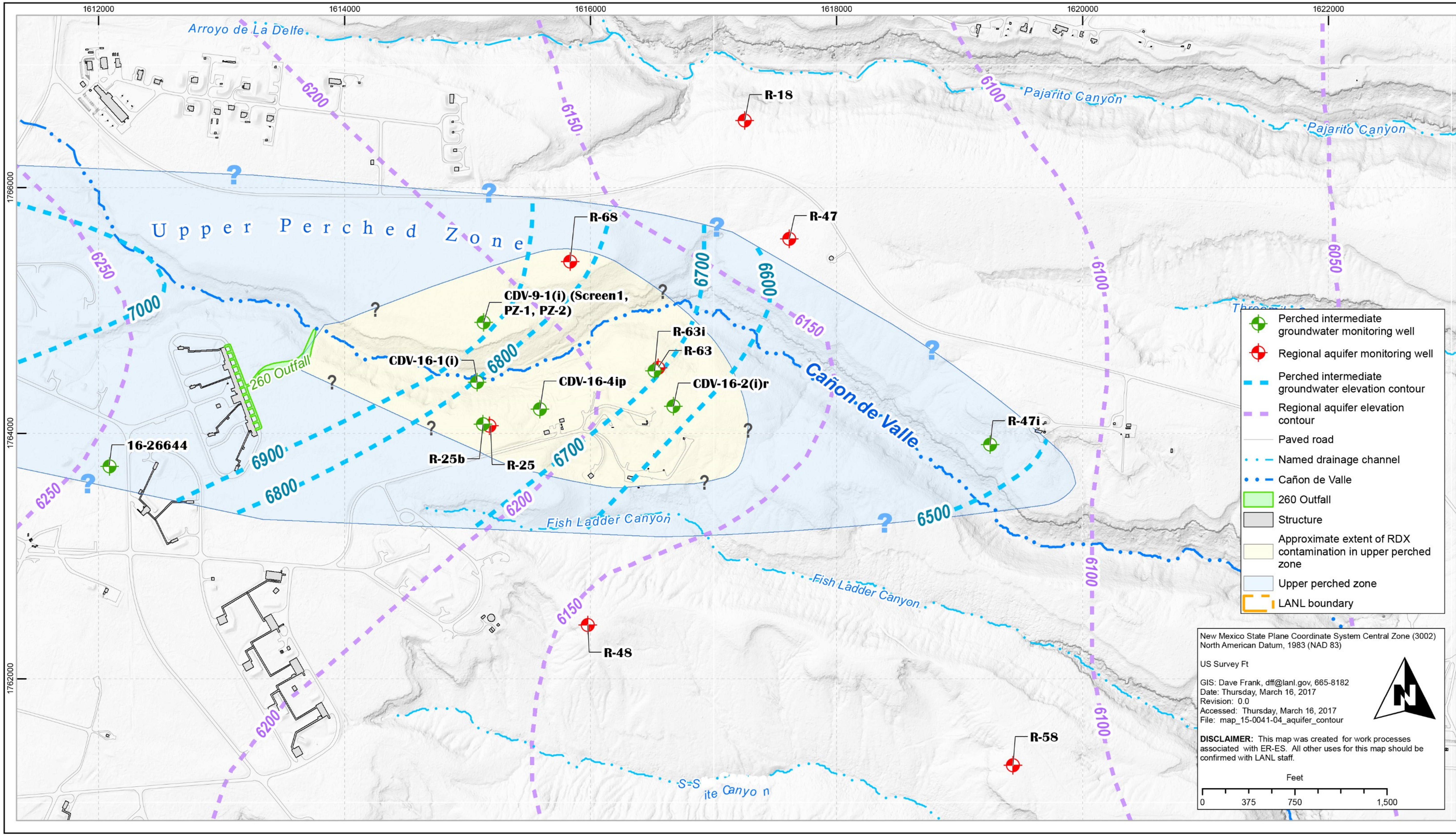

Figure 1.0-2 Perched-intermediate and regional groundwater wells in the vicinity of the 260 Outfall, and water table contours for intermediate (blue dashed lines) and regional groundwater (purple dashed lines)

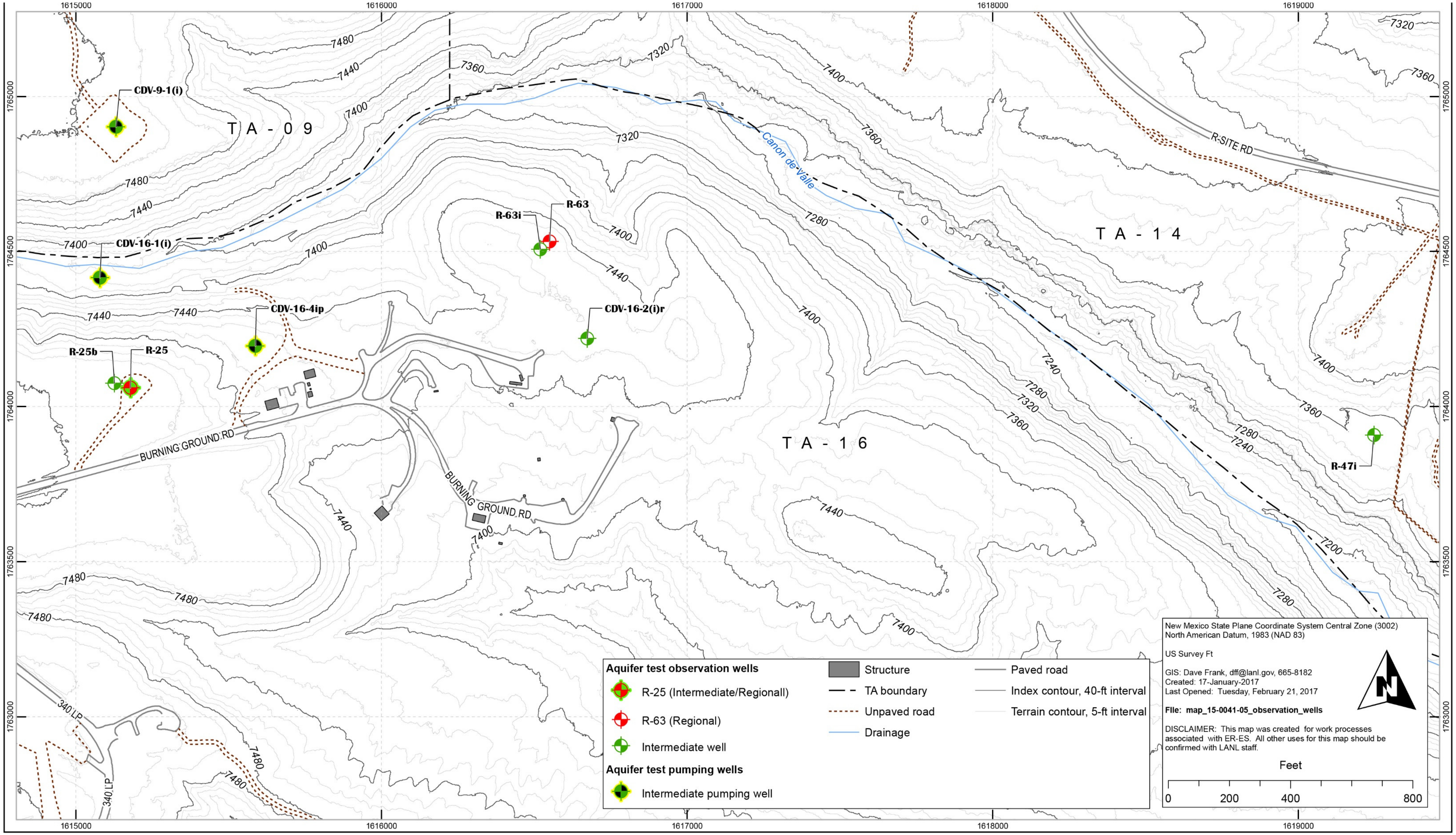

Figure 1.1-1 Locations of the pumping and observation wells

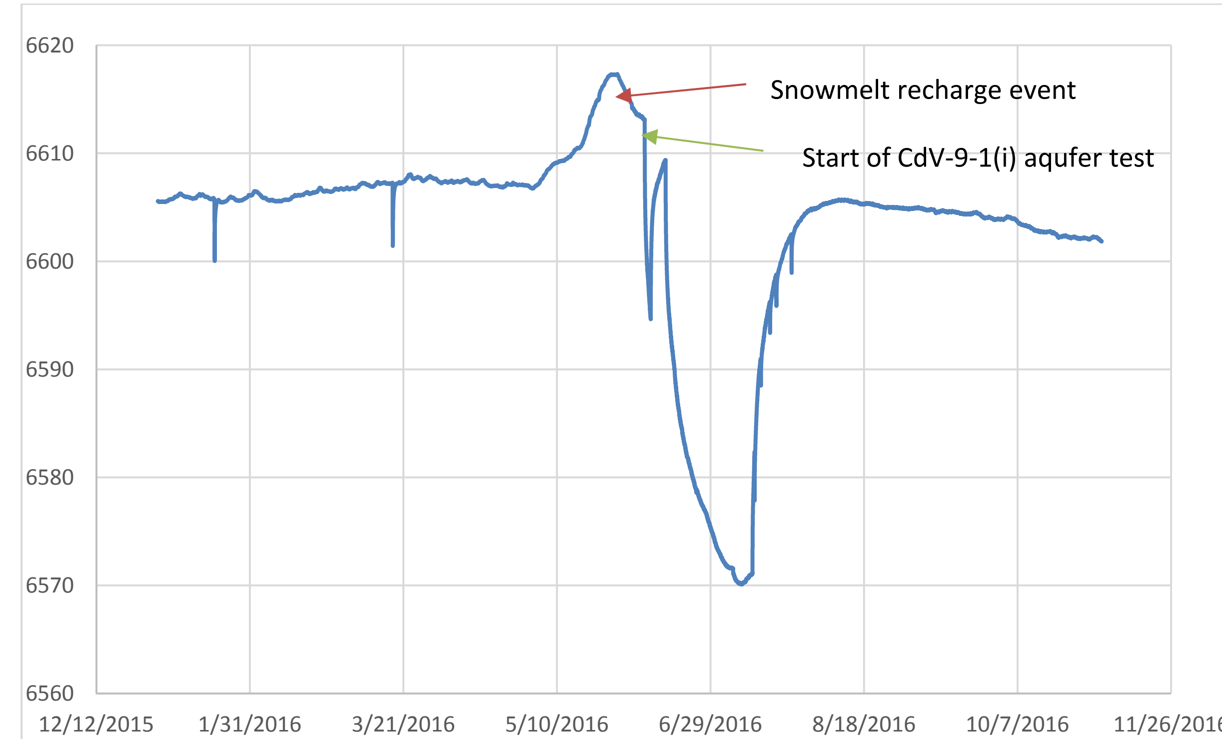

Figure 3.1-1 Water levels in CdV-9-1(i) S1 from January 1 to November 3 before and after pumping test activities

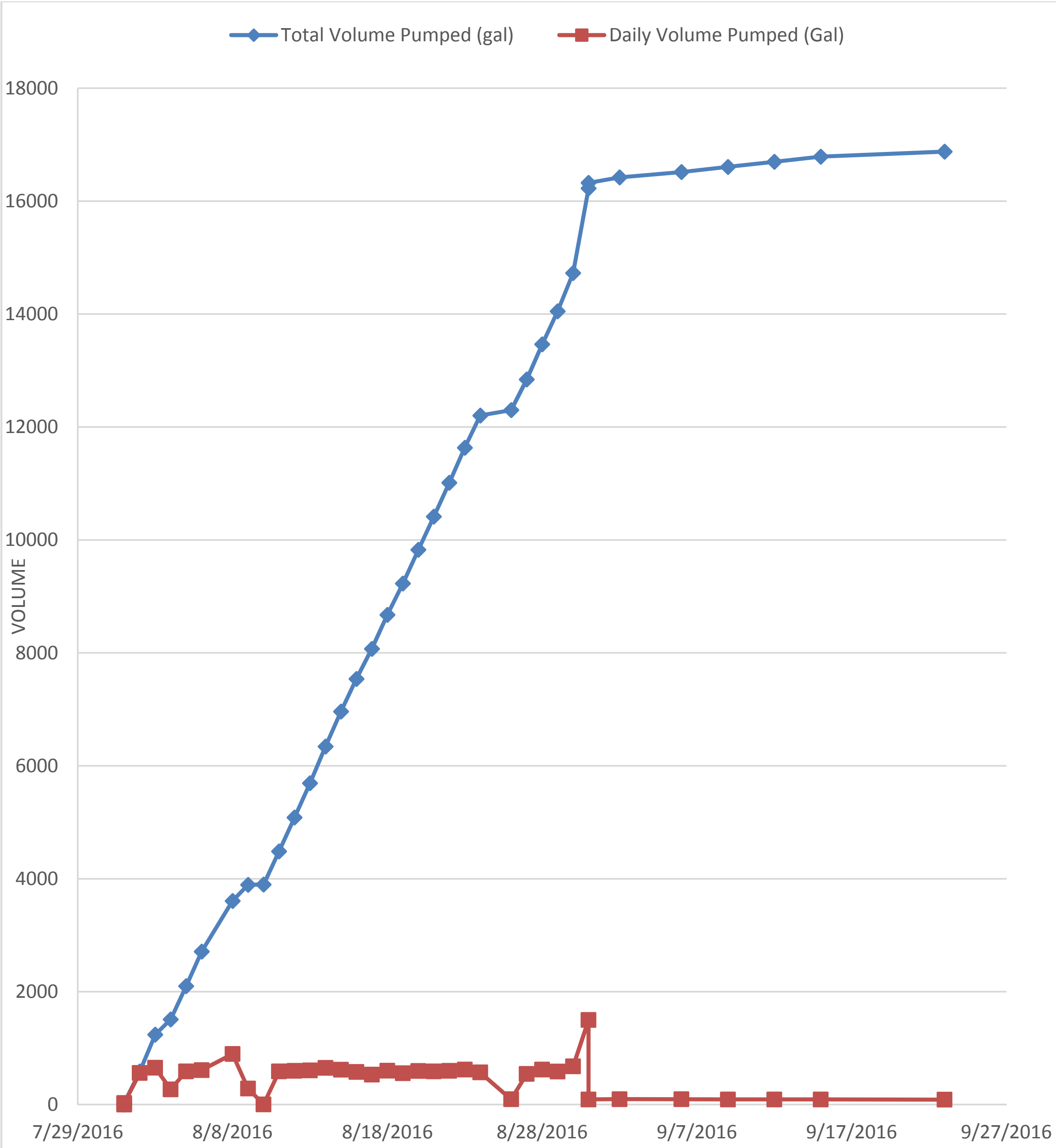

Figure 3.2-1 Cumulative volume pumped and daily pumping volume during the CdV-9-1(i) pumping test and rebound sampling period

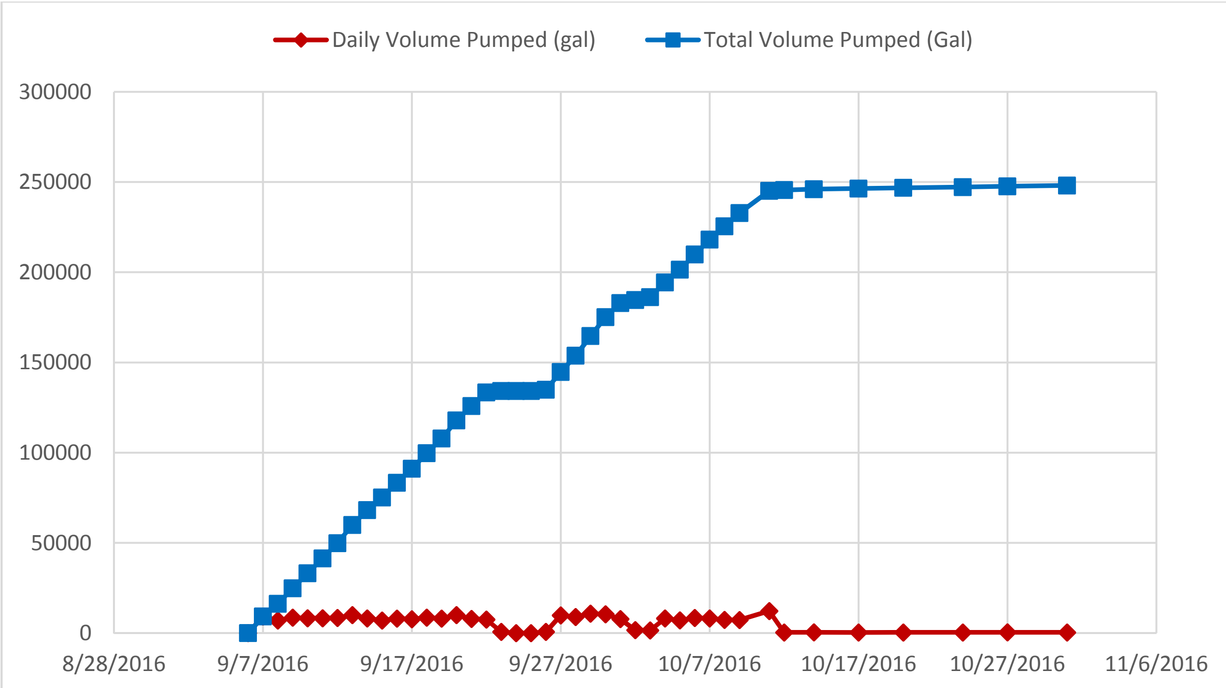

Figure 3.3-1 **Cumulative volume pumped and daily volume pumped during the CdV-16-4ip pumping test and rebound sampling period**

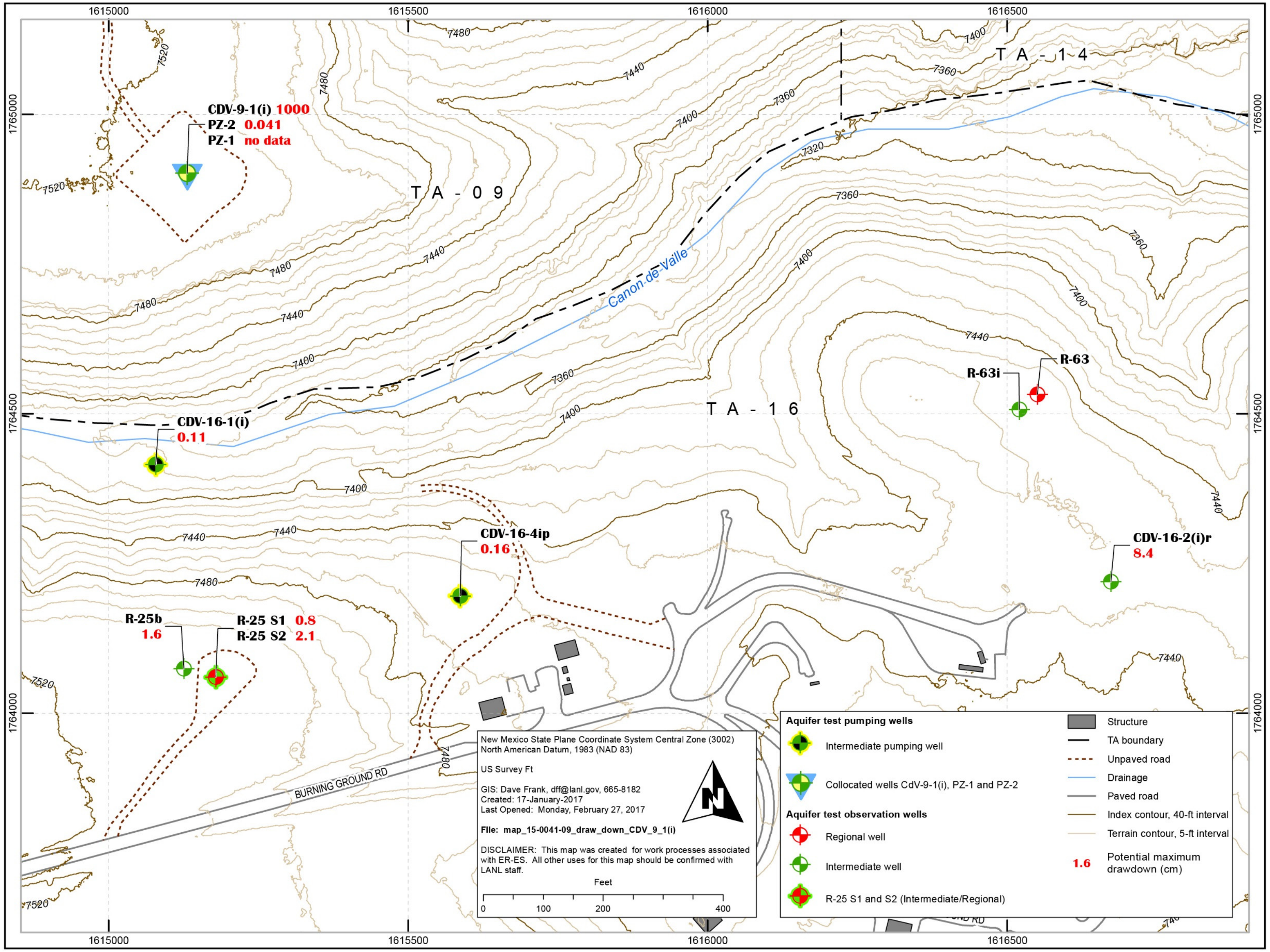

Figure 4.3-1 Estimated potential maximum drawdowns in nearby observation screens during pumping at CdV-9-1(i)

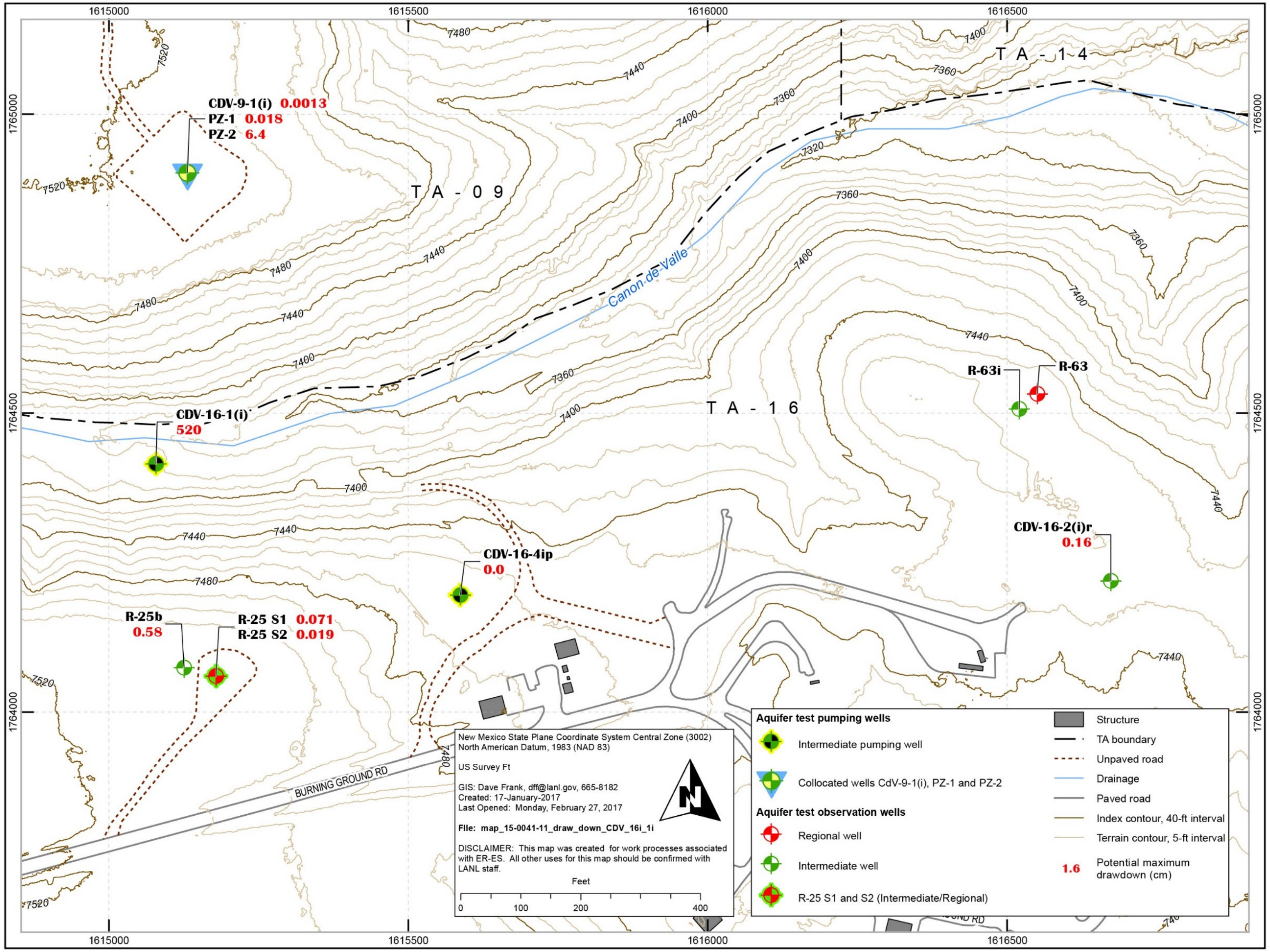

Figure 4.3-2 **Estimated potential maximum drawdowns in nearby observation screens during pumping at CdV-16-1(i)**

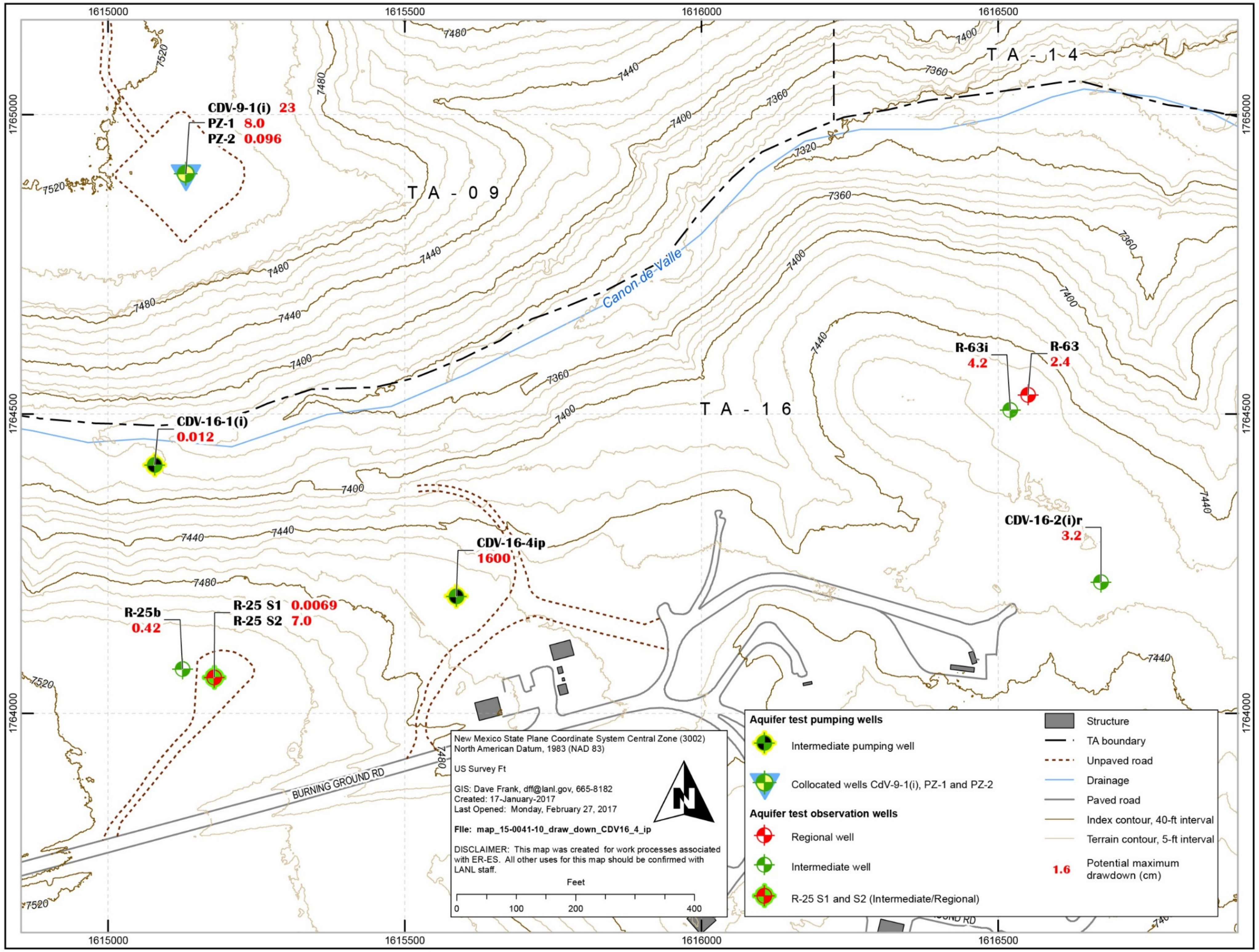

Figure 4.3-3 Estimated potential maximum drawdowns in nearby observation screens during pumping at CdV-16-4ip

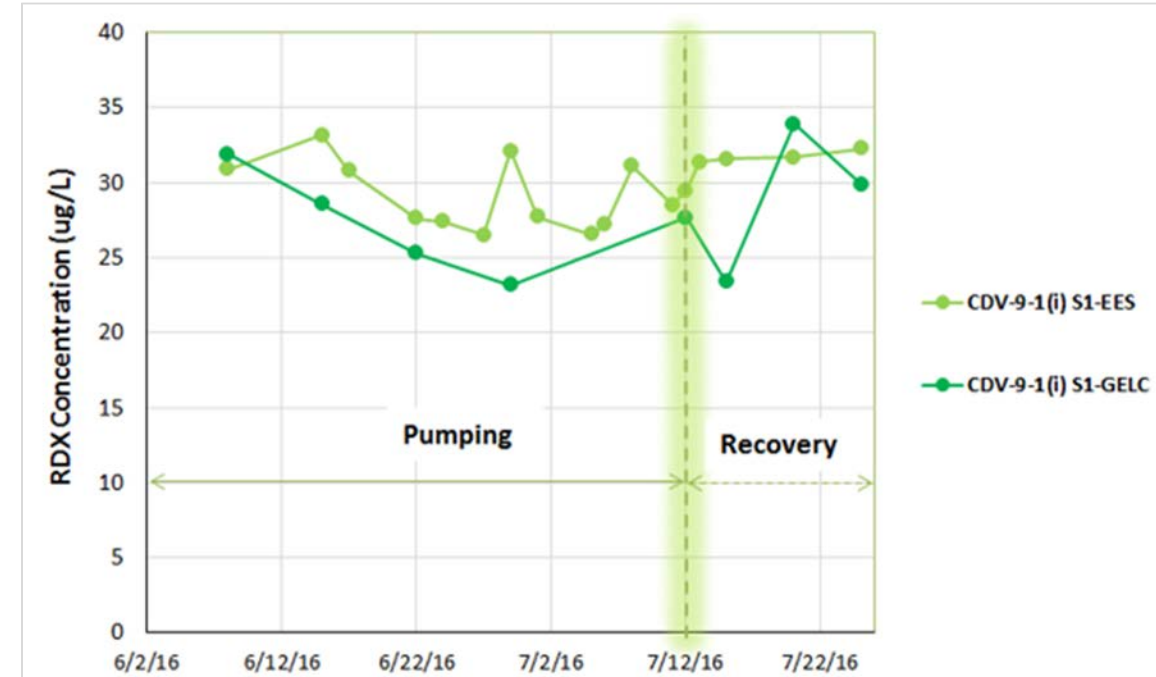

Figure 4.4-1 RDX concentrations measured during pumping and recovery at CdV-9-1(i)

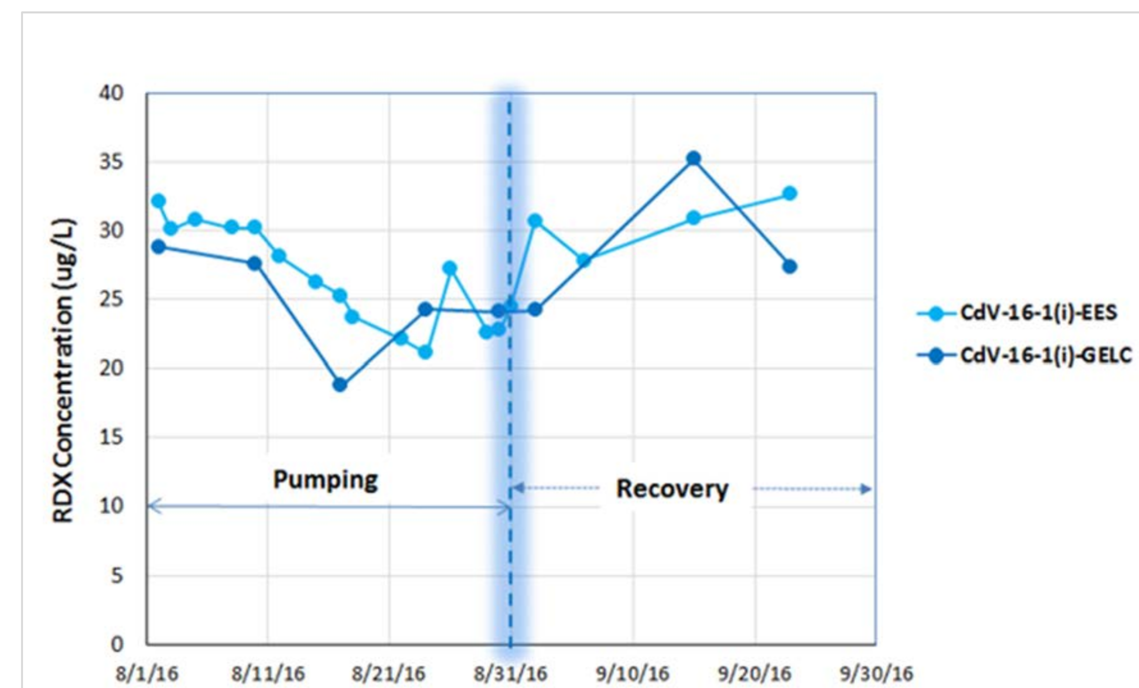

Figure 4.4-2 RDX concentrations measured during pumping and recovery at CdV-16-1(i)

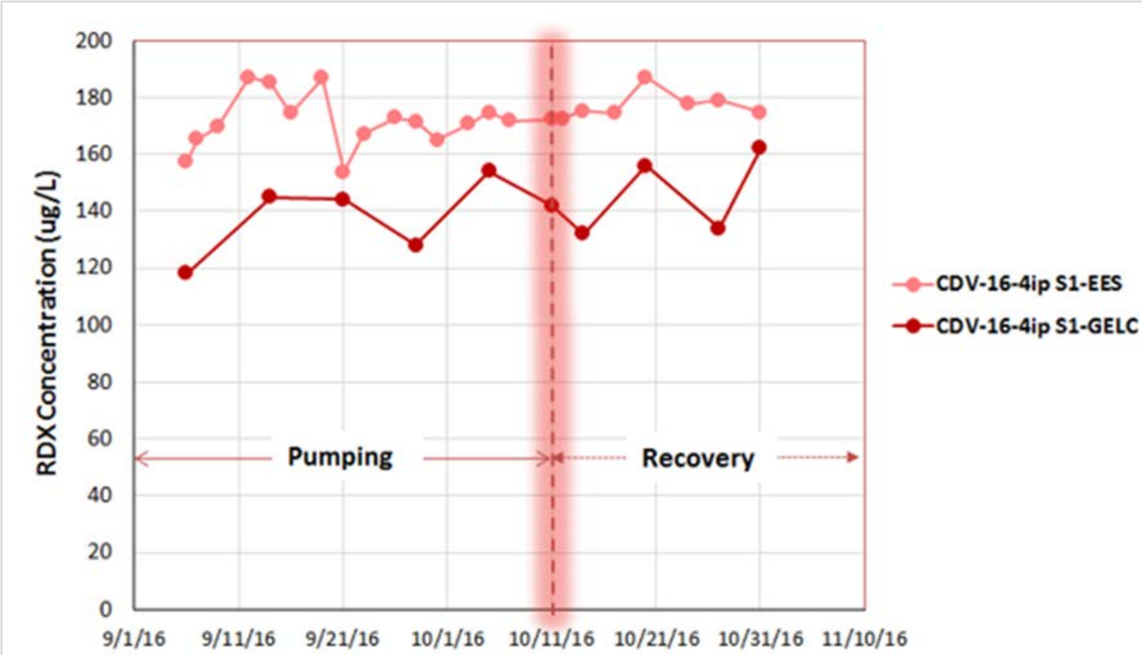

Figure 4.4-3 **RDX concentrations measured during pumping and recovery at CdV-16-4ip**

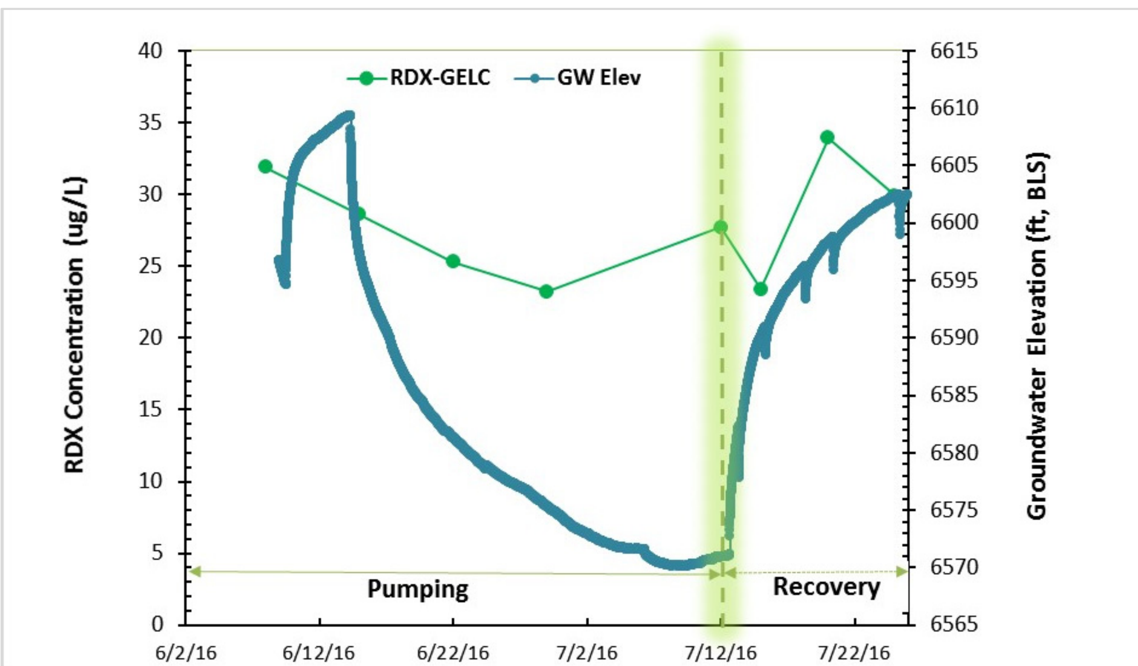

Figure 4.4-4 **RDX concentrations and groundwater levels during pumping and recovery at CdV-9-1(i)**

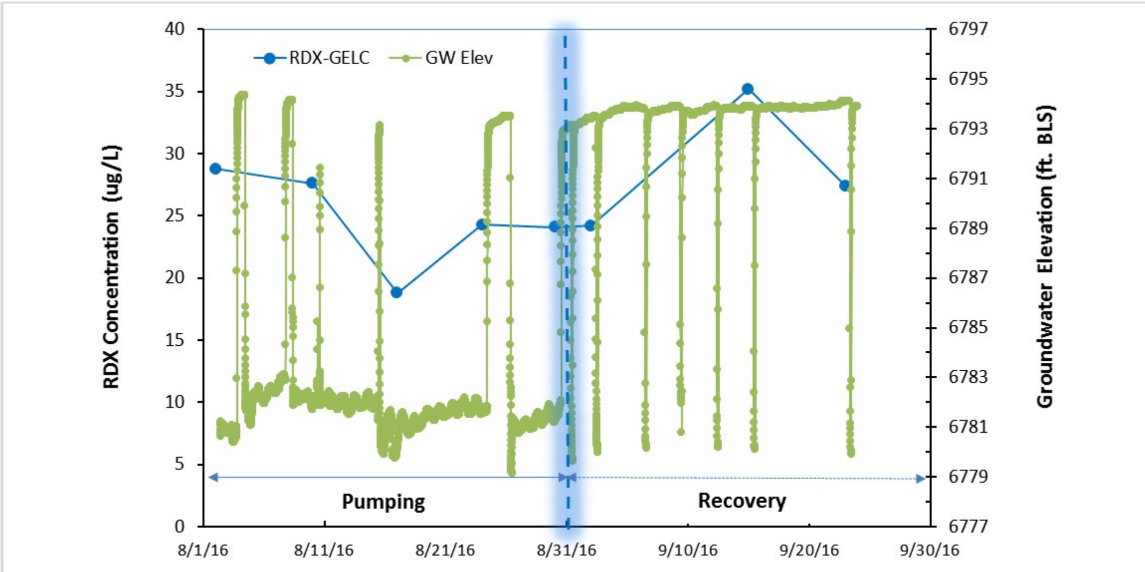

Figure 4.4-5 RDX concentrations and groundwater levels during pumping and recovery at CdV-16-1(i)

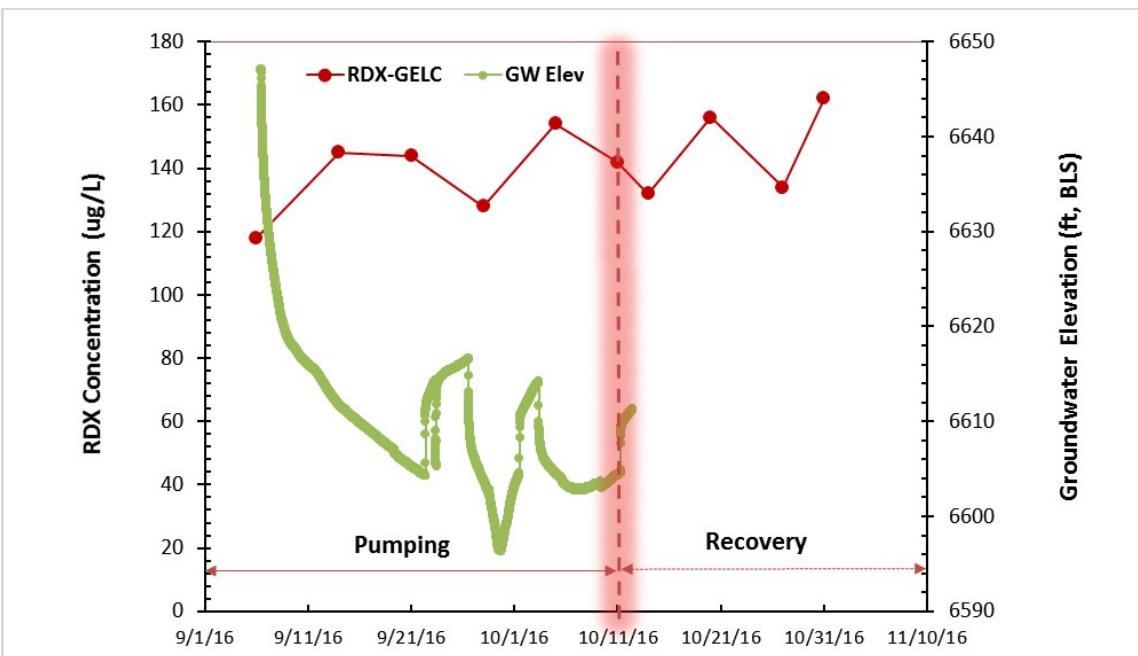

Figure 4.4-6 RDX concentrations and groundwater levels during pumping and recovery at CdV-16-4ip

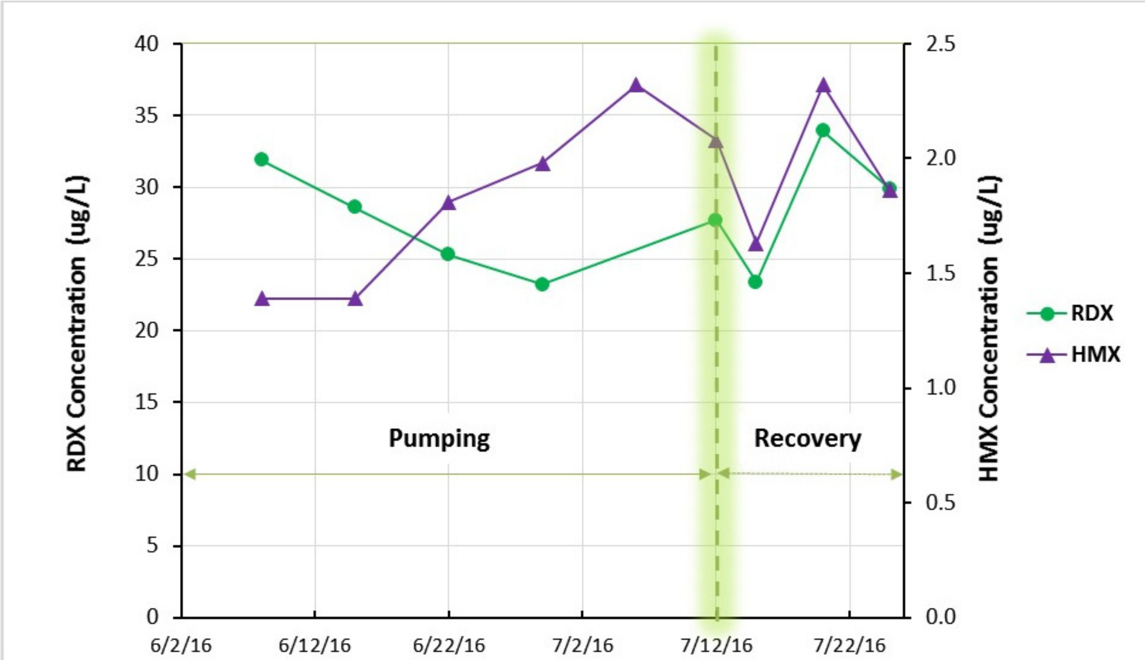

Figure 4.4-7 RDX and HMX concentrations during pumping and recovery at CdV-9-1(i)

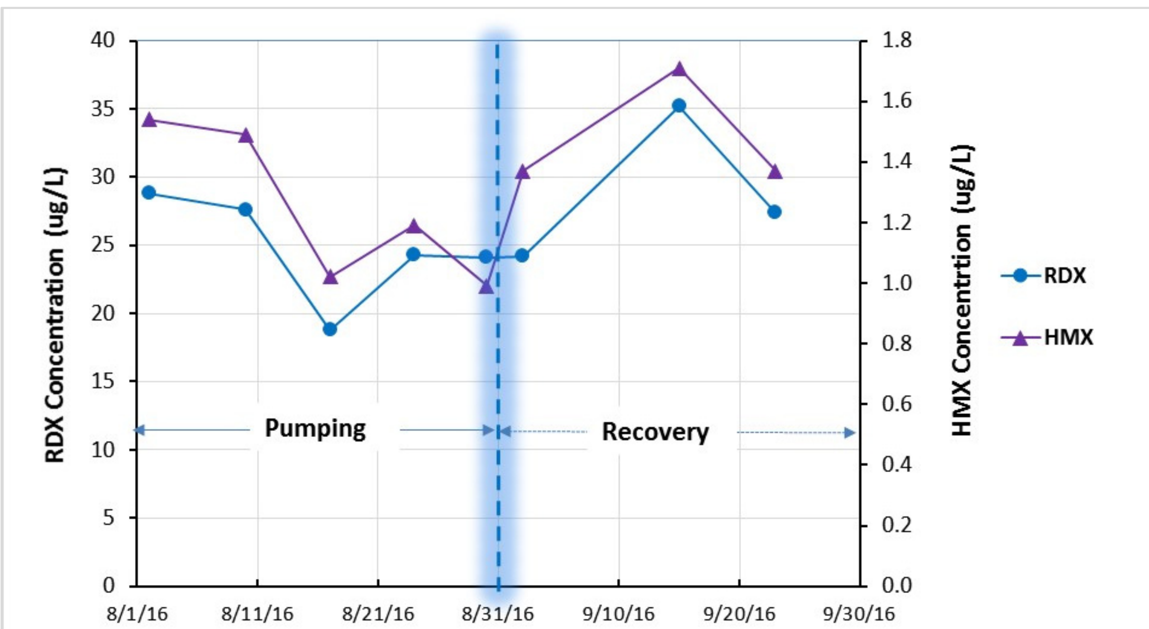

Figure 4.4-8 RDX and HMX concentrations during pumping and recovery at CdV-16-1(i)

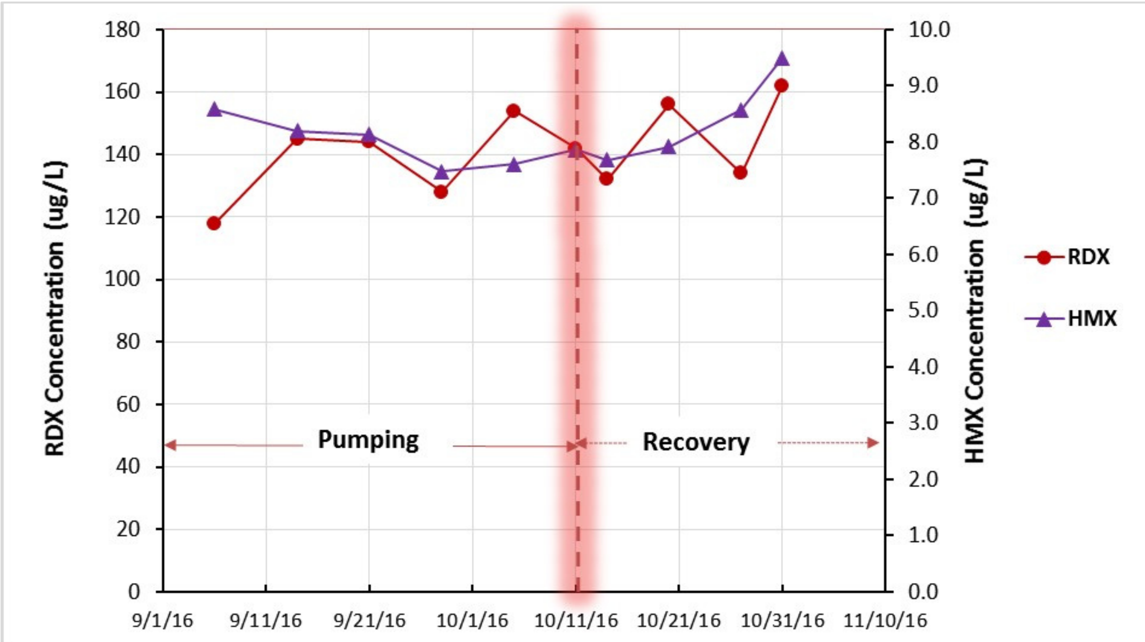

Figure 4.4-9 RDX and HMX concentrations during pumping and recovery at CdV-16-4ip

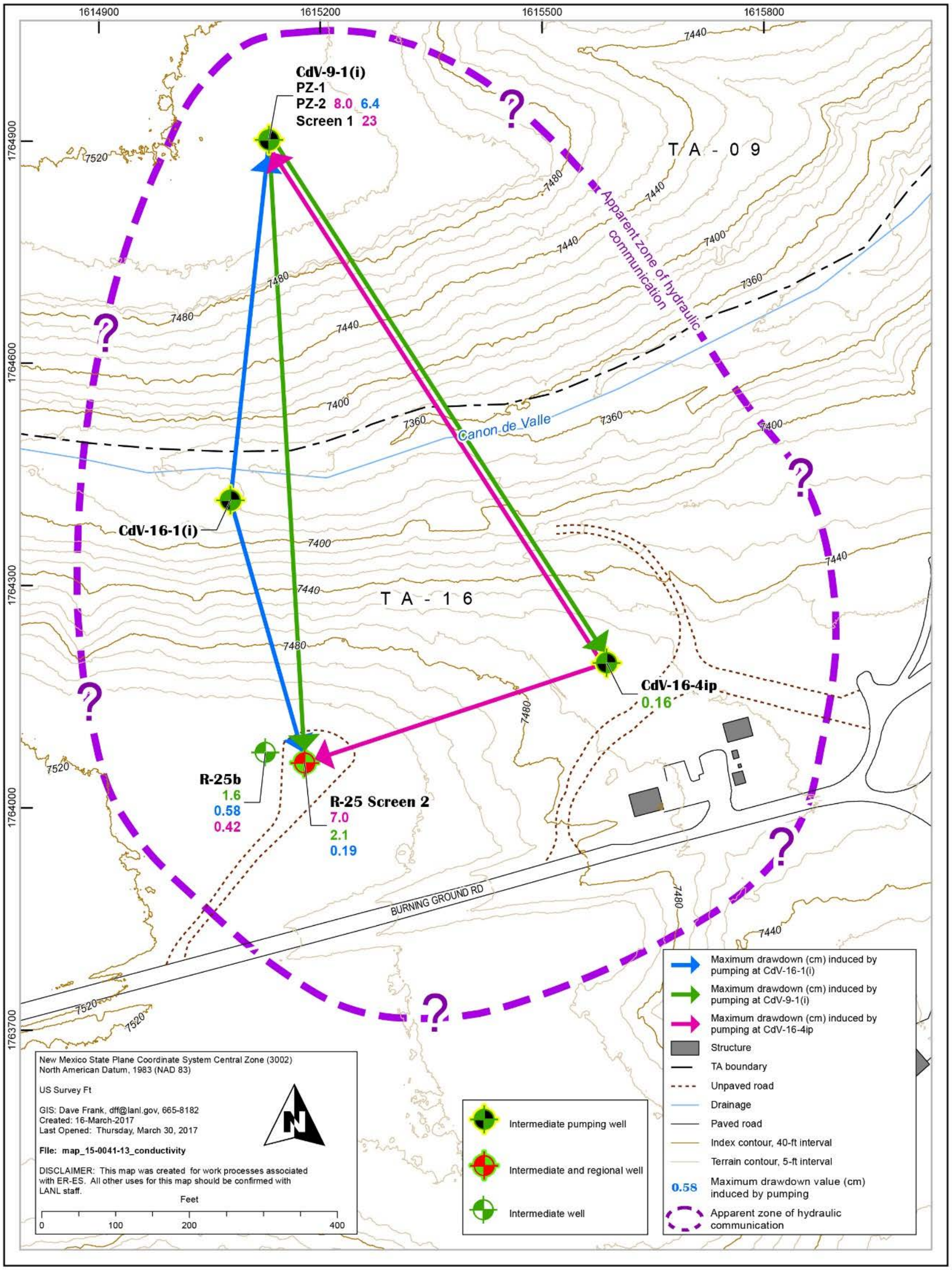

Figure 5.0-1 Primary area of hydraulic communication observed during pumping test and maximum predicted drawdowns observed in each well from pumping at nearby wells

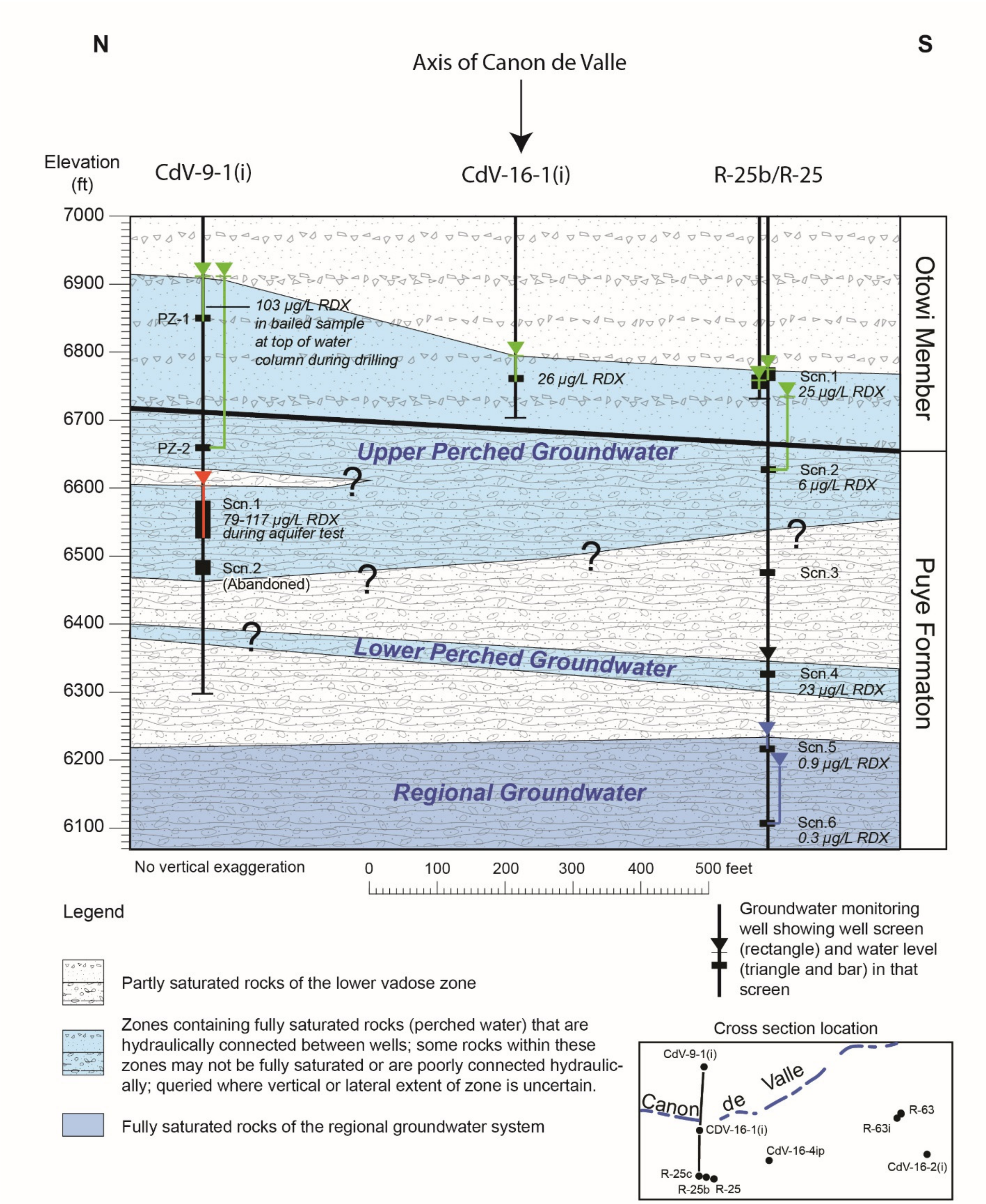

Figure 5.0-2a Revised geologic cross-section reflecting results from intermediate-system pumping test

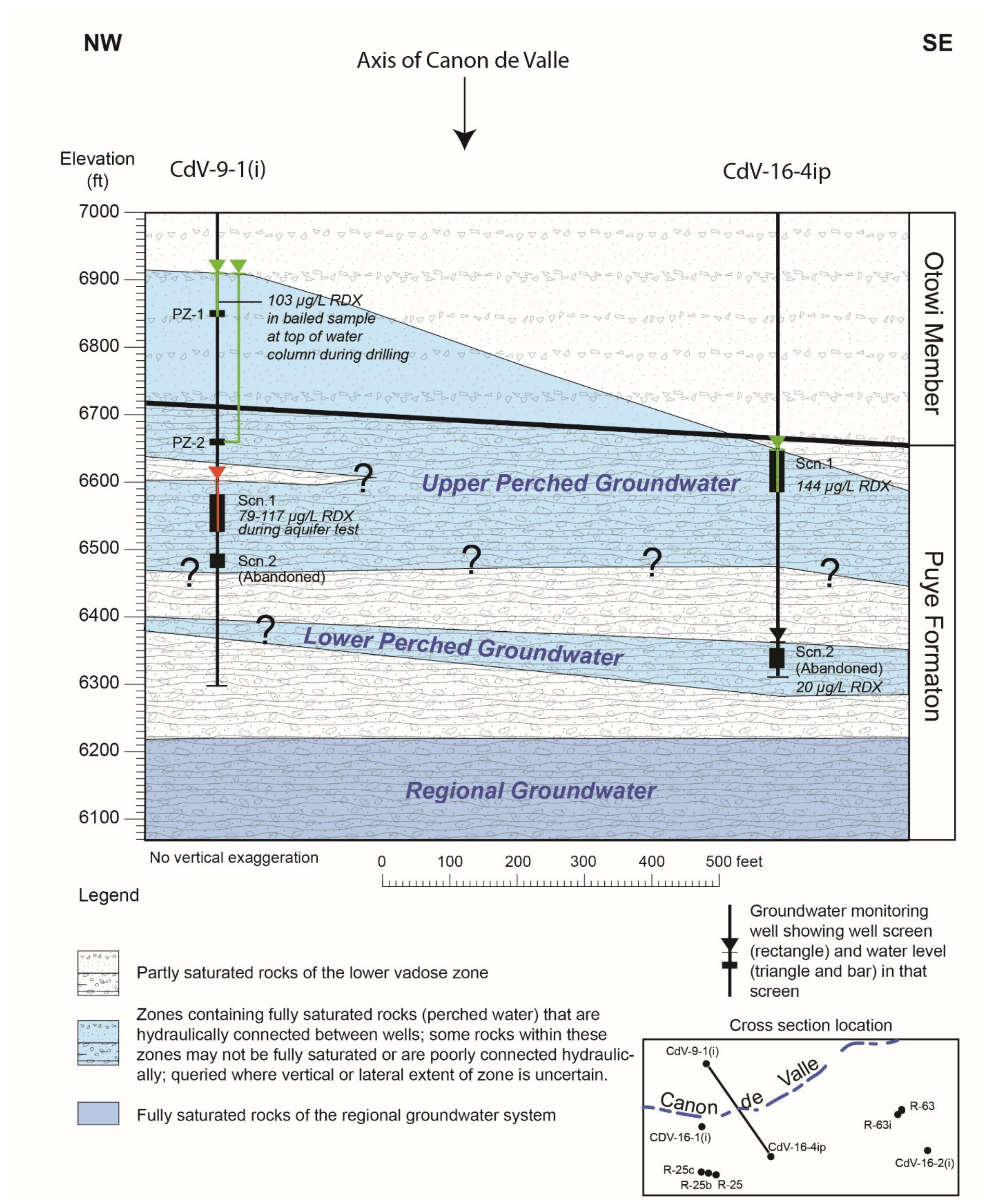

Figure 5.0-2b Revised geologic cross-section reflecting results from intermediate-system pumping test

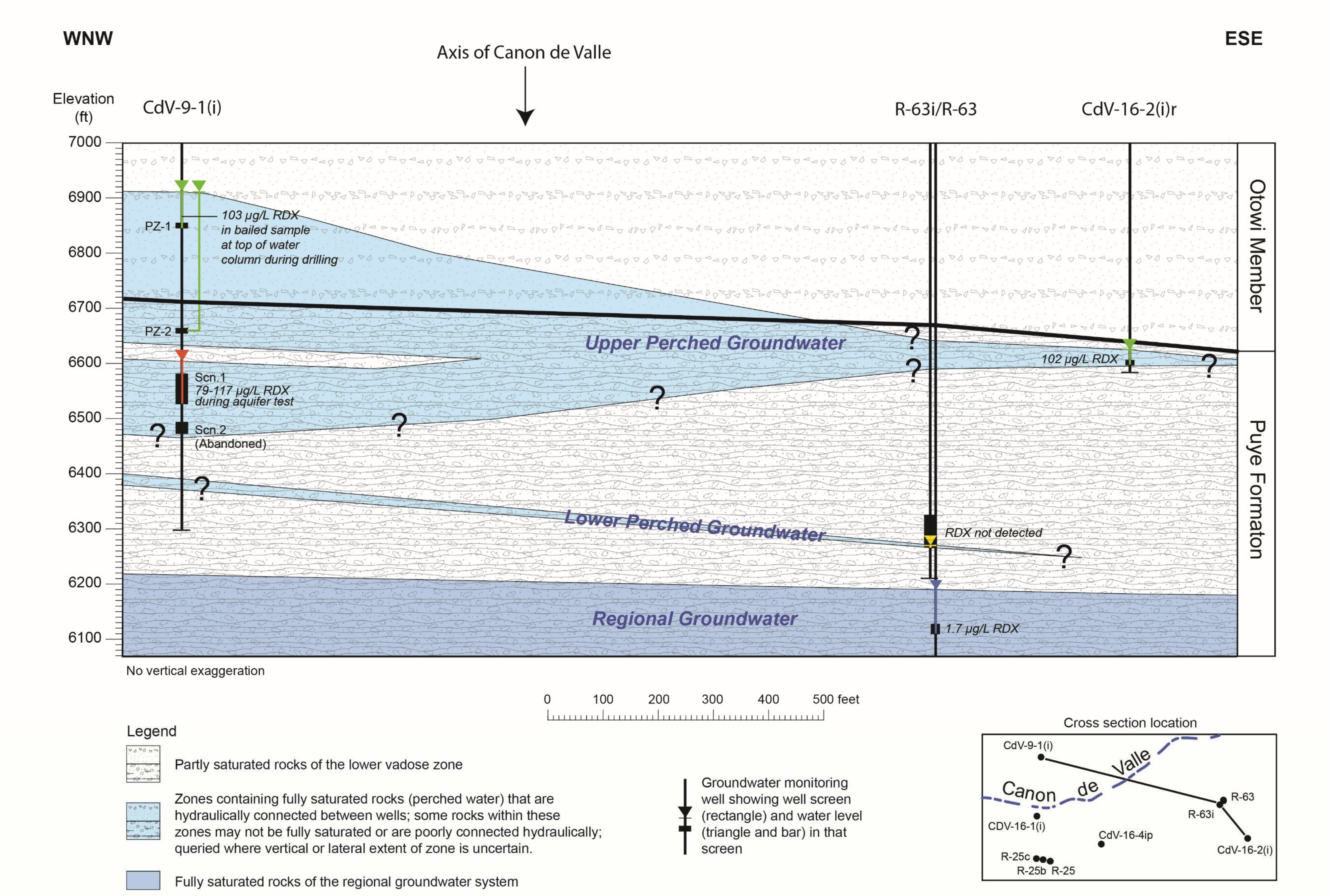

Figure 5.0-2c Revised geologic cross-section reflecting results from intermediate-system pumping test

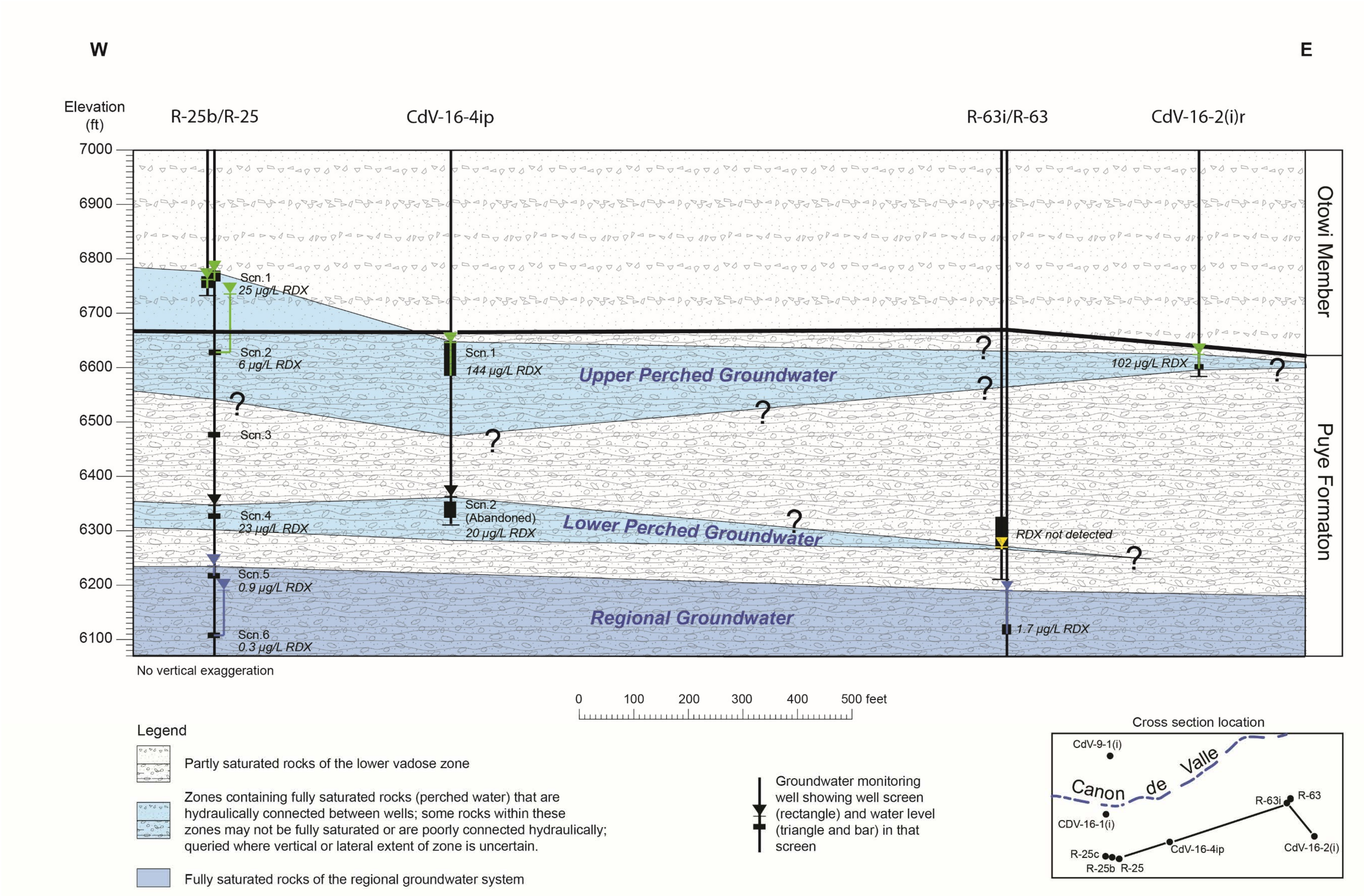

Figure 5.0-2d Revised geologic cross-section reflecting results from intermediate-system pumping test

Table 1.1-1
Lateral Distances Between Pumping and Observation Wells in Feet

Well Screen	Geologic Unit	Lateral Distance from Pumping Well CdV-9-1(i) (ft)	Lateral Distance from Pumping Well CdV-16-1(i) (ft)	Lateral Distance from Pumping Well CdV-16-4ip (ft)
CdV-16-4ip S1	Puye Formation	840.51	554.18	0.0
CdV-16-1(i)	Otowi Member, Bandelier Tuff	489.2	0.0	840.51
CdV-9-1(i) S1	Puye Formation	0.0	489.19	840.51
CdV-9-1(i) PZ-1	Otowi Member, Bandelier Tuff	0.0	489.19	840.51
CdV-9-1(i) PZ-2	Puye Formation	0.0	489.19	840.51
R-25b	Otowi Member, Bandelier Tuff	826.88	343.78	477.08
R-25 S1	Otowi Member, Bandelier Tuff	842.4	368.59	430.45
R-25 S2	Puye Formation	842.42	368.59	430.45
R-25 S4	Puye Formation	842.42	368.59	430.45
CdV-16-2(i)r	Puye Formation	1686.64	1607.01	331.1
R-47i	Puye Formation	4237.45	4202.54	3674.23
R-63i	Puye Formation	1444.45	1444.99	983.78
R-63	Puye Formation	1467.16	1477.16	1020.77

Table 2.2-1
Well Completion Details for the Pumping and Observation Wells Monitored during Pumping Test Activities

Well/Screen	Easting (ft)	Northing (ft)	Geologic Unit	Ground Surface Elevation (ft)	Reference Elevation (Brass cap) (ft)	Screen Length (ft)	Screen Depth Interval (ft)	Primary Sand-Pack Depth Interval (ft)	Screen Top Elevation (ft)	Screen Bottom Elevation (ft)	Water Table Elevation (ft) 02/23/2017*	Water Table Distance to Top of Screen (ft)
CdV-16-4ip S1	1615587.07	1764195.74	Puye Formation	7463.8	7463.91	63.6	815.6–879.2	809.8–884.9	6648.3	6584.7	6646.87	-1.4
CdV-16-1(i)	1615078.20	1764415.20	Otowi Member, Bandelier Tuff	7382.2	7382.17	10.0	624.0–634.0	613–644	6758.2	6748.2	6794.2	36.0
CdV-9-1(i) S1	1615130.71	1764901.56	Puye Formation	7517.1	7517.44	55.0	937.4–992.4	932.2–996.9	6580.0	6525.0	6603.79	23.8
CdV-9-1(i) PZ-1	1615130.71	1764901.56	Otowi Member, Bandelier Tuff	7517.1	7517.44	9.5	662.9–672.4	658.2–676.9	6854.5	6845.0	6910.47	55.9
CdV-9-1(i) PZ-2	1615130.71	1764901.56	Puye Formation	7517.1	7517.44	9.5	852.9–862.4	848.1–867.6	6664.5	6655.0	6910.56	246.0
R-25b	1615125.60	1764074.70	Otowi Member, Bandelier Tuff	7518.0	7517.00	20.8	750–770.8	745–776	6767.0	6746.2	6758.37	-8.6
R-25 S1	1615178.42	1764060.50	Otowi Member, Bandelier Tuff	7516.1	7516.10	20.8	737.6–758.4	732.0–762.0	6778.5	6757.7	6772.32	-6.2
R-25 S2	1615178.42	1764060.50	Puye Formation	7516.1	7516.10	10.8	882.6–893.4	878.0–897.0	6633.5	6622.7	6735.67	102.2
R-25 S4	1615178.42	1764060.50	Puye Formation	7516.1	7516.10	10.0	1184.6–1194.6	1180.0–1191.0	6331.5	6321.5	6345.57	14.1
CdV-16-2(i)r	1616673.24	1764219.40	Puye Formation	7456.4	7456.67	9.7	850.0–859.7	841–865.5	6606.7	6597.0	6623.44	16.8
R-47i	1619250.01	1763907.91	Puye Formation	7357.8	7358.41	20.6	840–860.6	835–866	6518.4	6497.8	6526.98	8.6
R-63i	1616520.27	1764507.14	Puye Formation	7455.3	7455.40	66.5	1122.5–1189.0	1117.6–1194.1	6332.9	6266.4	6270.49	-62.4
R-63	1616550.69	1764532.51	Puye Formation	7454.4	7454.57	20.3	1325.0–1345.3	1318.5–1352.5	6129.6	6109.3	6190.15	60.6

Note: Positive values (black text) indicate above top of screen; negative values (red text) indicate below top of screen.
* Water table elevation data from R-25 screens were measured on September 12, 2016; all other water table elevation data were measured on February 23, 2017.

Table 2.3-1
Sampling Analytes, Sample Ports, Analytical Laboratory, and Sampling Frequency for Samples Collected during Pumping Test Activities and Rebound Sampling

Analytical Suite	Sample Type	Sampling Valve Location/Source	Laboratory	Sample Collection Frequency
Metals	Characterization	Pumping Well Port: (VS-9-1i-1, VS-4ip-1, VS-16-1i-1)	GGRL	Pumping: 3 × week Rebound: 2 × week
Anions	Characterization	Pumping Well Port: (VS-9-1i-1, VS-4ip-1, VS-16-1i-1)	GGRL	Pumping: 3 × week Rebound: 2 × week
Alkalinity/pH	Characterization	Pumping Well Port: (VS-9-1i-1, VS-4ip-1, VS-16-1i-1)	GGRL	Pumping: 3 × week Rebound: 2 × week
RDX	Characterization	Pumping Well Port: (VS-9-1i-1, VS-4ip-1, VS-16-1i-1)	GGRL	Pumping: 3 × week Rebound: 2 × week
HEXMOD	Characterization	Pumping Well Port: (VS-9-1i-1, VS-4ip-1, VS-16-1i-1)	GEL Laboratories	Pumping: Weekly Rebound: Weekly
VOCs	Characterization	Pumping Well Port: (VS-9-1i-1, VS-4ip-1, VS-16-1i-1)	GEL Laboratories	Pumping: Weekly Rebound: Not required
TA-16 Tracers	Characterization	Pumping Well Port: (VS-9-1i-1, VS-4ip-1, VS-16-1i-1)	GGRL	Pumping: 3 × week Rebound: Weekly
RDX (Operational Samples)	Operational	After Primary GAC: (VS-HE-3A, VS-HE-3B, VS-HE-3C) Effluent Port: (VS-HE-4)	GGRL	Pumping: 3 × week Rebound: 2 × week
HEXMOD	Operational	After Primary GAC: (VS-HE-3A, VS-HE-3B, VS-HE-3C) Effluent Port: (VS-HE-4)	GEL Laboratories	Pumping: Weekly

Table 2.3-2
Samples Taken during Pumping and Recovery at CdV-9-1(i)

Sample ID	Date Collected	Time Collected	Pumping Rate (gpm)	RDX	NMED HEXMOD	Metals	Anions	Alkalinity /pH	Tracer+BR	VOCs	Test Phase
VS-HE-3A-16-121452	6/8/2016	9:25	1.97	X							Pumping
VS-HE-3B-16-121461	6/8/2016	9:25	1.97	X							Pumping
VS-HE-4-16-121479	6/8/2016	9:25	1.97	X	X						Pumping
VS-9-1i-16-121404	6/8/2016	9:50	1.97			X	X				Pumping
VS-9-1i-16-121401	6/8/2016	9:45	1.97	X	X			X	X		Pumping
VS-HE-3A-16-121449	6/15/2016	9:25	1.94	X							Pumping
VS-HE-3B-16-121458	6/15/2016	9:25	1.94	X							Pumping
VS-HE-4-16-121476	6/15/2016	9:25	1.94	X	X						Pumping
VS-9-1i-16-121395	6/15/2016	9:26	1.94			X	X				Pumping
VS-9-1i-16-121408	6/15/2016	9:26	1.94	X	X			X	X	X	Pumping
VS-HE-3A-16-121450	6/17/2016	9:18	1.95	X							Pumping
VS-HE-3B-16-121459	6/17/2016	9:18	1.95	X							Pumping
VS-HE-4-16-121477	6/17/2016	9:18	1.95	X							Pumping
VS-9-1i-16-121409	6/17/2016	9:18	1.95			X	X				Pumping
VS-9-1i-16-121394	6/17/2016	9:18	1.95	X					X		Pumping
VS-HE-3A-16-121450	6/20/2016	9:20	1.98	X							Pumping
VS-HE-3B-16-121459	6/20/2016	9:20	1.98	X							Pumping
VS-HE-4-16-121477	6/20/2016	9:20	1.98	X							Pumping
VS-9-1i-16-121409	6/20/2016	9:20	1.98			X	X				Pumping
VS-9-1i-16-121394	6/20/2016	9:20	1.98	X					X		Pumping
VS-HE-3A-16-123116	6/22/2016	9:29	2.015	X							Pumping
VS-HE-3B-16-123127	6/22/2016	9:20	2.015	X							Pumping
VS-HE-4-16-123138	6/22/2016	9:20	2.015	X	X						Pumping
VS-9-1i-16-123088	6/22/2016	9:20	2.015			X	X				Pumping
VS-9-1i-16-123102	6/22/2016	9:30	2.015	X	X			X	X		Pumping
VS-HE-3A-16-121451	6/24/2016	10:15	2.05	X							Pumping
VS-HE-3B-16-121460	6/24/2016	10:15	2.05	X							Pumping
VS-HE-4-16-121478	6/24/2016	10:15	2.05	X							Pumping
VS-9-1i-16-121410	6/24/2016	10:15	2.05			X	X				Pumping
VS-9-1i-16-121396	6/24/2016	10:15	2.05	X					X		Pumping
VS-HE-3A-16-121448	6/27/2016	9:30	1.98	X							Pumping
VS-HE-3B-16-121457	6/27/2016	9:30	1.98	X							Pumping
VS-HE-4-16-121475	6/27/2016	9:30	1.98	X							Pumping
VS-9-1i-16-121405	6/27/2016	9:30	1.98			X	X				Pumping

Table 2.3-2 (continued)

Sample ID	Date Collected	Time Collected	Pumping Rate (gpm)	RDX	NMED HEXMOD	Metals	Anions	Alkalinity /pH	Tracer+BR	VOCs	Test Phase
VS-9-1i-16-121400	6/27/2016	9:30	1.98	X					X		Pumping
VS-HE-3A-16-123117	6/29/2016	9:13	1.86	X							Pumping
VS-HE-3B-16-123128	6/29/2016	9:13	1.86	X							Pumping
VS-HE-4-16-123139	6/29/2016	9:13	1.86	X	X						Pumping
VS-9-1i-16-123089	6/29/2016	9:13	1.86			X	X				Pumping
VS-9-1i-16-123103	6/29/2016	9:13	1.86	X	X			X	X		Pumping
VS-HE-3A-16-123119	7/1/2016	9:55	1.86	X							Pumping
VS-HE-3B-16-123130	7/1/2016	9:55	1.86	X							Pumping
VS-HE-4-16-123141	7/1/2016	9:55	1.86	X							Pumping
VS-9-1i-16-123101	7/1/2016	9:55	1.86			X	X				Pumping
VS-9-1i-16-123110	7/1/2016	9:55	1.86	X					X		Pumping
VS-HE-3A-16-123120	7/5/2016	9:30	1.71	X							Pumping
VS-HE-3B-16-123131	7/5/2016	9:30	1.71	X							Pumping
VS-HE-4-16-123142	7/5/2016	9:30	1.71	X							Pumping
VS-9-1i-16-123100	7/5/2016	9:30	1.71			X	X				Pumping
VS-9-1i-16-123111	7/5/2016	9:30	1.71	X					X		Pumping
VS-HE-3A-16-123118	7/6/2016	9:15	1.87	X							Pumping
VS-HE-3B-16-123129	7/6/2016	9:15	1.87	X							Pumping
VS-HE-4-16-123140	7/6/2016	9:15	1.87	X	X						Pumping
VS-9-1i-16-123092	7/6/2016	9:15	1.87			X	X				Pumping
VS-9-1i-16-123106	7/6/2016	9:15	1.87	X	X			X	X	X	Pumping
VS-HE-3A-16-123124	7/8/2016	9:07	1.75	X							Pumping
VS-HE-3B-16-123135	7/8/2016	9:02	1.75	X							Pumping
VS-HE-4-16-123146	7/8/2016	9:02	1.75	X							Pumping
VS-9-1i-16-123099	7/8/2016	9:02	1.75			X	X				Pumping
VS-9-1i-16-123112	7/8/2016	9:02	1.75	X					X		Pumping
VS-HE-3A-16-123121	7/11/2016	10:10	1.68	X							Pumping
VS-HE-3B-16-123132	7/11/2016	10:10	1.68	X							Pumping
VS-HE-4-16-123143	7/11/2016	10:10	1.68	X							Pumping
VS-9-1i-16-123097	7/11/2016	10:10	1.68			X	X				Pumping
VS-9-1i-16-123113	7/11/2016	10:10	1.68	X					X		Pumping
VS-HE-3A-16-123123	7/12/2016	16:13	1.64	X							Pumping
VS-HE-3B-16-123134	7/12/2016	16:13	1.64	X							Pumping
VS-HE-4-16-123145	7/12/2016	16:13	1.64	X	X						Pumping
VS-9-1i-16-123091	7/12/2016	16:13	1.64			X	X				Pumping

Table 2.3-2 (continued)

Sample ID	Date Collected	Time Collected	Pumping Rate (gpm)	RDX	NMED HEXMOD	Metals	Anions	Alkalinity /pH	Tracer+BR	VOCs	Test Phase
VS-9-1i-16-123105	7/12/2016	16:13	1.64	X	X			X	X	X	Pumping
VS-9-1i-16-123098	7/13/2016	10:50	2.26			X	X				Rebound
VS-9-1i-16-123114	7/13/2016	10:50	2.26	X				X	X		Rebound
VS-9-1i-16-123093	7/15/2016	10:33	2.26			X	X				Rebound
VS-9-1i-16-123107	7/15/2016	10:33	2.26	X	X			X	X		Rebound
VS-9-1i-16-123094	7/18/2016	10:32	2.37			X	X				Rebound
VS-9-1i-16-123108	7/18/2016	10:32	2.37	X	X			X	X		Rebound
VS-9-1i-16-123090	7/20/2016	12:10	2.4			X	X				Rebound
VS-9-1i-16-123104	7/20/2016	12:10	2.4	X	X			X	X		Rebound
VS-9-1i-16-123096	7/25/2016	10:25	2.05			X	X				Rebound
VS-9-1i-16-123109	7/25/2016	10:25	2.05	X	X			X	X		Rebound

Note: Blank cell indicates samples for this analyte suite were not collected because they were not required.

Table 2.3-3
Samples Taken during Pumping and Recovery at CdV-16-1(i)

Sample ID	Date Collected	Time Collected	Pumping Rate (gpm)	RDX	NMED HEXMOD	Metals	Anions	Alkalinity /pH	Tracer+BR	VOCs	Test Phase
VS-HE2-02-16-124392	8/2/2016	11:40	0.491	X							Pumping
VS-HE2-03-16-124411				X							Pumping
VS-16-1i-16-121446						X	X				Pumping
VS-16-1i-16-0121431				X	X			X	X	X	Pumping
VS-HE2-02-16-124390	8/3/2016	10:15	0.481	X							Pumping
VS-HE2-03-16-124405				X	X						Pumping
VS-16-1i-16-121447						X	X				Pumping
VS-16-1i-16-121430				X				X	X		Pumping
VS-HE2-02-16-124389	8/5/2016	10:00	0.441	X							Pumping
VS-HE2-03-16-124409				X							Pumping
VS-16-1i-16-121445						X	X				Pumping
VS-16-1i-16-121433				X				X	X		Pumping
VS-HE2-02-16-124391	8/8/2016	11:04	0.471	X							Pumping
VS-HE2-03-16-124410				X							Pumping
VS-16-1i-16-121442						X	X				Pumping
VS-16-1i-16-121435				X				X	X		Pumping
VS-HE2-02-16-124403	8/10/2016	10:15	0.417	X							Pumping
VS-HE2-03-16-124404				X	X						Pumping
VS-16-1i-16-121443						X	X				Pumping
VS-16-1i-16-121434				X	X			X	X	X	Pumping
VS-HE2-02-16-124399	8/12/2016	9:58	0.412	X							Pumping
VS-HE2-03-16-124418				X							Pumping
VS-16-1i-16-121441						X	X				Pumping
VS-16-1i-16-121436				X				X	X		Pumping
VS-HE2-02-16-124398	8/15/2016	10:15	0.427	X							Pumping
VS-HE2-03-16-124417				X							Pumping
VS-16-1i-16-121444						X	X				Pumping
VS-16-1i-16-121432				X				X	X		Pumping
VS-HE2-02-16-124395	8/17/2016	9:10	0.397	X							Pumping
VS-HE2-03-16-124798				X	X						Pumping
VS-16-1i-16-124791						X	X				Pumping
VS-16-1i-16-124788				X	X			X	X	X	Pumping
VS-HE2-02-16-124397	8/18/2016	10:05	0.407	X							Pumping

Table 2.3-3 (continued)

Sample ID	Date Collected	Time Collected	Pumping Rate (gpm)	RDX	NMED HEXMOD	Metals	Anions	Alkalinity/pH	Tracer+BR	VOCs	Test Phase
VS-HE2-03-16-124416	8/18/2016	10:05	0.407	X							Pumping
VS-16-1i-16-121439						X	X				Pumping
VS-16-1i-16-121438				X				X	X		Pumping
VS-HE2-02-16-124396	8/22/2016	10:10	0.402	X							Pumping
VS-HE2-03-16-124415				X							Pumping
VS-16-1i-16-124790						X	X				Pumping
VS-16-1i-16-124789				X				X	X		Pumping
VS-HE2-02-16-124393	8/24/2016	11:03	0.412	X							Pumping
VS-HE2-03-16-124800				X	X						Pumping
VS-16-1i-16-124794						X	X				Pumping
VS-16-1i-16-124785				X	X			X	X	X	Pumping
VS-HE2-02-16-124801	8/26/2016	12:00	0.516	X							Pumping
VS-HE2-03-16-124408				X							Pumping
VS-16-1i-16-121440						X	X				Pumping
VS-16-1i-16-121437				X				X	X		Pumping
VS-HE2-02-16-124802	8/29/2016	9:50	0.422	X							Pumping
VS-HE2-03-16-124413				X							Pumping
VS-16-1i-16-124793						X	X				Pumping
VS-16-1i-16-124786				X				X	X		Pumping
VS-HE2-02-16-124394	8/30/2016	13:34	0.382	X							Pumping
VS-HE2-03-16-124799				X	X						Pumping
VS-16-1i-16-124792						X	X				Pumping
VS-16-1i-16-124787				X	X			X	X	X	Pumping
VS-HE2-02-16-124401	8/31/2016	12:28	0.475	X							Rebound
VS-HE2-03-16-124407				X							Rebound
VS-16-1i-16-124796						X	X				Rebound
VS-16-1i-16-124783				X				X	X		Rebound
VS-HE2-02-16-124803	9/2/2016	13:55	0.466	X							Rebound
VS-HE2-03-16-124406				X	X						Rebound
VS-16-1i-16-124795						X	X				Rebound
VS-16-1i-16-124784				X	X			X	X		Rebound
VS-HE2-02-16-124400	9/6/2016	14:45	0.575	X							Rebound
VS-HE2-03-16-124414				X							Rebound
VS-16-1i-16-124797						X	X				Rebound
VS-16-1i-16-124782				X				X	X		Rebound

Table 2.3-3 (continued)

Sample ID	Date Collected	Time Collected	Pumping Rate (gpm)	RDX	NMED HEXMOD	Metals	Anions	Alkalinity/pH	Tracer+BR	VOCs	Test Phase
VS-HE2-02-16-126026	9/9/2016	12:56	0.58	X							Rebound
VS-HE2-03-16-126031				X	X						Rebound
VS-16-1i-16-126020						X	X				Rebound
VS-16-1i-16-126023				X	X			X	X		Rebound
VS-HE2-02-16-126028	9/12/2016	12:50	0.595	X							Rebound
VS-HE2-03-16-126029				X	X						Rebound
VS-16-1i-16-126022						X	X				Rebound
VS-16-1i-16-126025				X				X	X		Rebound
VS-HE2-02-16-126187	9/15/2016	13:45	0.565	X							Rebound
VS-HE2-03-16-126188				X	X						Rebound
VS-16-1i-16-126190						X	X				Rebound
VS-16-1i-16-126189				X	X			X	X		Rebound
VS-HE2-02-16-126589	9/23/2016	12:26	0.64	X							Rebound
VS-HE2-03-16-126590				X	X						Rebound
VS-16-1i-16-126587						X	X				Rebound
VS-16-1i-16-126588				X	X			X	X		Rebound

Note: Blank cell indicates samples for this analyte suite were not collected because they were not required.

Table 2.3-4
Samples Taken during Pumping and Recovery at CdV-16-4ip

Sample ID	Date Collected	Time Collected	Pumping Rate (gpm)	RDX	NMED HEXMOD	Metals	Anions	Alkalinity/pH	Tracer+BR	VOCs	Pumping or Rebound?
VS-HE-3A-16-125269	9/6/2016	13:15	6.05	X							Pumping
VS-HE-3B-16-125278				X							Pumping
VS-HE-4-16-125287				X	X						Pumping
VS-4ip-16-121421						X	X				Pumping
VS-4ip-16-121416				X	X			X	X	X	Pumping
VS-HE-3A-16-125270	9/7/2016	14:05	5.909	X							Pumping
VS-HE-3B-16-125279				X							Pumping
VS-HE-4-16-125288				X							Pumping
VS-4ip-16-121423						X	X				Pumping
VS-4ip-16-121415				X				X	X		Pumping
VS-HE-3A-16-125274	9/9/2016	10:25	5.85	X							Pumping
VS-HE-3B-16-125283				X							Pumping
VS-HE-4-16-125292				X							Pumping
VS-4ip-16-121426						X	X				Pumping
VS-4ip-16-121412				X				X	X		Pumping
VS-HE-3A-16-125271	9/12/2016	9:35	5.75	X							Pumping
VS-HE-3B-16-125280				X							Pumping
VS-HE-4-16-125289				X							Pumping
VS-4ip-16-121424						X	X				Pumping
VS-4ip-16-121414				X				X	X		Pumping
VS-HE-3A-16-125276	9/14/2016	14:20	5.7	X							Pumping
VS-HE-3B-16-125285				X							Pumping
VS-HE-4-16-125294				X	X						Pumping
VS-4ip-16-121428						X	X				Pumping
VS-4ip-16-121419				X	X			X	X	X	Pumping
VS-HE-3A-16-125277	9/16/2016	9:59	5.75	X							Pumping
VS-HE-3B-16-125286				X							Pumping
VS-HE-4-16-125295				X							Pumping
VS-4ip-16-121429						X	X				Pumping
VS-4ip-16-121420				X				X	X		Pumping
VS-HE-3A-16-125275	9/19/2016	9:55	5.7	X							Pumping
VS-HE-3B-16-125284				X							Pumping
VS-HE-4-16-125293				X							Pumping

Table 2.3-4 (continued)

Sample ID	Date Collected	Time Collected	Pumping Rate (gpm)	RDX	NMED HEXMOD	Metals	Anions	Alkalinity/pH	Tracer+BR	VOCs	Pumping or Rebound?
VS-4ip-16-121427	9/19/2016	9:55	5.7			X	X				Pumping
VS-4ip-16-121418				X				X	X		Pumping
VS-HE-3A-16-126252	9/21/2016	12:55	5.89	X							Pumping
VS-HE-3B-16-126262				X							Pumping
VS-HE-4-16-126272				X	X						Pumping
VS-4ip-16-126232						X	X				Pumping
VS-4ip-16-126247				X	X			X	X	X	Pumping
VS-HE-3A-16-126250	9/23/2016	11:31	7.7	X							Pumping
VS-HE-3B-16-126260				X							Pumping
VS-HE-4-16-126270				X							Pumping
VS-4ip-16-126230						X	X				Pumping
VS-4ip-16-126245				X				X	X		Pumping
VS-HE-3A-16-126251	9/26/2016	16:03	7.8	X							Pumping
VS-HE-3B-16-126261				X							Pumping
VS-HE-4-16-126271				X							Pumping
VS-4ip-16-126231						X	X				Pumping
VS-4ip-16-126246				X				X	X		Pumping
VS-HE-3A-16-125272	9/28/2016	9:13	7.6	X							Pumping
VS-HE-3B-16-125281				X							Pumping
VS-HE-4-16-125290				X	X						Pumping
VS-4ip-16-121425						X	X				Pumping
VS-4ip-16-121413				X	X			X	X	X	Pumping
VS-HE-3A-16-125273	9/30/2016	9:52	6.658	X							Pumping
VS-HE-3B-16-125282				X							Pumping
VS-HE-4-16-125291				X							Pumping
VS-4ip-16-121422						X	X				Pumping
VS-4ip-16-121417				X				X	X		Pumping
VS-HE-3A-16-126253	10/3/2016	14:50	6.01	X							Pumping
VS-HE-3B-16-126263				X							Pumping
VS-HE-4-16-126273				X							Pumping
VS-4ip-16-126248				X				X	X		Pumping
VS-4ip-16-126233						X	X				Pumping
VS-HE-3A-16-126257	10/5/2016	10:07	5.802	X							Pumping
VS-HE-3B-16-126267				X							Pumping
VS-HE-4-16-126277				X	X						Pumping

Table 2.3-4 (continued)

Sample ID	Date Collected	Time Collected	Pumping Rate (gpm)	RDX	NMED HEXMOD	Metals	Anions	Alkalinity/pH	Tracer+BR	VOCs	Pumping or Rebound?
VS-4ip-16-126237	10/5/2016	10:07	5.802			X	X				Pumping
VS-4ip-16-126240				X	X			X	X	X	Pumping
VS-HE-3A-16-126256	10/7/2016	9:40	5.45	X							Pumping
VS-HE-3B-16-126266				X							Pumping
VS-HE-4-16-126276				X							Pumping
VS-4ip-16-126236						X	X				Pumping
VS-4ip-16-126239				X				X	X		Pumping
VS-HE-3A-16-126255	10/11/2016	8:15	3.88	X							Pumping
VS-HE-3B-16-126265				X							Pumping
VS-HE-4-16-126275				X	X						Pumping
VS-4ip-16-126235						X	X				Pumping
VS-4ip-16-126242				X	X			X	X	X	Pumping
VS-HE-3A-16-126254	10/12/2016	12:30	7.4	X							Rebound
VS-HE-3B-16-126264				X							Rebound
VS-HE-4-16-126274				X							Rebound
VS-4ip-16-126234						X	X				Rebound
VS-4ip-16-126243				X				X			Rebound
VS-HE-3A-16-126249	10/14/2016	11:10	7.5	X							Rebound
VS-HE-3B-16-126259				X							Rebound
VS-HE-4-16-126269				X							Rebound
VS-4ip-16-126229						X	X				Rebound
VS-4ip-16-126244				X	X			X	X		Rebound
VS-HE-3A-16-126258	10/17/2016	11:00	7.6	X							Rebound
VS-HE-3B-16-126268				X							Rebound
VS-HE-4-16-126278				X							Rebound
VS-4ip-16-126238						X	X				Rebound
VS-4ip-16-126241				X				X	X		Rebound
VS-HE-3A-17-127011	10/20/2016	14:52	7.6	X							Rebound
VS-HE-3B-17-127183				X							Rebound
VS-HE-4-17-127015				X							Rebound
VS-4ip-17-126990				X	X			X	X		Rebound
VS-4ip-17-126987						X	X				Rebound
VS-HE-3A-17-127009	10/24/2016	10:49	7.6	X							Rebound
VS-HE-3B-17-127197				X							Rebound
VS-HE-4-17-127017				X							Rebound

Table 2.3-4 (continued)

Sample ID	Date Collected	Time Collected	Pumping Rate (gpm)	RDX	NMED HEXMOD	Metals	Anions	Alkalinity/pH	Tracer+BR	VOCs	Pumping or Rebound?
VS-4ip-17-126989	10/24/2016	10:49	7.6			X	X				Rebound
VS-4ip-17-126992				X				X			Rebound
VS-HE-3A-17-127010	10/27/2016	11:07	7.7	X							Rebound
VS-HE-3B-17-127013				X							Rebound
VS-HE-4-17-127016				X							Rebound
VS-4ip-17-126988						X	X				Rebound
VS-4ip-17-126991				X	X			X	X		Rebound
VS-HE-3A-17-127322	10/31/2016	14:54	7.89	X							Rebound
VS-HE-3B-17-127325				X							Rebound
VS-HE-4-17-127328				X							Rebound
VS-4ip-17-127320						X	X				Rebound
VS-4ip-17-127321				X	X			X	X		Rebound

Note: Blank cell indicates samples for this analyte suite were not collected because they were not required.

Table 2.3-5
Field Water-Quality Parameters Measured during Pumping Test at CdV-9-1(i)

					Measurement Parameters						
Sample ID	Pumping Well	Date	Time	Pumping Rate (gpm)	pH	Temperature (Degree C)	Conductivity (µS/cm)	DO (mg/L)	ORP (mV)	Turbidity (NTU)	Test Phase
VS-HE-3A-16-121452	CdV-9-1(i)	6/8/2016	9:25	1.97	7.1	28	184	6.54	38.5	NC*	Pumping
VS-HE-3B-16-121461	CdV-9-1(i)	6/8/2016	9:25	1.97	7.1	28	184	6.54	38.5	NC	Pumping
VS-HE-4-16-121479	CdV-9-1(i)	6/8/2016	9:25	1.97	7.1	28	184	6.54	38.5	NC	Pumping
VS-9-1i-16-121404	CdV-9-1(i)	6/8/2016	9:50	1.97	7.1	28	184	6.54	38.5	NC	Pumping
VS-9-1i-16-121401	CdV-9-1(i)	6/8/2016	9:45	1.97	7.1	28	184	6.54	38.5	NC	Pumping
VS-HE-3A-16-121449	CdV-9-1(i)	6/15/2016	9:25	1.94	NC	NC	NC	NC	NC	NC	Pumping
VS-HE-3B-16-121458	CdV-9-1(i)	6/15/2016	9:25	1.94	NC	NC	NC	NC	NC	NC	Pumping
VS-HE-4-16-121476	CdV-9-1(i)	6/15/2016	9:25	1.94	NC	NC	NC	NC	NC	NC	Pumping
VS-9-1i-16-121395	CdV-9-1(i)	6/15/2016	9:26	1.94	NC	NC	NC	NC	NC	NC	Pumping
VS-9-1i-16-121408	CdV-9-1(i)	6/15/2016	9:26	1.94	NC	NC	NC	NC	NC	NC	Pumping
VS-HE-3A-16-121450	CdV-9-1(i)	6/17/2016	9:18	1.95	NC	NC	NC	NC	NC	NC	Pumping
VS-HE-3B-16-121459	CdV-9-1(i)	6/17/2016	9:18	1.95	NC	NC	NC	NC	NC	NC	Pumping
VS-HE-4-16-121477	CdV-9-1(i)	6/17/2016	9:18	1.95	NC	NC	NC	NC	NC	NC	Pumping
VS-9-1i-16-121409	CdV-9-1(i)	6/17/2016	9:18	1.95	NC	NC	NC	NC	NC	NC	Pumping
VS-9-1i-16-121394	CdV-9-1(i)	6/17/2016	9:18	1.95	NC	NC	NC	NC	NC	NC	Pumping
VS-HE-3A-16-121450	CdV-9-1(i)	6/20/2016	9:20	1.98	7.9	24.2	188	6.34	143	NC	Pumping
VS-HE-3B-16-121459	CdV-9-1(i)	6/20/2016	9:20	1.98	7.9	24.2	188	6.34	143	NC	Pumping
VS-HE-4-16-121477	CdV-9-1(i)	6/20/2016	9:20	1.98	7.9	24.2	188	6.34	143	NC	Pumping
VS-9-1i-16-121409	CdV-9-1(i)	6/20/2016	9:20	1.98	7.9	24.2	188	6.34	143	NC	Pumping
VS-9-1i-16-121394	CdV-9-1(i)	6/20/2016	9:20	1.98	7.9	24.2	188	6.34	143	NC	Pumping
VS-HE-3A-16-123116	CdV-9-1(i)	6/22/2016	9:29	2.015	7.5	24.4	240	4.05	83.6	NC	Pumping

Table 2.3-5 (continued)

Sample ID	Pumping Well	Date	Time	Pumping Rate (gpm)	Measurement Parameters: pH	Temperature (Degree C)	Conductivity (µS/cm)	DO (mg/L)	ORP (mV)	Turbidity (NTU)	Test Phase
VS-HE-3B-16-123127	CdV-9-1(i)	6/22/2016	9:20	2.015	7.5	24.4	240	4.05	83.6	NC	Pumping
VS-HE-4-16-123138	CdV-9-1(i)	6/22/2016	9:20	2.015	7.5	24.4	240	4.05	83.6	NC	Pumping
VS-9-1i-16-123088	CdV-9-1(i)	6/22/2016	9:20	2.015	7.5	24.4	240	4.05	83.6	NC	Pumping
VS-9-1i-16-123102	CdV-9-1(i)	6/22/2016	9:30	2.015	7.5	24.4	240	4.05	83.6	NC	Pumping
VS-HE-3A-16-121451	CdV-9-1(i)	6/24/2016	10:15	2.05	7.2	19.8	188	5.08	107	NC	Pumping
VS-HE-3B-16-121460	CdV-9-1(i)	6/24/2016	10:15	2.05	7.2	19.8	188	5.08	107	NC	Pumping
VS-HE-4-16-121478	CdV-9-1(i)	6/24/2016	10:15	2.05	7.2	19.8	188	5.08	107	NC	Pumping
VS-9-1i-16-121410	CdV-9-1(i)	6/24/2016	10:15	2.05	7.2	19.8	188	5.08	107	NC	Pumping
VS-9-1i-16-121396	CdV-9-1(i)	6/24/2016	10:15	2.05	7.2	19.8	188	5.08	107	NC	Pumping
VS-HE-3A-16-121448	CdV-9-1(i)	6/27/2016	9:30	1.98	7.2	22.7	222	3.32	155.8	NC	Pumping
VS-HE-3B-16-121457	CdV-9-1(i)	6/27/2016	9:30	1.98	7.2	22.7	222	3.32	155.8	NC	Pumping
VS-HE-4-16-121475	CdV-9-1(i)	6/27/2016	9:30	1.98	7.2	22.7	222	3.32	155.8	NC	Pumping
VS-9-1i-16-121405	CdV-9-1(i)	6/27/2016	9:30	1.98	7.2	22.7	222	3.32	155.8	NC	Pumping
VS-9-1i-16-121400	CdV-9-1(i)	6/27/2016	9:30	1.98	7.2	22.7	222	3.32	155.8	NC	Pumping
VS-HE-3A-16-123117	CdV-9-1(i)	6/29/2016	9:13	1.86	7.2	20.3	227	1.36	104.5	NC	Pumping
VS-HE-3B-16-123128	CdV-9-1(i)	6/29/2016	9:13	1.86	7.2	20.3	227	1.36	104.5	NC	Pumping
VS-HE-4-16-123139	CdV-9-1(i)	6/29/2016	9:13	1.86	7.2	20.3	227	1.36	104.5	NC	Pumping
VS-9-1i-16-123089	CdV-9-1(i)	6/29/2016	9:13	1.86	7.2	20.3	227	1.36	104.5	NC	Pumping
VS-9-1i-16-123103	CdV-9-1(i)	6/29/2016	9:13	1.86	7.2	20.3	227	1.36	104.5	NC	Pumping
VS-HE-3A-16-123119	CdV-9-1(i)	7/1/2016	9:55	1.86	7.3	16.9	195	5.82	123.4	NC	Pumping
VS-HE-3B-16-123130	CdV-9-1(i)	7/1/2016	9:55	1.86	7.3	16.9	195	5.82	123.4	NC	Pumping
VS-HE-4-16-123141	CdV-9-1(i)	7/1/2016	9:55	1.86	7.3	16.9	195	5.82	123.4	NC	Pumping
VS-9-1i-16-123101	CdV-9-1(i)	7/1/2016	9:55	1.86	7.3	16.9	195	5.82	123.4	NC	Pumping

Table 2.3-5 (continued)

Sample ID	Pumping Well	Date	Time	Pumping Rate (gpm)	Measurement Parameters						
					pH	Temperature (Degree C)	Conductivity (µS/cm)	DO (mg/L)	ORP (mV)	Turbidity (NTU)	Test Phase
VS-9-1i-16-123110	CdV-9-1(i)	7/1/2016	9:55	1.86	7.3	16.9	195	5.82	123.4	NC	Pumping
VS-HE-3A-16-123120	CdV-9-1(i)	7/5/2016	9:30	1.71	7.3	17	195	5.7	128.3	NC	Pumping
VS-HE-3B-16-123131	CdV-9-1(i)	7/5/2016	9:30	1.71	7.3	17	195	5.7	128.3	NC	Pumping
VS-HE-4-16-123142	CdV-9-1(i)	7/5/2016	9:30	1.71	7.3	17	195	5.7	128.3	NC	Pumping
VS-9-1i-16-123100	CdV-9-1(i)	7/5/2016	9:30	1.71	7.3	17	195	5.7	128.3	NC	Pumping
VS-9-1i-16-123111	CdV-9-1(i)	7/5/2016	9:30	1.71	7.3	17	195	5.7	128.3	NC	Pumping
VS-HE-3A-16-123118	CdV-9-1(i)	7/6/2016	9:15	1.87	7.2	16.9	195	5.68	309.2	NC	Pumping
VS-HE-3B-16-123129	CdV-9-1(i)	7/6/2016	9:15	1.87	7.2	16.9	195	5.68	309.2	NC	Pumping
VS-HE-4-16-123140	CdV-9-1(i)	7/6/2016	9:15	1.87	7.2	16.9	195	5.68	309.2	NC	Pumping
VS-9-1i-16-123092	CdV-9-1(i)	7/6/2016	9:15	1.87	7.2	16.9	195	5.68	309.2	NC	Pumping
VS-9-1i-16-123106	CdV-9-1(i)	7/6/2016	9:15	1.87	7.2	16.9	195	5.68	309.2	NC	Pumping
VS-HE-3A-16-123124	CdV-9-1(i)	7/8/2016	9:07	1.75	7.2	22.6	245	2.7	200.5	NC	Pumping
VS-HE-3B-16-123135	CdV-9-1(i)	7/8/2016	9:02	1.75	7.2	22.6	245	2.7	200.5	NC	Pumping
VS-HE-4-16-123146	CdV-9-1(i)	7/8/2016	9:02	1.75	7.2	22.6	245	2.7	200.5	NC	Pumping
VS-9-1i-16-123099	CdV-9-1(i)	7/8/2016	9:02	1.75	7.2	22.6	245	2.7	200.5	NC	Pumping
VS-9-1i-16-123112	CdV-9-1(i)	7/8/2016	9:02	1.75	7.2	22.6	245	2.7	200.5	NC	Pumping
VS-HE-3A-16-123121	CdV-9-1(i)	7/11/2016	10:10	1.68	7.1	26.5	324	-0.01	45.3	NC	Pumping
VS-HE-3B-16-123132	CdV-9-1(i)	7/11/2016	10:10	1.68	7.1	26.5	324	-0.01	45.3	NC	Pumping
VS-HE-4-16-123143	CdV-9-1(i)	7/11/2016	10:10	1.68	7.1	26.5	324	-0.01	45.3	NC	Pumping
VS-9-1i-16-123097	CdV-9-1(i)	7/11/2016	10:10	1.68	7.1	26.5	324	-0.01	45.3	NC	Pumping
VS-9-1i-16-123113	CdV-9-1(i)	7/11/2016	10:10	1.68	7.1	26.5	324	-0.01	45.3	NC	Pumping
VS-HE-3A-16-123123	CdV-9-1(i)	7/12/2016	16:13	1.64	7.1	37.8	364	0	45.3	NC	Pumping
VS-HE-3B-16-123134	CdV-9-1(i)	7/12/2016	16:13	1.64	7.1	37.8	364	0	45.3	NC	Pumping

Table 2.3-5 (continued)

Sample ID	Pumping Well	Date	Time	Pumping Rate (gpm)	Measurement Parameters						
					pH	Temperature (Degree C)	Conductivity (µS/cm)	DO (mg/L)	ORP (mV)	Turbidity (NTU)	Test Phase
VS-HE-4-16-123145	CdV-9-1(i)	7/12/2016	16:13	1.64	7.1	37.8	364	0	45.3	NC	Pumping
VS-9-1i-16-123091	CdV-9-1(i)	7/12/2016	16:13	1.64	7.1	37.8	364	0	45.3	NC	Pumping
VS-9-1i-16-123105	CdV-9-1(i)	7/12/2016	16:13	1.64	7.1	37.8	364	0	45.3	NC	Pumping
VS-9-1i-16-123098	CdV-9-1(i)	7/13/2016	10:50	2.26	7.3	18.3	175	6.11	140.5	NC	Rebound
VS-9-1i-16-123114	CdV-9-1(i)	7/13/2016	10:50	2.26	7.3	18.3	175	6.11	140.5	NC	Rebound
VS-9-1i-16-123093	CdV-9-1(i)	7/15/2016	10:33	2.26	7.3	15.8	185	6.35	139	NC	Rebound
VS-9-1i-16-123107	CdV-9-1(i)	7/15/2016	10:33	2.26	7.3	15.8	185	6.35	139	NC	Rebound
VS-9-1i-16-123094	CdV-9-1(i)	7/18/2016	10:32	2.37	7.3	15.8	186	6.2	141.7	NC	Rebound
VS-9-1i-16-123108	CdV-9-1(i)	7/18/2016	10:32	2.37	7.3	15.8	186	6.2	141.7	NC	Rebound
VS-9-1i-16-123090	CdV-9-1(i)	7/20/2016	12:10	2.4	7.3	16.1	187	6.21	185	NC	Rebound
VS-9-1i-16-123104	CdV-9-1(i)	7/20/2016	12:10	2.4	7.3	16.1	187	6.21	185	NC	Rebound
VS-9-1i-16-123096	CdV-9-1(i)	7/25/2016	10:25	2.05	7.9	25.3	189	5.17	262	NC	Rebound
VS-9-1i-16-123109	CdV-9-1(i)	7/25/2016	10:25	2.05	7.9	25.3	189	5.17	262	NC	Rebound

*NC = Not collected.

Table 4.1-1
Summary of Slug Test Results for CdV-9-1(i) Piezometers and Primary Screen

Well Screen	Initial Vertical Displacement (ft)	Assumed Saturated Thickness (ft)	Estimated Hydraulic Conductivity K (m/d)	Estimated Transmissivity T (m^2/d)	Estimated Initial Displacement (ft)
CdV-9-1(i) PZ-1	4.16 ft	72.6	2.884	63.83	4.042
CdV-9-1(i) PZ-2	95.2	182.5	0.003002	0.167	93.55
CdV-9-1(i) S1	17.36	123.9	0.046–0.182	1.74–6.87	17.36

Table 4-2-1
Summary of Observations Related to Hydraulic Connections and Estimated Potential Maximum Drawdowns in Observation Wells

	Observation Well or Screen	Geologic Unit	Summary of Observations Related to Hydraulic Connections	Estimated Potential Maximum Drawdown in Observation Well (m)		
				Pumping Well CdV-9-1(i)	Pumping Well CdV-16-1(i)	Pumping Well CdV-16-4ip
OBSERVATION WELLS	CdV-16-1(i)	Qbof	Water levels in CdV-16-1(i) were potentially influenced by pumping at CdV-16-4ip and CdV-9-1(i) in 2016.	0.0011	5.2	0.00012
	CdV-16-2ir	Tpf	Maximum predicted drawdowns of 0.084 m and 0.032 m were simulated during pumping of CdV-9-1(i) and CdV-16-4ip, respectively. However, lack of good correlations between observed and predicted water levels and "noise" in the CdV-16-2ir water-level data suggest drawdowns resulting from 2016 pumping test (and 2014 pumping test) are questionable and more likely reflect seasonality in this zone.	0.084	0.0016	0.032
	CdV-16-4ip S1	Tpf	Negligible drawdown from pumping at CdV-9-1(i) and CdV-16-1(i). However, when CdV-16-4ip was pumped, CdV-9-1(i) responded with 0.23-m drawdown, indicating likely hydraulic connection.	0.0016	0.0	16
	CdV-9-1(i) S1	Tpf	Water levels in CdV-9-1(i) S1 were not influenced by pumping at CdV-16-1(i). Pumping at CdV-16-4ip resulted in drawdown of 0.23 m in CdV-9-1(i); however, this estimated value may be influenced by a large-scale natural hydraulic event that was occurring immediately before and during the pumping test.	10	0.000013	0.23
	CdV-9-1(i) PZ-1	Qbof	Transducer cable to CdV-9-1(i) PZ-1 was faulty during the CdV-9-1(i) pumping test, and no conclusions can be drawn from the water-level data in PZ-1 during the CdV-9-1(i) pumping test. Transducer cable replaced July 27, 2016. No potential maximum drawdowns were predicted because of the shorter period of record; however, water levels in CdV-9-1(i) PZ-1 were very similar to levels in CdV-9-1(i) PZ-2.	0.00015	0.00018	0.00096
	CdV-9-1(i) PZ-2	Tpf	Pumping at CdV-16-1(i) generated maximum potential drawdown of 0.064 m in PZ-2, while pumping at CdV-16-4ip generated maximum potential drawdown of 8 cm in CdV-9-1(i) PZ-2. However, PZ-2 water levels were noisy, and there was a poor match between observed and predicted water levels, suggesting this possible connection is questionable.	0.00041	0.064	0.08
	R-25 S1	Qbof	Negligible influence of pumping in CdV-9-1(i) and CdV-16-4ip on water levels. May be weakly connected to CdV-9-1(i) based on hydraulic response during drilling of CdV-9-1(i)	0.0080	0.00071	0.000069
	R-25 S2	Tpf	Water levels in R-25 S2 show influence of pumping at CdV-9-1(i) and CdV-16-4ip, with simulated maximum drawdowns of 0.021 m and 0.07 m in 2016. Relatively good match between observed and model-predicted water levels indicate pumping effects in R-25 S2 during 2016 testing are likely. CdV-16-4ip pumping test data collected in 2014 confirmed the connection between CdV-16-4ip and R-25 S2.	0.021	0.0019	0.07
	R-25 S4	Tpf	Water levels in R-25 S4 showed no responses to pumping at CdV-9-1(i) S1, CdV-16-1(i), and CdV-16-4ip during the 2016 pumping test. A possible response was observed during the longer-term testing in 2014, but it may have been coincidental with other water-level perturbations.	0.0034	0.0040	0.0046
	R-25b	Qbof	Water levels in R-25b show limited responses to pumping in CdV-9-1(i) (0.016 m) and CdV-16-4ip (0.0042 m) in 2016. Drawdown responses are almost negligible.	0.016	0.0058	0.0042
	R-47i	Tpf	Pumping at CdV-9-1(i) resulted in simulated drawdown of 0.041 m, while pumping at CdV-16-4ip resulted in simulated drawdown of 0.019 m. Modelling data do not fit data well but suggest some connection to CdV-16-4ip exists. Fluctuation in water levels may potentially be attributed to other seasonal hydrologic processes.	0.041	0.00034	0.019
	R-63	Tpf	R-63 is influenced by pumping at water supply wells PM-4 and PM-5. CdV-16-4ip appeared to influence drawdown at R-63, with 0.024 m of predicted drawdown during the 2016 pumping test. However, the 2014 test showed no influence, and this connection is implausible.	0.0014	0.00099	0.024
	R-63i	Tpf	Water-level data set extremely noisy. Pumping at CdV-9-1(i) and CdV-16-4ip may influence water levels at R-63i, with simulated drawdowns of 0.12 m and 0.042 m. Relatively poor match between observed and predicted water levels indicate pumping effects at R-63i are questionable.	0.12	0.058	0.042

Notes: Drawdowns are in meters. The detections of pumping impacts at each observation well are labeled as certain (red), potential (blue), and unlikely (grey).

Table 4.5-1
Summary of Total Volumes Pumped and RDX Removed during Active Pumping at Wells CdV-9-1(i), CdV-16-1(i), and CdV-16-4ip

Well	Average RDX during Pumping (µg/L)	Total Volume Pumped (gal.)	Total Liters Pumped	RDX Removed (kg)	RDX Removed (lb)
CdV-9-1(i)	29.2	82,003	310,415	0.00905	0.01995
CdV-16-1(i)	26.9	16,227	61,426	0.00165	0.00364
CdV-16-4ip	171.7	245,120	927,880	0.1593	0.3511
Total	n/a*	**343,350**	**1,299,721**	**0.170**	**0.375**

*n/a = Not applicable.

Appendix A

As-built Diagrams and Borehole Stratigraphy
for CdV-9-1(i), CdV-16-1(i), and CdV-16-4ip

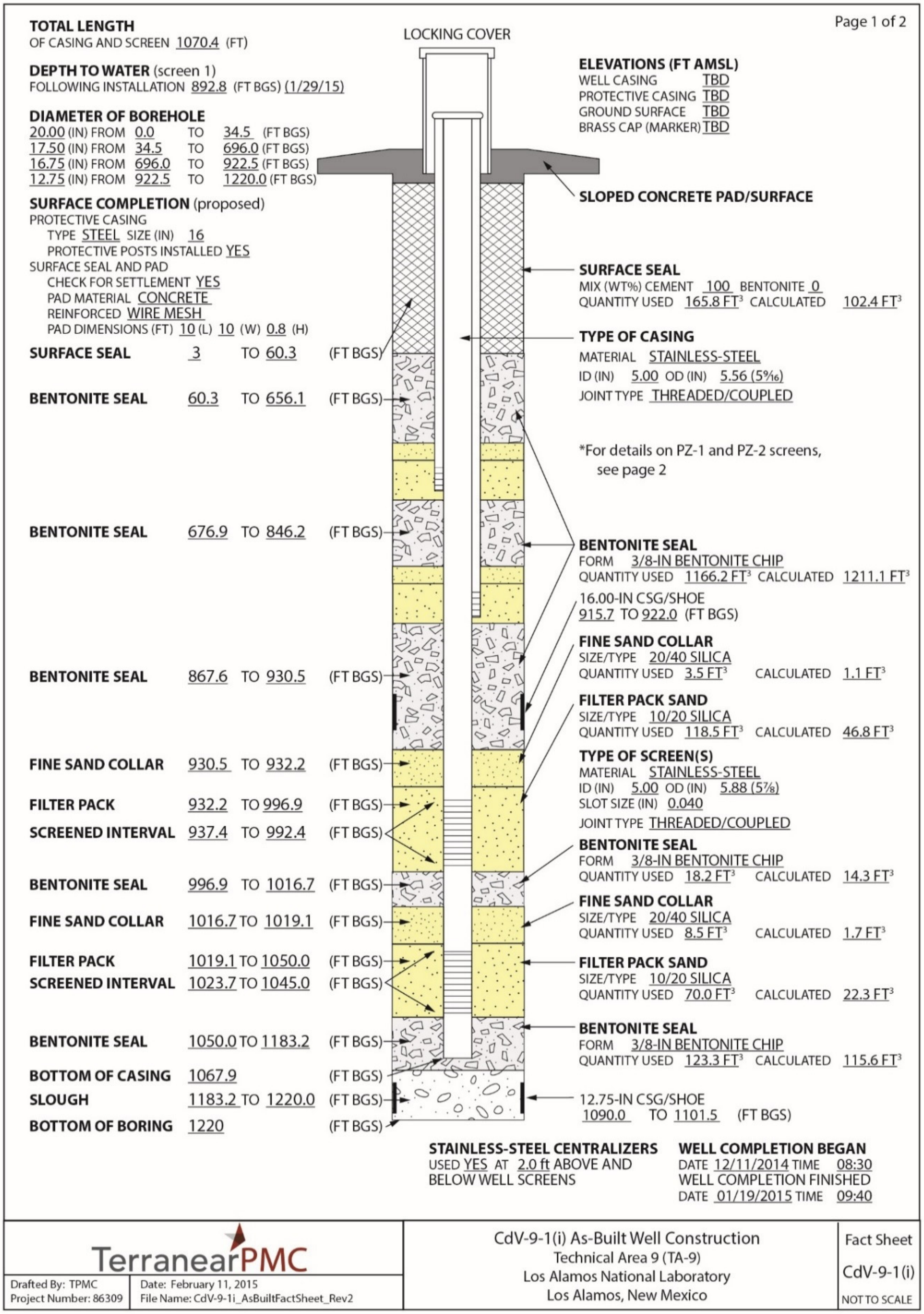

Figure A-1 As-built well construction for CdV-9-1(i) page 1 of 2

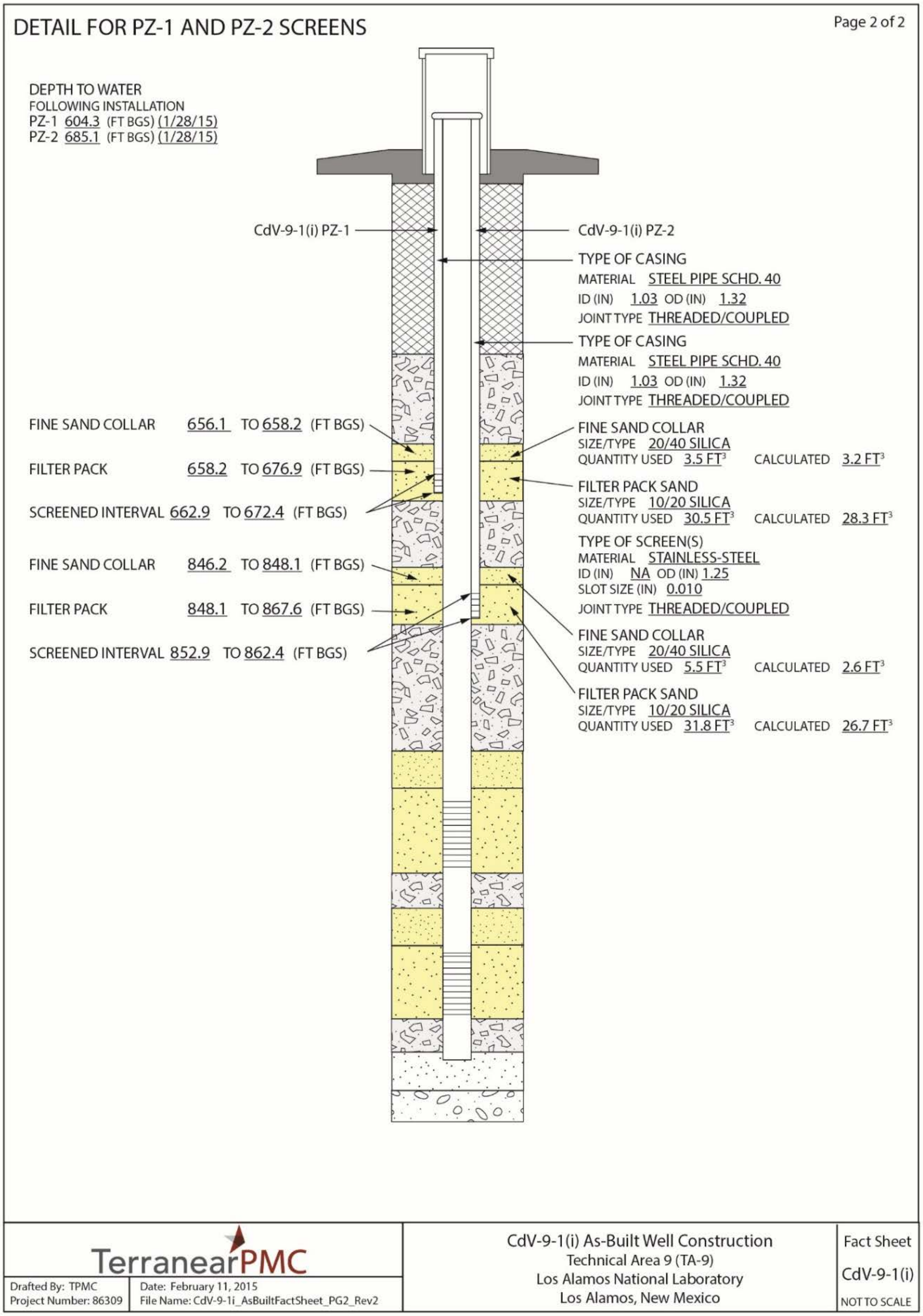

Figure A-2 As-built well construction for CdV-9-1(i) page 2 of 2

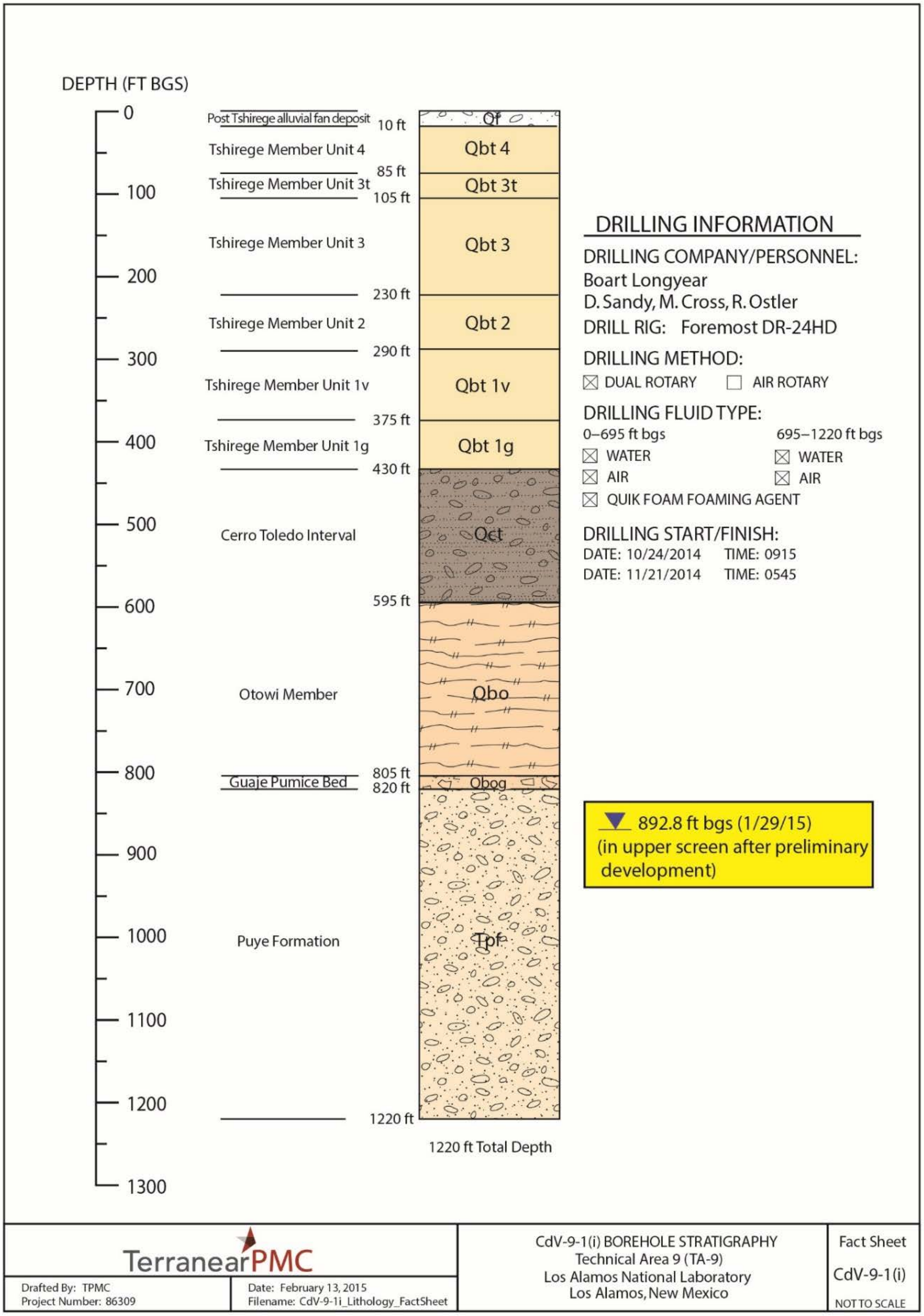

Figure A-3 Borehole stratigraphy for CdV-9-1(i)

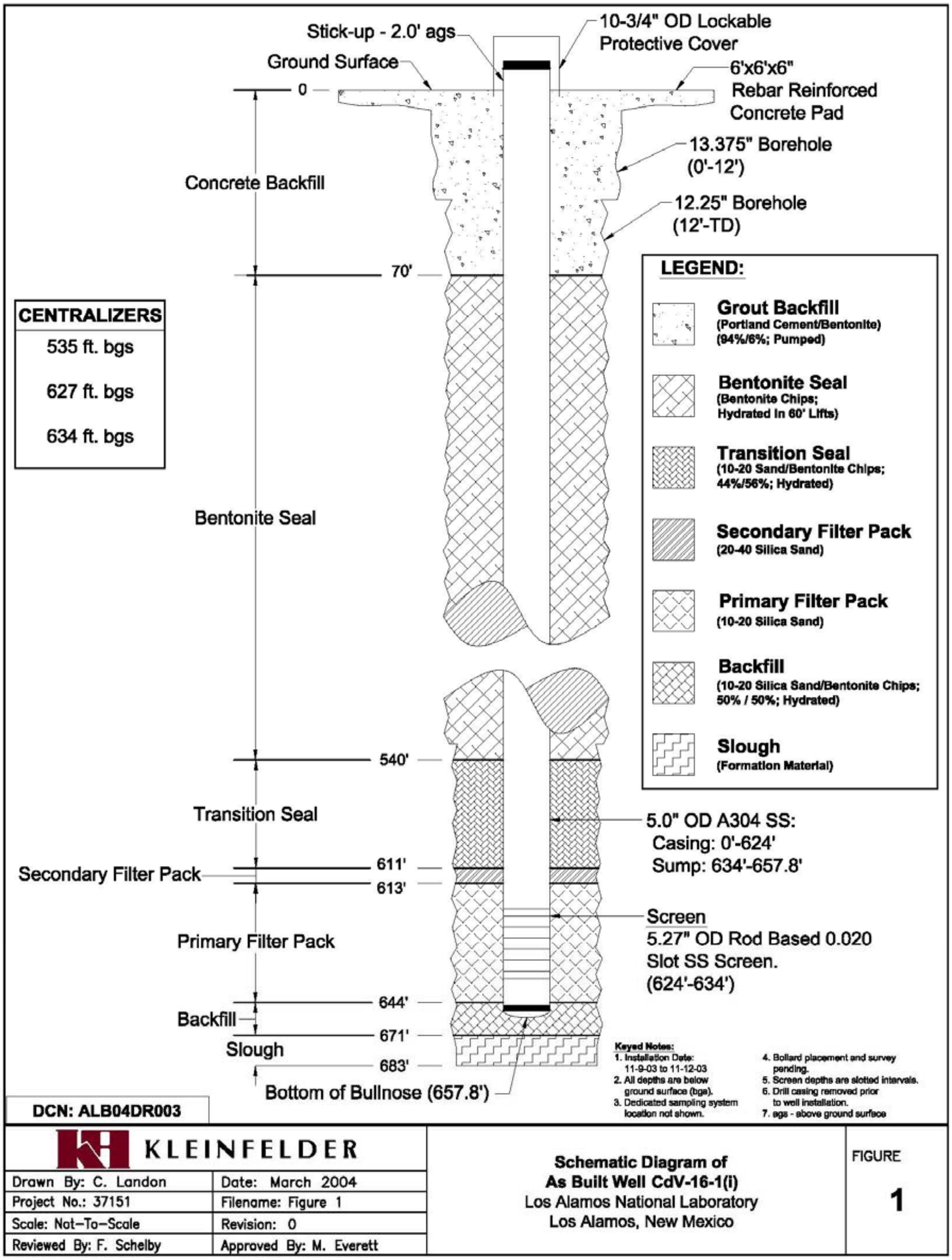

Figure A-4 As-built well construction for CdV-16-1(i)

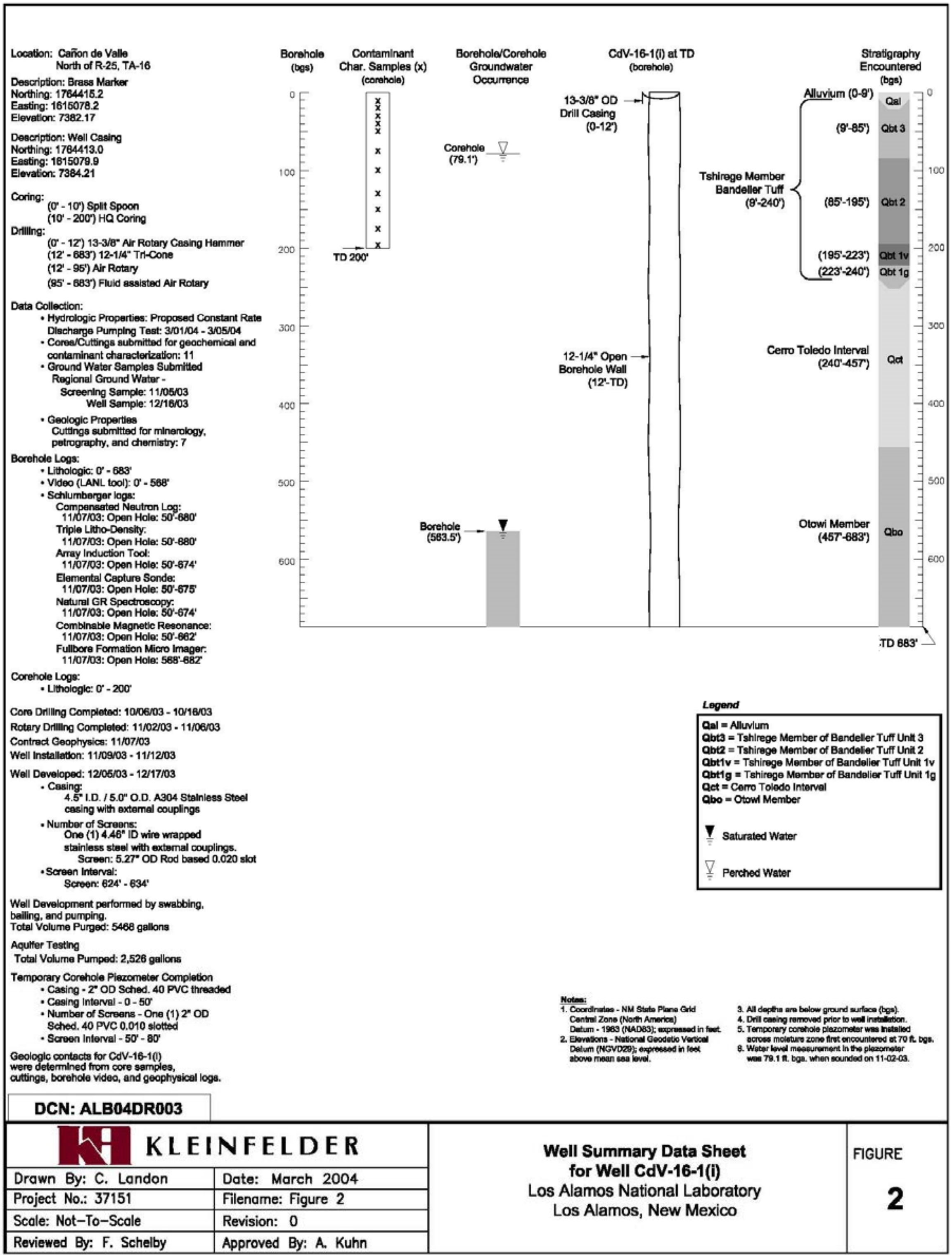

Figure A-5 Borehole stratigraphy for CdV-16-1(i)

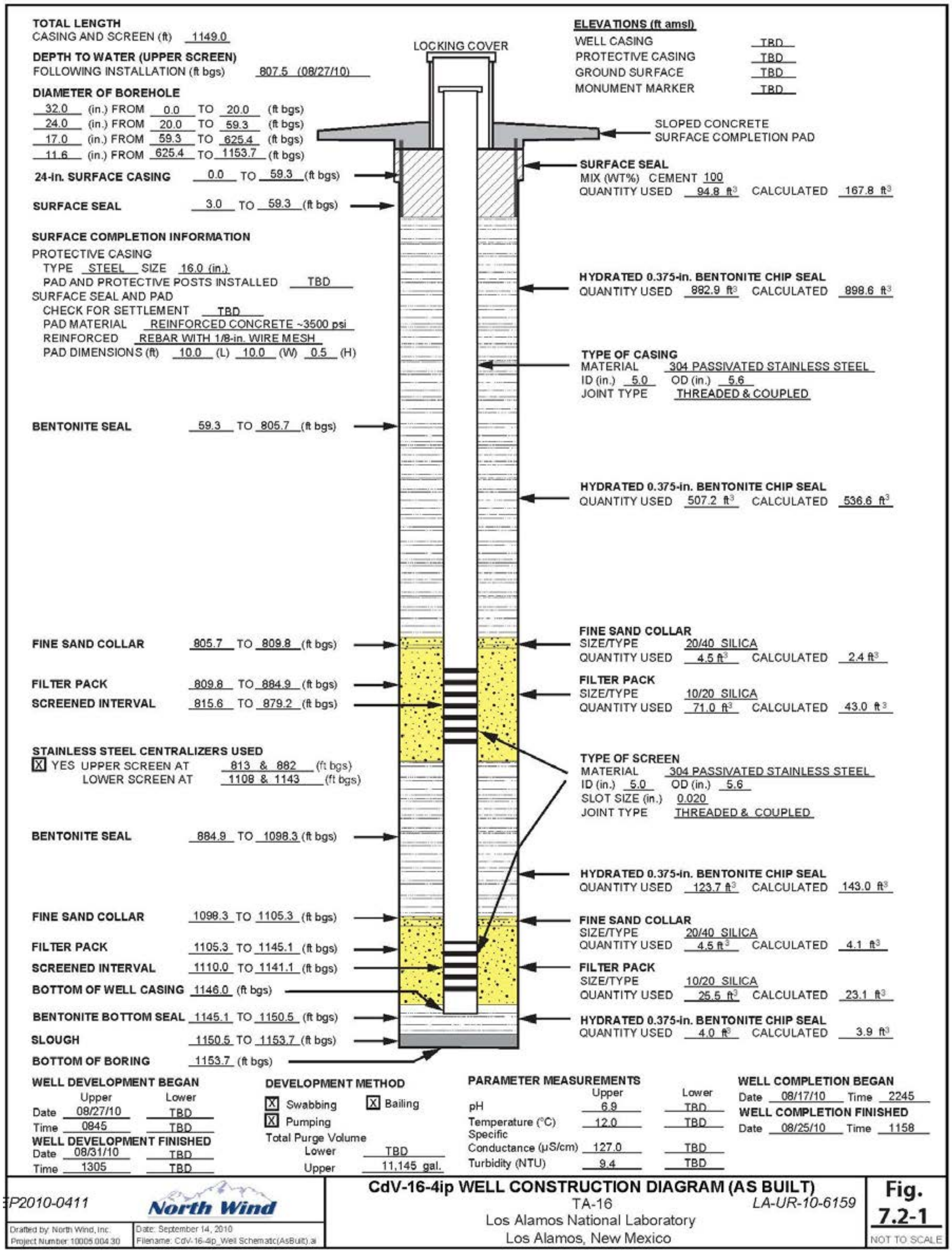

Figure A-6 As-built well construction for CdV-16-4ip

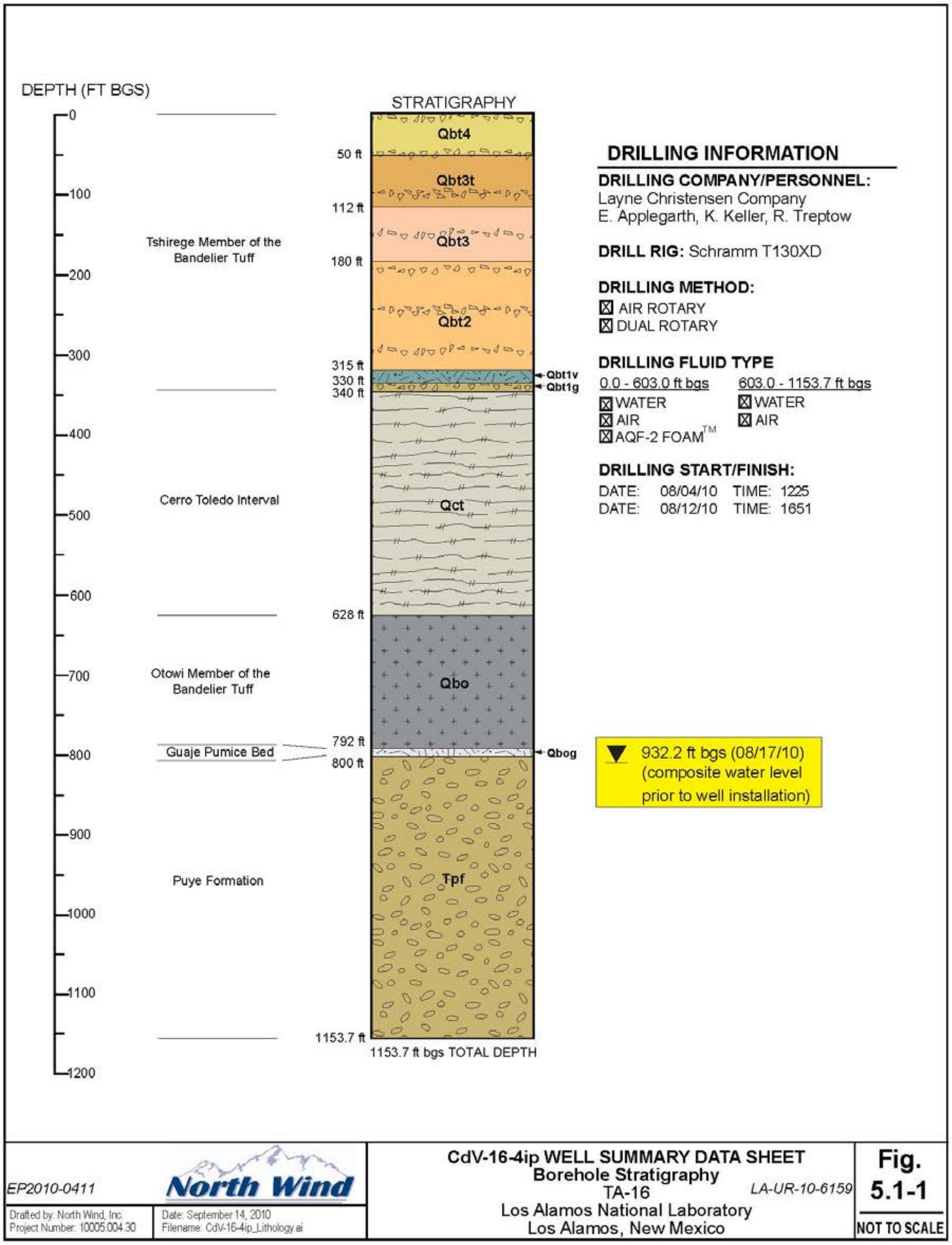

Figure A-7　Borehole stratigraphy for CdV-16-4ip

Appendix B

Water-Level Data for Pumping and Observation Wells
(on CD included with this document)

Appendix C

Analytical Data Collected for Characterization and Compliance Sampling during Pumping and Recovery (on CD included with this document)

Appendix D

Analysis of Pumping Test Data for Well CdV-9-1(i)

D-1.0 INTRODUCTION

This appendix describes the analysis of the pumping tests conducted from June 7 to July 27, 2016, at well CdV-9-1(i), located in Technical Area 09. The CdV-9-1(i) tests were conducted at the main well screen (from depth 937.4 to 992.4 ft with a screen length of 55 ft) to characterize the saturated perched sediments and estimate the hydraulic properties of the upper Puye Formation. The thickness of the perched horizon within the upper Puye Formation impacted by the pumping test is assumed to be 100 ft. The water-level elevation was 6613.12 ft before this test began at 13:36 pm on June 7.

Well CdV-9-1(i) was pumped first from 14:40 on June 7 to 9:31 on June 9, and then the pumping stopped for a 5-d monitoring period of water-level recovery. The pump was restarted at 9:50 on June 14 and continued until 15:28 on July 12, 2016 (Figure D-1). The pump ran at various rates (between 2.05 and 1.64 gallons per minute [gpm]). During the recovery period after July 12, five 1-h rebound sampling events occurred on July 13, 15, 18, 20, and 25, with pumping rates of 2.26, 2.3, 2.37, 2.4 and 2.05 gpm, respectively, and these rebound pumping events were also considered in pumping test analyses (Figure D-2). During the period of field pumping activities from June 7 to July 27 the cumulative amount of water pumped out from well CdV-9-1(i) was 82731 gal. (Figure D-3). Since the changes in the pumping rates had a large impact on the observed drawdowns, an analytical model capable of representing variability in the pumping rates was selected to analyze the pumping test data; the observed daily-based pumping-rate fluctuations were applied as a model input. The observed water levels were converted to corrected displacements or drawdowns (in ft) by using the observed water level at 13:36 on June 7 as an initial water level. The observed water levels are applied as a model calibration targets.

It was assumed the perched layer (horizon) within the Puye Formation is a partially penetrated unconfined saturated zone that is homogeneous and anisotropic. The perched layer is assumed to have a uniform thickness (without boundary effects). The software AQTESOLV (Duffield 2007, 601723) is used to interpret the pumping test data. Three theoretical models, Theis (1934-1935, 098241); Neuman (1974, 085421); and Cooper-Jacob (1946, 098236), which are built into the software AQTESOLV, were applied for interpreting the pumping test data and estimating hydraulic (groundwater flow) parameters of the saturation zone, including hydraulic conductivity, storage coefficient, specific yield, and anisotropic factor. The interpretation of the slug tests at PZ-1, PZ-2, and screen 1 in CdV-9-1(i) is included in Attachment D-1.

D-2.0 THEIS MODEL

First, the Theis model (Theis 1934–1935, 098241) was used to fit the observed drawdown and recovery data. The Theis model was originally derived for simulating the transient flow towards a fully penetrating well in a horizontally-distributed confined aquifer with uniform thickness and homogeneous hydraulic properties. The solution assumes a line source for the pumped well and therefore neglects the wellbore storage (Theis 1934–1935, 098241):

$$s = \frac{Q}{4\pi T}\int_u^\infty \frac{e^{-y}}{y}dy = \frac{Q}{4\pi T}W(u), \qquad \textbf{Equation D-1}$$

$$u = \frac{r^2\mu}{4Tt}, \qquad \textbf{Equation D-2}$$

where, *s* is drawdown (L); *Q* is pumping rate [L^3/T]; *T* is transmissivity [L^2/T]; *r* is radial distance [L]; μ is storativity [dimensionless]; *t* is time [T]; and *W*(*u*) is the Theis well function. Hantush (Hantush 1961, 098237; Hantush 1961, 106003) modified the Theis model for simulating the effects of partial penetration in a aquifer of uniform thickness:

$$s = \frac{Q}{4\pi T}\left\{W(u) + \frac{2b}{\pi(l-d)}\sum_{n=1}^{\infty}\frac{1}{n}\left[\sin\left(\frac{n\pi l}{b}\right) - \sin\left(\frac{n\pi d}{b}\right)\right]\cos\left(\frac{n\pi z}{b}\right)W\left(u, \sqrt{\frac{K_z}{K_r}}\frac{n\pi r}{b}\right)\right\},$$ **Equation D-3**

where, *b* is aquifer thickness [L]; *d* is depth to top of pumping well screen [L]; *d′* is depth to top of observation well screen [L]; *l* is depth to bottom of pumping well screen [L]; *l′* is depth to bottom of observation well screen [L]; $\frac{K_z}{K_r}$ is vertical to horizontal hydraulic conductivity anisotropy [dimensionless]; *r* is radial distance; *b* is aquifer thickness; K_z is vertical conductivity; K_r is horizontal conductivity; *W(u,β)* is the Hantush-Jacob well function ($\beta = \sqrt{\frac{K_z}{K_r}}\frac{n\pi r}{b}$); and *z* is depth to piezometer opening [L].

AQTESOLV (Duffield 2007, 601723) incorporates the Theis solution (Theis 1934-1935, 098241), and Hantush (Hantush 1961, 098237; Hantush 1961, 106003) modified solution for simulating in a partially penetrated well for confined and unconfined aquifers. In this case, Jacob's correction for partial dewatering of water table (unconfined) aquifers allows for use of the Theis solution for unconfined aquifers as well. The Jacob's correction was applied as implemented in the software AQTESOLV, which also uses the principle of superposition in time to account for variable-pumping rate tests, including recovery. The well structure and pumping-rate data are shown in Table D-1.

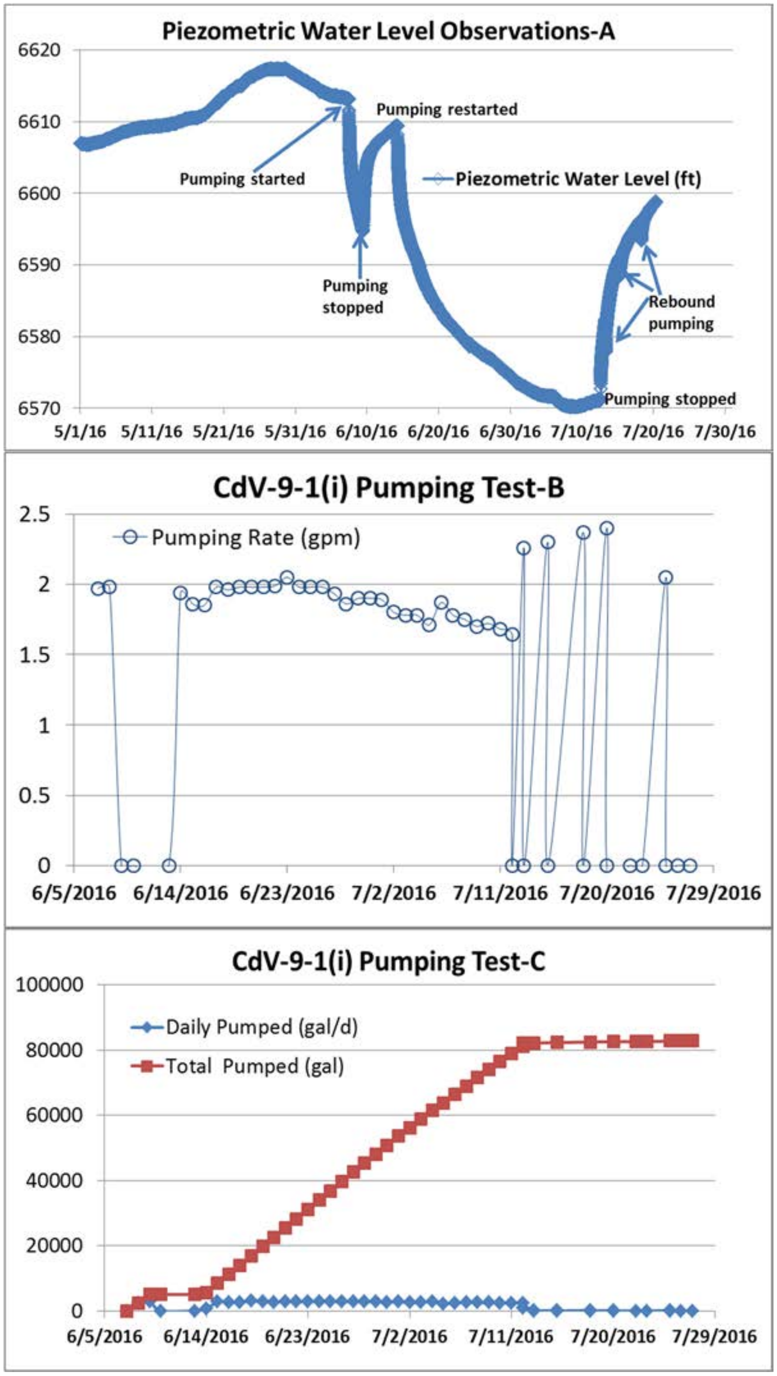

Figure D-1 Water-level observations (A), pumping rate fluctuations (B), and total pumped water (C) during the CdV-9-1(i) pumping test

Table D-2 presents estimated parameters using Theis models. The estimated transmissivity is 0.808 m^2/d, the horizontal hydraulic conductivity is 0.027 m/d, and the storage coefficient is 0.183. The computed drawdowns from the Theis model fit the observations reasonably well (Figure D-2).

Table D-1
CdV-9-1(i) Pumping Test Data Provided as AQTESOLV Input for the Theis Model

Data Set: E:\EP2016\AquiferTest\CdV-9-1i\CdV-9-1i_S1_unconfined_TheisAll2.aqt
Title: CdV-9-1iTest
Date: 01/20/17
Time: 09:42:55

PROJECT INFORMATION

Company: LANL
Client: zd
Project: ep
Location: Puye
Test Date: 2016
Test Well: CdV-9-1i

AQUIFER DATA

Saturated Thickness: 100. ft
Anisotropy Ratio (Kz/Kr): 0.01

PUMPING WELL DATA

No. of pumping wells: 1

Pumping Well No. 1: CdV9_1iMainSall2

X Location: 0. ft
Y Location: 0. ft

Casing Radius: 8. ft
Well Radius: 6.38 ft

Partially Penetrating Well
Depth to Top of Screen: 44.6 ft
Depth to Bottom of Screen: 83.8 ft

No. of pumping periods: 47

Pumping Period Data

Time (day)	Rate (gal/min)	Time (day)	Rate (gal/min)	Time (day)	Rate (gal/min)
0.	1.97	19.78	1.93	35.03	0.
0.7847	1.98	20.78	1.86	35.79	2.26
1.785	0.	21.78	1.9	35.84	0.
6.799	1.94	22.78	1.9	37.79	2.3
7.785	1.86	23.78	1.89	37.83	0.
8.787	1.85	24.78	1.8	40.79	2.37
9.785	1.98	25.8	1.78	40.83	0.
10.85	1.96	26.9	1.78	42.86	2.4
11.84	1.98	27.78	1.71	42.9	0.
12.78	1.98	28.78	1.87	44.78	0.
13.78	1.98	29.78	1.78	45.78	0.
14.78	1.99	30.78	1.75	47.79	2.05
15.78	2.05	31.78	1.7	47.83	0.
16.8	1.98	32.78	1.72	48.78	0.
17.78	1.98	33.79	1.68	49.78	0.
18.78	1.98	34.78	1.64		

OBSERVATION WELL DATA

Table D-2
Estimated Parameters Using the Theis Model

Pumping Test
Aquifer Model: Unconfined
Solution Method: Theis

VISUAL ESTIMATION RESULTS

Estimated Parameters

Parameter	Estimate	
T	0.8078	m^2/day
S	0.1829	
Kz/Kr	0.01	
b	100.	ft

K = T/b = 0.0265 m/day (3.067E-5 cm/sec)
Ss = S/b = 0.001829 1/ft

AUTOMATIC ESTIMATION RESULTS

Estimated Parameters

Parameter	Estimate	Std. Error	Approx. C.I.	t-Ratio	
T	0.8078	0.004992	+/- 0.009805	161.8	m^2/day
S	0.1829	0.003651	+/- 0.007171	50.1	
Kz/Kr	0.01	not estimated			
b	100.	not estimated			ft

C.I. is approximate 95% confidence interval for parameter
t-ratio = estimate/std. error
No estimation window

K = T/b = 0.0265 m/day (3.067E-5 cm/sec)
Ss = S/b = 0.001829 1/ft

Parameter Correlations

	T	S
T	1.00	-0.91
S	-0.91	1.00

Residual Statistics

for weighted residuals

Sum of Squares . . . . 2094.9 ft^2
Variance . . . . 3.545 ft^2
Std. Deviation. . . . . . . 1.883 ft
Mean . . . . 0.6571 ft
No. of Residuals 593
No. of Estimates 2

D-3.0 NEUMAN MODEL

The Neuman model (Neuman 1974, 085421) was used to fit the observed drawdown data as well as the recovery data. By adding a new parameter "specific yield" to address the delayed gravity response of the unconfined aquifer, Neuman (1974, 085421) derived an analytical solution for simulating the transient flow to a fully or partially penetrating well in a homogeneous, anisotropic unconfined aquifer with delayed gravity response. Therefore, the pumping test analyses using Neuman model also provide information about the properties of the unsaturated zone in addition to the properties of the saturated zone. The Neuman model assumes instantaneous drainage at the water table. The solution also assumes a line source for the pumped well and therefore neglects wellbore storage.

$$s = \frac{Q}{4\pi T}\int_0^\infty 4yJ_0(y\sqrt{\beta})\{u_0(y) + \textstyle\sum_{n=1}^\infty u_n(y)\}dy, \qquad \textbf{Equation D-4}$$

$$\beta = \frac{r^2K_z}{b^2K_r}, \qquad \textbf{Equation D-5}$$

where, J_0 is Bessel function of first kind and zero order and u_0 and u_n are functions for computing drawdowns in a piezometer or in a partially penetrating observation well (Neuman 1974, 085421). The drawdown in a piezometer is calculated using the following two equations:

$$u_0(y) = \frac{\left[1-\exp\left(-t_s\beta(y^2-\gamma_0^2)\right)\right]\cosh(\gamma_0 Z_D)}{[y^2+(1+\sigma)\gamma_0^2-\frac{(y^2-\gamma_0^2)^2}{\sigma}]\cosh(\gamma_0)}\cdot\frac{\sinh(\gamma_0(1-d_D))-\sinh(\gamma_0(1-l_D))}{(l_D-d_D)\sinh(\gamma_0)}, \qquad \textbf{Equation D-6}$$

$$u_n(y) = \frac{\left[1-\exp\left(-t_s\beta(y^2-\gamma_0^2)\right)\right]\cos(\gamma_0 Z_D)}{[y^2+(1+\sigma)\gamma_0^2-\frac{(y^2-\gamma_0^2)^2}{\sigma}]\cos(\gamma_0)}\cdot\frac{\sin(\gamma_0(1-d_D))-\sin(\gamma_0(1-l_D))}{(l_D-d_D)\sin(\gamma_0)}, \qquad \textbf{Equation D-7}$$

where d_D is dimensionless depth to top of pumping well screen (d/b); l_D is dimensionless depth to bottom of pumping well screen (1/b); Z_D is dimensionless elevation of piezometer opening above base of aquifer (z/b); $t_s = \frac{Tt}{Sr^2}$; S is storativity; and S_y is specific yield; and the gamma term (γ_0) is computed numerically (Duffield 2007, 601723).

the Neuman model (as implemented in the software AQTESOLV) is used to estimate the hydraulic parameters by matching the observed drawdowns during the pumping test. The model predicted drawdowns fitted the observation data reasonably well. The estimated parameters are presented in Table D-3. The estimated transmissivity is 0.686 m^2/d, the hydraulic conductivity is 0.023 m/d, the storage coefficient is 0.133, and the specific yield is 0.28, which is close to the available prior estimates for porosity of the Puye Formation. The parameter β is a coefficient to describe the hydraulic conductivity anisotropic ratio ($\frac{r^2}{b^2}\frac{K_z}{K_r}$). In this model, the parameter β is 4.0×10^{-5}, and the anisotropic ratio of $\frac{K_z}{K_r}$ is equal to 0.01.

Table D-3
Estimated Parameters Using the Neuman Model

Aquifer Model: Unconfined
Solution Method: Neuman

Estimated Parameters

Parameter	Estimate	Std. Error	Approx. C.I.	t-Ratio	
T	0.6862	0.1	+/- 0.1965	6.859	m^2/day
S	0.1331	0.005154	+/- 0.01012	25.83	
Sy	0.28	1.968E+5	+/- 3.866E+5	1.423E-6	
ß	4.07E-5	0.0004965	+/- 0.0009752	0.08197	

C.I. is approximate 95% confidence interval for parameter
t-ratio = estimate/std. error
No estimation window

K = T/b = 0.02251 m/day (2.606E-5 cm/sec)
Ss = S/b = 0.001331 1/ft

Parameter Correlations

	T	S	Sy	ß
T	1.00	0.46	-0.98	-0.99
S	0.46	1.00	-0.60	-0.56
Sy	-0.98	-0.60	1.00	1.00
ß	-0.99	-0.56	1.00	1.00

Residual Statistics

for weighted residuals

Sum of Squares . . . . 1513.7 ft^2
Variance . . . . 2.57 ft^2
Std. Deviation. . . . . . . 1.603 ft
Mean . . . . 0.2816 ft
No. of Residuals 593
No. of Estimates 4

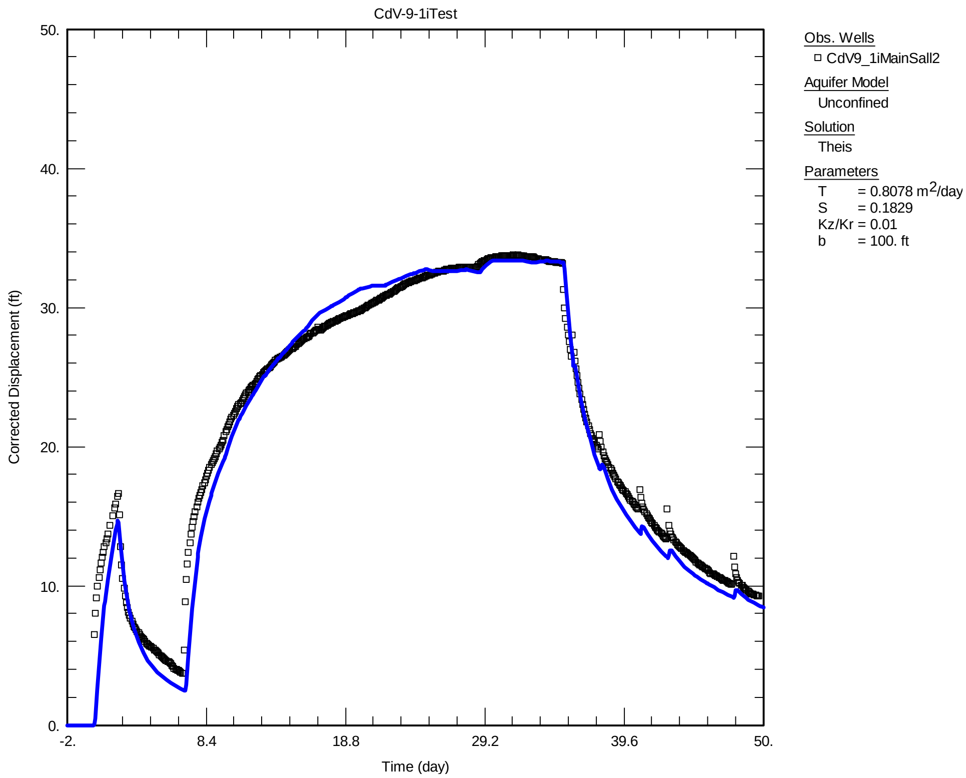

Figure D-2 Representation of the CdV-9-1(i) pumping test using the Theis model

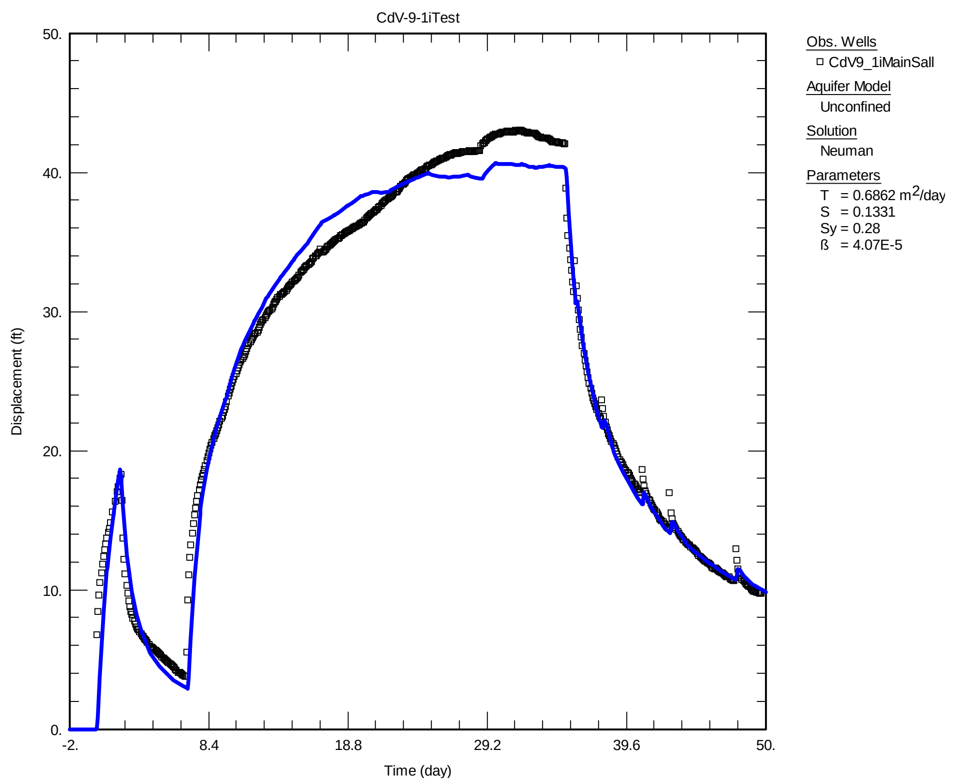

Figure D-3 Representation of the CdV-9-1(i) pumping test using the Neuman model

D-4.0 COOPER-JACOB MODEL

The Cooper-Jacob (1946, 098236) solution was originally developed to analyze pumping tests in a confined aquifer. The Cooper-Jacob solution can be applied for pumping test analyses in unconfined aquifers through the correction of drawdown data as described by Kruseman et al. (1991, 106681):

$$s' = s - s^2/2b$$ **Equation D-8**

where s' is corrected displacement [L], s is observed displacement [L], and b is saturated aquifer thickness [L]. The corrected displacement (s') predicted by this equation reaches a maximum of one-half the aquifer saturated thickness ($0.5b$) when the observed displacement is equal to the aquifer saturated thickness ($s = b$). The Cooper-Jacob equation is a simplified approximation of the Theis equation and is valid whenever the u value is less than about 0.05. For small radius values (e.g., corresponding to borehole radii), u is less than 0.05 at very early pumping times and is therefore less than 0.05 for most or all measured drawdown values. Thus, for the pumped well, the Cooper-Jacob equation usually can be considered a valid approximation of the Theis equation. According to the Cooper-Jacob method, the time-drawdown data are plotted on a semilog graph, with time plotted on the logarithmic scale. A straight line of best fit is constructed through the data points and transmissivity is calculated using:

$$T = \frac{264Q}{\Delta s}$$ **Equation D-9**

where, Δs = change in head over one log cycle of the graph [L]. Because this test well completed on the Pajarito Plateau is partially penetrating, an alternate solution considered for assessing aquifer conditions is the Hantush equation for partially penetrating wells (Hantush 1961, 098237; Hantush 1961, 106003) as

$$s = \frac{Q}{4\pi T}\left[W(u) + \frac{2b^2}{\pi^2(l-d)(l'-d')}\sum_{n=1}^{\infty}\frac{1}{n^2}\left(\sin\frac{n\pi l}{b} - \sin\frac{n\pi d}{b}\right)\left(\sin\frac{n\pi l'}{b} - \sin\frac{n\pi d'}{b}\right)W\left(u, \sqrt{\frac{K_z}{K_r}}\frac{n\pi r}{b}\right)\right]$$ **Equation D-10**

The definitions of the variables and parameters in Equation D-10 are the same as those in Equation D-3. The Cooper-Jacob model (which is coded in the software AQTESOLV) is used to estimate the hydraulic parameters by matching the observed drawdowns during the recovery period. The model predicted drawdowns could fit the main trend of the corrected displacements (Figure D-4). The estimated parameters are listed in Table D-4. The estimated transmissivity is 0.987 m^2/d, the hydraulic conductivity is 0.031 m/d, and the storage coefficient is 0.0048. Because the recovery data that can be used for parameter estimation with the Cooper-Jacob model are very limited, the estimated parameters may include high uncertainty (e.g., the storage coefficient).

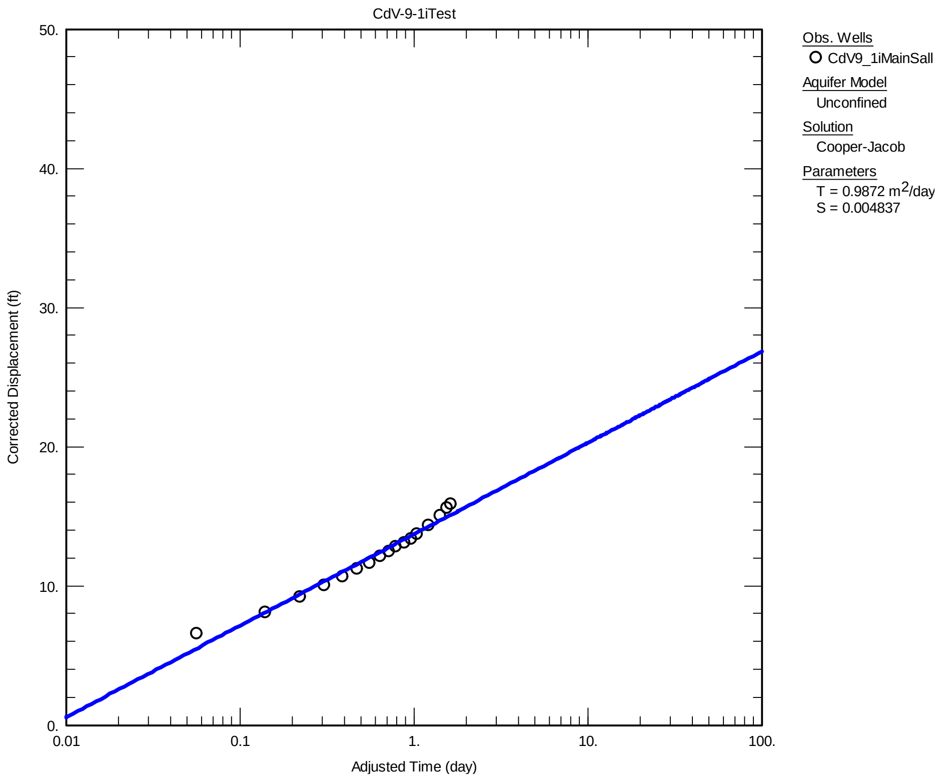

Figure D-4 The fitting results of the CdV-9-1(i) pumping test using the Cooper-Jacob model

Table D-4
Estimated Parameters with the Cooper-Jacob Model for the Perched Layer Screen at CdV-9-1(i) Screen 1

SOLUTION

Pumping Test
Aquifer Model: Unconfined
Solution Method: Cooper-Jacob

VISUAL ESTIMATION RESULTS

Estimated Parameters

Parameter	Estimate	
T	0.9872	m^2/day
S	0.004837	

K = T/b = 0.03239 m/day (3.749E-5 cm/sec)
Ss = S/b = 4.837E-5 1/ft

AUTOMATIC ESTIMATION RESULTS

Estimated Parameters

Parameter	Estimate	Std. Error	Approx. C.I.	t-Ratio	
T	0.9872	0.04435	+/- 0.0945	22.26	m^2/day
S	0.004837	0.0007408	+/- 0.001579	6.529	

C.I. is approximate 95% confidence interval for parameter
t-ratio = estimate/std. error
No estimation window

K = T/b = 0.03239 m/day (3.749E-5 cm/sec)
Ss = S/b = 4.837E-5 1/ft

Parameter Correlations

	T	S
T	1.00	-0.97
S	-0.97	1.00

Residual Statistics

for weighted residuals

Sum of Squares . . . . 4.04 ft^2
Variance . . . . 0.2694 ft^2
Std. Deviation. . . . . . . 0.519 ft
Mean . . . . -0.0007735 ft
No. of Residuals 17
No. of Estimates 2

D-5.0 COMPARISON AMONG THE THEIS, NEUMAN, AND COOPER-JACOB MODEL RESULTS

The model fitting results of the pumping test data using the three models are compared in Table D-5. Overall, the Theis model matches the drawdown portion of the curve where the maximum drawdowns are observed. However, this model does not capture the early and late-time (recovery) data very well. The computed drawdowns during the early recovery periods are higher than the corresponding observations. The Neuman model matches the early and late-time (recovery) data better but underestimates the drawdowns at the peak of the curve. The objective function values or the sum of squares and variance obtained from the Neuman model are lower than those derived from the Theis model, which means the parameters estimated from the Neuman model are less uncertain or more robust than those obtained using the Theis model. For this reason, the parameters estimated by the Neuman model are believed most representative. The Cooper-Jacob model only uses the late-time recovery data (it uses fewer data than the Theis and Neuman models) and the estimation variance is much smaller, which means the estimated parameters from this model have the lowest uncertainty.

It is important to note that the imperfect data matching may be caused by the assumption that the perched layer (tested saturation zone) has a uniform thickness, while in reality the perched layer thickness may increase to the west and decrease to the east (Figure D-5). Because uniform thickness is assumed, the hydraulic conductivity may be underestimated while the estimated transmissivity may represent an averaged value. Further study using more complex numerical models that consider variable thicknesses may be needed for more accurate descriptions of the pumping test data.

Table D-5 includes also the results from the Theis model analyses presented in Appendix G of this report. The results obtained in Appendix G for transmissivity are consistent with the estimates obtained here. Table D-5 also includes previous estimates from Appendix F of the “Completion Report for Intermediate Aquifer Well CdV-9-1(i)” (LANL 2015, 600503). The previous estimates of transmissivity and hydraulic conductivity are consistently higher than the estimates provided here (Table D-5) perhaps because of differences in size of the saturated zone interrogated during the two pumping tests. The 2015 pumping test was conducted over only 3 d. However, during the 2016 test, a water-level record over about 30 d of pumping was collected. The results presented here suggest that the effective hydraulic properties of the saturated zone interrogated during the 2016 pumping test are lower than the hydraulic properties of the saturated zone interrogated during the 2015 pumping test. This potentially suggests scaling effect of the hydraulic properties. The new estimates provide more reliable estimates of the pumped zone at a larger scale; the 2015 estimates are more representative of the hydraulic properties near the pumped screen. The differences in the previous and new pumping test estimates also potentially demonstrate pronounced heterogeneity of the pumped saturated zone; similar heterogeneity effects were also discussed based on the interoperation of the 2015 pumping test (LANL 2015, 600503). Any future hydraulic predictions for long-term pumping of CdV-9-1(i) should be based on the new hydraulic estimates.

Table D-5
Estimated Hydraulic Parameters for CdV-9-1(i) S1
Using the Theis, Neuman, and Cooper-Jacob Models

Parameters	Theis	Neuman	Cooper-Jacob	Theis Model Analysis[a]	Previous Estimates[b]
Hydraulic conductivity (m/d)	0.027	0.023	0.032	n/a[c]	0.396
Transmissivity (m^2/d)	0.808	0.686	0.987	0.66	3.73–7.64
Storage coefficient (-)	0.183	0.133	4.84×10^{-3}	n/a	0.01–0.2
Anisotropy ratio Kz/Kr (-)	0.01	0.01	0.01	n/a	0.01–1.0
Sum of Squared Residuals (ft^2)	2094.9	1513.7	4.04[d]	n/a	n/a
Variance (ft^2)	3.55	2.57	0.269	n/a	n/a

[a] Theis model analysis presented in Appendix G of this report.

[b] Estimates derived from the well completion report for well CdV-9-1(i) (LANL, 2015, 600503).

[c] n/a = Not applicable.

[d] The Cooper-Jacob model only uses recovery data, while Theis and Neuman models use the entire observational record.

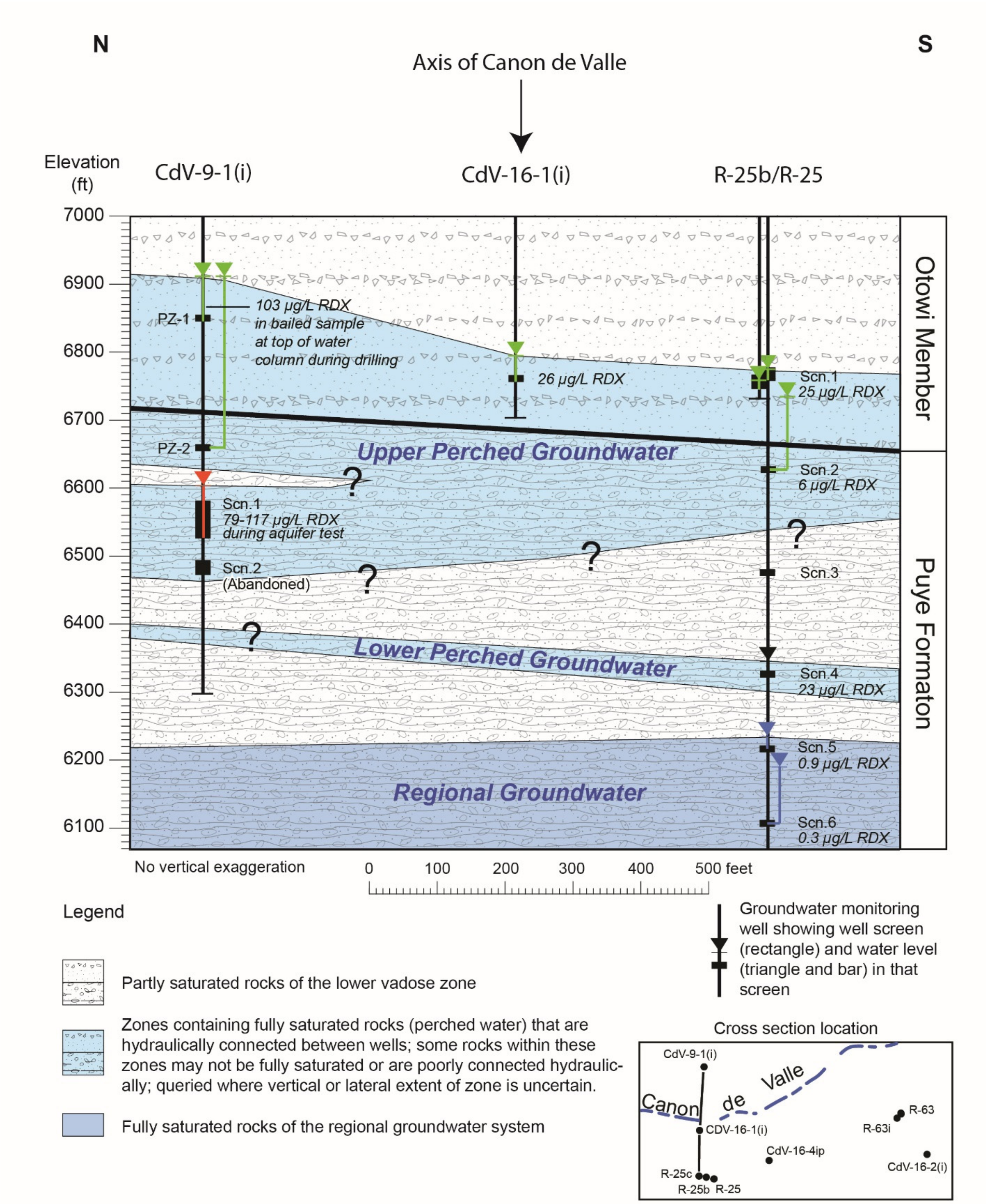

Figure D-5 **North-south geologic cross-section for the lower portion of the vadose zone at CdV-9-1(i), CdV-16-1(i), and R-25/R-25b**

D-6.0 IMPACT OF THE CdV-9-1(i) PUMPING TEST ON SURROUNDING MONITORING WELLS

During the pumping test of well CdV-9-1(i), the water levels in the surrounding wells [e.g. CdV-9-1(i) PZ-2, CdV-16-1(i), CdV-16-4ip, R-25b, and R-63/R-63i] were also monitored. The observed water levels in these wells were used to analyze the impacts of the CdV-9-1(i) test at these monitoring wells. Detailed model-based analyses of these data are provided in Appendix G of this report. This appendix provides a qualitative and quantitative assessment of the water-level data to identify potential pumping effects caused by CdV-9-1(i) on the surrounding monitoring wells.

Before the observed pressure data from the monitoring wells were analyzed, the calibrated Theis model presented in section 2 above was applied to simulate the drawdowns in monitoring wells at different lateral distances: 40, 80, 150, 400, 800 and 1200 ft away from the pumping well. The computed results are shown in Figure D-6. The predicted influence delay times and drawdowns will be used as references to analyze the impacts on surrounding wells at different lateral distances. It should be noted that the Theis model is calibrated against the CdV-9-1(i) data only, but it is applied to predict the drawdowns away from the pumping well. Note that the Theis model is also applied to estimate the drawdown at some lateral distance from the pumping well. However, the distance between the pumping and monitoring screens discussed below have three-dimensional components; some of the distances are strictly vertical. Therefore, there is no explicit expectation that the comparisons presented below between the Theis-predicted and observed drawdowns are theoretically justifiable. Still, the Theis-predicted drawdowns provide some insights into the expected system behavior.

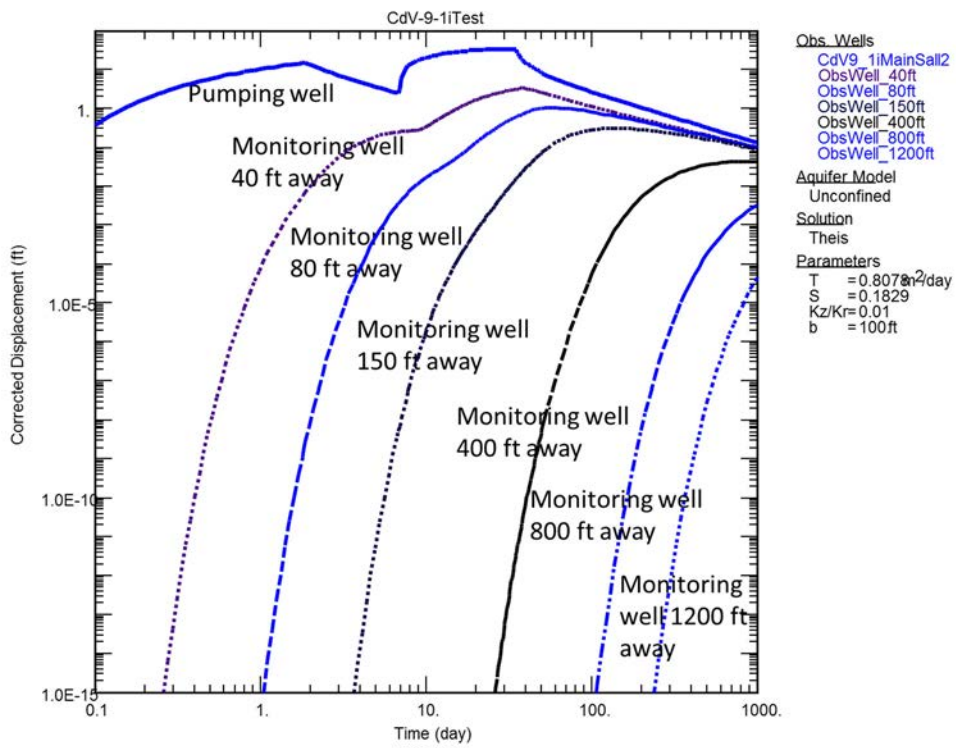

Figure D-6 Theis model-predicted drawdowns for monitoring wells at different lateral distances away from the pumping well CdV-9-1(i)

CdV-9-1(i)-PZ-1: In examining the telemetry data obtained from PZ-1 piezometers over the CdV-9-1(i) pumping test period, it was noted that the transducer was not performing well. Therefore, the monitoring data from PZ-1 are problematic and will not be included in this analysis.

CdV-9-1(i)-PZ-2: Figure D-7A shows the observed water levels of screen PZ-2 from May 1 to July 20, 2016. Since the pumping test was conducted at screen 1 or the middle perched water layer of well CdV-9-1(i) and screen PZ-2 was installed within the upper perched water layer (see Figure D-5), both screens had a vertical separation of about 80 ft. In Figure D-6, for a monitoring well of 80 ft lateral distance from the pumping well, the influence delay time is about 1 d. The potentially observed hydraulic response at the PZ-2 was delayed for about 10 d (see Figure D-7b). The predicted maximum drawdowns (about 0.75 ft or 20 cm at about 25 d after the pumping test) in Figure D-6 are for the monitoring wells in the same saturation zone; the distances are lateral from the pumping well. The predicted drawdowns in Figure D-6 also do not account for the effects of three-dimensional groundwater flow. The PZ-2 screen is installed in a different perched layer, and the hydraulic connection between these two perched layers is not known. The differences in the hydraulic heads in the two perches zones screened by CdV-9-1(i) PZ-2 and CdV-9-1(i) screen 1 suggest the hydraulic connection is not very good (Figure D-5). The potentially observed drawdowns at the PZ-2 between June 20 and July 12 (see Figure D-7b) are about 0.33 ft or 10 cm.

CdV-16-1(i): Figure D-8 presents the observed water levels of CdV-16-1(i) from May 31 to July 20, 2016. The diamond-shaped symbols are the observed raw water levels, and the green line represents the water levels corrected by removing barometric pressure and Earth-tide effects with the software BETCO (Rasmussen and Crawford 1997, 094014; Spane 2002, 602105; Toll 2005, 602226; Van Camp and Vauterin 2005, 602227; Toll and Rasmussen 2007, 104799) and CHipBETA (a code developed by Los Alamos National Laboratory that is similar to BETCO). The pumping test was conducted at screen 1 or within the middle perched water layer of well CdV-9-1(i) and the CdV-16-1(i) screen was installed within the upper perched water layer (see Figure D-5). Horizontally, CdV-16-1(i) is about 400 ft away from the pumping well CdV-9-1(i), and the observed hydraulic response at well CdV-16-1(i) was delayed about 12 d. The pumping at screen 1 was started on June 7, and an apparent average drawdown (about 0.18 ft or 5 cm) was observed at the CdV-16-1(i) between June 18 and July 12 (see Figure D-8). Figure D-6 shows the predicted influence delay time is about 22 d for a monitoring well at a distance of 400 ft. Therefore, the observed average drawdown (5 cm) after the end of June may have been influenced by the pumping test at CdV-9-1(i).

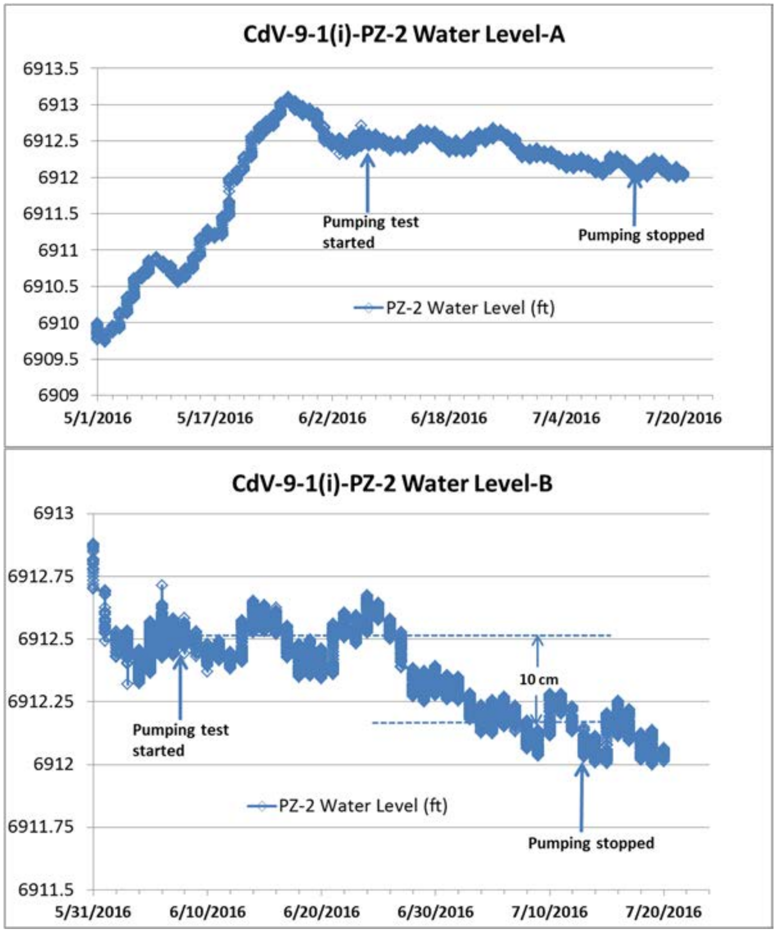

Figure D-7 Observed water levels at CdV-9-1(i) PZ-2 over various periods

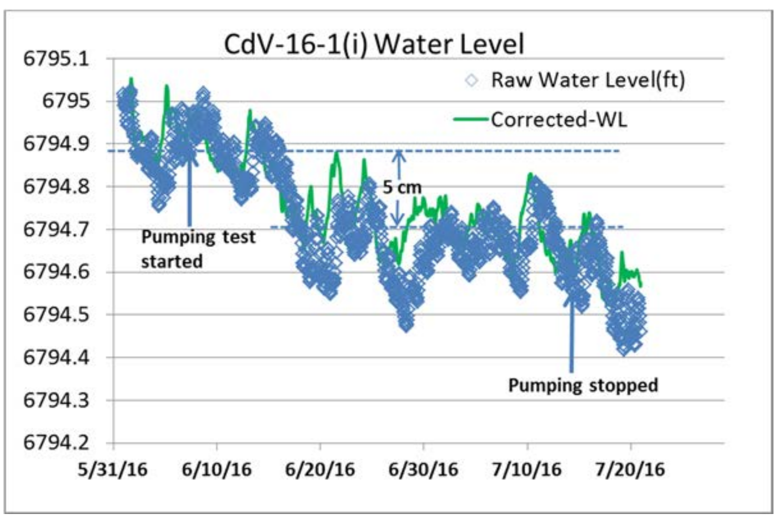

Figure D-8 Observed water levels at CdV-16-1(i) during the pumping test at CdV-9-1(i) screen 1

CdV-16-4ip: Figure D-9 shows the observed water levels of CdV-16-4ip screen 1 from May 31 to July 20, 2016. The screen of CdV-16-4ip is installed within the upper perched water layer, and horizontally this well is about 800 ft away from pumping well CdV-9-1(i). Pumping at CdV-16-1(i) does not appear to cause a hydraulic response in CdV-16-4ip. The predicted results in Figure D-6 also demonstrate that there should be about 100 d for the pumping test to influence on a monitoring well at a distance of 800 ft.

R-25b: Figure D-10 shows the observed water levels of R-25b from June 4 to June 24, 2016. The screen of R-25b was installed within the upper perched water layer (see Figure D-5), and horizontally this well is about 800 ft away from pumping well CdV-9-1(i). The observed changes of water levels at this well were mainly from seasonal or natural variations. No obvious water-level decline occurred during the pumping test period.

R-25: The hydrographs for well R-25 screens 1, 2, 4 and 6 also showed very little barometric pressure response, suggesting that none of the R-25 screen zones had an apparent response to pumping at CdV-9-1(i).

R-63/R-63i: Figures D-11 and D-12 present the observed water levels of screens R-63 and R-63i from May 31 to July 20, 2016. Screens R-63 and R-63i were installed within the lower perched water layer and the regional aquifer, respectively (see Figure D-13), and horizontally this well is about 1200 ft away from pumping well CdV-9-1(i). The predicted results shown in Figure D-6 demonstrate that more than 200 d for the pumping test are needed to influence on a monitoring well at a distance of 1200 ft. The observed water levels at screen R-63 were flat and no obvious pumping-test effect was noted.

Figure D-12 shows an average drawdown of about 0.14 ft or 4 cm at the well screen of R-63i during the pumping test period. However, the observed water levels showed a declining trend before the test (before June 7), and during the test the trend continued until almost the end. The observed drawdown (4 cm) is likely from seasonal variations of water levels. But any faults and fractures in the area may build a good hydraulic connection between the pumping well CdV-9-1(i) and monitoring well R-63 and R-63i, thus leading to some quicker response than the predicted results of Figure D-6. This condition was not considered in the in Figure D-6. Therefore, the pumping test at well CdV-9-1(i) generally had no impact on the water levels at the wells R-63 and R-63i.

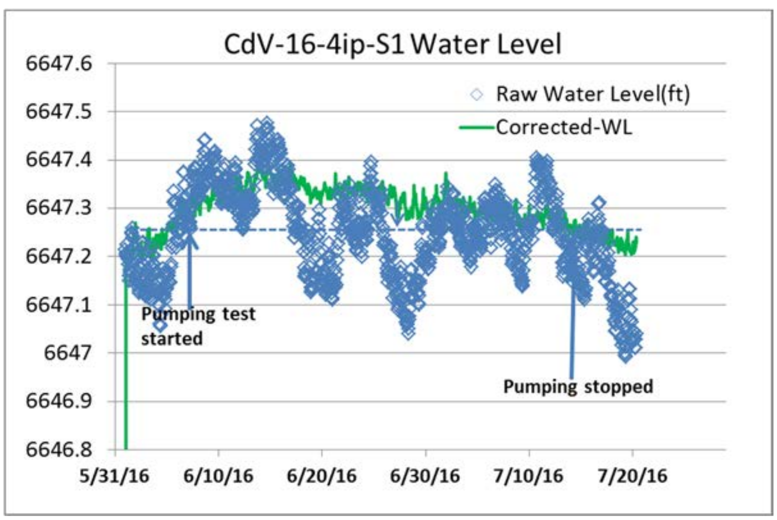

Figure D-9 **Observed water levels at CdV-16-4ip during the pumping test at CdV-9-1(i).**

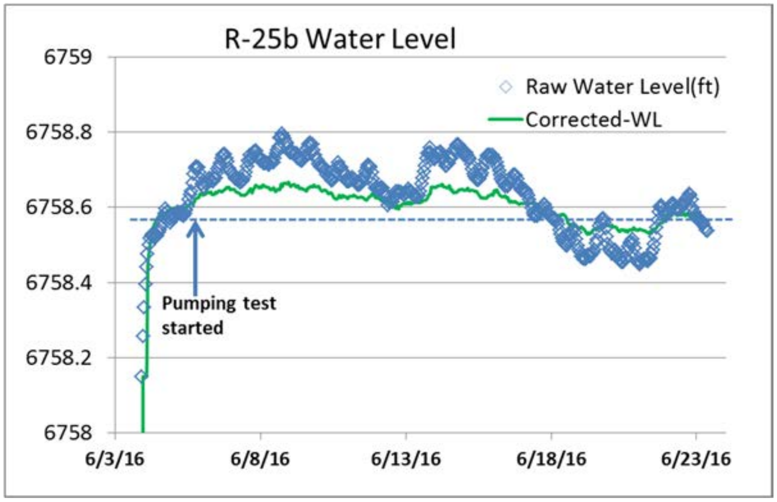

Figure D-10 **Observed water levels at R-25b during the pumping test at CdV-9-1(i)**

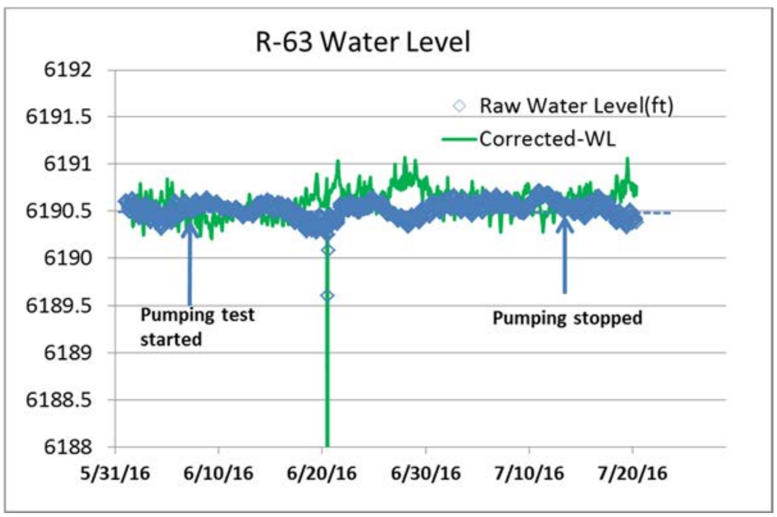

Figure D-11 **Observed water levels at R-63 during the pumping test at CdV-9-1(i)**

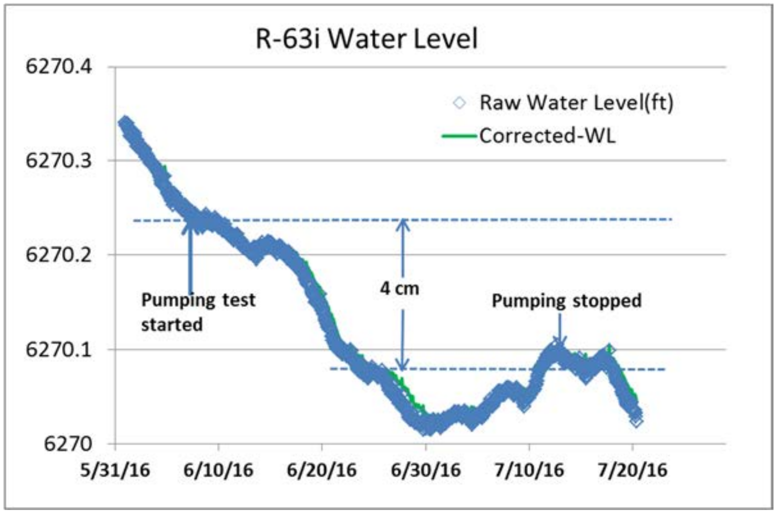

Figure D-12 **Observed water levels at R-63i during the pumping test at CdV-9-1(i)**

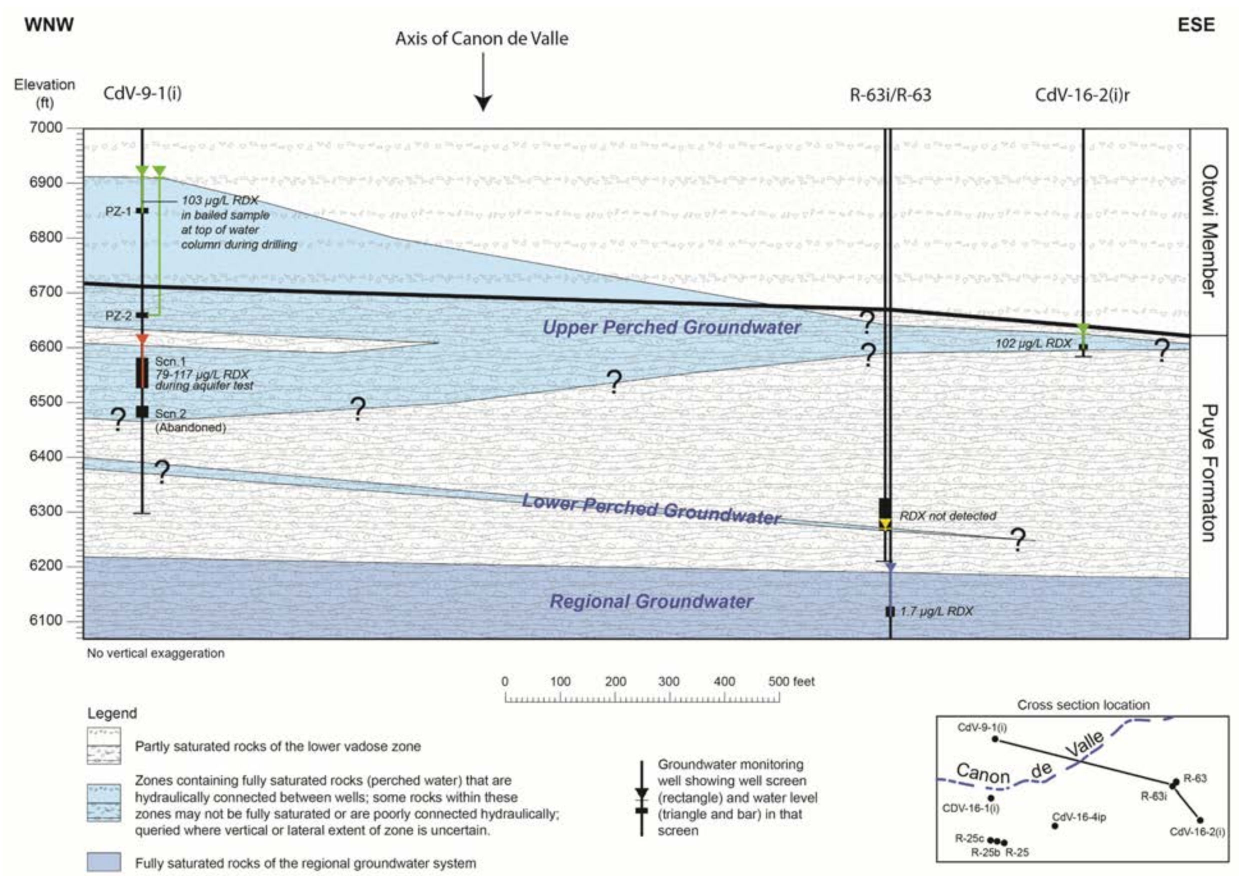

Figure D-13 **West-northwest to east-southeast geologic cross-section through the upper, middle, and lower perched zones (saturation layers) of the vadose zone at CdV-9-1(i), CdV-16-2(i)r, and R-63/R-63i**

D-7.0 SUMMARY

The pumping test at CdV-9-1(i) allowed the hydraulic properties of the perched zone to be estimated by inverse modeling. The different models are applied to estimate the hydraulic parameters. The Theis, Neuman, and Cooper-Jacob models produced a reasonable representation of the observed drawdowns and reasonable and similar hydraulic parameter estimates. The estimated transmissivity of the perched zone is 0.686 m^2/d based on the Neuman method, which is believed to provide the most representative value of the three models (section D-5.0). The hydraulic conductivity is difficult to estimate because the effective thickness of the perched zone is not fully known. The effective thickness is impacted not only by the vertical extent of the saturation but also by anisotropy and screen thickness. Taking into account the screen thickness is 55 ft, the effective thickness of the perched zone is assumed to be 100 ft. As a result, the estimated horizontal hydraulic conductivity is about 0.023 m/d, based on the Neuman method. The estimated storage coefficient is estimated to be about 0.133, which is a reasonable value for unconfined saturation zone conditions. The specific yield of the vadose zone is estimated to be 0.28, which is close to the available previous estimates for porosity of the Puye Formation (theoretically, specific yield is expected to be close to the total water-filled porosity). The anisotropic ratio between vertical and horizontal permeability is estimated to be about 0.01 which is reasonable for the Puye Formation.

The pumping test at CdV-9-1(i) may have produced drawdowns at CdV-9-1(i) PZ-2 and CdV-16-1(i). Given the apparent hydraulic separation between the upper and middle zones of saturation and larger lateral distances at the site (Figure D-5), the observed water-level declines in other monitoring wells may have been caused by other natural hydrogeologic factors (e.g., seasonal fluctuations).

D-8.0 REFERENCES

The following list includes all documents cited in this appendix. Parenthetical information following each reference provides the author(s), publication date, and ERID or ESHID. This information is also included in text citations. ERIDs were assigned by the Environmental Programs Directorate's Records Processing Facility (IDs through 599999), and ESHIDs are assigned by the Environment, Safety, and Health (ESH) Directorate (IDs 600000 and above). IDs are used to locate documents in the Laboratory's Electronic Document Management System and, where applicable, in the master reference set.

Copies of the master reference set are maintained at the New Mexico Environment Department Hazardous Waste Bureau and the ESH Directorate. The set was developed to ensure that the administrative authority has all material needed to review this document, and it is updated with every document submitted to the administrative authority. Documents previously submitted to the administrative authority are not included.

Bouwer, H., May-June 1989. "The Bouwer and Rice Slug Test -- An Update," *Ground Water,* Vol. 27, No. 3, pp. 304-309. (Bouwer 1998, 602218)

Bouwer, H., and R.C. Rice, June 1976. "A Slug Test for Determining Hydraulic Conductivity of Unconfined Aquifers With Completely or Partially Penetrating Wells," *Water Resources Research,* Vol. 12, No. 3, pp. 423-428. (Bouwer and Rice 1976, 064056)

Cooper, H.H., Jr., and C.E. Jacob, August 1946. "A Generalized Graphical Method for Evaluating Formation Constants and Summarizing Well-Field History," *American Geophysical Union Transactions,* Vol. 27, No. 4, pp. 526-534. (Cooper and Jacob 1946, 098236)

Duffield, G.M., June 16, 2007. "AQTESOLV for Windows, Version 4.5, User's Guide," HydroSOLVE, Inc., Reston, Virginia. (Duffield 2007, 601723)

Hantush, M.S., July 1961. "Drawdown around a Partially Penetrating Well," *Journal of the Hydraulics Division, Proceedings of the American Society of Civil Engineers,* Vol. 87, No. HY 4, pp. 83-98. (Hantush 1961, 098237)

Hantush, M.S., September 1961. "Aquifer Tests on Partially Penetrating Wells," Journal of the Hydraulics Division, Proceedings of the American Society of Civil Engineers, pp. 171–195. (Hantush 1961, 106003)

Kruseman, G.P., N.A. de Ridder, and J.M. Verweij, 1991. Excerpted page from *Analysis and Evaluation of Pumping Test Data*, International Institute for Land Reclamation and Improvement, Netherlands. (Kruseman et al. 1991, 106681)

LANL (Los Alamos National Laboratory), June 2015. "Completion Report for Intermediate Aquifer Well CdV-9-1(i)," Los Alamos National Laboratory document LA-UR-15-23954, Los Alamos, New Mexico. (LANL 2015, 600503)

Neuman, S.P., April 1974. "Effect of Partial Penetration on Flow in Unconfined Aquifers Considering Delayed Gravity Response," *Water Resources Research,* Vol. 10, No. 2, pp. 303-312. (Neuman 1974, 085421)

Rasmussen, T.C., and L.A. Crawford, 1997. "Identifying and Removing Barometric Pressure Effects in Confined and Unconfined Aquifers," *Ground Water,* Vol. 35, No. 3, pp. 502-511. (Rasmussen and Crawford 1997, 094014)

Spane, F.A., 2002. "Considering Barometric Pressure in Groundwater Flow Investigations," *Water Resources Research,* Vol. 38, No. 6, pp. 1-18. (Spane 2002, 602105)

Theis, C.V., 1934-1935. "The Relation Between the Lowering of the Piezometric Surface and the Rate and Duration of Discharge of a Well Using Ground-Water Storage," *American Geophysical Union Transactions,* Vol. 15-16, pp. 519-524. (Theis 1934-1935, 098241)

Toll, N.J., October 2005. "User's Manual for BETCO Version 1.00," Sandia National Laboratories. (Toll, N.J. 2005, 602226)

Toll, N.J., and T.C. Rasmussen, January–February 2007. "Removal of Barometric Pressure Effects and Earth Tides from Observed Water Levels," *Ground Water,* Vol. 45, No. 1, pp. 101–105. (Toll and Rasmussen 2007, 104799)

Van Camp, M., and P. Vauterin, 2005. "Tsoft: Graphical and Interactive Software for the Analysis of Time Series and Earth Tides," *Computers & Geosciences,* Vol. 31, pp. 631-640. (Van Camp and Vauterin 2005, 602227)

Attachment D-1

Interpretation of the Slug Tests
Conducted at CdV-9-1(i))

D1-1.0 PZ-1 SLUG TEST

This attachment presents the interpretation results of three slug tests (PZ-1, PZ-2, and S1) at well CdV-9-1(i). The Bouwer-Rice model is used to estimate hydraulic conductivity (Bouwer and Rice 1976, 064056; Bouwer 1998, 602218). The PZ-1 slug test was conducted within the Otowi Member, in a layer of patched water with a thickness of 72.6 ft, and a depth from 604.3 ft to 676.9 ft. The screen of PZ-1 extends from depth 662.9 to 672.4 ft with a screen length of 9.5 ft. The well structure parameters and the estimated conductivity are provided in Tables D1-1 and D1-2. The fitting results are presented in Figure D1-1. The Bouwer-Rice model was used to estimate the hydraulic conductivity of the patched layer. The estimated conductivity is 2.88 m/d, which is higher than the previous information for the Otowi Member (consisting primarily of Bandelier Tuff) because of the relatively high uncertainty of the observed displacements (see Figure D1-1).

Table D1-1
PZ-1 Well Structure and Observation Data

Data Set: E:\EP2016\slugtest\PZ1_try1_slugTest_halfTest_visual.aqt
Title: PZ-1
Date: 05/31/16
Time: 10:44:17

PROJECT INFORMATION

Company: LANL
Client: zd
Project: EP_modeling
Location: Otowi Member
Test Date: 2015
Test Well: PZ-1

AQUIFER DATA

Saturated Thickness: 72.6 ft
Anisotropy Ratio (Kz/Kr): 1.

SLUG TEST WELL DATA

Test Well: PZ-1

X Location: 0. ft
Y Location: 0. ft

Initial Displacement: 4.16 ft
Static Water Column Height: 72.6 ft
Casing Radius: 10. ft
Well Radius: 8.75 ft
Well Skin Radius: 8.75 ft
Screen Length: 9.5 ft
Total Well Penetration Depth: 68.1 ft
Corrected Casing Radius (Butler Method): 2.374 ft
Expected Initial Displacement: 1. ft

Table D1-2
Estimated Conductivity for the Patched Water Layer Within the Otowi Member

Corrected Casing Radius (Butler Method): 2.374 ft
Expected Initial Displacement: 1. ft

No. of Observations: 51

Observation Data

Time (sec)	Displacement (ft)	Time (sec)	Displacement (ft)
0.	4.16	5100.	0.18
300.	2.07	5400.	0.13
600.	0.94	5700.	0.15
900.	1.41	6000.	0.08
1200.	0.86	6300.	0.19
1500.	0.43	6600.	0.16
1800.	0.38	6900.	0.05
2100.	0.33	7200.	0.17
2400.	0.3	7500.	0.13
2700.	0.24	7800.	0.13
3000.	0.25	8100.	0.1
3300.	0.19	8400.	0.1
3600.	0.19	8700.	0.09
3900.	0.18	9000.	0.09
4200.	0.12	9300.	0.17
4500.	0.16	9600.	0.07
4800.	0.2	9900.	0.09

SOLUTION

Slug Test
Aquifer Model: Unconfined
Solution Method: Bouwer-Rice
ln(Re/rw): 0.4101

VISUAL ESTIMATION RESULTS

Estimated Parameters

Parameter	Estimate	
K	2.884	m/day
y0	4.042	ft

K = 0.003339 cm/sec
T = K*b = 63.83 m²/day (7.388 sq. cm/sec)

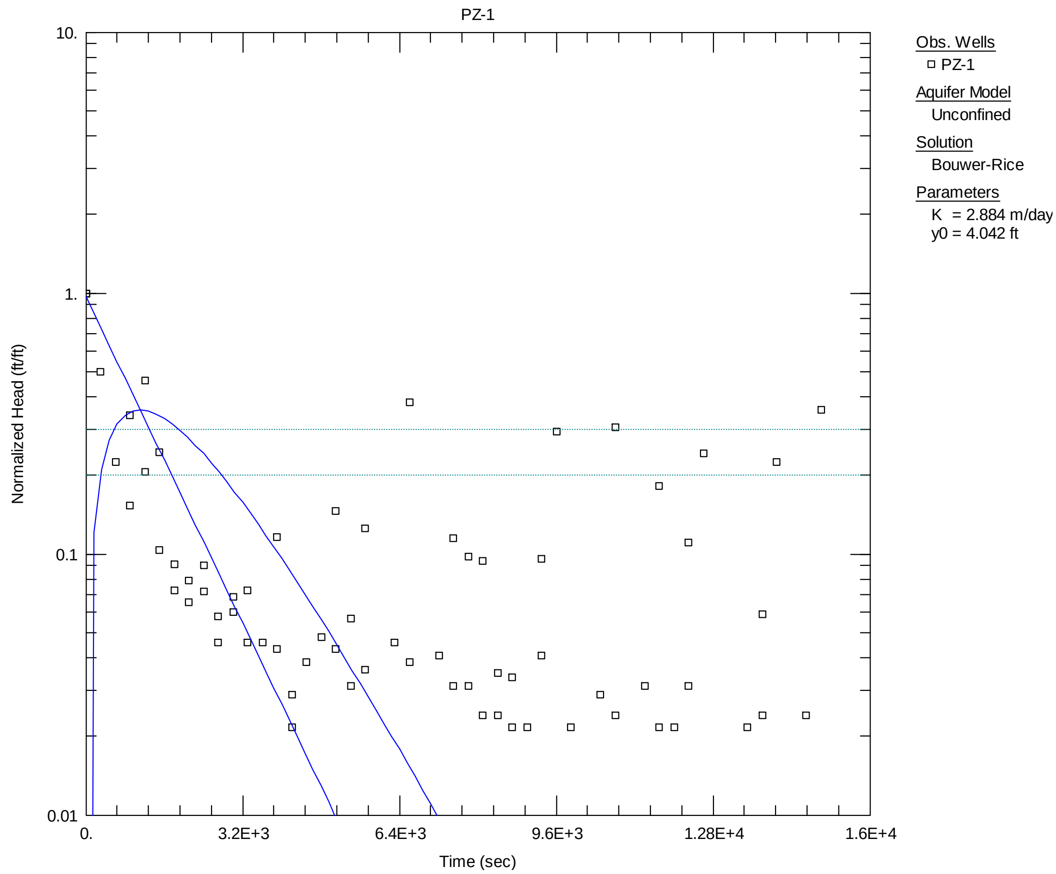

Figure D1-1 The fitting results using the Bouwer-Rice model

D1-2.0 PZ-2 SLUG TEST

The PZ-2 test was conducted at the bottom of the Otowi Member and the top of the Puye Formation, in the upper patched water with a thickness of 182.5 ft, and a depth from 685.1 ft to 867.6 ft. The screen of PZ-2 extends from depth 852.9 to 862.4 ft with a screen length of 9.5 ft. The well structure parameters and the estimated conductivity (0.003 m/d) are listed in Tables D1-3 and D1-4. The fitting results of the PZ-2 test are presented in Figure D1-2. These results are obtained by assuming an anisotropy factor of 1. When the factor is reduced to 0.1 and 0.01, the estimated conductivity increases to 0.0083 and 0.0154 m/d, respectively, while the fittings are the similar to each other. These results indicate that the horizontal conductivity is negatively correlated with the anisotropy factor (Figure D1-3).

Table D1-3
PZ-2 Well Structure and Observation Data

Data Set: E:\EP2016\slugtest\PZ2_try0_slugTest_halfTest_anisotropy0_1.aqt
Title: PZ2
Date: 05/24/16
Time: 10:04:23

PROJECT INFORMATION

Company: LANL
Client: zd
Project: EP_modeling
Location: Qbo_TopTpf
Test Date: 2015
Test Well: PZ2

AQUIFER DATA

Saturated Thickness: 182.5 ft
Anisotropy Ratio (Kz/Kr): 1.

SLUG TEST WELL DATA

Test Well: PZ2

X Location: 0. ft
Y Location: 0. ft

Initial Displacement: 95.2 ft
Static Water Column Height: 182.5 ft
Casing Radius: 10. ft
Well Radius: 8.38 ft
Well Skin Radius: 8.38 ft
Screen Length: 9.5 ft
Total Well Penetration Depth: 177.3 ft
Corrected Casing Radius (Butler Method): 0.5592 ft
Expected Initial Displacement: 1. ft

No. of Observations: 981

Observation Data

Time (sec)	Displacement (ft)	Time (sec)	Displacement (ft)	Time (sec)	Displacement (ft)
0.	95.2	9.81E+4	22.24	1.962E+5	4.548
300.	94.82	9.84E+4	22.07	1.965E+5	4.456
600.	94.4	9.87E+4	21.98	1.968E+5	4.454
900.	93.96	9.9E+4	21.93	1.971E+5	4.445
1200.	93.49	9.93E+4	21.78	1.974E+5	4.468
1500.	92.98	9.96E+4	21.73	1.977E+5	4.363
1800.	92.43	9.99E+4	21.57	1.98E+5	4.349
2100.	91.8	1.002E+5	21.52	1.983E+5	4.4
2400.	91.28	1.005E+5	21.41	1.986E+5	4.329
2700.	90.76	1.008E+5	21.33	1.989E+5	4.267
3000.	90.28	1.011E+5	21.19	1.992E+5	4.249
3300.	89.66	1.014E+5	21.14	1.995E+5	4.263
3600.	89.2	1.017E+5	21.01	1.998E+5	4.215
3900.	88.68	1.02E+5	20.96	2.001E+5	4.179
4200.	88.18	1.023E+5	20.85	2.004E+5	4.162
4500.	87.69	1.026E+5	20.72	2.007E+5	4.131
4800.	87.22	1.029E+5	20.62	2.01E+5	4.124
5100.	86.68	1.032E+5	20.61	2.013E+5	4.071
5400.	86.23	1.035E+5	20.47	2.016E+5	4.087
5700.	85.84	1.038E+5	20.44	2.019E+5	4.066
6000.	85.41	1.041E+5	20.29	2.022E+5	4.053

Table D1-4
Estimated Conductivity for the Patched Water Layer at Bottom of the Otowi Member and Top Layer of Puye Formation

SOLUTION

Slug Test
Aquifer Model: Unconfined
Solution Method: Bouwer-Rice
ln(Re/rw): 0.4641

VISUAL ESTIMATION RESULTS

Estimated Parameters

Parameter	Estimate	
K	0.003002	m/day
y0	93.55	ft

K = 3.474E-6 cm/sec
T = K*b = 0.167 m²/day (0.01933 sq. cm/sec)

AUTOMATIC ESTIMATION RESULTS

Estimated Parameters

Parameter	Estimate	Std. Error	Approx. C.I.	t-Ratio	
K	0.003002	3.86E-6	+/- 7.574E-6	777.6	m/day
y0	93.55	0.08456	+/- 0.1659	1106.2	ft

C.I. is approximate 95% confidence interval for parameter
t-ratio = estimate/std. error
No estimation window

K = 3.474E-6 cm/sec
T = K*b = 0.167 m²/day (0.01933 sq. cm/sec)

Parameter Correlations

	K	y0
K	1.00	0.71
y0	0.71	1.00

Residual Statistics

for weighted residuals

Sum of Squares . . . . 392.7 ft^2
Variance . . . . 0.4011 ft^2
Std. Deviation. . . . . . . 0.6333 ft
Mean . . . . -0.2355 ft
No. of Residuals 981
No. of Estimates 2

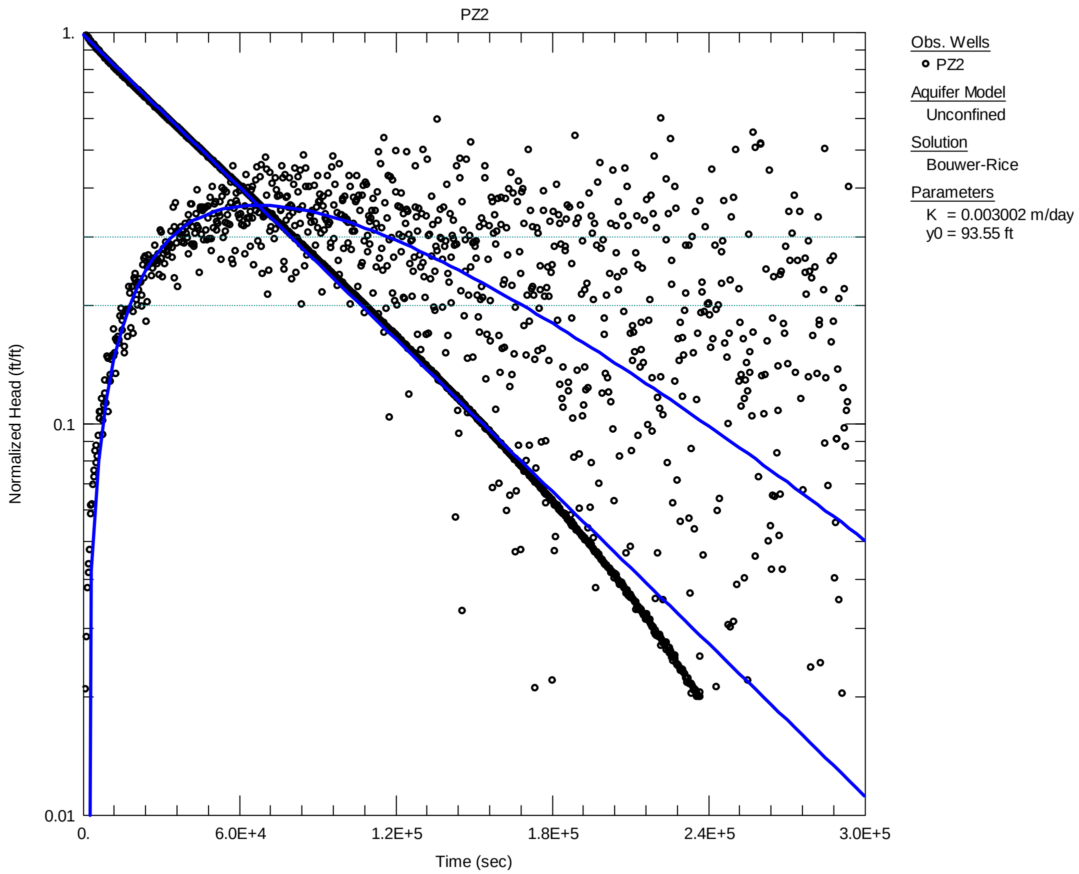

Figure D1-2 The fitting results of PZ-2 test using the Bouwer-Rice model

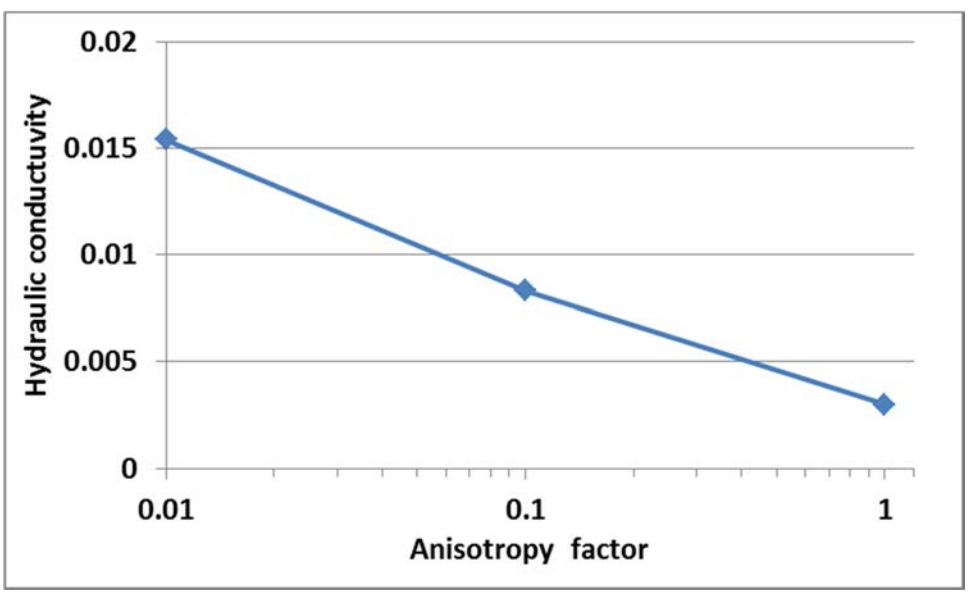

Figure D1-3 The horizontal hydraulic conductivity and anisotropy factor estimated from PZ-2 test

D1-3.0 SCREEN 1 SLUG TEST

The screen 1 (S1) test was conducted at the middle of the Puye Formation, which has a thickness of 123.9 ft, and a depth from 892.8 ft to 1016.7 ft. Screen 1 extends from a depth of 937.4 to 992.4 ft with a screen length of 55 ft. The fitting results of the S1 test in the early time are presented in Figure D1-4. These results (conductivity of 0.0459 m/d) are obtained by assuming an anisotropy factor of 1. When the factor is reduced to 0.1 and 0.01, the estimated conductivity increases to 0.0773 and 0.1065 m/d, respectively, while the fittings are the similar to each other. Figure D1-4 shows a much steep slope in the late-time data. Therefore, the late-time data were used to explore more interpretations. Figure D1-5 shows the fitting results of the late-time data and the estimated conductivity is 0.0848 m/d with an anisotropy factor of 1. When the factor is reduced to 0.1 and 0.01, the estimated conductivity increases to 0.135 and 0.1819 m/d, respectively. These three conductivity values can be converted to log permeabilities of −13.0, −12.8, and −12.67 log(m^2), respectively. These results also indicate that the horizontal conductivity is negatively correlated with the anisotropy factor (Figure D1-6). In summary, the estimated hydraulic conductivity has a range between 0.046 and 0.182 m/d, which is larger than the estimated results of the pumping test at the same screen of CdV-9-1(i). The hydraulic conductivity estimated from pumping test has a range from 0.023 to 0.032 m/d, which is more reliable since the pumping test, which has a larger pumping rate and a much longer pumping time, collects much more reliable observation data.

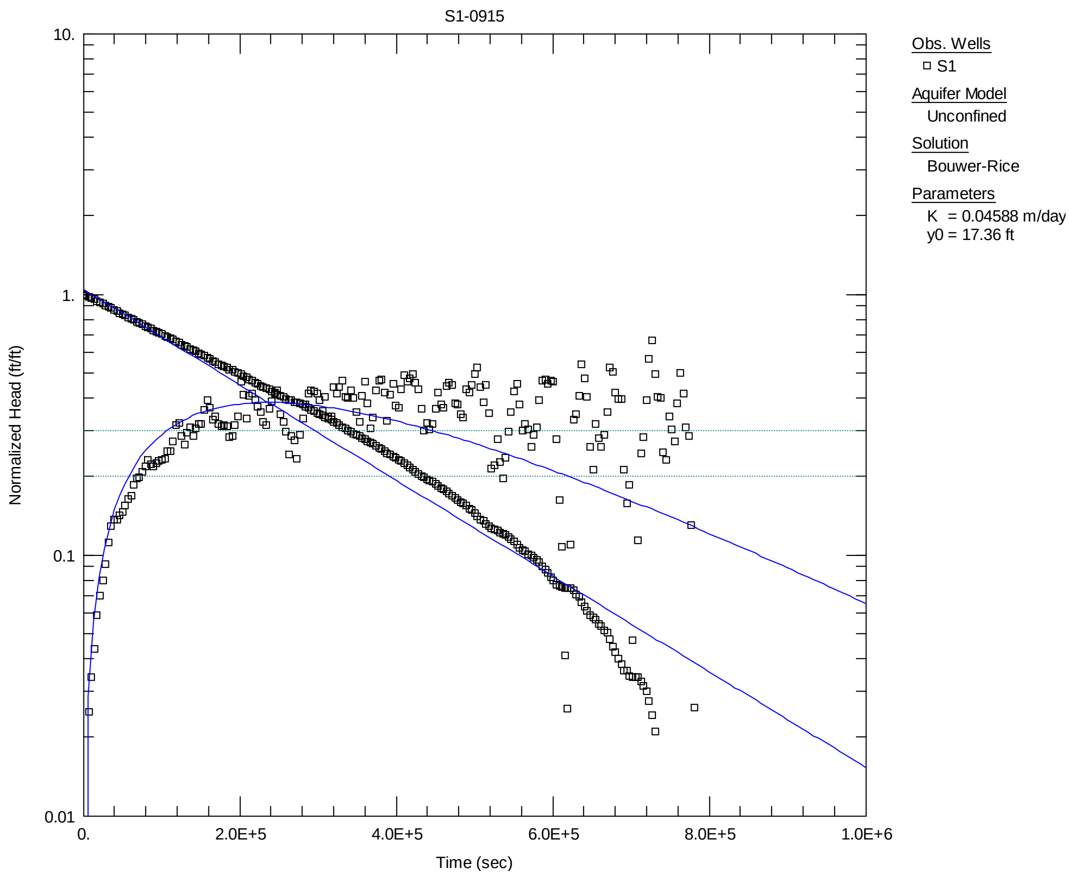

Figure D1-4 The fitting results of S1 test (early-time data) using the Bouwer-Rice model

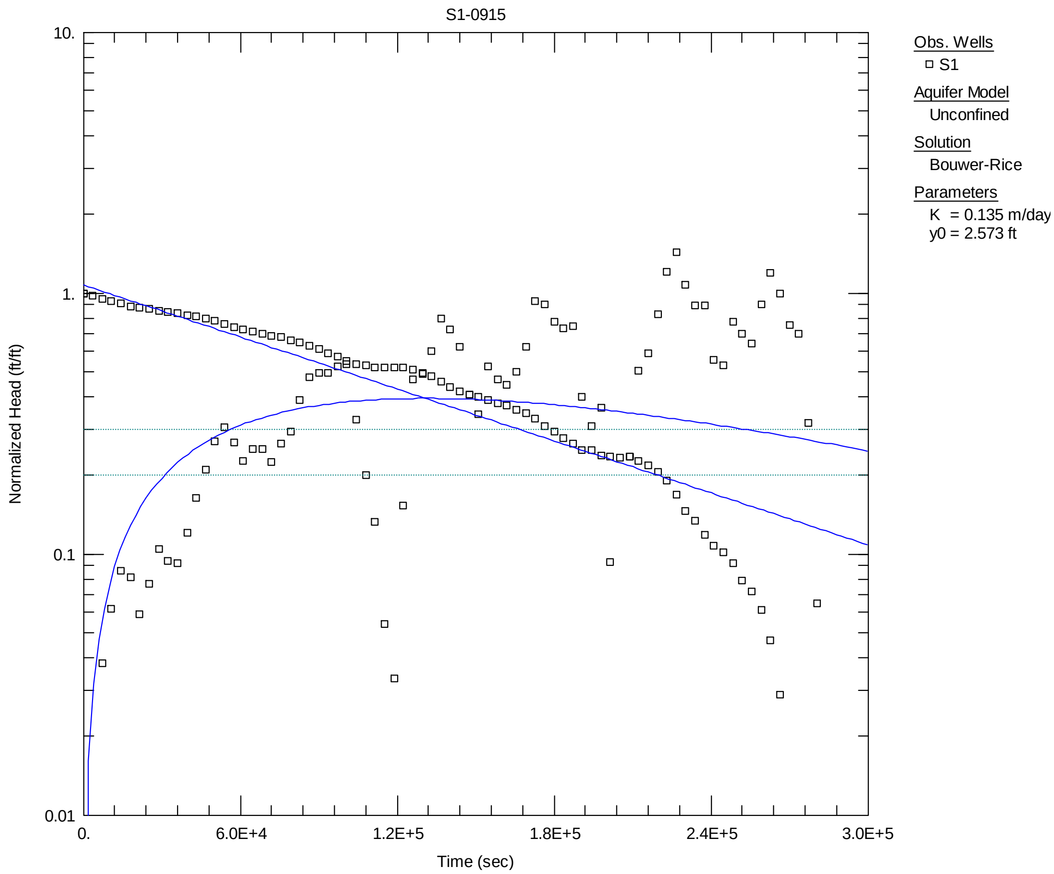

Figure D1-5 The fitting results of S1 test (late-time data) using the Bouwer-Rice model

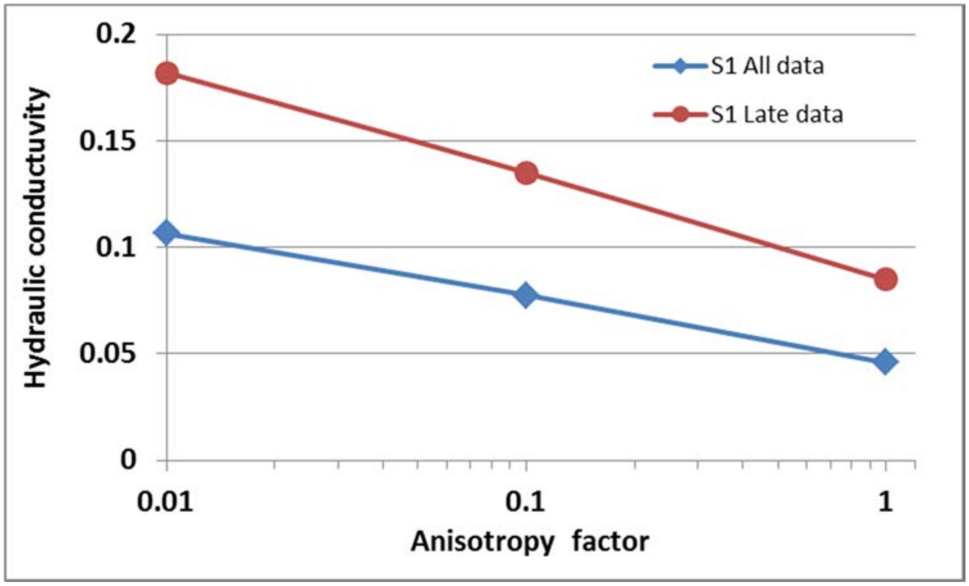

Figure D1-6 The estimated hydraulic conductivity and the anisotropy factor from S1 test

D1-4.0 REFERENCES

The following list includes all documents cited in this attachment. Parenthetical information following each reference provides the author(s), publication date, and ERID or ESHID. This information is also included in text citations. ERIDs were assigned by the Environmental Programs Directorate's Records Processing Facility (IDs through 599999), and ESHIDs are assigned by the Environment, Safety, and Health (ESH) Directorate (IDs 600000 and above). IDs are used to locate documents in the Laboratory's Electronic Document Management System and, where applicable, in the master reference set.

Copies of the master reference set are maintained at the New Mexico Environment Department Hazardous Waste Bureau and the ESH Directorate. The set was developed to ensure that the administrative authority has all material needed to review this document, and it is updated with every document submitted to the administrative authority. Documents previously submitted to the administrative authority are not included.

Bouwer, H., May-June 1989. "The Bouwer and Rice Slug Test -- An Update," *Ground Water,* Vol. 27, No. 3, pp. 304-309. (Bouwer 1998, 602218)

Bouwer, H., and R.C. Rice, June 1976. "A Slug Test for Determining Hydraulic Conductivity of Unconfined Aquifers With Completely or Partially Penetrating Wells," *Water Resources Research,* Vol. 12, No. 3, pp. 423-428. (Bouwer and Rice 1976, 064056)

Appendix E

Analysis of Pumping Test Data for Well CdV-16-1(i)

E-1.0 INTRODUCTION

This appendix describes the analysis of the pumping tests conducted from August 1 to September 23, 2016, at well CdV 16-1(i), located in Technical Area 09. The CdV 16-1(i) tests were conducted at the main well screen (from 6748.2 to 6758.2 ft with a screen length of 10 ft) to characterize the upper perched-water layer and estimate the hydraulic properties of the Otowi Member. The thickness of the perched horizon within the Otowi Member affected during the pumping test is assumed to be 100 ft. The water level was at elevation 6794.6 ft before this test (at 15:19 pm on August 1, 2016).

The pumping well [CdV 16-1(i)] was pumped first from 15:19 on August 1 to 9:30 on August 31 with variable pumping rates between 0.38 and 0.6 gallons per minute (gpm), The tests were stopped and restarted seven times during that period. During the 23-d recovery period, seven rebounds occurred, and each rebound pumping was conducted for about 3 h with rates from 0.47 to 0.64 gpm. The pump rate and water-level variations were monitored, as shown in Figure E-1A and E-1B. The complex pumping, stopping, restarting, and rebound activities were considered in the pumping-test analyses as well (Figure E-1B). Since the changed pumping rates had a large impact on the observed drawdowns and modeling results, analytical models capable of representing variability in the pumping rates were selected to analyze the pumping test; the observed daily-based pumping-rate fluctuations were a model input. The observed water levels were converted to corrected displacements or drawdowns (in feet) by using the observed water level at 15:19 on August 1 as the initial water level (Figure E-1C). Some spikes in the observed water levels (Figure E-1A and E-1C) were removed to reduce the uncertainty or errors in the observation data. The observed water levels are applied as a model calibration targets.

It was assumed that the perched layer (horizon) within the lower Otowi Member’s tuff is a partially penetrated unconfined saturated zone, which is homogeneous and anisotropic. The perched layer is assumed to have a uniform thickness (without boundary effects). The software AQTESOLV (Duffield 2007, 601723) was used to interpret the pumping test data. Three theoretical models, Theis (1934-1935, 098241); Neuman (1974, 085421); and Cooper-Jacob (1946, 098236), are built into the software AQTESOLV and applied for interpreting the pumping test data and estimating hydraulic (groundwater flow) parameters of the saturated zone, including hydraulic conductivity, storage coefficient, specific yield, and anisotropic factor.

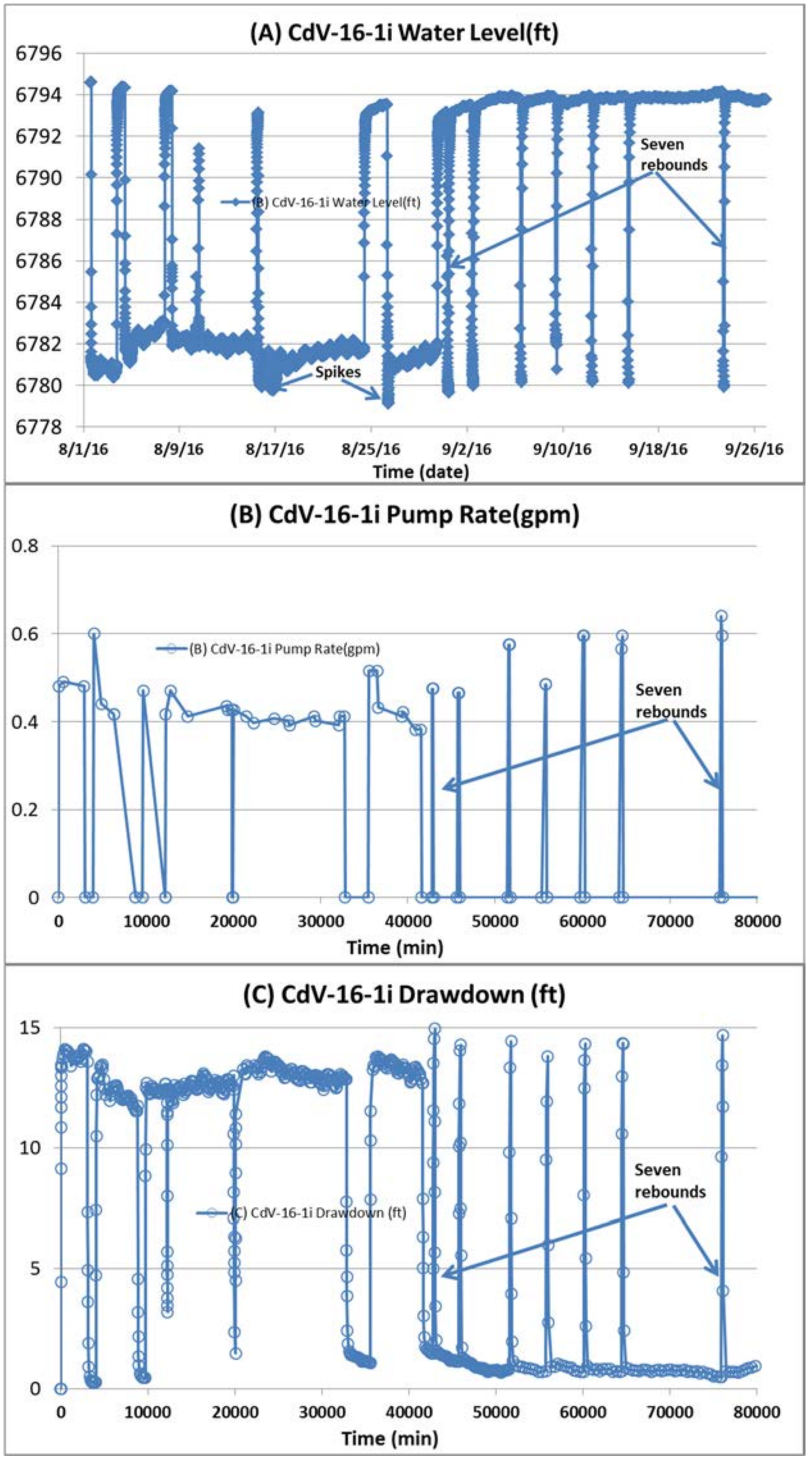

Figure E-1 The original water-level observations (A), pumping-rate fluctuations (B), and corrected water drawdowns (C) for the CdV 16-1(i) pumping test

E-2.0 THEIS MODEL

First, Theis model (Theis 1934–1935, 098241) was used to fit the observed drawdown and recovery data. The Theis model was originally derived for simulating the transient flow towards a fully penetrating well in a horizontally distributed confined aquifer with uniform thickness and homogeneous hydraulic properties. The solution assumed a line source for the pumped well and therefore neglects the wellbore storage (Theis 1934–1935, 098241):

$$s = \frac{Q}{4\pi T}\int_u^\infty \frac{e^{-y}}{y}\,dy = \frac{Q}{4\pi T}W(u), \qquad \textbf{Equation E-1}$$

$$u = \frac{r^2\mu}{4Tt}, \qquad \textbf{Equation E-2}$$

where, *s* is drawdown (L); *Q* is pumping rate [L^3/T]; *T* is transmissivity [L^2/T]; *r* is radial distance [L]; μ is storativity [dimensionless]; *t* is time [T]; and *W*(*u*) is the Theis well function.

Hantush (Hantush 1961, 098237; Hantush 1961, 106003) modified the Theis model for simulating the effects of partial penetration in a uniform-thickness aquifer. The partial penetration correction is as follows:

$$s = \frac{Q}{4\pi T}\left\{W(u) + \frac{2b}{\pi(l-d)}\sum_{n=1}^{\infty}\frac{1}{n}\left[\sin\left(\frac{n\pi l}{b}\right) - \sin\left(\frac{n\pi d}{b}\right)\right]\cos\left(\frac{n\pi z}{b}\right)W\left(u, \sqrt{\frac{K_z}{K_r}}\frac{n\pi r}{b}\right)\right\}, \qquad \textbf{Equation E-3}$$

where, *b* is aquifer thickness [L]; *d* is depth to top of pumping well screen [L]; *d'* is depth to top of observation well screen [L]; *l* is depth to bottom of pumping well screen [L]; *l'* is depth to bottom of observation well screen [L]; *Kz/Kr* is vertical to horizontal hydraulic conductivity anisotropy [dimensionless]; *W(u,β)* is the Hantush-Jacob well function; and *z* is depth to piezometer opening [L].

AQTESOLV (Duffield 2007, 601723) incorporates the Theis solution and modified Hantush solution (Hantush 1961, 098237; Hantush 1961, 106003) for simulating water flow in confined and unconfined aquifers. In this case, Jacob’s correction for partial dewatering of water-table (unconfined) aquifers allows the use of the Theis solution for unconfined aquifers as well. Jacob’s correction were applied as implemented in the software AQTESOLV. AQTESOLV also uses the principle of superposition in time to account for variable-pumping rate tests including recovery. The well structure and pumping-rate data are shown in Table E-1. Table E-2 presents estimated parameters using Theis models. The estimated transmissivity is 0.976 m^2/d, horizontal hydraulic conductivity is 0.032 m/d, and the storage coefficient is 0.001. The computed drawdowns from the Theis model fit the observations reasonably well (Figure E-2).

Table E-1
CdV 16-1(i) Pumping Test Observation
Data Provided as AQTESOLV Input for the Theis Model

Data Set: E:\EP2016\AquiferTest\CdV-16-1i\CdV-16-1i__unconfined_Theis1.aqt
Title: CdV-16-1iTest
Date: 01/17/17
Time: 10:55:14

PROJECT INFORMATION

Company: LANL
Client: zd
Project: ep
Location: Puye
Test Date: 2016
Test Well: CdV-16-1i

AQUIFER DATA

Saturated Thickness: 100. ft
Anisotropy Ratio (Kz/Kr): 0.4991

PUMPING WELL DATA

No. of pumping wells: 1

Pumping Well No. 1: CdV16_1iMain

X Location: 0. ft
Y Location: 0. ft

Casing Radius: 8. ft
Well Radius: 6.38 ft

Partially Penetrating Well
Depth to Top of Screen: 54. ft
Depth to Bottom of Screen: 64. ft

No. of pumping periods: 73

Pumping Period Data

Time (min)	Rate (gal/min)	Time (min)	Rate (gal/min)	Time (min)	Rate (gal/min)
0.	1.0E-5	2.436E+4	0.397	4.588E+4	0.466
6.	0.481	2.47E+4	0.407	4.6E+4	0.
576.	0.491	2.632E+4	0.402	5.143E+4	0.
946.	0.481	2.847E+4	0.392	5.157E+4	0.575
3076.	0.	2.929E+4	0.412	5.164E+4	0.575
3936.	0.	2.941E+4	0.402	5.176E+4	0.
4051.	0.6	3.214E+4	0.392	5.532E+4	0.
4136.	0.441	3.226E+4	0.412	5.577E+4	0.485
4221.	0.417	3.274E+4	0.412	5.584E+4	0.485
6361.	0.401	3.283E+4	0.	5.596E+4	0.
8841.	0.	3.547E+4	0.	5.973E+4	0.
9606.	0.	3.558E+4	0.516	6.01E+4	0.595
9711.	0.417	3.609E+4	0.516	6.019E+4	0.595
1.223E+4	0.	3.609E+4	0.432	6.028E+4	0.
1.226E+4	0.	3.931E+4	0.412	6.423E+4	0.
1.226E+4	0.417	3.943E+4	0.422	6.448E+4	0.565
1.282E+4	0.471	4.09E+4	0.382	6.459E+4	0.595
1.303E+4	0.412	4.153E+4	0.382	6.466E+4	0.

Table E-2
Estimated Parameters Using the Theis Model
for the Perched Layer of the Otowi Member Formation

SOLUTION

Pumping Test
Aquifer Model: Unconfined
Solution Method: Theis

VISUAL ESTIMATION RESULTS

Estimated Parameters

Parameter	Estimate	
T	0.9756	m^2/day
S	0.001163	
Kz/Kr	0.4991	
b	100.	ft

K = T/b = 0.03201 m/day (3.705E-5 cm/sec)
Ss = S/b = 1.163E-5 1/ft

AUTOMATIC ESTIMATION RESULTS

Estimated Parameters

Parameter	Estimate	Std. Error	Approx. C.I.	t-Ratio	
T	0.9756	0.004617	+/- 0.009067	211.3	m^2/day
S	0.001163	5.898E-5	+/- 0.0001158	19.73	
Kz/Kr	0.4991	not estimated			
b	100.	not estimated			ft

C.I. is approximate 95% confidence interval for parameter
t-ratio = estimate/std. error
No estimation window

K = T/b = 0.03201 m/day (3.705E-5 cm/sec)
Ss = S/b = 1.163E-5 1/ft

Parameter Correlations

	T	S
T	1.00	-0.60
S	-0.60	1.00

Residual Statistics

for weighted residuals

Sum of Squares .... 494.6 ft^2
Variance .... 0.8189 ft^2
Std. Deviation....... 0.9049 ft
Mean .... -0.03984 ft
No. of Residuals 606
No. of Estimates 2

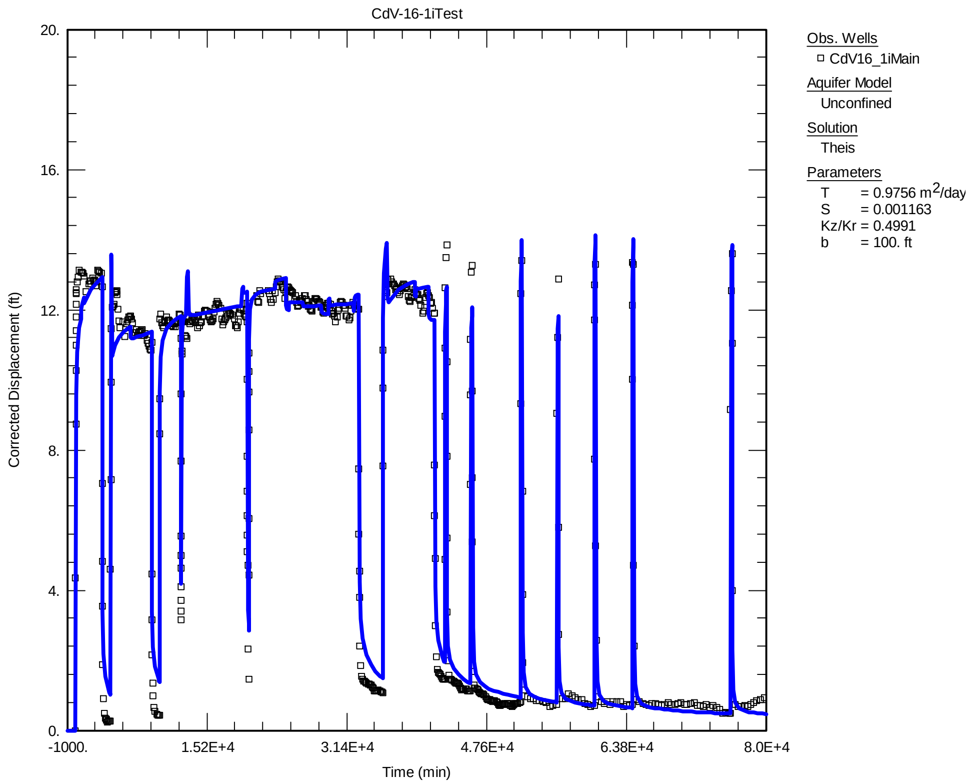

Figure E-2　Representation of the CdV 16-1(i) pumping test using the Theis model

E-3.0 NEUMAN MODEL

The Neuman model (Neuman 1974, 085421) was used to fit the observed drawdown and recovery data as well. By adding a new parameter, "specific yield," to address the delayed gravity response of the unconfined aquifer, Neuman (1974, 085421) derived an analytical solution for simulating the transient flow to a fully or partially penetrating well in a homogeneous, anisotropic unconfined aquifer with delayed gravity response. Therefore, the pumping test analyses using Neuman model also provide information about the properties of the unsaturated zone as well as of the saturated zone. The Neuman model assumes instantaneous drainage at the water table. The solution also assumes a line source for the pumped well and therefore neglects wellbore storage.

$$s = \frac{Q}{4\pi T}\int_0^\infty 4yJ_0(y\sqrt{\beta})\{u_0(y) + \textstyle\sum_{n=1}^{\infty} u_n(y)\}dy, \qquad \textbf{Equation E-4}$$

$$\beta = \frac{r^2K_z}{b^2K_r}, \qquad \textbf{Equation E-5}$$

where, J_0 is Bessel function of first kind and zero order; u_0 and u_n are functions for computing drawdowns in a piezometer or in a partially penetrating observation well (Neuman 1974, 085421). The drawdown in a piezometer is calculated using the following two equations:

$$u_0(y) = \frac{\left[1-\exp\left(-t_s\beta\left(y^2-\gamma_0^2\right)\right)\right]\cosh(\gamma_0 z_D)}{\left[y^2+(1+\sigma)\gamma_0^2-\frac{\left(y^2-\gamma_0^2\right)^2}{\sigma}\right]\cosh(\gamma_0)}\cdot\frac{\sinh\left(\gamma_0(1-d_D)\right)-\sinh\left(\gamma_0(1-l_D)\right)}{(l_D-d_D)\sinh(\gamma_0)}, \qquad \textbf{Equation E-6}$$

$$u_n(y) = \frac{\left[1-\exp\left(-t_s\beta\left(y^2-\gamma_0^2\right)\right)\right]\cos(\gamma_0 Z_D)}{[y^2+(1+\sigma)\gamma_0^2-\frac{\left(y^2-\gamma_0^2\right)^2}{\sigma}]\cos(\gamma_0)} \cdot \frac{\sin\left(\gamma_0(1-d_D)\right)-\sin\left(\gamma_0(1-l_D)\right)}{(l_D-d_D)\sin(\gamma_0)}, \qquad \textbf{Equation E-7}$$

where d_D is dimensionless depth to top of pumping well screen (d/b); l_D is dimensionless depth to bottom of pumping well screen (1/b); Z_D is dimensionless elevation of piezometer opening above base of aquifer (z/b); and the gamma terms are computed numerically.

The Neuman model (built into the software AQTESOLV) was used to estimate the hydraulic parameters by matching the observed drawdowns during the pumping test. The model predicted drawdowns fitted the observation data reasonably well. The estimated parameters are listed in Table E-3. The estimated transmissivity is 0.822 m^2/d, the hydraulic conductivity is 0.027 m/d, storage coefficient is 0.0012, and specific yield is 0.02. The parameter β is a coefficient to describe the hydraulic conductivity anisotropic ratio ($\frac{r^2}{b^2}\frac{K_z}{K_r}$), where, r is radial distance, b is aquifer thickness, K_z is vertical conductivity, and K_r is horizontal conductivity. In this model, the parameter β is 0.002, and the anisotropic ratio of $\frac{K_z}{K_r}$ is equal to 0.5.

Table E-3
Estimated Parameters with the Neuman Model for Perched Layer

Aquifer Model: Unconfined
Solution Method: Neuman

Estimated Parameters

Parameter	Estimate	Std. Error	Approx. C.I.	t-Ratio	
T	0.8219	0.1355	+/- 0.2662	6.064	m^2/day
S	0.001199	7.506E-5	+/- 0.0001474	15.98	
Sy	0.02	0.01007	+/- 0.01979	1.985	
ß	0.002032	0.0009223	+/- 0.001811	2.204	

C.I. is approximate 95% confidence interval for parameter
t-ratio = estimate/std. error
No estimation window

K = T/b = 0.02696 m/day (3.121E-5 cm/sec)
Ss = S/b = 1.199E-5 1/ft

Parameter Correlations

	T	S	Sy	ß
T	1.00	0.80	-0.94	-1.00
S	0.80	1.00	-0.72	-0.81
Sy	-0.94	-0.72	1.00	0.93
ß	-1.00	-0.81	0.93	1.00

Residual Statistics

for weighted residuals

Sum of Squares . . . . 424.4 ft^2
Variance . . . . 0.705 ft^2
Std. Deviation. . . . . . . 0.8396 ft
Mean . . . . 0.147 ft
No. of Residuals 606
No. of Estimates 4

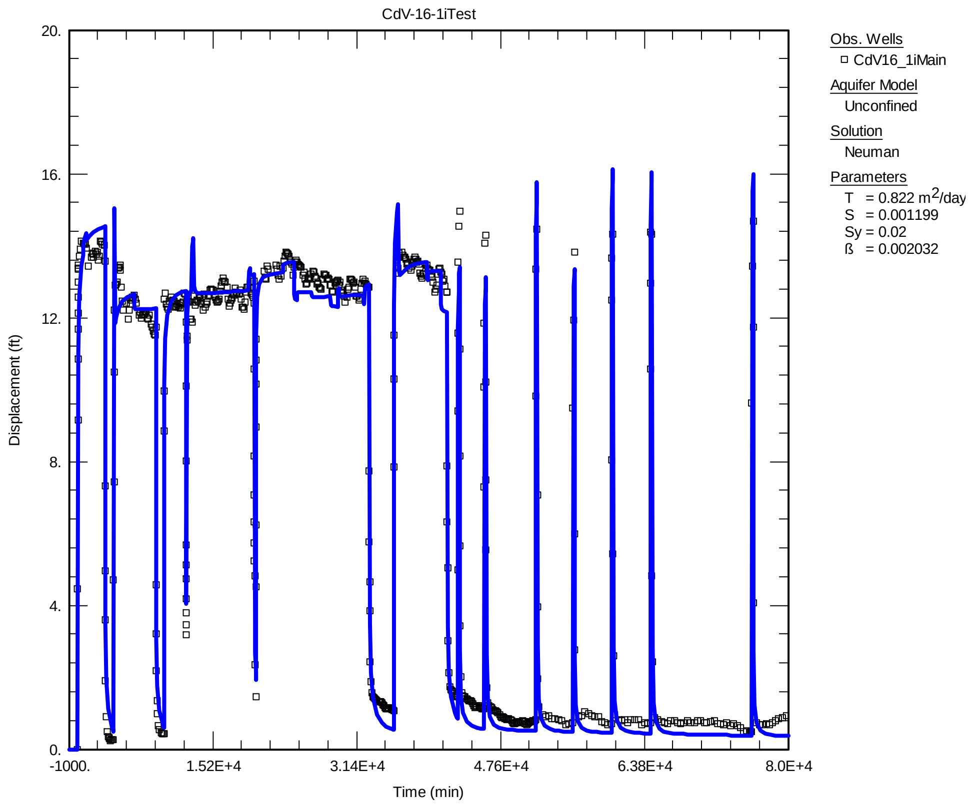

Figure E-3 The fitting results of the CdV 16-1(i) pumping test using the Neuman model

E-4.0 COOPER-JACOB MODEL

The Cooper-Jacob (1946, 098236) solution was originally developed to analyze pumping tests in confined aquifers. The Cooper-Jacob method can be applied for analysis of pumping-test in unconfined aquifers through the correction of drawdown data as described by Kruseman and de Ridder (1991, 106681):

$$s' = s - s^2/2b$$ **Equation E-8**

where s' is corrected displacement [L], s is observed displacement [L], and b is saturated aquifer thickness [L]. The corrected displacement (s') predicted by this equation reaches a maximum of one-half the aquifer saturated thickness (0.5b) when the observed displacement is equal to the saturated thickness of the aquifer ($s = b$). The Cooper-Jacob equation is a simplified approximation of the Theis equation and is valid whenever the u value is less than about 0.05. For small radius values (e.g., corresponding to borehole radii), u is less than 0.05 at very early pumping times and is therefore less than 0.05 for most or all measured drawdown values. Thus, for the pumped well, the Cooper-Jacob equation usually can be considered a valid approximation of the Theis equation. According to the Cooper-Jacob method, the time-drawdown data are plotted on a semilog graph, with time plotted on the logarithmic scale. A straight line of best fit is constructed through the data points and transmissivity is calculated using the following equation:

$$T = \frac{264Q}{\Delta s}$$ **Equation E-9**

where, Δs = change in head over one log cycle of the graph [L]. Because this test well, completed on the Pajarito Plateau, is partially penetrating, an alternate solution considered for assessing aquifer conditions is the Hantush equation for partially penetrating wells (Hantush 1961, 098237; Hantush 1961, 106003) as:

$$s = \frac{Q}{4\pi T}\left[W(u) + \frac{2b^2}{\pi^2(l-d)(l'-d')}\sum_{n=1}^{\infty}\frac{1}{n^2}\left(\sin\frac{n\pi l}{b} - \sin\frac{n\pi d}{b}\right)\left(\sin\frac{n\pi l'}{b} - \sin\frac{n\pi d'}{b}\right)W\left(u, \sqrt{\frac{K_z}{K_r}}\frac{n\pi r}{b}\right)\right]$$ **Equation E-10**

The definitions of the variables and parameters in Equation 10 are the same as those in Equation 3.

The Cooper-Jacob model (built into the software AQTESOLV) was used to estimate the hydraulic parameters by matching the observed drawdowns during the recovery period. The model predicted drawdowns could fit the main trend of the corrected displacements (Figure E-4). The estimated parameters are listed in Table E-4. The estimated transmissivity is 0.931 m^2/d, the hydraulic conductivity is 0.031 m/d, and the storage coefficient is 1.0×10^{-8}, which is too small. Because rebounds occurred during the recovery time, the recovery data that can be used for parameter estimation with the Cooper-Jacob model are very limited, and the estimated parameters may include high uncertainty (e.g., the storage coefficient).

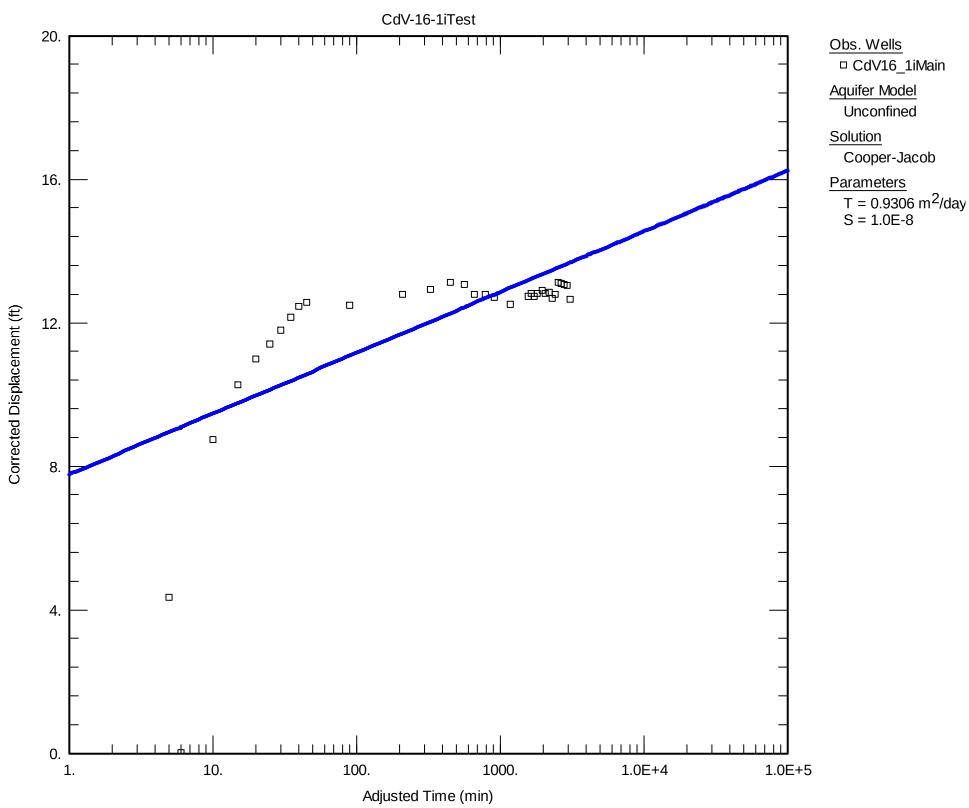

Figure E-4 The fitting results of the CdV 16-1(i) pumping test using the Cooper-Jacob model

Table E-4
Estimated Parameters with the Cooper-Jacob Model for Perched Layer

Aquifer Model: Unconfined
Solution Method: Cooper-Jacob

Estimated Parameters

Parameter	Estimate	Std. Error	Approx. C.I.	t-Ratio	
T	0.9306	0.1358	+/- 0.2769	6.852	m^2/day
S	1.0E-8	2.299E-8	+/- 4.687E-8	0.4351	

C.I. is approximate 95% confidence interval for parameter
t-ratio = estimate/std. error
No estimation window

K = T/b = 0.03053 m/day (3.534E-5 cm/sec)
Ss = S/b = 1.0E-10 1/ft

Parameter Correlations

	T	S
T	1.00	-0.99
S	-0.99	1.00

Residual Statistics

for weighted residuals

Sum of Squares . . . . 59.85 ft^2
Variance . . . . 1.931 ft^2
Std. Deviation. . . . . . . 1.39 ft
Mean . . . . 0.05696 ft
No. of Residuals 33
No. of Estimates 2

E-5.0 COMPARISON AMONG THE THEIS, NEUMAN, AND COOPER-JACOB MODEL RESULTS

The model-fitting results of the pumping test data using the three models are listed in Table E-5. Overall, the Theis model matches the drawdown portion of the curve where the maximum drawdowns are observed. However, this model does not capture the early and late-time (recovery) data very well, or the computed drawdowns during the early recovery periods are higher than those corresponding observations. The Neuman model matches better the early and late-time (recovery) data, but it underestimates the drawdowns for the seven rebounds during the late recovery period. The objective function values or the sum of squares and variance obtained from the Neuman model are lower than those of the Theis model, which means the parameters estimated derived from the Neuman model less uncertain or more robust than those from Theis model. The Cooper-Jacob model only uses the late-time recovery data (it uses less data than the Theis and Neuman models), and the estimation variance is much larger, which means the estimated parameters from this model has highest uncertainty. Based on these observations, the Neuman model is believed to provide the most representative estimates for the parameters.

It is important to note that the imperfect data matching may be caused by the assumption that the perched layer (tested saturation zone) has a uniform thickness, while in reality the perched layer thickness may increase to the west and decrease to the east. Given the assumption of uniform thickness, hydraulic conductivity may be underestimated while the estimated transmissivity may represent an averaged value. Further study, with more complex numerical model with variable thicknesses, may be needed for more accurate descriptions of the pumping test data.

Table E-5 includes also the results from the Theis model analyses presented in Appendix G of this report. The results obtained for transmissivity and presented in in Appendix G are consistent with the estimates obtained here. Table E-5 also includes previous estimates from pumping/slug test analysis (Kleinfelder 2004, 087844, Appendix E). The previous estimates are generally consistent with the new estimates provided here.

Table E-5
Estimated Hydraulic Parameters for CdV-16-1(i)
Using the Theis, Neuman, and Cooper-Jacob Models

Parameters	Theis	Neuman	Cooper-Jacob	Theis Model Analysis[a]	Previous Estimates[b]
Hydraulic conductivity (m/d)	0.032	0.027	0.031	n/a[c]	0.061-0.204
Transmissivity (m^2/d)	0.976	0.822	0.931	0.82	n/a
Storage coefficient (−)	1.2×10^{-3}	1.2×10^{-3}	10^{-8}	n/a	0.1
Anisotropy ratio Kz/Kr (−)	0.499	0.5	0.5	n/a	0.1-1.0
Sum of squared residuals (ft^2)	494.6	424.4	59.85[d]	n/a	n/a
Variance (ft^2)	0.819	0.705	1.931	n/a	n/a

[a] Theis model analysis presented in Appendix G of this report.

[b] Estimates derived from pumping/slug test analysis presented in “Hydrologic Testing Report and Test Data, February 27 to March 4, 2004” (Kleinfelder 2004, 087844).

[c] n/a = Not applicable.

[d] The Cooper-Jacob model only uses recovery data, while Theis and Neuman models use the entire observational record.

E-6.0 IMPACT OF THE CdV 16-1(i) TEST ON SURROUNDING MONITORING WELLS

During the pumping test of well CdV-16-1(i), the water levels in the surrounding wells [e.g. CdV-9-1(i) PZ-1 and PZ-2, CdV-16-4ip, R-25b, R-25 screens 1 and 2, and R-63/R-63i] were also monitored. Analysis of the cross-well responses during the pumping of CdV 16-1(i) is presented in Appendix G.

E-7.0 REFERENCES

The following list includes all documents cited in this appendix. Parenthetical information following each reference provides the author(s), publication date, and ERID or ESHID. This information is also included in text citations. ERIDs were assigned by the Environmental Programs Directorate's Records Processing Facility (IDs through 599999), and ESHIDs are assigned by the Environment, Safety, and Health (ESH) Directorate (IDs 600000 and above). IDs are used to locate documents in the Laboratory's Electronic Document Management System and, where applicable, in the master reference set.

Copies of the master reference set are maintained at the New Mexico Environment Department Hazardous Waste Bureau and the ESH Directorate. The set was developed to ensure that the administrative authority has all material needed to review this document, and it is updated with every document submitted to the administrative authority. Documents previously submitted to the administrative authority are not included.

Cooper, H.H., Jr., and C.E. Jacob, August 1946. "A Generalized Graphical Method for Evaluating Formation Constants and Summarizing Well-Field History," *American Geophysical Union Transactions,* Vol. 27, No. 4, pp. 526-534. (Cooper and Jacob 1946, 098236)

Duffield, G.M., June 16, 2007. "AQTESOLV for Windows, Version 4.5, User's Guide," HydroSOLVE, Inc., Reston, Virginia. (Duffield 2007, 601723)

Hantush, M.S., July 1961. "Drawdown around a Partially Penetrating Well," *Journal of the Hydraulics Division, Proceedings of the American Society of Civil Engineers,* Vol. 87, No. HY 4, pp. 83-98. (Hantush 1961, 098237)

Hantush, M.S., September 1961. "Aquifer Tests on Partially Penetrating Wells," Journal of the Hydraulics Division, Proceedings of the American Society of Civil Engineers, pp. 171–195. (Hantush 1961, 106003)

Kleinfelder, May 7, 2004. "Final Well CdV-16-1(i) Completion Report," report prepared for Los Alamos National Laboratory, Project No. 37151/9.12, Albuquerque, New Mexico. (Kleinfelder 2004, 087844)

Kruseman, G.P., N.A. de Ridder, and J.M. Verweij, 1991. Excerpted page from *Analysis and Evaluation of Pumping Test Data*, International Institute for Land Reclamation and Improvement, Netherlands. (Kruseman et al. 1991, 106681)

Neuman, S.P., April 1974. "Effect of Partial Penetration on Flow in Unconfined Aquifers Considering Delayed Gravity Response," *Water Resources Research,* Vol. 10, No. 2, pp. 303-312. (Neuman 1974, 085421)

Theis, C.V., 1934-1935. "The Relation Between the Lowering of the Piezometric Surface and the Rate and Duration of Discharge of a Well Using Ground-Water Storage," *American Geophysical Union Transactions,* Vol. 15-16, pp. 519-524. (Theis 1934-1935, 098241)

Appendix F

Analysis of Pumping Test Data for Well CdV-16-4ip

F-1.0 INTRODUCTION

This appendix describes the analysis of the pumping tests conducted from September 6 to October 31, 2016, at well CdV-16-4ip, located in Technical Area 16. The CdV-16-4ip tests were conducted at the main well screen (from 6584.7 to 6648.3 ft with a screen length of 63.6 ft) to estimate the hydraulic properties of the Puye Formation. The thickness of the perched horizon within the Puye Formation is assumed to be 100 ft. The water level was at elevation 6647.2 ft before this test began at 11:10 on September 6.

The pumping well (CdV-16-4ip) was pumped first from 11:10 on September 6 to 7:30 on October 11, with variable pumping rates between 3.88 and 7.8 gallons per minute (gpm). During that period, the pump was stopped and restarted three times. During the 20-d recovery period, rebound sampling events occurred over seven periods, during which pumping was conducted for about 1 to 2 h with rates from 7.4 to 7.9 gpm. The pumping rates and water-level variations were monitored as shown in Figure F-1A and F-1B. The complex pumping, stopping, restarting, and rebound activities were considered in the analysis of pumping test results (Figure F-1B). Since the changed pumping rates had a large impact on the observed drawdowns and modeling results, analytical models capable of representing variations in the pumping rates to analyze the pumping test were selected; the observed daily-based pumping-rate fluctuations were a model input. The observed water levels were converted to corrected displacements or drawdowns (in feet) by using the observed water level at 11:10 September 6 as the initial water level (Figure F-1C). The observed water-levels are applied as a model calibration targets.

It was assumed the perched layer (horizon) within the Puye Formation is a partially penetrated, unconfined saturated zone that is homogeneous and anisotropic. The perched layer is assumed to have a uniform thickness (without boundary effects). The software AQTESOLV (Duffield 2007, 601723) is used to interpret the pumping test data. Three theoretical models, Theis (1934-1935, 098241); Neuman (1974, 085421); and Cooper-Jacob (1946, 098236), which are built into the software AQTESOLV, are applied in analyzing the pumping test data and estimating hydraulic (groundwater flow) parameters of the saturated zone, which include hydraulic conductivity, storage coefficient, specific yield, and anisotropic factor.

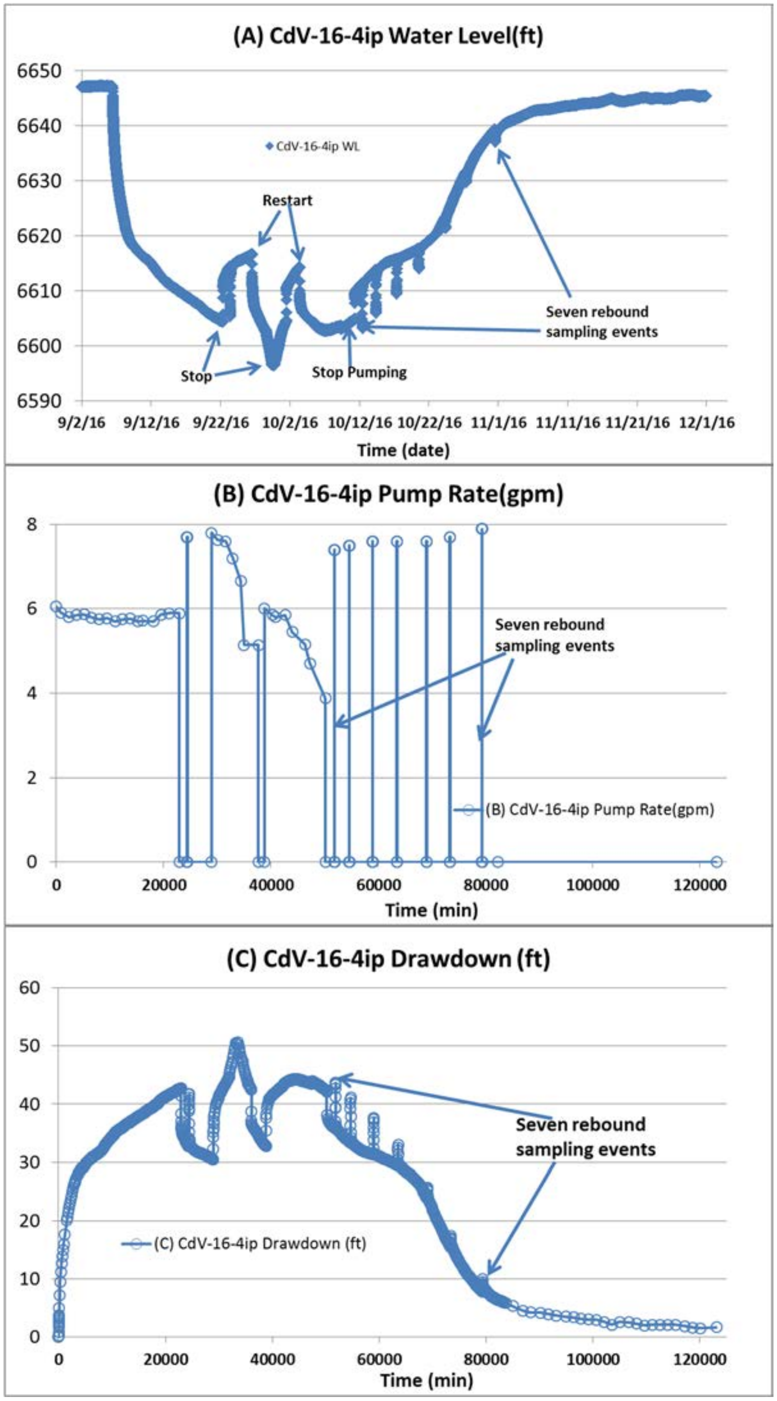

Figure F-1 **The original water level observations (A), pumping rate fluctuations (B), and corrected water drawdowns (C) for the CdV-16-4ip pumping test**

F-2.0 PARAMETER ESTIMATION WITH THE THEIS MODEL

First, the Theis model (Theis 1934–1935, 098241) was used to fit the observed drawdown and recovery data. The Theis model was originally derived for simulating the transient flow towards a fully penetrating well in a horizontally-distributed confined aquifer with uniform thickness and homogeneous hydraulic properties. The solution assumes a line source for the pumped well and therefore neglects the wellbore storage (Theis 1934–1935, 098241):

$$s = \frac{Q}{4\pi T}\int_u^\infty \frac{e^{-y}}{y}\,dy = \frac{Q}{4\pi T}W(u), \qquad \textbf{Equation F-1}$$

$$u = \frac{r^2\mu}{4Tt}\,, \qquad \textbf{Equation F-2}$$

where, *s* is drawdown (L); *Q* is pumping rate [L^3/T]; *T* is transmissivity [L^2/T]; *r* is radial distance [L]; μ is storativity [dimensionless]; *t* is time [T]; and *W*(*u*) is the Theis well function.

Hantush (Hantush 1961, 098237; Hantush 1961, 106003) modified the Theis model for simulating the effects of partial penetration in an aquifer of uniform thickness. The partial penetration correction is as follows:

$$s = \frac{Q}{4\pi T}\left\{W(u) + \frac{2b}{\pi(l-d)}\sum_{n=1}^{\infty}\frac{1}{n}\left[\sin\left(\frac{n\pi l}{b}\right) - \sin\left(\frac{n\pi d}{b}\right)\right]\cos\left(\frac{n\pi z}{b}\right)W(u, \sqrt{\frac{K_z}{K_r}}\frac{n\pi r}{b})\right\}, \qquad \textbf{Equation F-3}$$

where, *b* is aquifer thickness [L]; *d* is depth to top of pumping well screen [L]; *d'* is depth to top of observation well screen [L]; *l* is depth to bottom of pumping well screen [L]; *l'* is depth to bottom of observation well screen [L]; $\frac{K_z}{K_r}$ is vertical to horizontal hydraulic conductivity anisotropy [dimensionless]; *r* is radial distance; *b* is aquifer thickness; K_z is vertical conductivity; K_r is horizontal conductivity; *W(u,β)* is the Hantush-Jacob well function ($\beta = \sqrt{\frac{K_z}{K_r}}\frac{n\pi r}{b}$); and *z* is depth to piezometer opening [L].

AQTESOLV (Duffield 2007, 601723) incorporates the Theis solution and the modified Hantush solution (Hantush 1961, 098237; Hantush 1961, 106003) for simulating water flow in confined and unconfined aquifers. In this case, Jacob's correction for partial dewatering of water table (unconfined) aquifers allows for use of the Theis solution for unconfined aquifers as well. The Jacob's correction was applied as implemented in the software AQTESOLV, which also uses the principle of superposition in time to account for variable-pumping rate tests including recovery. The well structure and pumping-rate data are shown in Table F-1. Table F-2 presents estimated parameters using Theis model. The estimated transmissivity is 1.157 m^2/d, horizontal hydraulic conductivity is 0.042 m/d, and the storage coefficient is 0.35. The estimated effective thickness of the saturated layer is 89.5 ft. The computed drawdowns from the Theis model can fit the observations reasonably well (Figure F-2).

Table F-1
CdV-16-4ip Pumping Test Data
Provided as AQTESOLV Input for the Theis Model

Data Set: E:\EP2016\AquiferTest\CdV-16-4ip\CdV-16-4ip_S1_unconfined_Theis.aqt
Title: CdV-16-4ipTest
Date: 01/25/17
Time: 13:36:09

PROJECT INFORMATION

Company: LANL
Client: zd
Project: ep
Location: TA9
Test Date: 2016
Test Well: CdV-16-4ip

AQUIFER DATA

Saturated Thickness: 89.45 ft
Anisotropy Ratio (Kz/Kr): 0.1707

PUMPING WELL DATA

No. of pumping wells: 1

Pumping Well No. 1: CdV16_4ipMainSall

X Location: 0. ft
Y Location: 0. ft

Casing Radius: 8. ft
Well Radius: 6.38 ft

Partially Penetrating Well
Depth to Top of Screen: 2. ft
Depth to Bottom of Screen: 65.6 ft

No. of pumping periods: 71

Pumping Period Data

Time (min)	Rate (gal/min)	Time (min)	Rate (gal/min)	Time (min)	Rate (gal/min)
0.	7.2	3.114E+4	7.63	5.447E+4	0.
2210.	5.909	3.164E+4	7.6	5.803E+4	0.
2310.	5.8	3.299E+4	7.2	5.803E+4	7.6
3740.	5.85	3.302E+4	6.658	5.898E+4	7.6
5160.	5.87	3.329E+4	5.143	5.913E+4	0.
6545.	5.79	3.566E+4	5.143	6.248E+4	0.
7980.	5.75	3.566E+4	0.	6.248E+4	7.6
9480.	5.78	3.778E+4	0.	6.354E+4	7.6
1.095E+4	5.7	3.778E+4	6.01	6.354E+4	0.
1.233E+4	5.75	3.83E+4	5.85	6.799E+4	0.
1.38E+4	5.77	3.923E+4	5.802	6.805E+4	7.6
1.518E+4	5.7	4.267E+4	5.85	6.855E+4	7.6
1.617E+4	5.72	4.352E+4	5.45	6.859E+4	0.
1.812E+4	5.7	4.539E+4	5.16	7.333E+4	0.
1.95E+4	5.86	4.726E+4	4.71	7.333E+4	7.7
2.097E+4	5.89	4.816E+4	3.88	7.338E+4	7.7
2.243E+4	5.89	4.964E+4	0.	7.348E+4	0.
2.256E+4	0.	5.031E+4	0.	7.932E+4	0.
2.334E+4	0.	5.061E+4	7.4	7.933E+4	7.89
2.344E+4	7.7	5.127E+4	7.4	7.938E+4	7.89
2.445E+4	7.7	5.157E+4	0.	7.938E+4	0.
2.445E+4	0.	5.201E+4	0.	8.237E+4	0.
2.744E+4	0.	5.331E+4	7.5	1.231E+5	0.
2.744E+4	7.8	5.447E+4	7.5		

Table F-2
Estimated Parameters Using the Theis Model for the Puye Formation

Pumping Test
Aquifer Model: Unconfined
Solution Method: Theis

VISUAL ESTIMATION RESULTS

Estimated Parameters

Parameter	Estimate	
T	1.156	m^2/day
S	0.35	
Kz/Kr	0.1707	
b	89.45	ft

K = T/b = 0.04245 m/day (4.913E-5 cm/sec)
Ss = S/b = 0.003917 1/ft

AUTOMATIC ESTIMATION RESULTS

Estimated Parameters

Parameter	Estimate	Std. Error	Approx. C.I.	t-Ratio	
T	1.157	1.702	+/- 3.34	0.6799	m^2/day
S	0.35	0.5073	+/- 0.9958	0.6899	
Kz/Kr	0.1717	0.2181	+/- 0.4281	0.7872	
b	89.35	128.6	+/- 252.4	0.6949	ft

C.I. is approximate 95% confidence interval for parameter
t-ratio = estimate/std. error
No estimation window

K = T/b = 0.04247 m/day (4.916E-5 cm/sec)
Ss = S/b = 0.003917 1/ft

Parameter Correlations

	T	S	Kz/Kr	b
T	1.00	1.00	-0.79	1.00
S	1.00	1.00	-0.77	1.00
Kz/Kr	-0.79	-0.77	1.00	-0.77
b	1.00	1.00	-0.77	1.00

Residual Statistics

for weighted residuals

Sum of Squares . . . . 1.399E+4 ft^2
Variance . . . . 17.67 ft^2
Std. Deviation. . . . . . . 4.203 ft
Mean . . . . 0.7437 ft
No. of Residuals 796
No. of Estimates 4

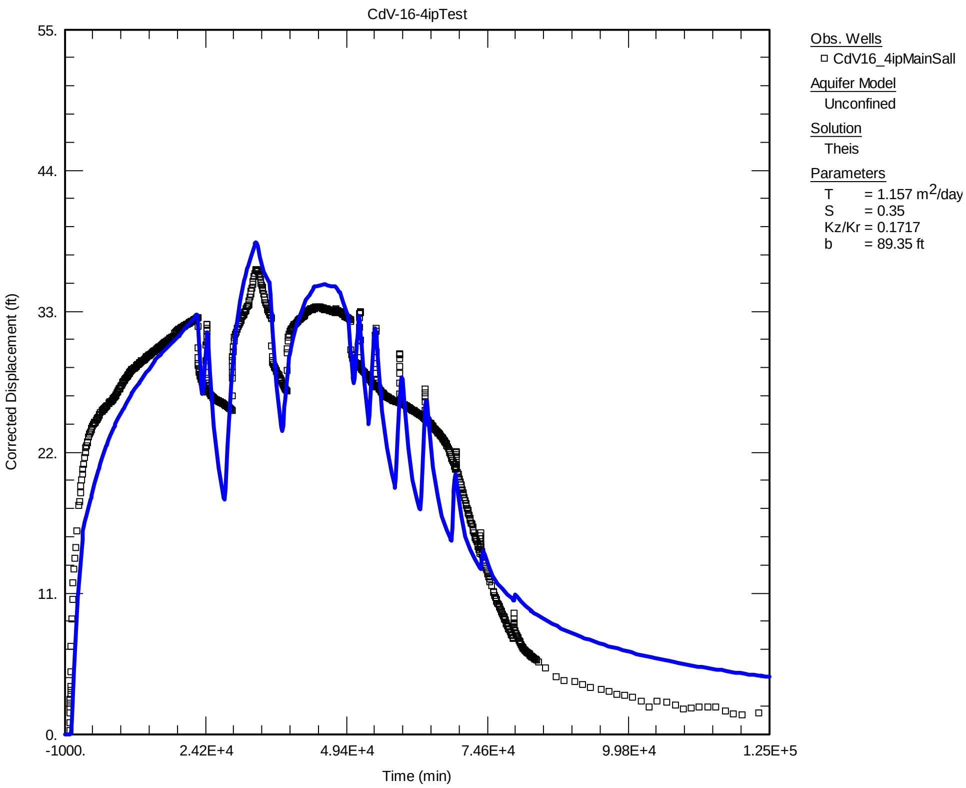

Figure F-2　Representation of the CdV-16-4ip pumping test using the Theis model

F-3.0 NEUMAN MODEL

The Neuman model (Neuman 1974, 085421) was used to fit the observed drawdown and recovery data as well. By adding a new parameter, “specific yield,” to address the delayed gravity response of the unconfined aquifer, Neuman (1974, 085421) derived an analytical solution for simulating the transient flow to a fully or partially penetrating well in a homogeneous, anisotropic unconfined aquifer with delayed gravity response. Therefore, the pumping test analyses using Neuman model also provide information about the properties of the unsaturated zone in addition to the properties of the saturated zone. The Neuman model assumes instantaneous drainage at the water table. The solution also assumes a line source for the pumped well and therefore neglects wellbore storage.

$$s = \frac{Q}{4\pi T}\int_0^\infty 4yJ_0(y\sqrt{\beta})\{u_0(y) + \textstyle\sum_{n=1}^{\infty} u_n(y)\}dy, \qquad \textbf{Equation F-4}$$

$$\beta = \frac{r^2 K_z}{b^2 K_r}, \qquad \textbf{Equation F-5}$$

where, J_0 is Bessel function of first kind and zero order and u_0 and u_n are functions for computing drawdowns in a piezometer or in a partially penetrating observation well (Neuman 1974, 085421). The drawdown in a piezometer is calculated using the following two equations:

$$u_0(y) = \frac{\left[1-\exp\left(-t_s\beta(y^2-\gamma_0^2)\right)\right]\cosh(\gamma_0 z_D)}{[y^2+(1+\sigma)\gamma_0^2-\frac{(y^2-\gamma_0^2)^2}{\sigma}]\cosh(\gamma_0)}\cdot\frac{\sinh(\gamma_0(1-d_D))-\sinh(\gamma_0(1-l_D))}{(l_D-d_D)\sinh(\gamma_0)}, \qquad \textbf{Equation F-6}$$

$$u_n(y) = \frac{\left[1-\exp\left(-t_s\beta\left(y^2-\gamma_0^2\right)\right)\right]\cos(\gamma_0 Z_D)}{\left[y^2+(1+\sigma)\gamma_0^2-\frac{\left(y^2-\gamma_0^2\right)^2}{\sigma}\right]\cos(\gamma_0)} \cdot \frac{\sin\left(\gamma_0(1-d_D)\right)-\sin\left(\gamma_0(1-l_D)\right)}{(l_D-d_D)\sin(\gamma_0)}, \quad \textbf{Equation F-7}$$

where d_D is dimensionless depth to top of pumping well screen (d/b); l_D is dimensionless depth to bottom of pumping well screen (1/b); Z_D is dimensionless elevation of piezometer opening above base of aquifer (z/b); and the gamma term (γ_0) are computed numerically; $t_s = \frac{Tt}{Sr^2}$; S is storativity; and S_y is specific yield.

By using the Neuman model (built into the software AQTESOLV), the hydraulic parameters were estimated by matching the observed drawdowns during the pumping test. The model predicted drawdowns fitted the observation data reasonably well. The estimated parameters are listed in Table F-3. The estimated transmissivity is 1.045 m^2/d, the hydraulic conductivity is 0.035 m/d, the storage coefficient is 0.285, and the specific yield is 0.35. The parameter β is a coefficient to describe the hydraulic conductivity anisotropic ratio ($\frac{r^2}{b^2}\frac{K_z}{K_r}$). In this model, the parameter β is 1.45$\times 10^{-4}$ and the anisotropic ratio of $\frac{K_z}{K_r}$ are equal to 0.037.

Table F-3
Estimated Parameters for the Perched Layer Using with Neuman Model

Pumping Test
Aquifer Model: Unconfined
Solution Method: Neuman

VISUAL ESTIMATION RESULTS

Estimated Parameters

Parameter	Estimate	
T	1.046	m^2/day
S	0.285	
Sy	0.35	
ß	0.0001448	

K = T/b = 0.03472 m/day (4.018E-5 cm/sec)
Ss = S/b = 0.002882 1/ft

AUTOMATIC ESTIMATION RESULTS

Estimated Parameters

Parameter	Estimate	Std. Error	Approx. C.I.	t-Ratio	
T	1.045	0.04608	+/- 0.09046	22.67	m^2/day
S	0.2847	0.008708	+/- 0.01709	32.7	
Sy	0.35	4.176	+/- 8.197	0.08382	
ß	0.0001525	0.0002016	+/- 0.0003958	0.7563	

C.I. is approximate 95% confidence interval for parameter
t-ratio = estimate/std. error
No estimation window

K = T/b = 0.03466 m/day (4.011E-5 cm/sec)
Ss = S/b = 0.002879 1/ft

Parameter Correlations

	T	S	Sy	ß
T	1.00	-0.39	0.82	-0.96
S	-0.39	1.00	0.06	0.15
Sy	0.82	0.06	1.00	-0.93
ß	-0.96	0.15	-0.93	1.00

Residual Statistics

for weighted residuals

Sum of Squares . . . . 8333.9 ft^2
Variance . . . . 10.52 ft^2
Std. Deviation. . . . . . . 3.244 ft
Mean . . . . 0.02461 ft
No. of Residuals 796
No. of Estimates 4

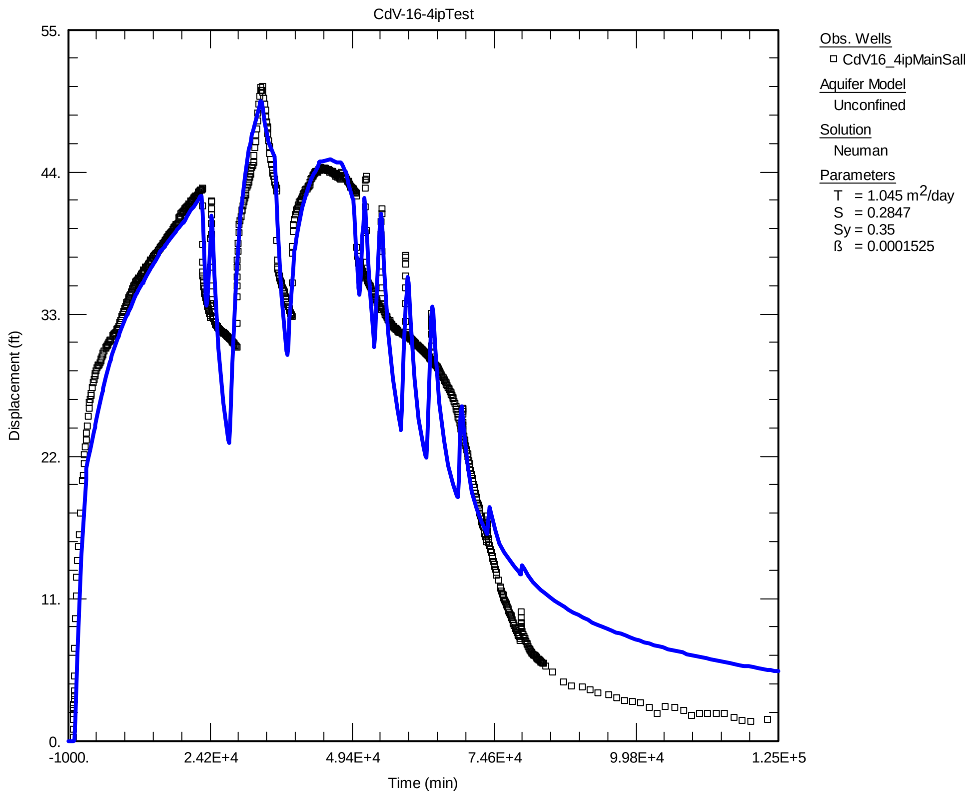

Figure F-3 The fitting results of the CdV-16-4ip pumping test using the Neuman model

F-4.0 COOPER-JACOB MODEL

The Cooper-Jacob solution (Cooper and Jacob 1946, 098236) was originally developed to analyze pumping tests in confined aquifer. The Cooper-Jacob solution can be applied to analyze pumping test in unconfined aquifers through the correction of drawdown data as described by Kruseman and de Ridder (1991, 106681):

$$s' = s - s^2/2b \qquad \textbf{Equation F-8}$$

where s' is corrected displacement [L], s is observed displacement [L], and b is saturated aquifer thickness [L]. The corrected displacement (s') predicted by this equation reaches a maximum of one-half the aquifer saturated thickness (0.5b) when the observed displacement is equal to the aquifer saturated thickness ($s = b$). The Cooper-Jacob equation is a simplified approximation of the Theis equation and is valid whenever the u value is less than about 0.05. For small radius values (e.g., corresponding to borehole radii), u is less than 0.05 at very early pumping times and therefore is less than 0.05 for most or all measured drawdown values. Thus, for the pumped well, the Cooper-Jacob equation usually can be considered a valid approximation of the Theis equation. According to the Cooper-Jacob method, the time-drawdown data are plotted on a semilog graph, with time plotted on the logarithmic scale. A straight line of best fit is constructed through the data points, and transmissivity is calculated using the following equation:

$$T = \frac{264Q}{\Delta s} \qquad \textbf{Equation F-9}$$

where, Δs = change in head over one log cycle of the graph [L]. Because this test well completed on the Pajarito Plateau is partially penetrating, an alternate solution considered for assessing aquifer conditions is the Hantush equation for partially penetrating wells (Hantush 1961, 106003; Hantush 1961, 098237) as:

$$s = \frac{Q}{4\pi T}\left[W(u) + \frac{2b^2}{\pi^2(l-d)(l'-d')}\sum_{n=1}^{\infty}\frac{1}{n^2}\left(\sin\frac{n\pi l}{b} - \sin\frac{n\pi d}{b}\right)\left(\sin\frac{n\pi l'}{b} - \sin\frac{n\pi d'}{b}\right)W\left(u, \sqrt{\frac{K_z}{K_r}}\frac{n\pi r}{b}\right)\right]$$ **Equation F-10**

The definitions of the variables and parameters in Equation F-10 are the same as those in Equation F-3.

The Cooper-Jacob model (built into the software AQTESOLV) was used to estimate the hydraulic parameters by matching the observed drawdowns during the recovery period. The model predicted drawdowns could fit the main trend of the corrected displacements (Figure F-4). The estimated parameters are listed in Table F-4. The estimated transmissivity is 1.606 m^2/d, the hydraulic conductivity is 0.059 m/d, and the storage coefficient is 0.031, which is much smaller than those estimated with Theis and Neuman models. Because seven rebound periods occurred during the recovery time, the recovery data that can be used to estimate parameters with the Cooper-Jacob model are very limited, and the estimated parameters may have high uncertainty (e.g., the storage coefficient).

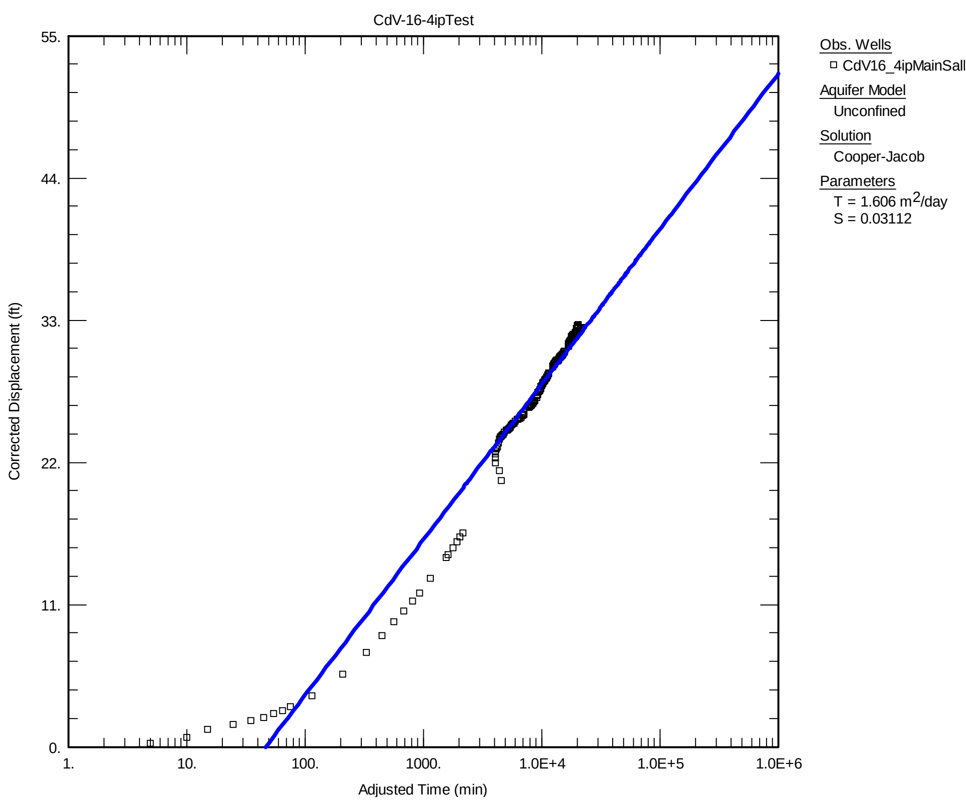

Figure F-4 The fitting results of the CdV-16-4ip pumping test using the Cooper-Jacob model

Table F-4
Estimated Parameters with the Cooper-Jacob Model for the Perched Layer

Pumping Test
Aquifer Model: Unconfined
Solution Method: Cooper-Jacob

VISUAL ESTIMATION RESULTS

Estimated Parameters

Parameter	Estimate	
T	1.606	m^2/day
S	0.03112	

K = T/b = 0.05889 m/day (6.817E-5 cm/sec)
Ss = S/b = 0.0003479 1/ft

AUTOMATIC ESTIMATION RESULTS

Estimated Parameters

Parameter	Estimate	Std. Error	Approx. C.I.	t-Ratio	
T	1.606	0.02516	+/- 0.04964	63.81	m^2/day
S	0.03112	0.002153	+/- 0.004248	14.46	

C.I. is approximate 95% confidence interval for parameter
t-ratio = estimate/std. error
No estimation window

K = T/b = 0.05889 m/day (6.817E-5 cm/sec)
Ss = S/b = 0.0003479 1/ft

Parameter Correlations

	T	S
T	1.00	-0.96
S	-0.96	1.00

Residual Statistics

for weighted residuals

Sum of Squares . . . . 968.7 ft^2
Variance . . . . 5.293 ft^2
Std. Deviation. . . . . . . 2.301 ft
Mean . . . . 0.05131 ft
No. of Residuals 185
No. of Estimates 2

F-5.0 COMPARISON AMONG THE THEIS, NEUMAN, AND COOPER-JACOB MODEL RESULTS

The model fitting results of the pumping test data using the three models are presented in Table F-5. Overall, the Theis and Neuman models match the observed drawdowns of the pumping period reasonably well. However, these two models do not capture very well the recovery data and the seven rebound sampling events, and the computed drawdowns during the recovery period are higher than those corresponding observations. In general, the objective function values or the sum of squares and variance obtained from the Neuman model are lower than those of the Theis model, which means the parameters estimated from the Neuman model are less uncertain or more robust than those derived from the Theis model. The Cooper-Jacob model only uses the late-time recovery data and the estimation variance is much smaller since it uses less data than the Theis and Neuman models. The Neuman model is believed to provide the most representative estimates for the parameters.

It is important to note that the imperfect data matching may be caused by the assumption that the Puye Formation has a uniform saturated thickness, while in reality the saturated thickness may vary at different locations. Because uniform saturated thickness is assumed, hydraulic conductivity may be underestimated while the estimated transmissivity may represent an averaged value. Further study using a more complex numerical model that considers variable saturated thicknesses may be needed for more accurate descriptions of the pumping test data.

Table F-5 includes also the results from the Theis model analyses presented in Appendix G of this report. The results obtained in Appendix G for transmissivity are consistent with the estimates obtained here.

Table F-5
Estimated Hydraulic Parameters for CdV-16-4ip
Using the Theis, Neuman, and Cooper-Jacob Models

Parameters	Theis	Neuman	Cooper-Jacob	Theis Model Analysis[a]
Hydraulic conductivity (m/d)	0.042	0.035	0.059	n/a[b]
Transmissivity T (m^2/d)	1.156	1.046	1.606	1.9
Storage coefficient S (−)	0.35	0.285	0.031	n/a
Anisotropy ratio Kz/Kr (−)	0.171	0.037	0.171	n/a
Sum of squared residuals (ft^2)	13990	8333.9	968.7[c]	n/a
Variance (ft^2)	17.67	10.52	5.29	n/a

[a]Theis model analysis presented in Appendix G of this report.

[b]n/a = Not applicable

[c]The Cooper-Jacob model only uses recovery data while Theis and Neuman models use entire observation data.

F-6.0 IMPACT OF THE CdV-16-4ip TEST ON SURROUNDING MONITORING WELLS

During the pumping test of well CdV-16-4ip, the water levels in the surrounding wells [e.g. CdV-9-1(i)-PZ-1 and PZ-2, CdV-16-1i, R-25b, R-25 screens 1 and 2, and R-63/R-63i] were also monitored. The analysis of these data is provided in Appendix G of this report.

F-7.0 REFERENCES

The following list includes all documents cited in this appendix. Parenthetical information following each reference provides the author(s), publication date, and ERID or ESHID. This information is also included in text citations. ERIDs were assigned by the Environmental Programs Directorate's Records Processing Facility (IDs through 599999), and ESHIDs are assigned by the Environment, Safety, and Health (ESH) Directorate (IDs 600000 and above). IDs are used to locate documents in the Laboratory's Electronic Document Management System and, where applicable, in the master reference set.

Copies of the master reference set are maintained at the New Mexico Environment Department Hazardous Waste Bureau and the ESH Directorate. The set was developed to ensure that the administrative authority has all material needed to review this document, and it is updated with every document submitted to the administrative authority. Documents previously submitted to the administrative authority are not included.

Cooper, H.H., Jr., and C.E. Jacob, August 1946. "A Generalized Graphical Method for Evaluating Formation Constants and Summarizing Well-Field History," *American Geophysical Union Transactions,* Vol. 27, No. 4, pp. 526-534. (Cooper and Jacob 1946, 098236)

Duffield, G.M., June 16, 2007. "AQTESOLV for Windows, Version 4.5, User's Guide," HydroSOLVE, Inc., Reston, Virginia. (Duffield 2007, 601723)

Hantush, M.S., July 1961. "Drawdown around a Partially Penetrating Well," *Journal of the Hydraulics Division, Proceedings of the American Society of Civil Engineers,* Vol. 87, No. HY 4, pp. 83-98. (Hantush 1961, 098237)

Hantush, M.S., September 1961. "Aquifer Tests on Partially Penetrating Wells," Journal of the Hydraulics Division, Proceedings of the American Society of Civil Engineers, pp. 171–195. (Hantush 1961, 106003)

Kruseman, G.P., N.A. de Ridder, and J.M. Verweij, 1991. Excerpted page from *Analysis and Evaluation of Pumping Test Data*, International Institute for Land Reclamation and Improvement, Netherlands. (Kruseman et al. 1991, 106681)

Neuman, S.P., April 1974. "Effect of Partial Penetration on Flow in Unconfined Aquifers Considering Delayed Gravity Response," *Water Resources Research,* Vol. 10, No. 2, pp. 303-312. (Neuman 1974, 085421)

Theis, C.V., 1934-1935. "The Relation Between the Lowering of the Piezometric Surface and the Rate and Duration of Discharge of a Well Using Ground-Water Storage," *American Geophysical Union Transactions,* Vol. 15-16, pp. 519-524. (Theis 1934-1935, 098241)

Appendix G

Pumping Test Results for CdV-9-1(i),
CdV-16-1(i), and CdV-16-4ip

G-1.0 Introduction

This appendix summarizes modeling methodology and results related to the analysis of 2016 pumping tests with the primary objective of inferring new information about cross-hole hydraulic conductivity of the vadose zone at the Technical Area 16 (TA-16) site of RDX (hexahydro-1,3,5-trinitro-1,3,5-triazine) contamination site. In 2016, pumping tests were conducted in CdV-9-1(i) (TA-09), CdV-16-1(i) (TA-09), and CdV-16-4ip (TA-16). The CdV-9-1(i) tests were conducted at the main well screen (screen 1), located within the Puye Formation (937.4- to 992.4-ft depth with a screen length of 55 ft). The CdV-16-1(i) tests were also conducted at the main well screen, located within the upper perched-water layer of the Otowi Member (6748.2- to 6758.2-ft depth with a screen length of 10 ft). Finally, the CdV-16-4ip tests were conducted at the main well screen (screen 1), also located within the Puye Formation (6584.7- to 6648.3-ft depth with a screen length of 63.6 ft).

CdV-9-1(i), CdV-16-1(i), and CdV-16-4ip were pumped in the summer and early fall of 2016, and the pumping regimes are shown in Figure G-1. During each individual test, the pumps were shut off intermittently. Average pumping rates are reported below for the times the pumps were active. Pumping at CdV-9-1(i) occurred from June 7 to July 27, 2016, with an average pumping rate of 1.95 gallons per minute (gpm). Pumping at CdV-16-1(i) occurred from August 1 to September 23, with an average pumping rate of 0.437 gpm. Pumping at CdV-16-4ip occurred from September 6 to October 31, with an average pumping rate of 6.08 gpm.

During the tests, the water levels were observed at the following monitoring well locations: CdV-9-1(i) screen 1, CdV-9-1(i) piezometer 1 (PZ-1), CdV-9-1(i) piezometer 2 (PZ-2), CdV-16-1(i), CdV-16-2ir, CdV-16-4ip screen 1, R-25 screen 1, R-25 screen 2, R-25 screen 4, R-25b, R-47i, R-63, and R-63i. The wells where the pumping tests occurred were also used as observation wells. Also, all the wells except R-63 are intermediate screened potentially in the same zone of saturation as CdV-16-4ip. The analyzed water-level data were obtained from a database storing all the observed water levels at the Los Alamos National Laboratory (LANL or the Laboratory) site. Pumping rates were also obtained from a similar database. The barometric data were obtained from http://weather.lanl.gov for the meteorological station at TA-54. Pumping records for the supply wells were obtained from Los Alamos County.

G-2.0 ANALYSIS OF WATER-LEVEL DATA OBSERVED AT PUMPING WELLS

CdV-9-1(i)

CdV-9-1(i) screen 1 water levels during the CdV-9-1(i) pump test exhibited drawdown recovery behavior that may be more indicative of low complexity and less stratification (Figure G-2) when compared with data collected at CdV-16-4ip, for example. Before pumping began, an unidentified hydrologic event resulted in a surge in water level at this well (the water level rise might have been caused by an infiltration event). This event was also potentially observed in CdV-9-1(i) PZ-2 and may indicate a hydrologic transient that cannot be represented using the analytical modeling tools applied here.

The moderate pumping rates (~2 gpm) at CdV-9-1(i) resulted in water-level decline of ~40 ft. The first stage of pumping was relatively short, resulting in a moderate decline in water level to ~6593 ft, followed by recovery after the pump was shut off and prolonged drawdown during the second (longest) stage of pumping, which occurred from June 14 to July 11, 2016, and resulted in a maximum decline in water level to ~6570 ft. This decline was followed by intermittent pumping at a slightly higher rate, which caused sharp declines in water level; these decreases did not drastically influence recovery to background water levels. The general rate of water-level decrease during prolonged pumping (second stage) was initially rapid but declined over time, potentially indicating an approach to steady-state drawdown for pumping rates of 1.8 to 2.0 gpm. Absence of drastic declines in water level before the minimum water level is reached suggests dewatering of the borehole did not occur. No major inflection points are apparent in the water-level curves, suggesting major hydrostratigraphic contacts or boundaries may not exist in the vicinity of the pumped screen interval.

CdV-16-1(i)

Changes in water levels of CdV-16-1(i) during the pump test are difficult to interpret because of the low pumping rates during the test (Figure G-3). The maximum decline in water-level elevation observed at the pumping well was ~17 ft and corresponds to a water level of ~6778 ft. Extended duration pumping at ~0.4 gpm resulted in an accelerated decrease in water level until a relatively steady plateau was reached at ~6781 ft, potentially indicating the achievement of a steady-state flow regime at this pumping rate. During periods where pumping ceased, the water level quickly recovered to levels close to the background prepumping condition. The recovery data did not show inflection points in recovery temporal trends that could suggest hydraulic effects caused by hydrostratigraphic contacts or boundary effects. The absence of any substantial decreases in water level before the minimum level was reached, further suggests dewatering of the borehole did not occur at the applied pumping rates.

CdV-16-4ip

The water level at CdV-16-4ip screen 1 during pumping demonstrates the complexity in the pumped zone of saturation and potential stratification in this area (Figure G-4). A similar water-level profile was observed during both the 2011 and 2014 pump tests of the same screen (LANL 2011, 111608, Figure B-7.0-1; LANL 2014, 600004, Figure B-2). Initially, pumping at ~6 gpm caused a rapid decline in water level to an elevation of ~6620 ft (Figure G-4), followed by a decrease in the rate of water-level decline until the elevation reached ~6605 ft when pumping stopped. Some recovery in water level occurred at ~6615 ft until pumping restarted. Subsequent pump cycles resulted in accelerated decreases in water level, especially when pumping rates are the highest (~7.8 gpm), although a plateau in observed water level occurred during pumping from October 3 to 11 as a result of incremental decreases in pumping rate. The minimum water level observed was ~6595 ft, resulting in a maximum decrease in water level of ~50 ft. However, below 6602 ft, the water level declined very rapidly, suggesting dewatering of the borehole. During the final stage of the pump test, short-duration pumping occurred intermittently, causing sharp decreases in water level that did not drastically interfere with recovery to background water levels. As with the 2014 pump test, inflection points in the water-level recovery curve at ~6615 and ~6620 ft suggest that hydrostratigraphic contacts affect the flow towards the saturated zone pumped by well; the elevations of the inflection points in the water-level recovery curve potentially identify the elevations of these hydrostratigraphic contacts. More permeable hydrostratigraphic zones are potentially located between ~6600 and ~6620 ft. However, the groundwater flow along these more permeable zones is not sufficient to provide sustainable pumping of CdV-16-4ip at a rate of 6 to 8 gpm.

G-3.0 ANALYSIS OF WATER-LEVEL DATA AT THE NEARBY MONITORING WELLS

Figures G-5 to G-19 show the water levels at the monitoring wells near CdV-9-1(i), CdV-16-1(i), and CdV-16-4ip during the pumping test period after removal of barometric pressure effects. The observation wells are CdV-9-1(i) screen 1, CdV-9-1(i) PZ-1, CdV-9-1(i) PZ-2, CdV-16-1(i), CdV-16-2ir, CdV-16-4ip screen 1, R-25 screen 1, R-25 screen 2, R-25 screen 4, R-25b, R-47i, R-63, and R-63i. The barometric pressure and tidal effects in the observed water levels are removed using a Laboratory-developed code called CHipBETA that utilizes the methodology developed by Toll and Rasmussen (2007, 104799). The code allows for automated removal of the barometric and tidal effects in the water-level data. After the barometric pressure and tidal effects are removed, the pumping effects in the water-level data were analyzed using the method described in Harp and Vesselinov (2011, 227709). The analyses utilize two open-source codes also developed at the Laboratory: WELLS (http://wells.lanl.gov) and MADS (http://mads.lanl.gov). WELLS is applied to simulate the drawdowns caused by the pumping. MADS is applied to (1) deconstruct pumping impacts caused by different pumping wells and (2) estimate hydrogeologic properties of the tested saturation zone by matching the simulated and observed hydraulic heads at the observation wells. In general, the model analysis using this approach was found to be difficult because of low pumping rates and because many of these observation wells are in the intermediate-perched zone, where additional physical processes may not be explicitly included in the model (e.g., capillarity, variably saturated flow) and additional signals may not be adequately removed during data preprocessing (e.g., barometric pressure fluctuations not removed by the approach of Toll and Rasmussen [2007, 104799]). Although these factors resulted in an imperfect model fit, this approach was still found to be an effective tool that aids in understanding hydraulic cross-hole connectivity between wells at the site.

Figures G-5 to G-19 present the results of this analysis. Each figure shows the model-based deconstruction of the water-level transients observed in each monitoring well. The upper panels in each figure depict the observed and simulated water levels at the monitoring well, and the lowest panel depicts the individual contributions of each pump test to drawdown at the observation well. Dashed lines in the lowest panel represent a general linear trend of water-level decline that is independent of responses that may be attributable to pumping associated with the aquifer tests. The trend in water-level decline is not explicitly represented in the model but may influence interpretation of water-level responses (these values are included while calculating simulated “total” hydraulic head). For all observation wells, the model was calibrated using water-level data from the 2016 pumping tests. Since longer water-level records are available, CdV-16-4ip screen 1, R-25 screen 2, R-25b, R-47i, and R-63 were also calibrated using the 2014 pump test along with the 2016 tests. Although longer water-level records exist for CdV-16-2ir, CdV-16-1(i), and R-25 screen 1, irregularities (i.e., measurement error, sensor drift) in the water-level data between the 2014 and 2016 pumping tests made model calibration using the entire dataset difficult, so these results are not included.

The following is a summary of the interpretation of modeling results for the observation wells analyzed. In addition to Figures G-5 to G-19, the maximum simulated drawdown contribution of each pumping well that occurs at each observation well in 2016 is presented in Table G-1. Drawdown contributions less than 1 cm are considered to be negligible.

(1) Analysis of CdV-9-1(i) screen 1 (Figure G-5) is dominated by drawdown from pumping at this well, and simulations suggest negligible impact of pumping at CdV-16-1(i). The analysis also suggests the pumping at CdV-16-4ip screen 1 is also affecting the water level in CdV-9-1(i) screen 1, with a maximum drawdown contribution of 23 cm (Table G-1). The influence of CdV-16-4ip screen 1 on CdV-16-4ip screen 1 is examined more closely in Figure G-6. The figure reveals that this relationship is somewhat questionable because the model under predicts drawdown from CdV-16-4ip screen 1 pumping. Furthermore, the rate of decrease in water levels fluctuates considerably for the duration of the CdV-16-4ip screen 1 pump test, despite fairly consistent pumping rates. The changes in water levels are more likely the result of additional hydrogeological processes occurring during the pumping tests that affect water-level transients [e.g., the water level sharply increases in May 2016 before the CdV-9-1(i) screen 1 pumping starts; after that the water level slowly rebounds]. It is expected the water-level increase may have been caused by infiltration. These types of processes are not captured in the current model analyses.

(2) CdV-9-1(i) PZ-1 analysis (Figure G-7) suggests negligible impact of any 2016 pumping tests on water levels at this screen.

(3) By contrast, CdV-9-1(i) PZ-2 model analysis (Figure G-8) suggests some impact of pumping at CdV-16-1(i) and CdV-16-4ip on water levels at this screen, although the maximum drawdown contribution is less than 10 cm (Table G-1). Considering the noise in the CdV-9-1(i) PZ-2 water levels as well as the lack of a good match between the observed and model-predicted water levels (Figure G-8), it would seem pumping effects at CdV-9-1(i) PZ-2 during the 2016 pumping tests are somewhat questionable.

(4) Analysis of CdV-16-1(i) (Figure G-9) is dominated by drawdown from pumping at this well, and simulations suggest negligible impact of pumping at CdV-9-1(i) and CdV-16-4ip.

(5) Analysis of CdV-16-2ir (Figure G-10) shows some impact of pumping with a maximum contribution of 8.4 cm from CdV-9-1(i) and 3.2 cm from CdV-16-4ip (Table G-1). However, the noise in the CdV-16-2ir water levels as well as the lack of a good match between the observed and model-predicted water levels (Figure G-10) indicate the pumping effects at CdV-16-2ir during the 2016 pumping tests are somewhat questionable.

(6) Figure G-11 shows simulated and observed water levels at CdV-16-4ip screen 1 for both 2014 and 2016 tests. The model is capable of simulating the large drawdowns that result from pumping at this well, but drawdown resulting from pumping at the other wells is negligible.

(7) Analysis of R-25 screen 1 (Figure G-12) reveals negligible influence of pumping tests on water levels.

(8) R-25 screen 2 water levels (Figure G-13) show some influence of pumping at CdV-9-1(i) and CdV-16-4ip. Figure G-13 shows that water levels in R-25 screen 2 responded to both the 2014 and 2016 pumping tests at CdV-16-4ip, with a maximum drawdown contribution of 7.0 cm in 2016 (Table G-1). The maximum contribution of pumping at CdV-9-1(i) in 2016 to drawdown in R-25 screen 2 was 2.1 cm (Table G-1). The relatively good match between the observed and model-predicted water levels (Figure G-13) indicates that the pumping effects at R-25 screen 2 during the 2016 tests are more certain.

(9) For R-25 screen 4, separate model calibrations were attempted for the 2014 and 2016 pumping tests. However, water-level data appear to be unreliable, which may be a result of plugging or inadequate sensitivity of the pressure transducer. During the 2014 pumping test (Figure G-14), the model predicted a response in observed water levels R-25 screen 4 to pumping at CdV-16-4ip. However, the modeled drawdown does not accurately coincide with the pumping start and end times, the pumping effects at R-25 screen 4 during the 2014 tests are questionable. During the 2016 test (Figure G-15), changes in observed water levels at R-25 screen 4 were negligible, resulting in erroneous model fit and maximum predicted drawdown contributions less than 0.0046 m.

(10) R-25b analysis (Figure G-16) shows some response of water levels in this well to pumping in CdV-9-1(i) and CdV-16-4ip during both the 2014 and 2016 tests, although these responses are practically negligible (the drawdown contribution was 1.6 cm in 2016).

(11) Analysis of R-47i (Figure G-17) also shows that pumping at CdV-16-4ip influences water levels during both the 2014 and 2016 tests. Drawdown at this well resulting from pumping at CdV-9-1(i) is also simulated with a maximum response of 4.1 cm. However, the signal from CdV-16-4ip is

very small, with a maximum drawdown contribution of only 1.9 cm. Furthermore, the model does not fit the data very well, and a fluctuation in water levels that mirrors the decreases in water levels during the 2014 and 2016 pump tests also occurs in August 2015. It is possible these decreases may be attributed to some other seasonal hydrologic process not captured in our current model analyses.

(12) Analysis of R-63 (Figure G-18) included pumping at Los Alamos County water supply wells PM-4 and PM-5 because the well screen is located in the regional aquifer, and these wells appear responsible for the larger water-level fluctuations. This analysis included data from 2014 to 2016. CdV-16-4ip pumping also appears to influence drawdown at R-63, albeit to a small degree with only a 2.4-cm maximum contribution (Table G-1). This drawdown contribution does not clearly match any discernable trend in the observed water levels at R-63 and, therefore, is questionable. Previous reports suggest no impact of CdV-16-4ip pumping on R-63 pressures from the vertical hydraulic separation between the pumping and observation screens: CdV-16-4ip is pumping a perched zone in the vadose zone above the regional aquifer; R-63 is screened in the regional aquifer.

(13) Although the water-level dataset for R-63i is extremely noisy (Figure G-19), modeling captured at least some of the fluctuations observed at this well. It appears that pumping at CdV-16-4ip and CdV-16-1(i) may influence water levels at R-63i because they resulted in maximum simulated drawdown contributions of 4.2 and 12 cm, respectively. Still, relatively poor match between the observed and model-predicted water levels (Figure G-19) indicate pumping effects at R-63i during the 2016 pumping tests are somewhat questionable.

The calibrated parameter values are presented in Table G-2. For each observation well model analysis, transmissivity (m^2/d) and storativity (m) are calibrated for each pumping well. These values represent the effective transmissivity and storativity between the observation and pumping wells. In general, large storativity estimates are caused by low sensitivity of observation well drawdowns to pumping transients, and large transmissivities estimates are caused by negligible influence of pumping on drawdown at the observation well. Exceedingly large transmissivities and small storativies do not represent real physical values but instead indicate lack of hydraulic connectivity. Table G-2 lists only effective transmissivity and storativity estimates that are considered reasonable and representative of drawdowns that are sufficiently well identified based on the available data. (Estimated parameters that resulted in drawdown contributions less than 1 cm were considered unrepresentative and ignored.)

G-4.0 REFERENCES

The following list includes all documents cited in this appendix. Parenthetical information following each reference provides the author(s), publication date, and ERID or ESHID. This information is also included in text citations. ERIDs were assigned by the Environmental Programs Directorate's Records Processing Facility (IDs through 599999), and ESHIDs are assigned by the Environment, Safety, and Health (ESH) Directorate (IDs 600000 and above). IDs are used to locate documents in the Laboratory's Electronic Document Management System and, where applicable, in the master reference set.

Copies of the master reference set are maintained at the New Mexico Environment Department Hazardous Waste Bureau and the ESH Directorate. The set was developed to ensure that the administrative authority has all material needed to review this document, and it is updated with every document submitted to the administrative authority. Documents previously submitted to the administrative authority are not included.

LANL (Los Alamos National Laboratory), January 2011. "Completion Report for Intermediate Well CdV-16-4ip," Los Alamos National Laboratory document LA-UR-11-0187, Los Alamos, New Mexico. (LANL 2011, 111608)

LANL (Los Alamos National Laboratory), October 2014. "Interim Measures Report for Source-Removal Testing at Well CdV-16-4ip," Los Alamos National Laboratory document LA-UR-14-27065, Los Alamos, New Mexico. (LANL 2014, 600004)

Toll, N.J., and T.C. Rasmussen, January–February 2007. "Removal of Barometric Pressure Effects and Earth Tides from Observed Water Levels," *Ground Water,* Vol. 45, No. 1, pp. 101–105. (Toll and Rasmussen 2007, 104799)

Vesselinov, V.V., and D.R. Harp, October 2011. "Adaptive Hybrid Optimization Strategy for Calibration and Parameter Estimation of Physical Models," Los Alamos National Laboratory document LA-UR-11-11755, Los Alamos, New Mexico. (Vesselinov and Harp 2011, 227709)

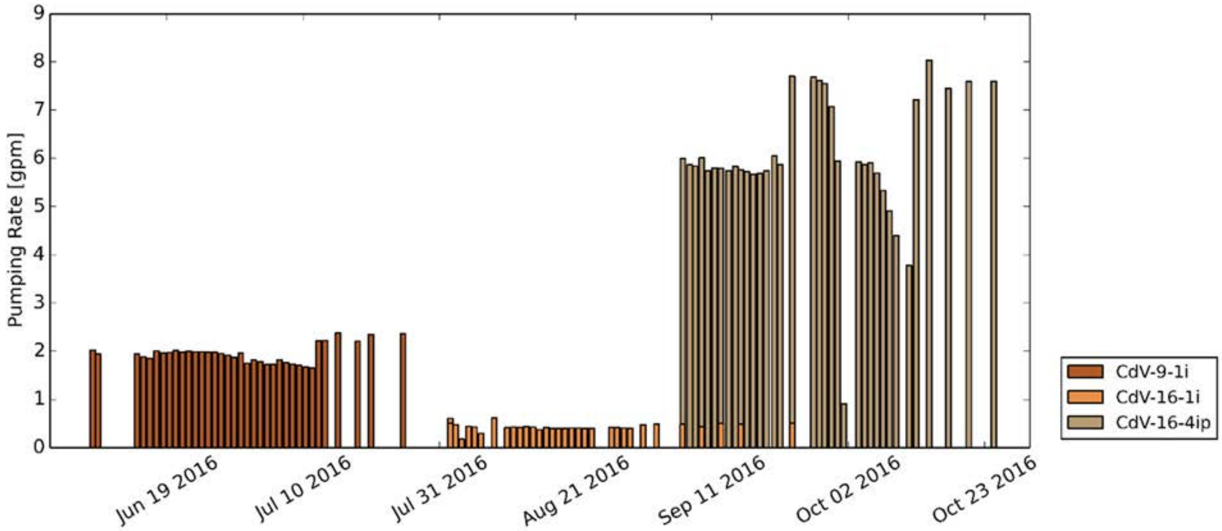

Figure G-1 **Daily averaged pumping rate (gpm) during 2016 pumping tests conducted at CdV-9-1(i), CdV-16-1(i), and CdV-16-4ip**

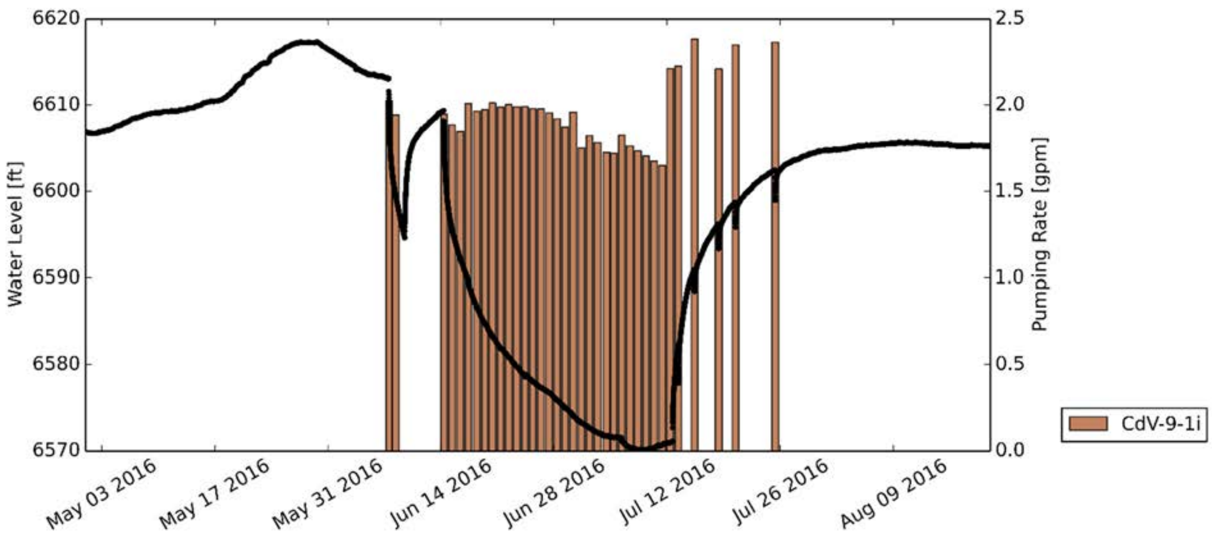

Figure G-2 **Water-level elevation (ft) and pumping rates (gpm) at CdV-9-1(i) during 2016 pumping tests. Note that a water level increase occurs in May 2016 immediately before the pumping test started; this increase may have been caused by an infiltration event.**

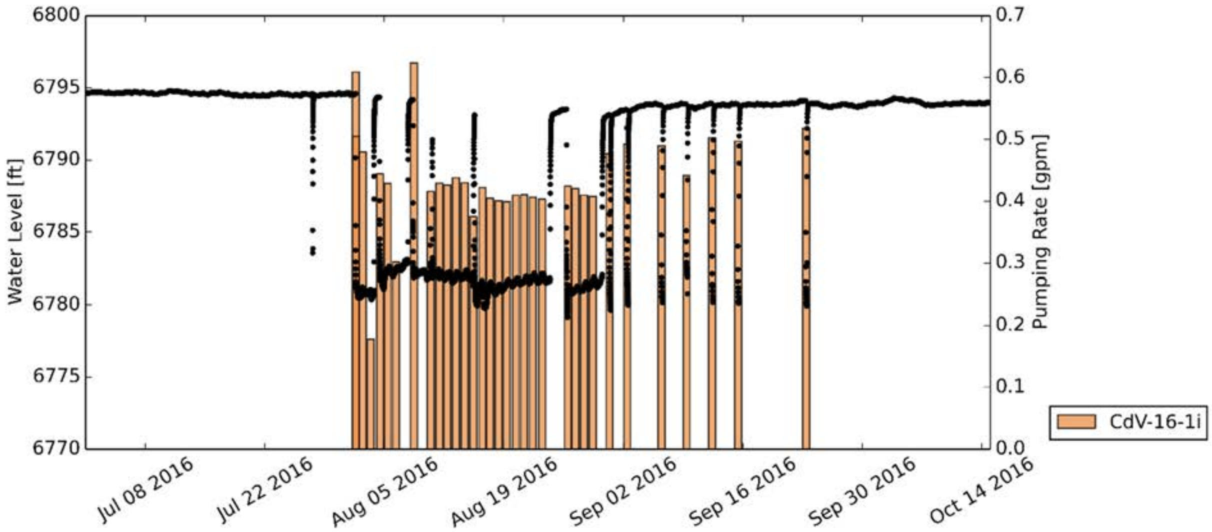

Figure G-3 Water-level elevation (ft) and pumping rates (gpm) at CdV-16-1(i) during 2016 pumping tests

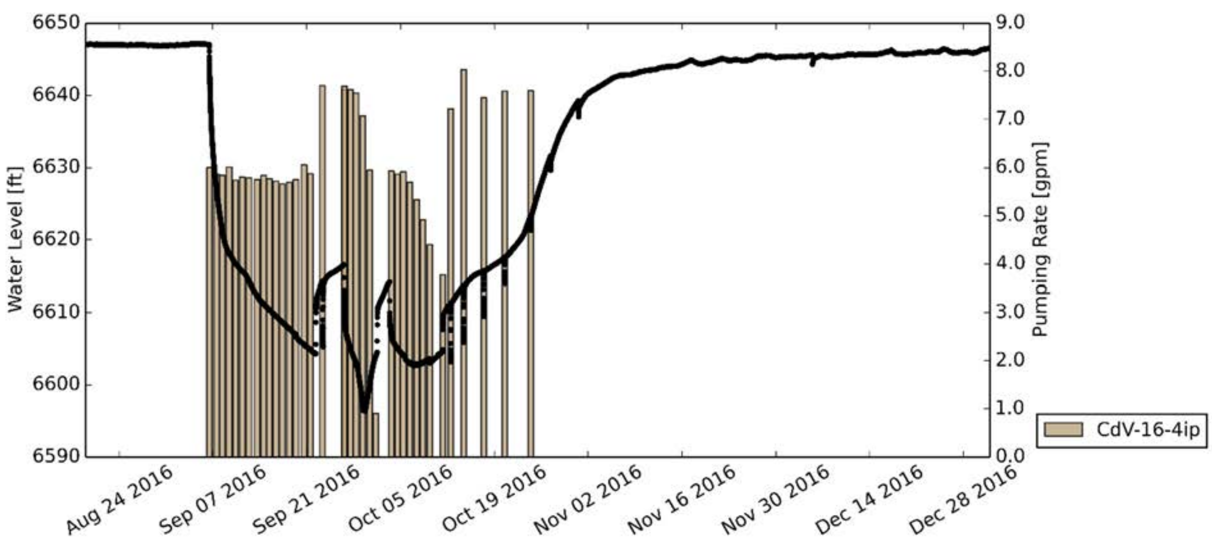

Figure G-4 Water-level elevation (ft) and pumping rates (gpm) at CdV-16-4ip during 2016 pumping tests

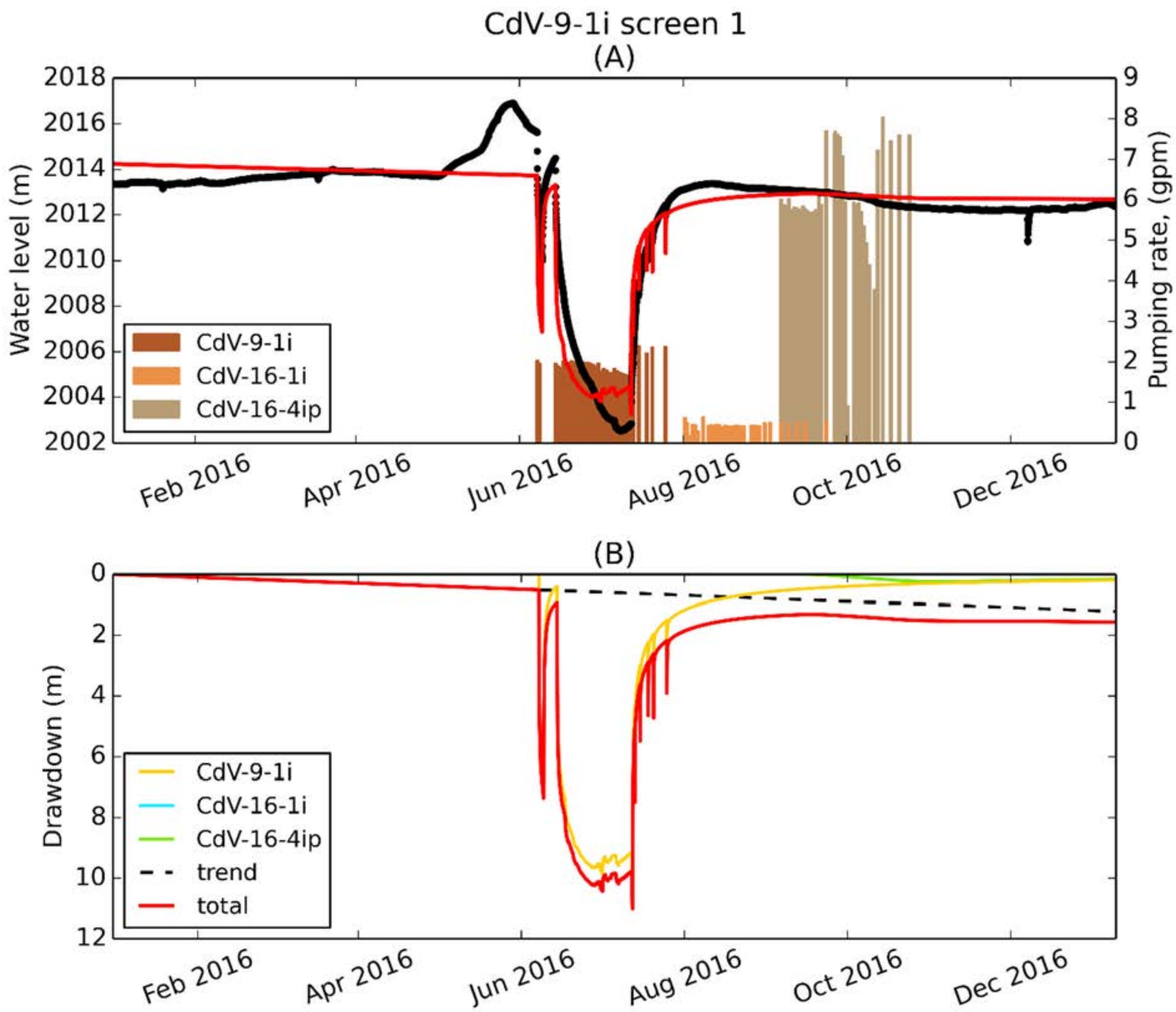

Figure G-5 **Calibrated model results for CdV-9-1(i) screen 1. Panel A shows observed (black dots) and simulated (red line) water levels (m) during the 2016 pumping tests, and panel B shows the simulated drawdowns (m) during the 2016 pumping tests.**

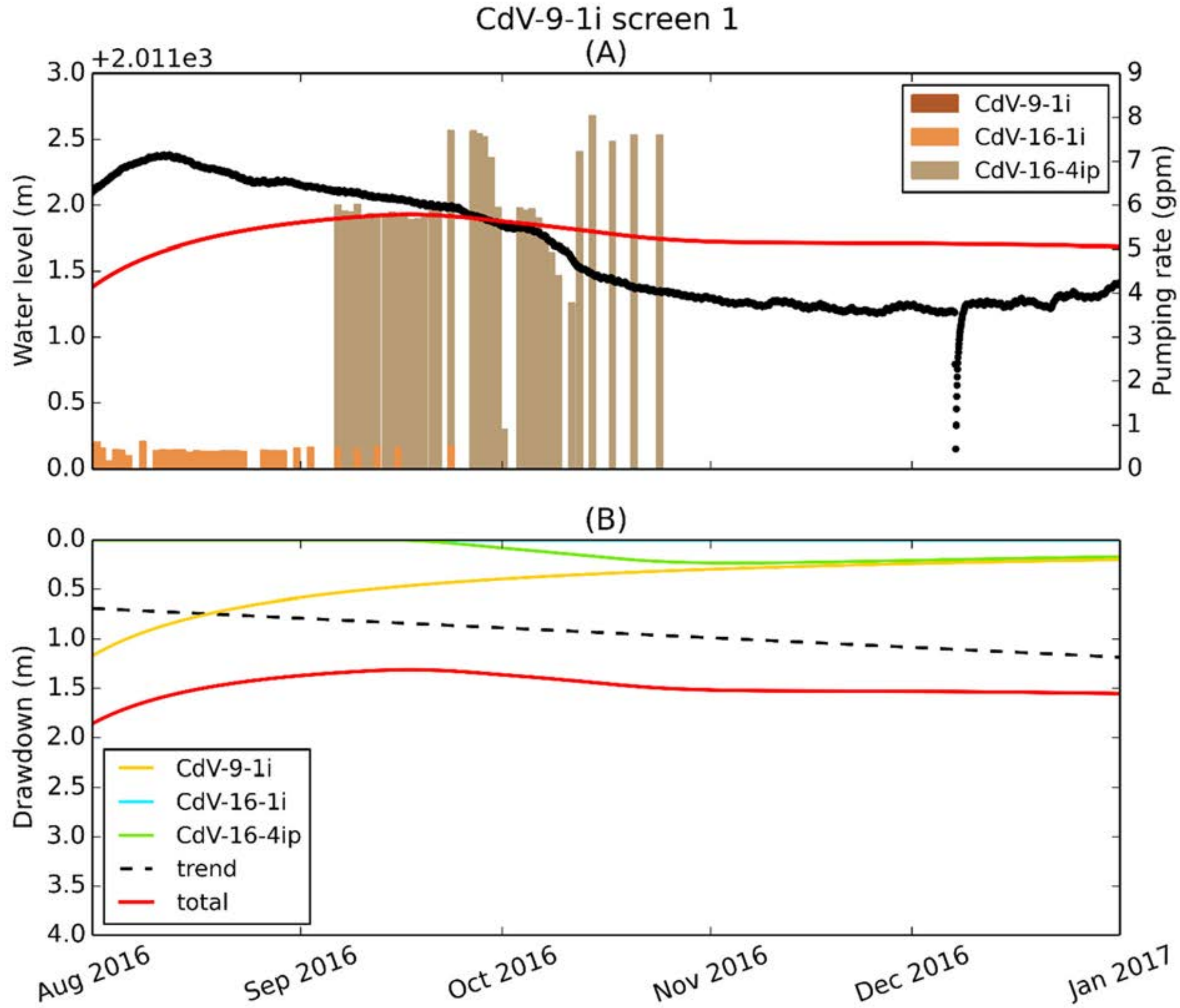

Figure G-6 **Enlarged calibrated model results for CdV-9-1(i) screen 1. The figure shows the same model predictions as Figure G-5 but focuses on the period of CdV-16-4ip pumping. Panel A shows observed (black dots) and simulated (red line) water levels (m) during the 2016 pumping tests, and panel B shows the simulated drawdowns (m) during the 2016 pumping tests.**

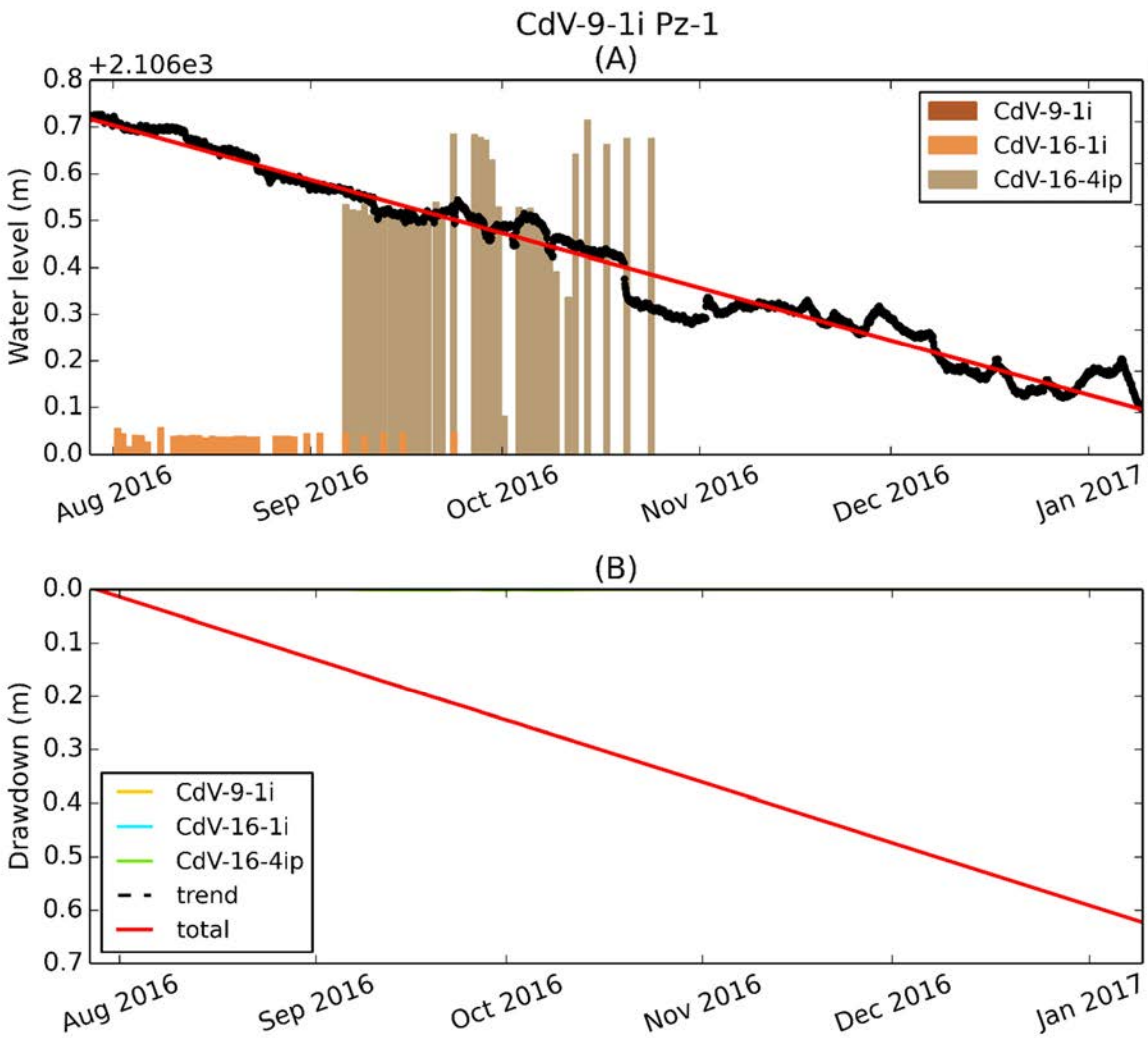

Figure G-7 **Calibrated model results for CdV-9-1(i) PZ-1. Panel A shows observed (black dots) and simulated (red line) water levels (m) during the 2016 pumping tests, and panel B shows the simulated drawdowns (m) during the 2016 pumping tests. CdV-9-1(i) pumping is not shown in panel A because it occurred outside the time frame discussed in this appendix.**

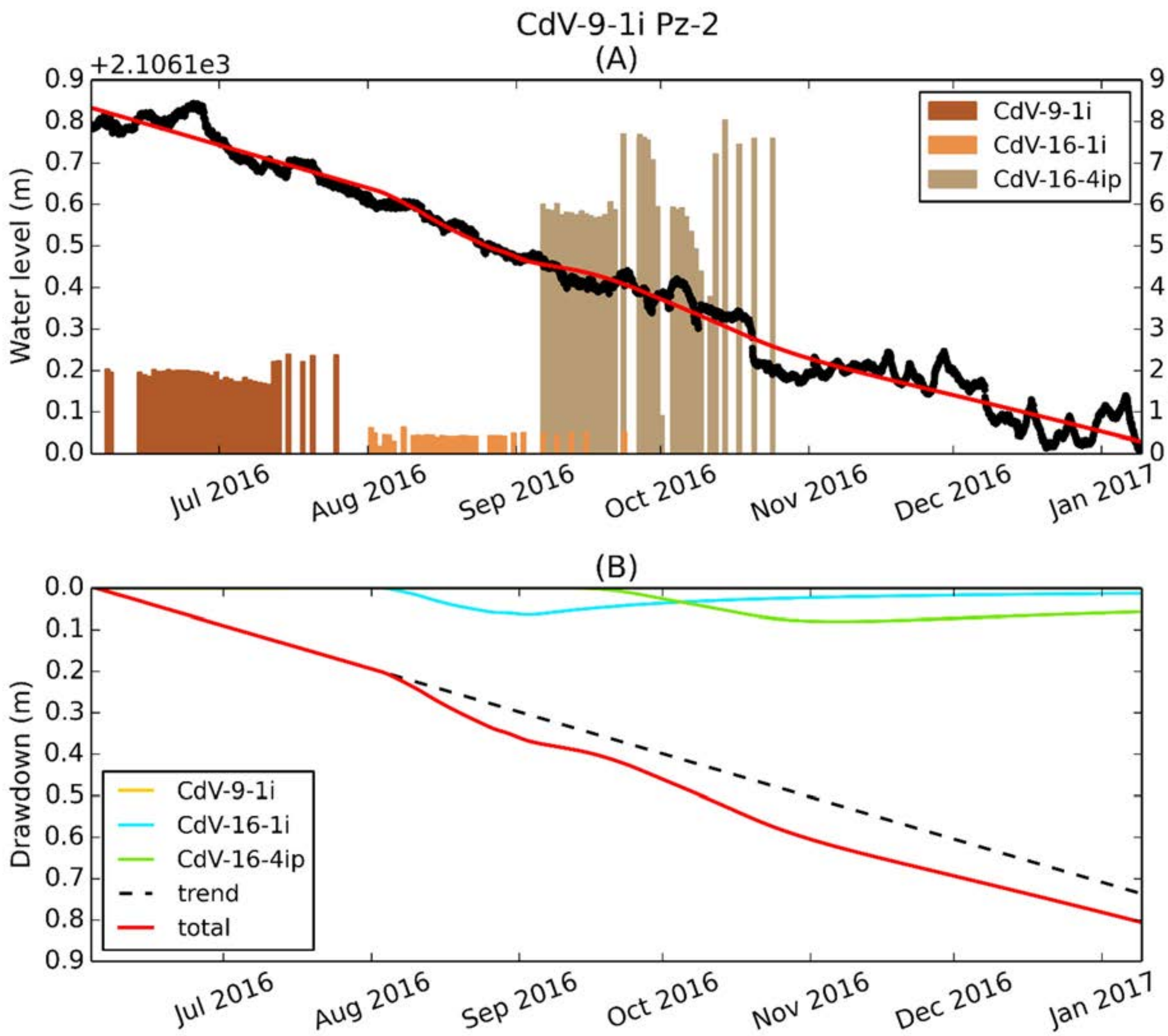

Figure G-8 **Calibrated model results for CdV-9-1(i) PZ-2. Panel A shows observed (black dots) and simulated (red line) water levels (m) during the 2016 pumping tests, and panel B shows the simulated drawdowns (m) during the 2016 pumping tests.**

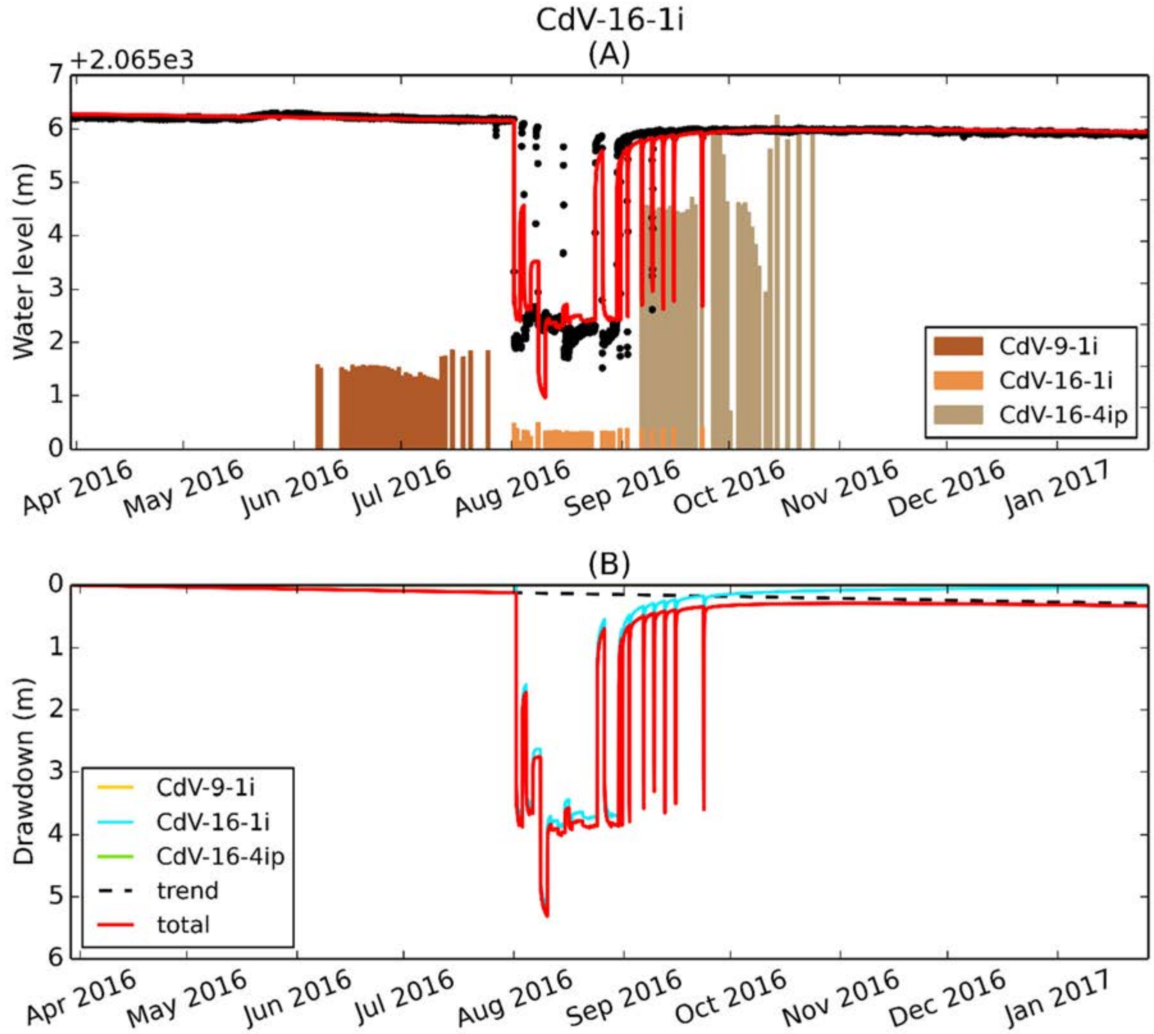

Figure G-9 **Calibrated model results for CdV-16-1(i). Panel A shows observed (black dots) and simulated (red line) water levels (m) during the 2016 pumping tests, and panel B shows the simulated drawdowns (m) during the 2016 pumping tests.**

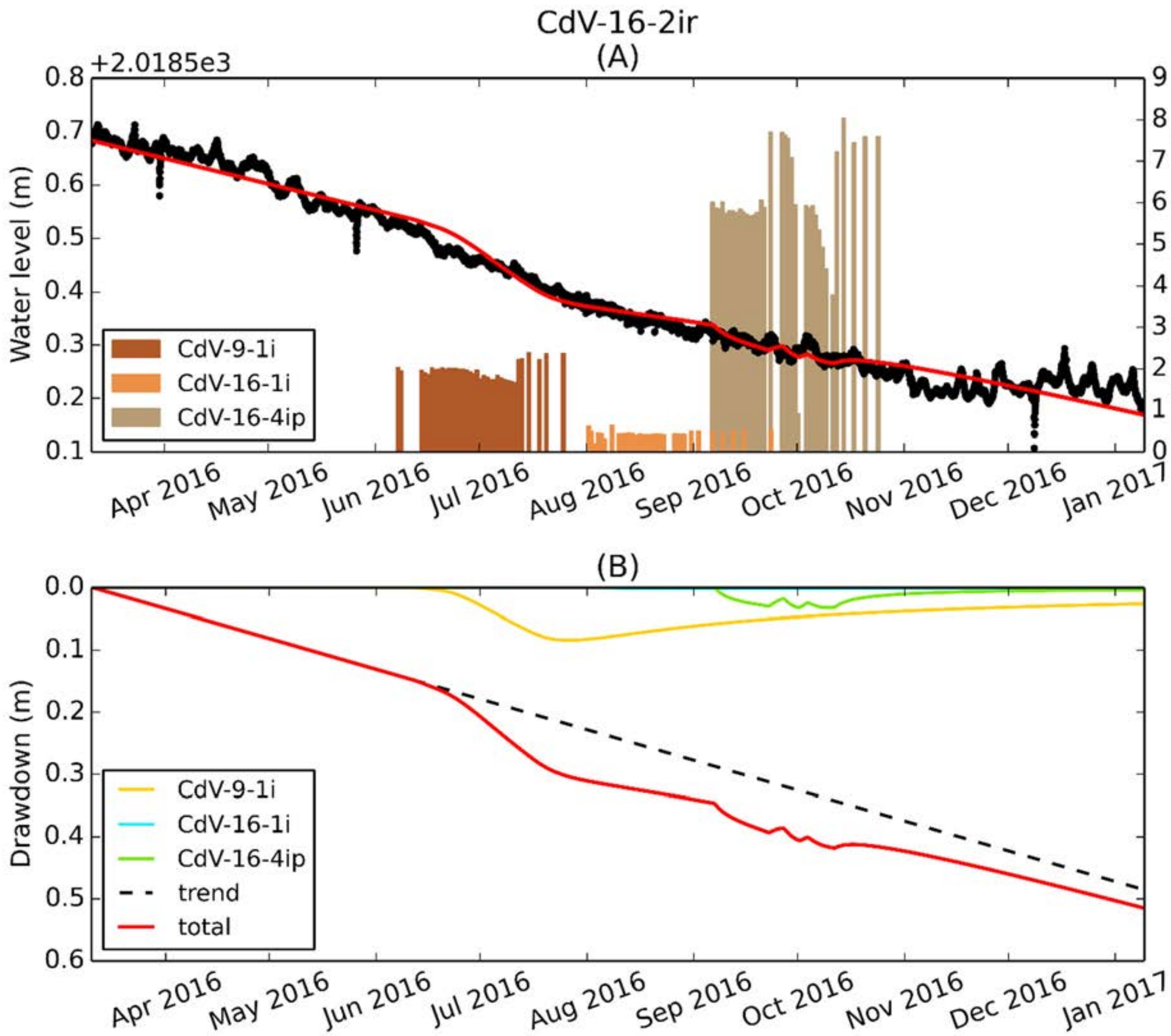

Figure G-10 Calibrated model results for CdV-16-2ir. Panel A shows observed (black dots) and simulated (red line) water levels (m) during the 2016 pumping tests, and panel B shows the simulated drawdowns (m) during the 2016 pumping tests.

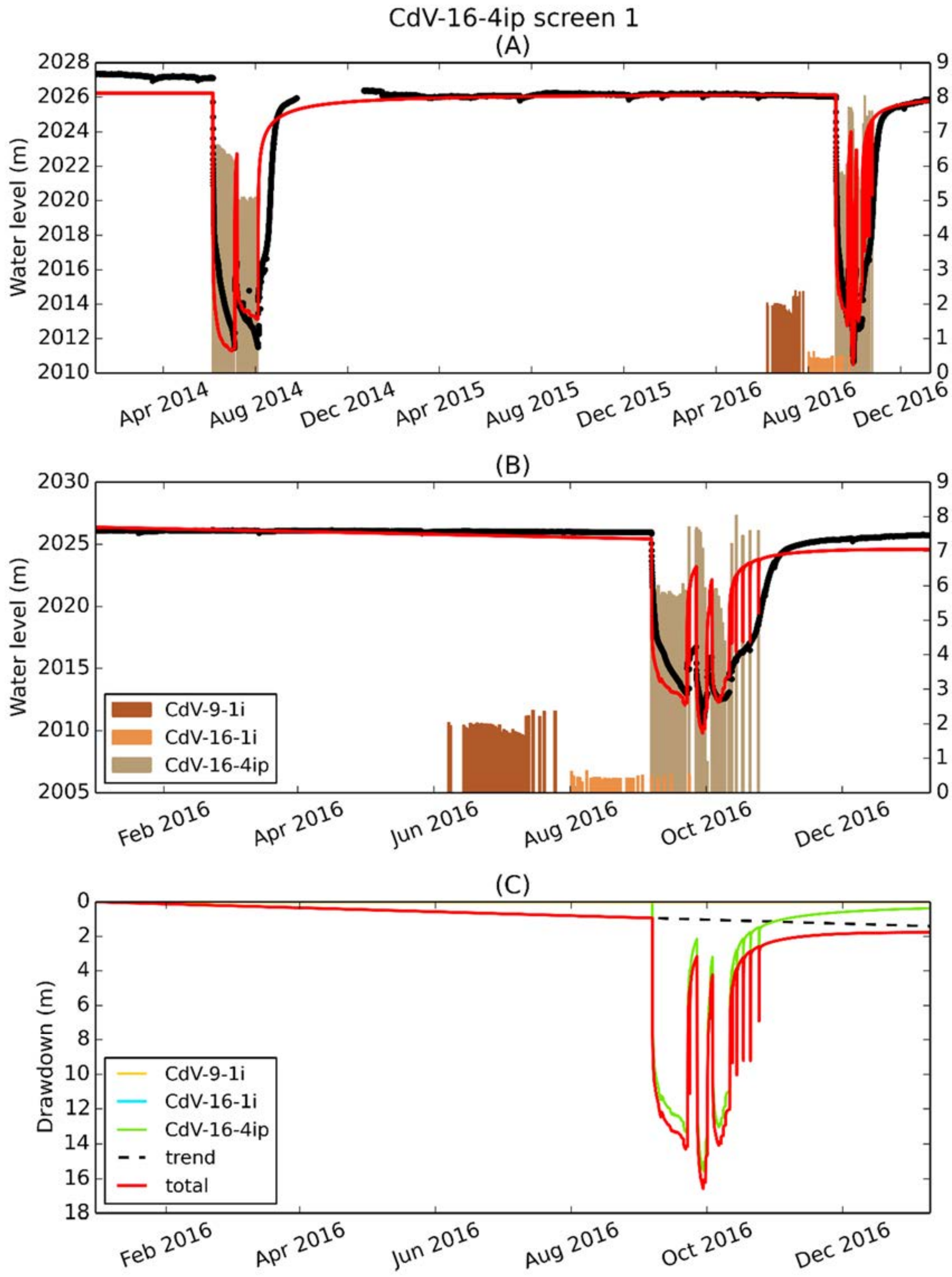

Figure G-11 Calibrated model results for CdV-16-4ip screen 1. Panel A shows observed (black dots) and simulated (red line) water levels (m) during both the 2014 and 2016 pumping tests, panel B shows observed (black dots) and simulated (red line) water levels (m) during the 2016 pumping tests only, and panel C shows the simulated drawdowns (m) during the 2016 pumping tests only.

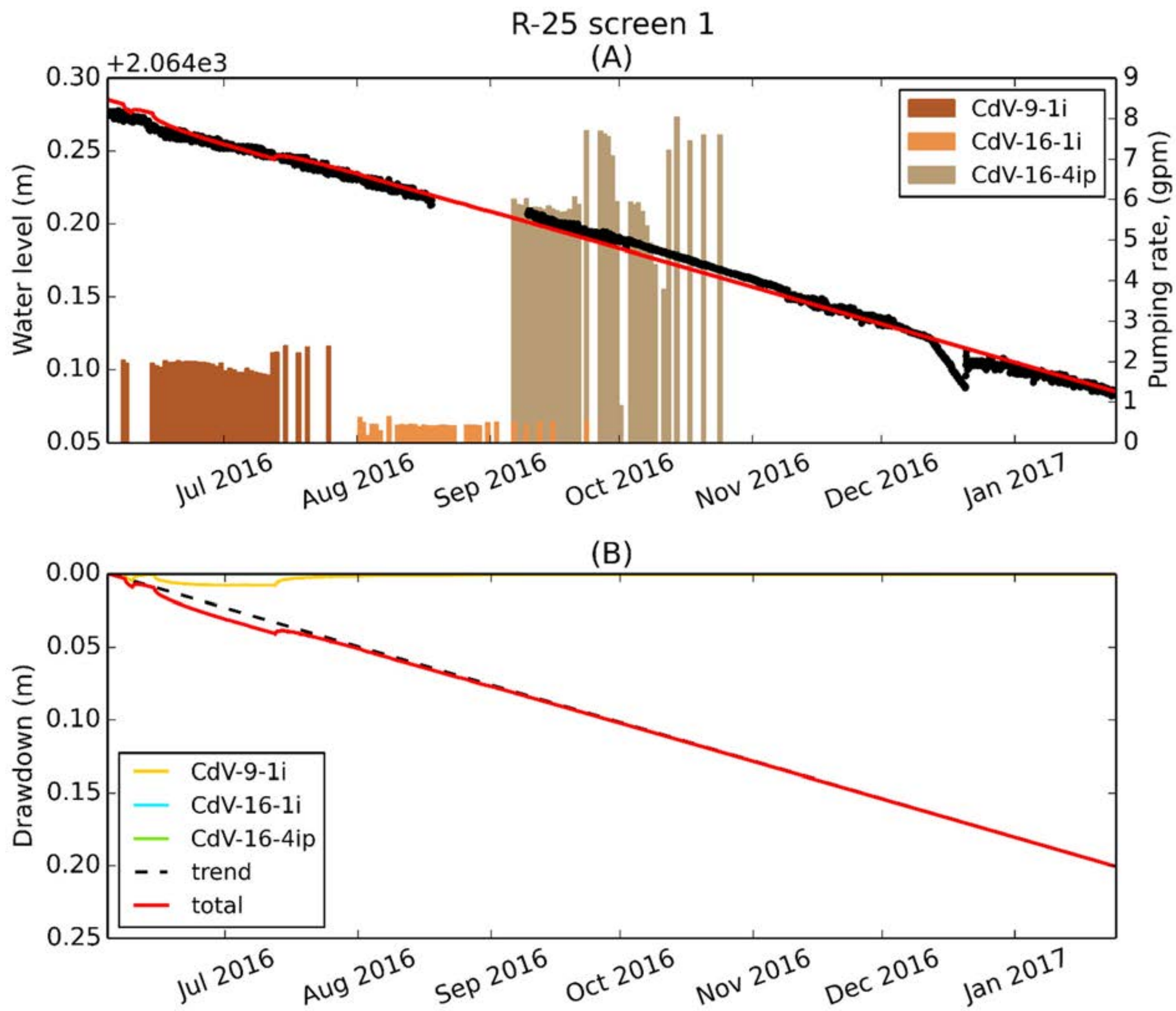

Figure G-12 Calibrated model results for R-25 screen 1. Panel A shows observed (black dots) and simulated (red line) water levels (m) during the 2016 pumping tests, and panel B shows the simulated drawdowns (m) during the 2016 pumping tests.

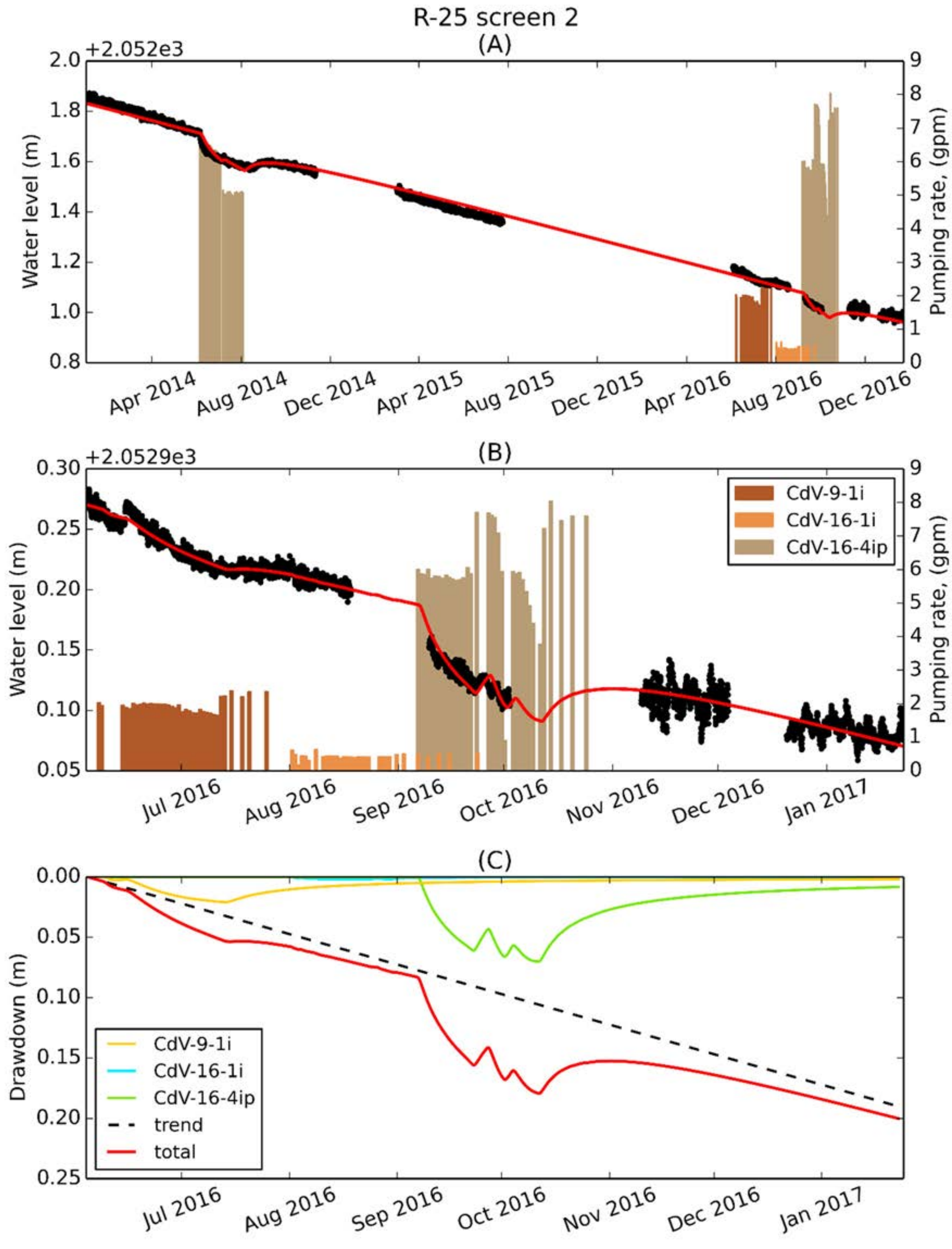

Figure G-13 Calibrated model results for R-25 screen 2. Panel A shows observed (black dots) and simulated (red line) water levels (m) during both the 2014 and 2016 pumping tests, panel B shows observed (black dots) and simulated (red line) water levels (m) during the 2016 pumping tests only, and panel C shows the simulated drawdowns (m) during the 2016 pumping tests only.

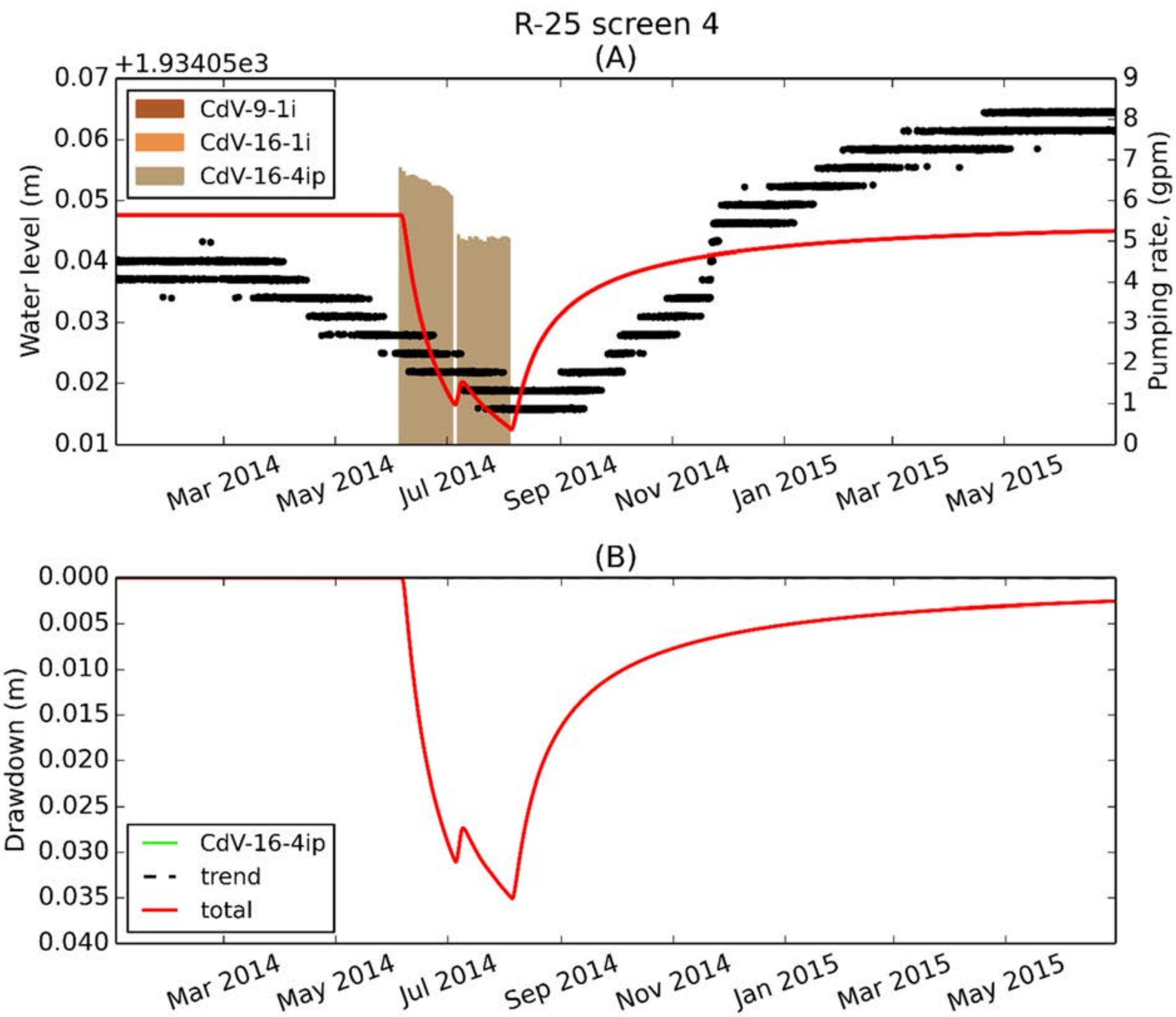

Figure G-14 Calibrated model results for R-25 screen 4. Panel A shows observed (black dots) and simulated (red line) water levels (m) during the 2014 pumping tests, and panel B shows the simulated drawdowns (m) during the 2014 pumping tests.

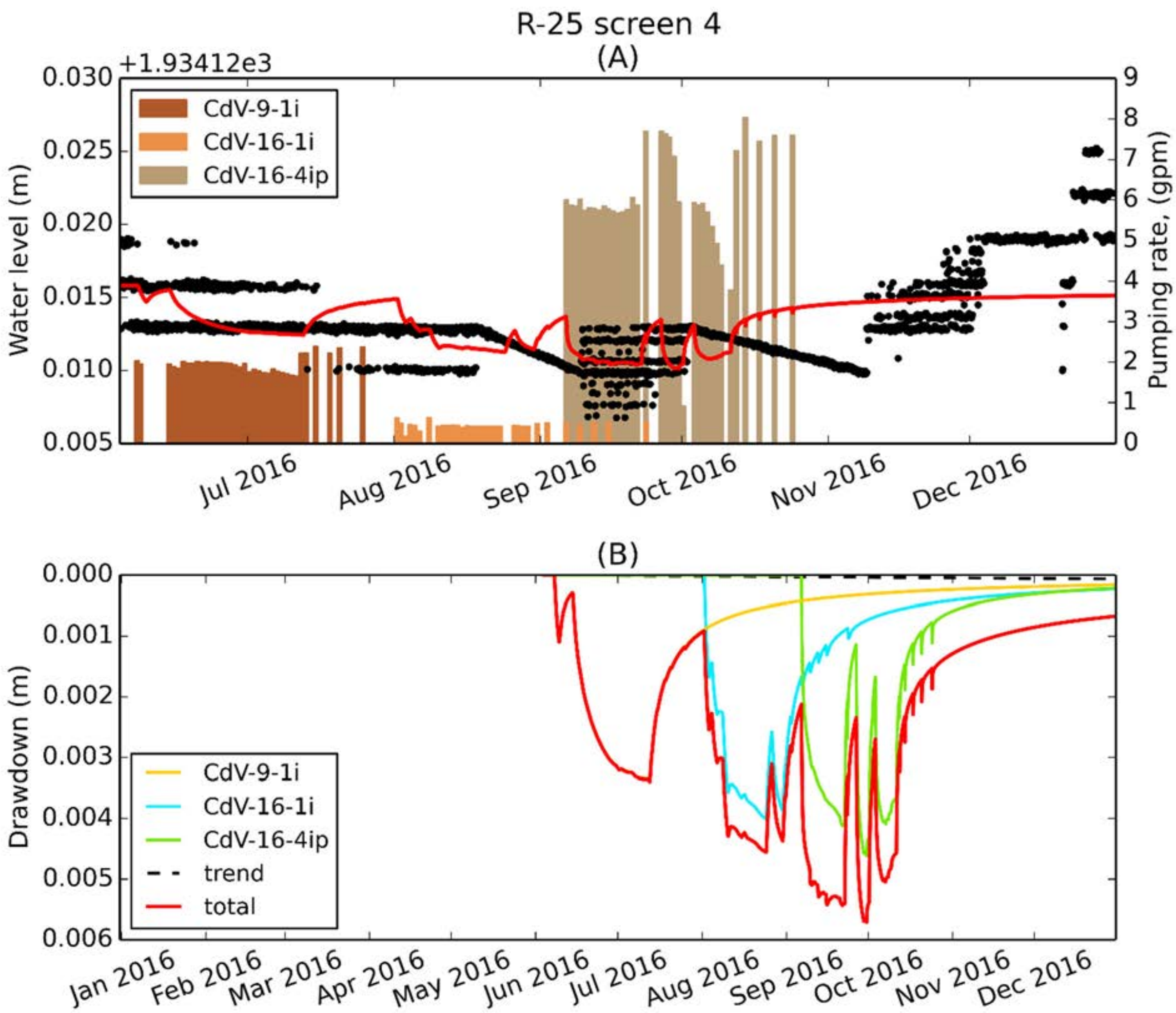

Figure G-15 Calibrated model results for R-25 screen 4. Panel A shows observed (black dots) and simulated (red line) water levels (m) during the 2016 pumping tests, and panel B shows the simulated drawdowns (m) during the 2016 pumping tests.

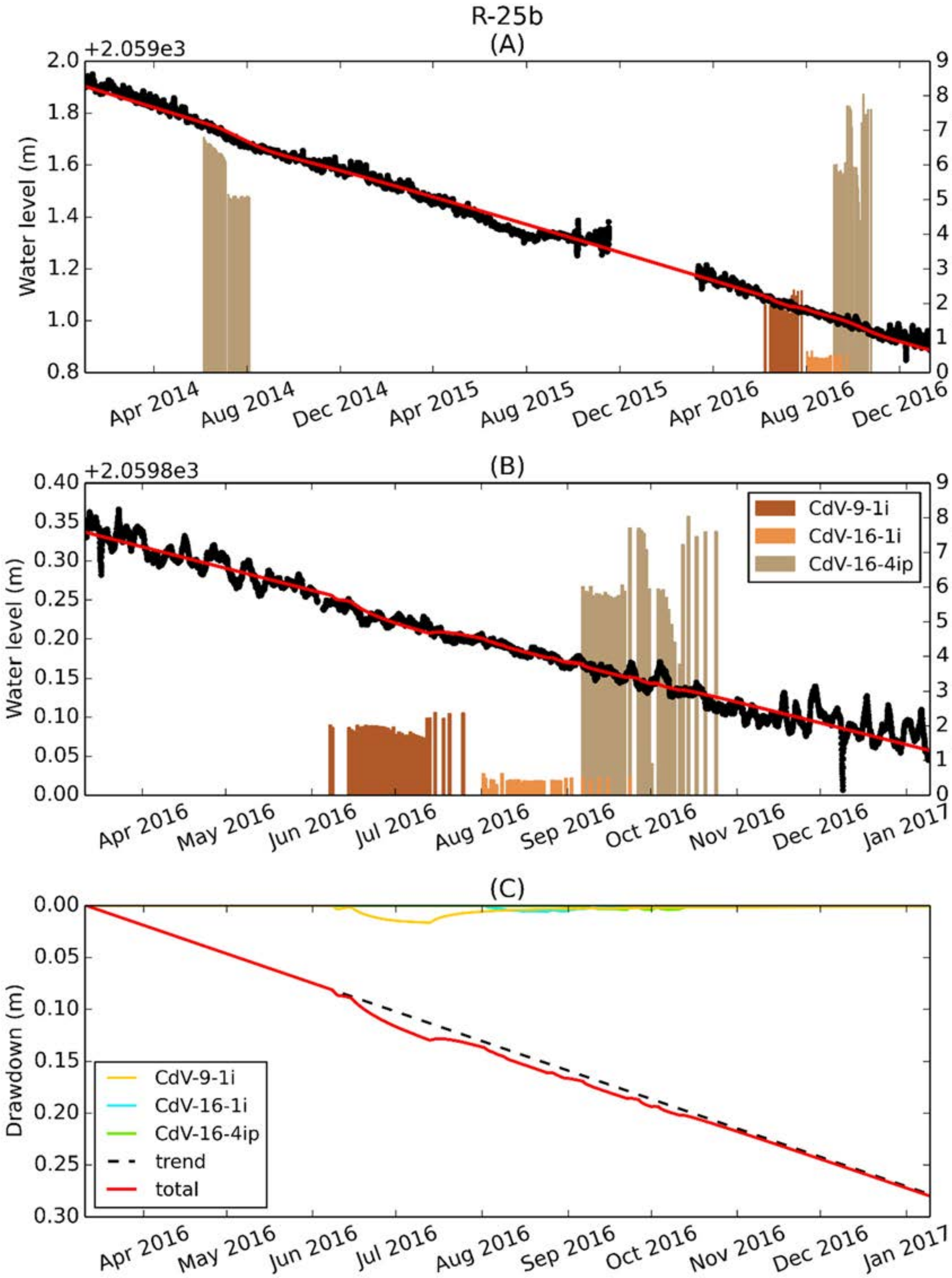

Figure G-16 Calibrated model results for R-25b. Panel A shows observed (black dots) and simulated (red line) water levels (m) during both 2014 and 2016 pumping tests, panel B shows observed (black dots) and simulated (red line) water levels (m) during the 2016 pumping tests only, and panel C shows the simulated drawdowns (m) during the 2016 pumping tests only.

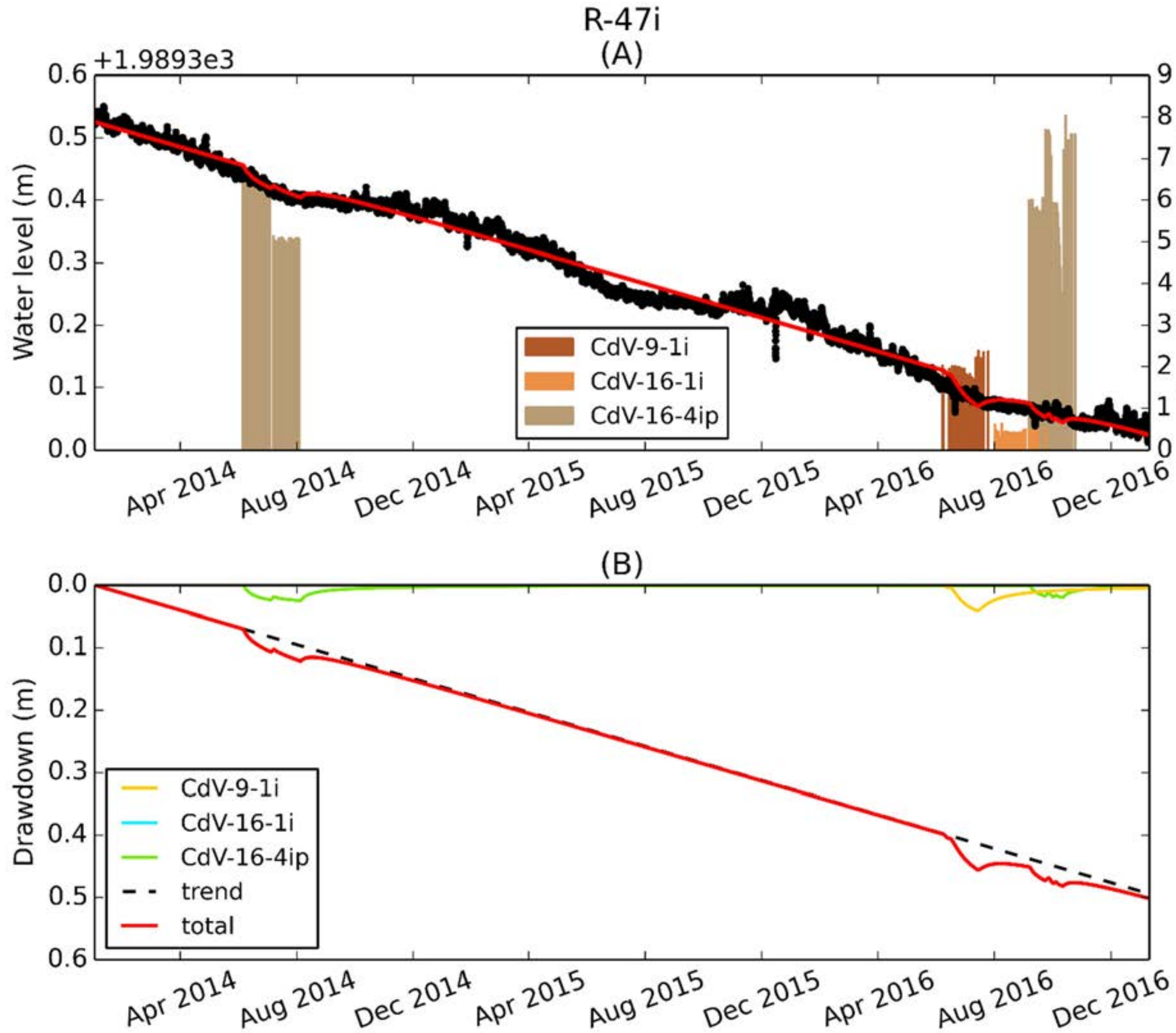

Figure G-17 **Calibrated model results for R-47i. Panel A shows observed (black dots) and simulated (red line) water levels (m) during both the 2014 and 2016 pumping tests, and panel B shows the simulated drawdowns (m) during both 2014 and 2016 pumping tests.**

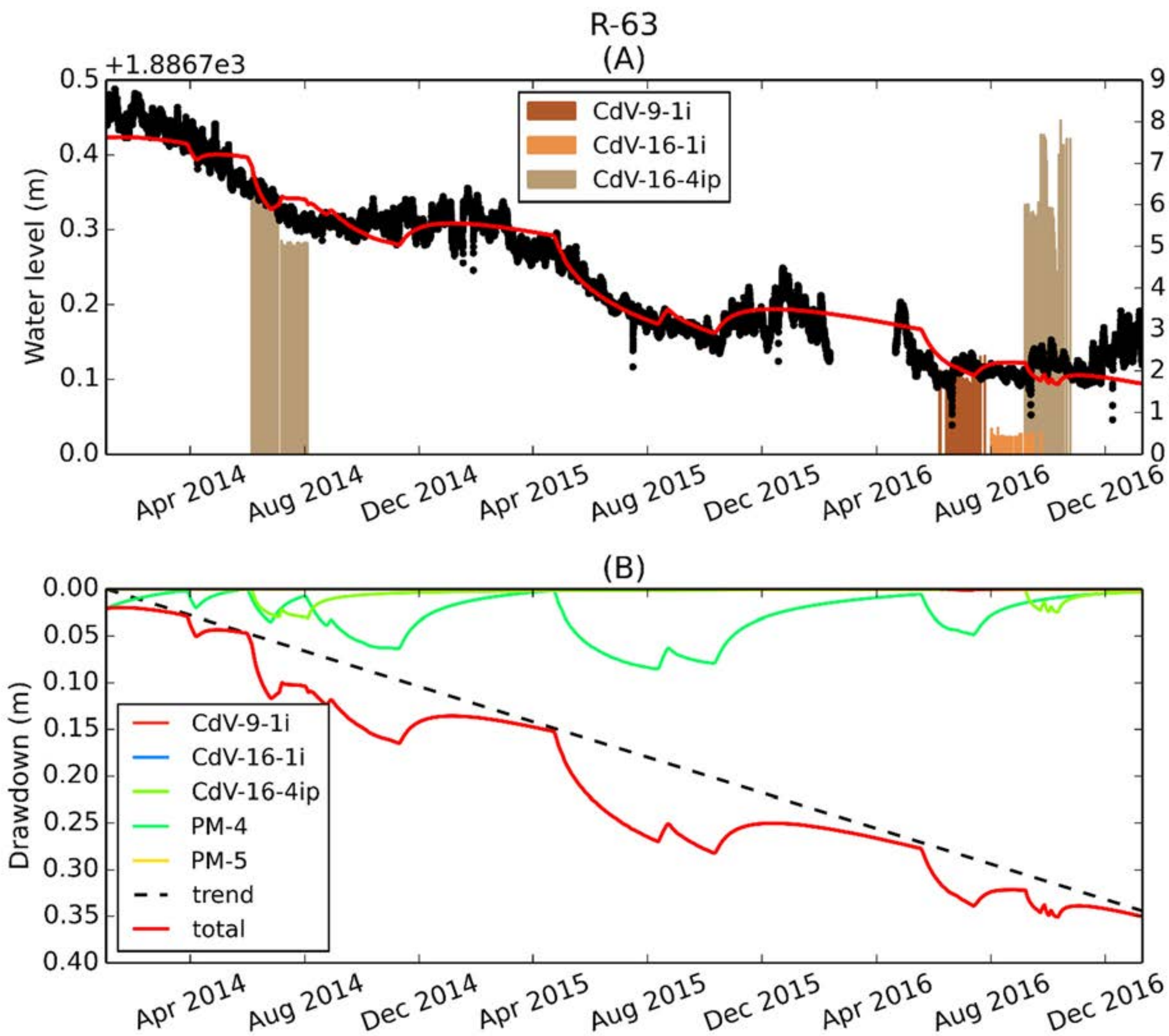

Figure G-18 Calibrated model results for R-63. Panel A shows observed (black dots) and simulated (red line) water levels (m) during both 2014 and 2016 pumping tests, and panel B shows the simulated drawdowns (m) during both 2014 and 2016 pumping tests.

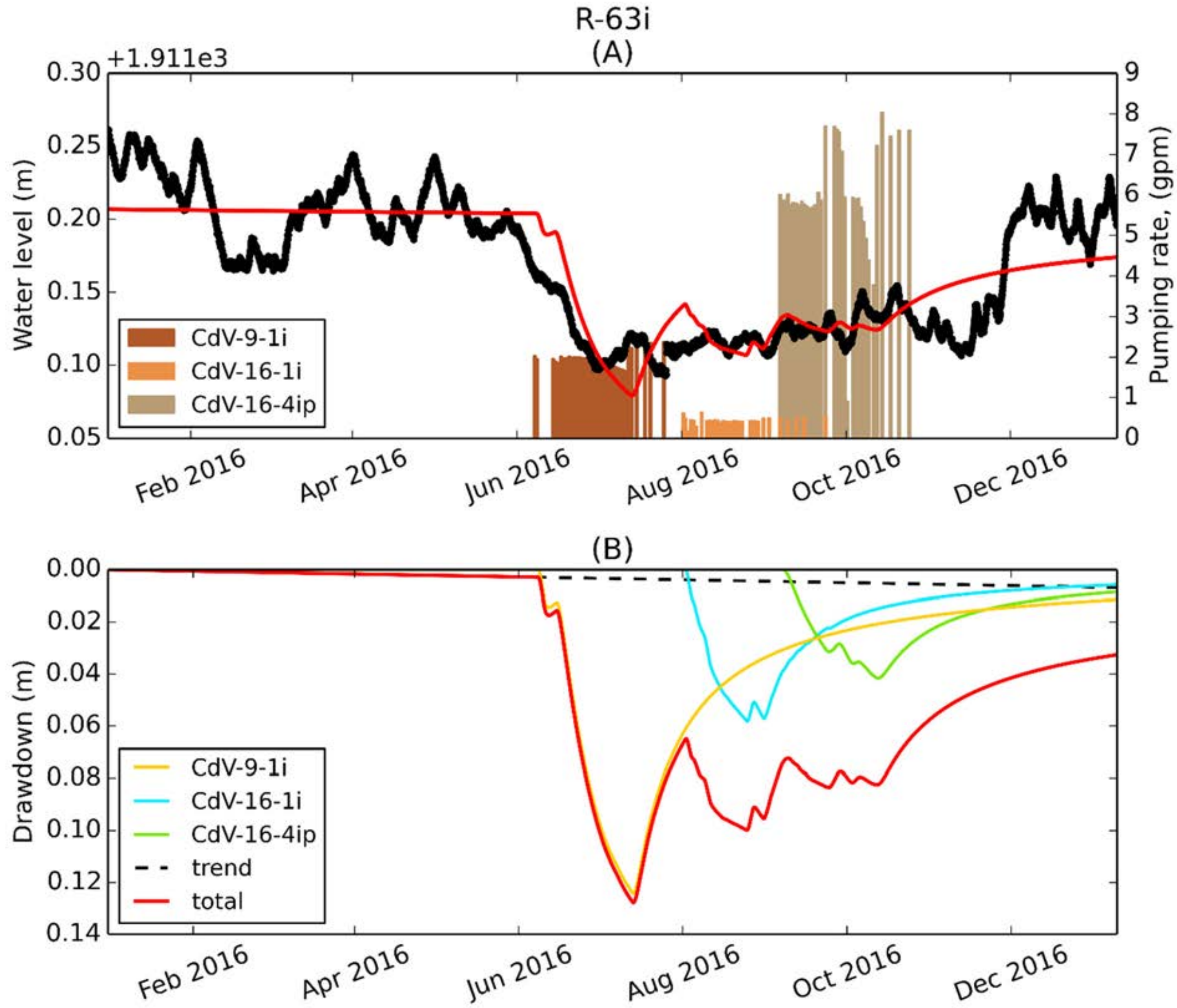

Figure G-19 **Calibrated model results for R-63i. Panel A shows observed (black dots) and simulated (red line) water levels (m) during the 2016 pumping test, and panel B shows the simulated drawdowns (m) during the 2016 pumping test.**

Table G-1
Estimated Potential Maximum Drawdown in 2016 at Each Screen from Pumping at Wells CdV-9-1(i), CdV-16-1(i), and CdV-16-4ip

		Pumping Wells		
		CdV-9-1(i)	CdV-16-1(i)	CdV-16-4ip
Observation Wells	CdV-9-1(i) screen 1	10	0.000013	0.23
	CdV-9-1(i) Pz-1	0.00015	0.00018	0.00096
	CdV-9-1(i) Pz-2	0.00041	0.064	0.080
	CdV-16-1(i)	0.0011	5.2	0.00012
	CdV-16-2ir	0.084	0.0016	0.032
	CdV-16-4ip screen 1	0.0016	0.0	16
	R-25 screen 1	0.0080	0.00071	0.000069
	R-25 screen 2	0.021	0.0019	0.070
	R-25 screen 4 (2014)	—*	—	0.035
	R-25 screen 4 (2016)	0.0034	0.0040	0.0046
	R-25b	0.016	0.0058	0.0042
	R-47i	0.041	0.00034	0.019
	R-63	0.0014	0.00099	0.024
	R-63i	0.12	0.058	0.042

Notes: Drawdowns are in meters. The detections of pumping impacts at each observation well are labeled as certain (red), potential (blue), and unlikely (grey).

*— = No drawdown detected from pumping at observation locations R-25 screen 4.

Table G-2
Estimated Transmissivity and Storativity Between Observation and Pumping Wells

		Parameters					
		CdV-9-1(i) Screen 1		CdV-16-1(i)		CdV-16-4ip Screen 1	
	Wells	T [m²/d]	*S* [–]	T [m²/d]	*S* [–]	T [m²/d]	*S* [–]
Observation Wells	CdV-9-1(i) screen 1	0.66	0.99[a]	—[b]	—	3.1	0.0070
	CdV-9-1(i) PZ-1	—	—	—	—	—	—
	CdV-9-1(i) PZ-2	—	—	2.7	0.0043	8.4	0.021
	CdV-16-1(i)	—	—	0.82	0.00037[a]	—	—
	CdV-16-2ir	4.3	0.0015	—	—	200	0.0066
	CdV-16-4ip screen 1	—	—	—	—	1.9	1.0[a]
	R-25 screen 1	—	—	—	—	—	—
	R-25 screen 2	67	0.014	—	—	73	0.029
	R-25 screen 4 (2014)	—	—	—	—	150	0.120
	R-25 screen 4 (2016)	—	—	—	—	—	—
	R-25b	130	0.010	—	—	—	—
	R-47i	27	0.00033	—	—	290	0.0013
	R-63	—	—	—	—	260	0.011
	R-63i	11	0.00079	5.9	0.00026	78	0.016

Notes: Large storativity is caused by low sensitivity of the observed water-level transients at the observation well to the pumping transients. Large transmissivity suggests negligible influence of pumping on observed drawdown. Calibrated parameters resulting in drawdown contributions less than 1 cm were considered unrepresentative and omitted (dashes).

[a] Storativity estimates obtained at the pumping wells are questionable and are not representative of the hydraulic properties.

[b] — = No hydraulic properties are estimated.

Appendix H

Additional Geochemical Data Plots

This appendix includes additional plots of geochemical parameters measured during the extended aquifer testing at wells CdV-9-1(i), CdV-16-1(i), and CdV-16-4ip. It includes plots for the following.

- RDX (hexahydro-1,3,5-trinitro-1,3,5-triazine) degradation products MNX (hexahydro-1-nitroso-3,5-dinitro-1,3,5-triazine); DNX (hexahydro-1,3-dinitro-5-nitro-1,3,5-triazine); and TNX (hexahydro-1,3,5-trinitroso-1,3,5-triazine) during pumping and recovery at each of the three wells (Figure H-1)
- RDX and HMX (1,3,5,7-tetranitro-1,3,5,7,-tetracyclo-octane), along with the RDX degradation products MNX, DNX, and TNX, during pumping and recovery at each of the three wells (Figure H-2)
- TNT [trinitrotoluene(2,4,6-)] and its degradation products during pumping and recovery at each of the three wells (Figure H-3)
- Volatile organic compounds MTBE (methyl-t-butyl ether), PCE (tetrachloroethylene), and TCE (trichloroethene) during pumping and recovery at each of the three wells (Figure H-4)
- Nitrate and chloride during pumping and recovery at each of the three wells (Figure H-5)
- Barium and boron during pumping and recovery at each of the three wells (Figure H-6)

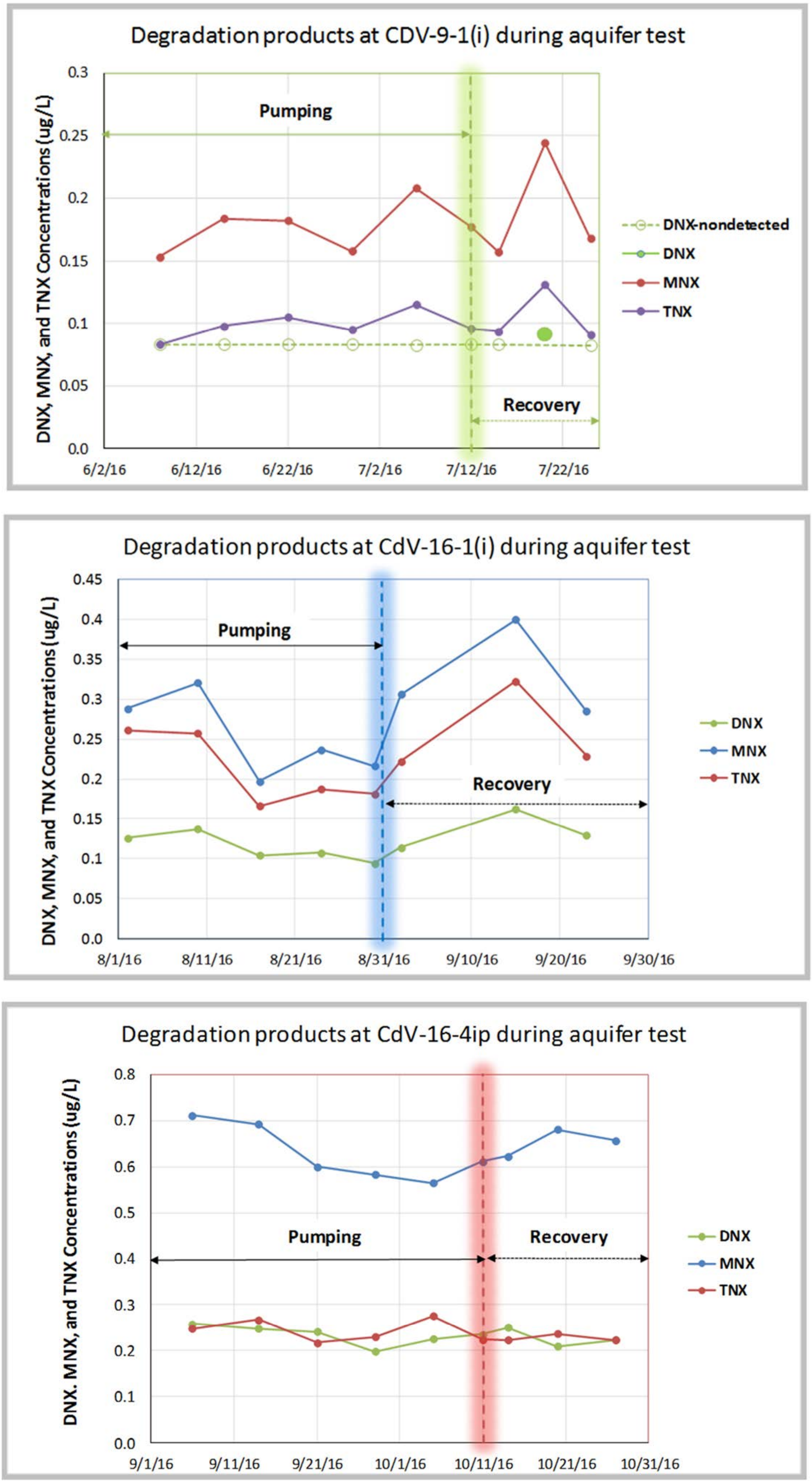

Figure H-1 RDX degradation products MNX, DNX, and TNX

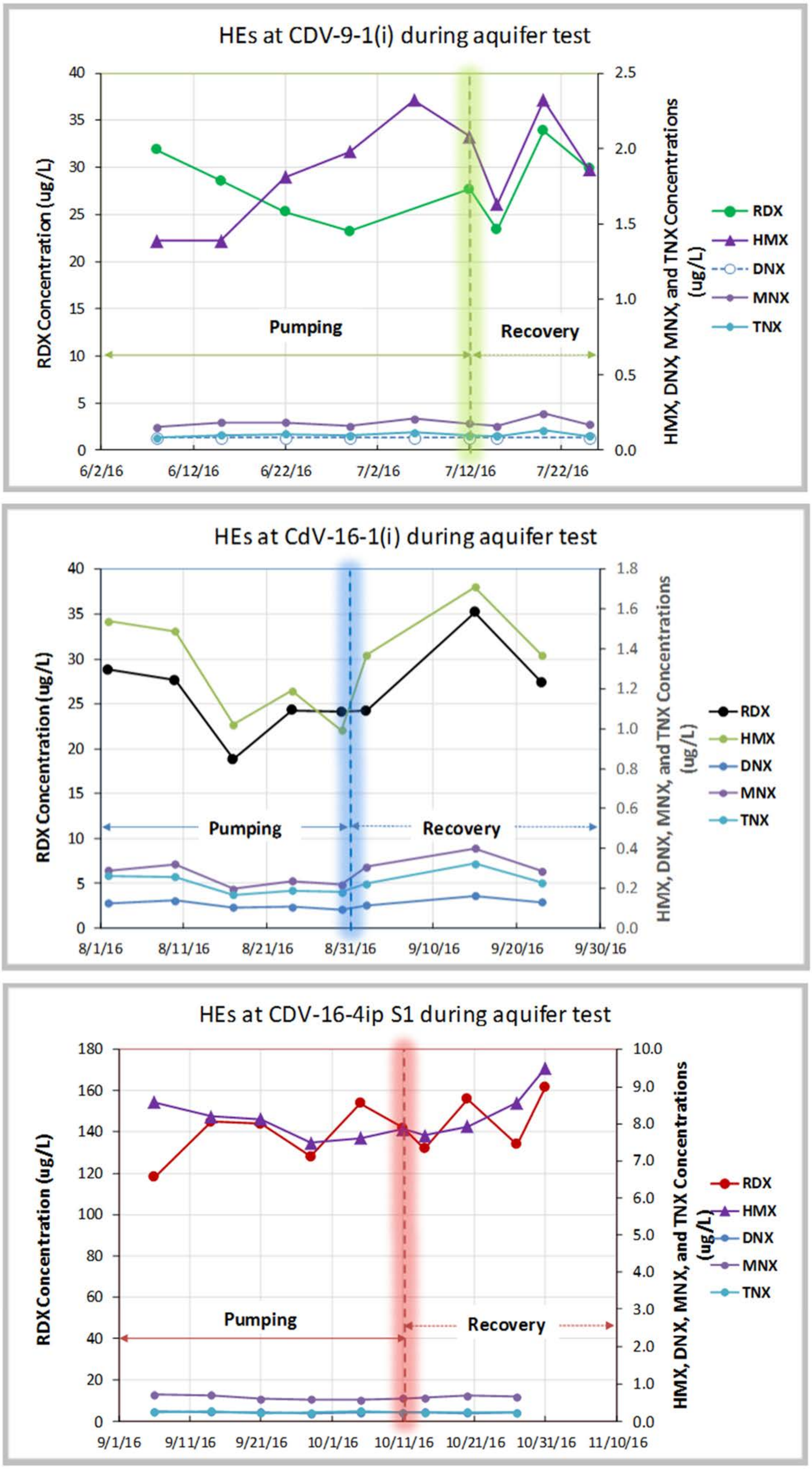

Figure H-2 RDX and HMX along with the RDX degradation products MNX, DNX, and TNX

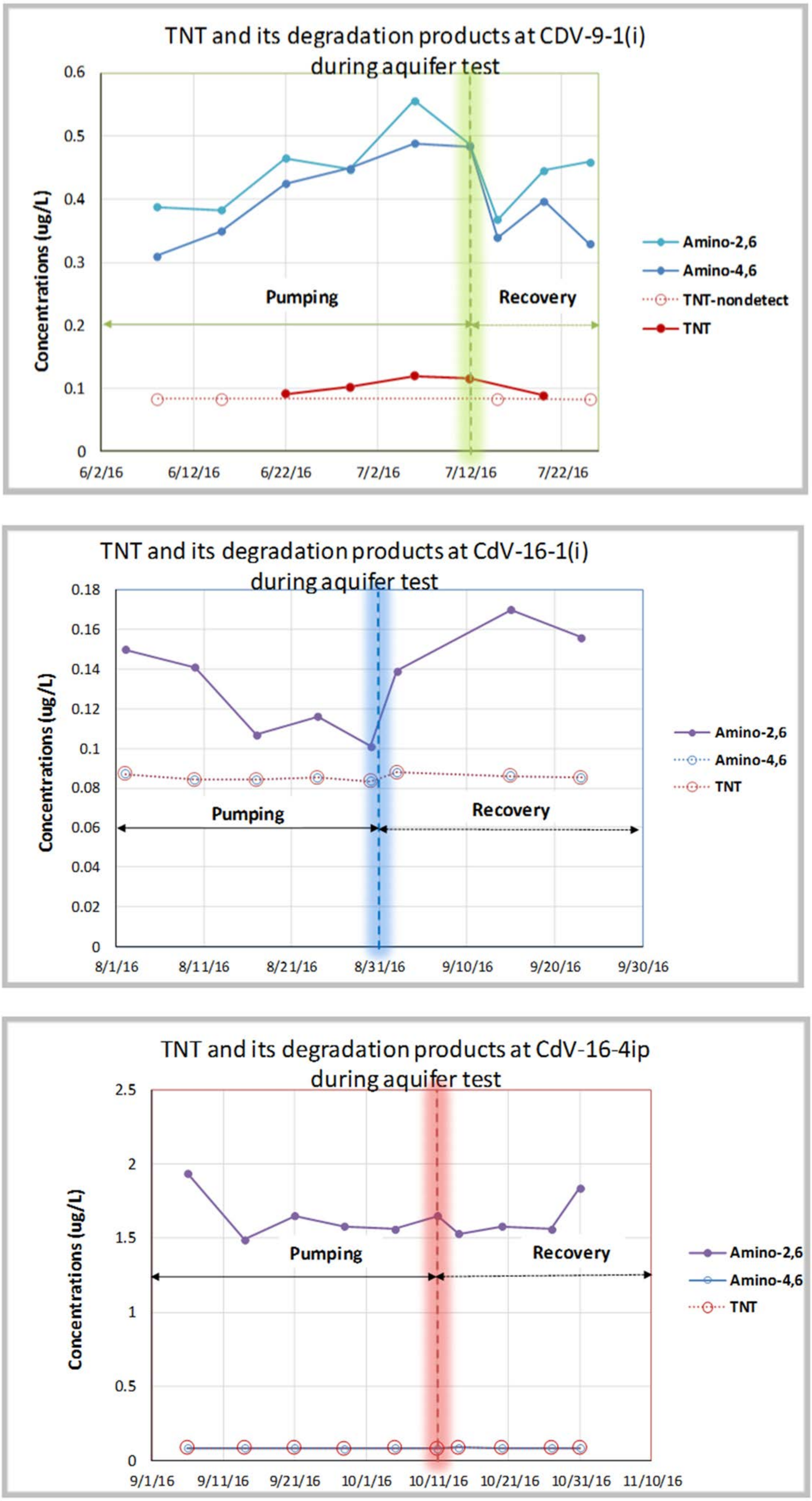

Figure H-3 **TNT and its degradation products**

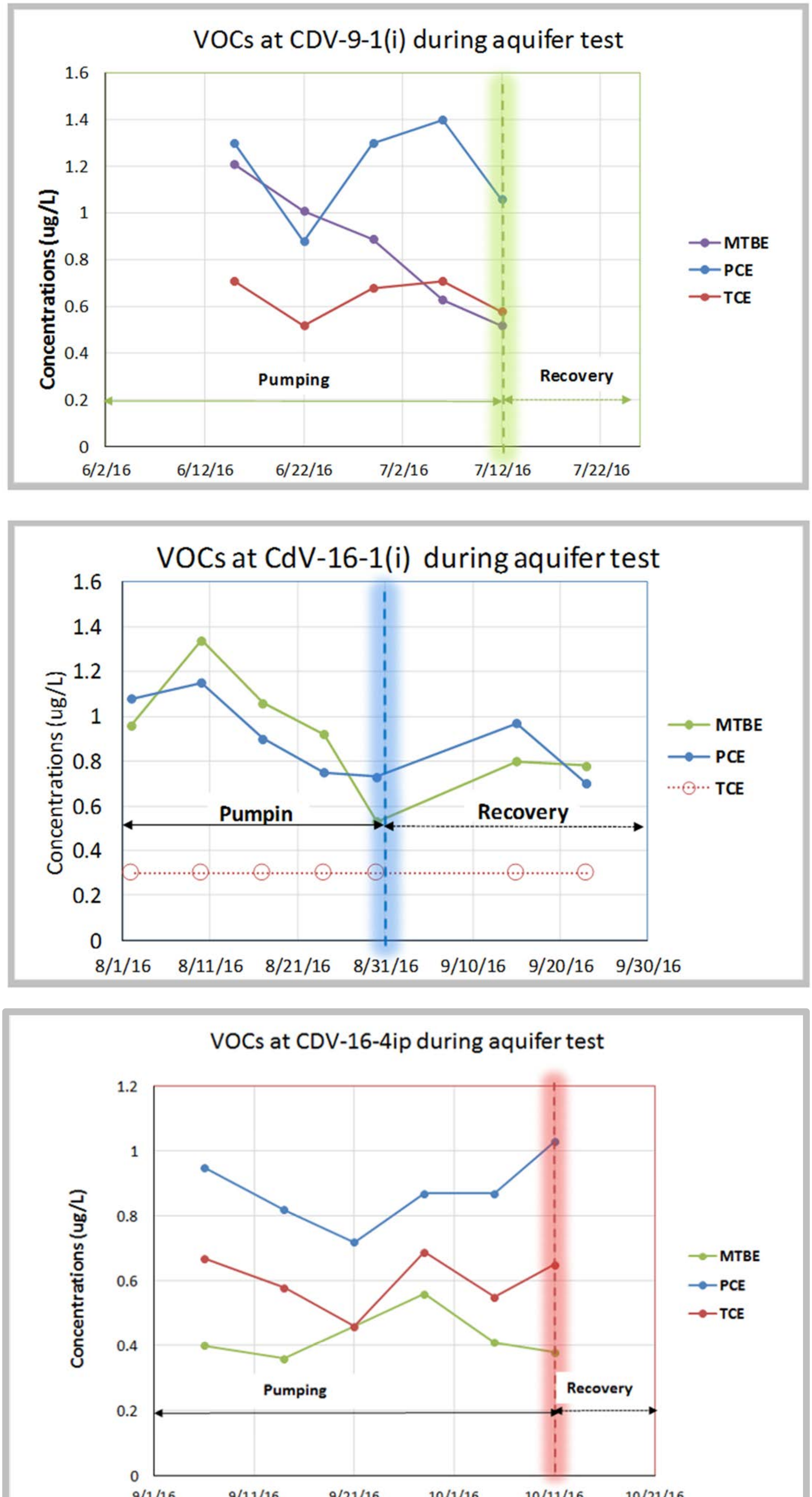

Figure H-4 **VOCs MTBE, PCE, and TCE**

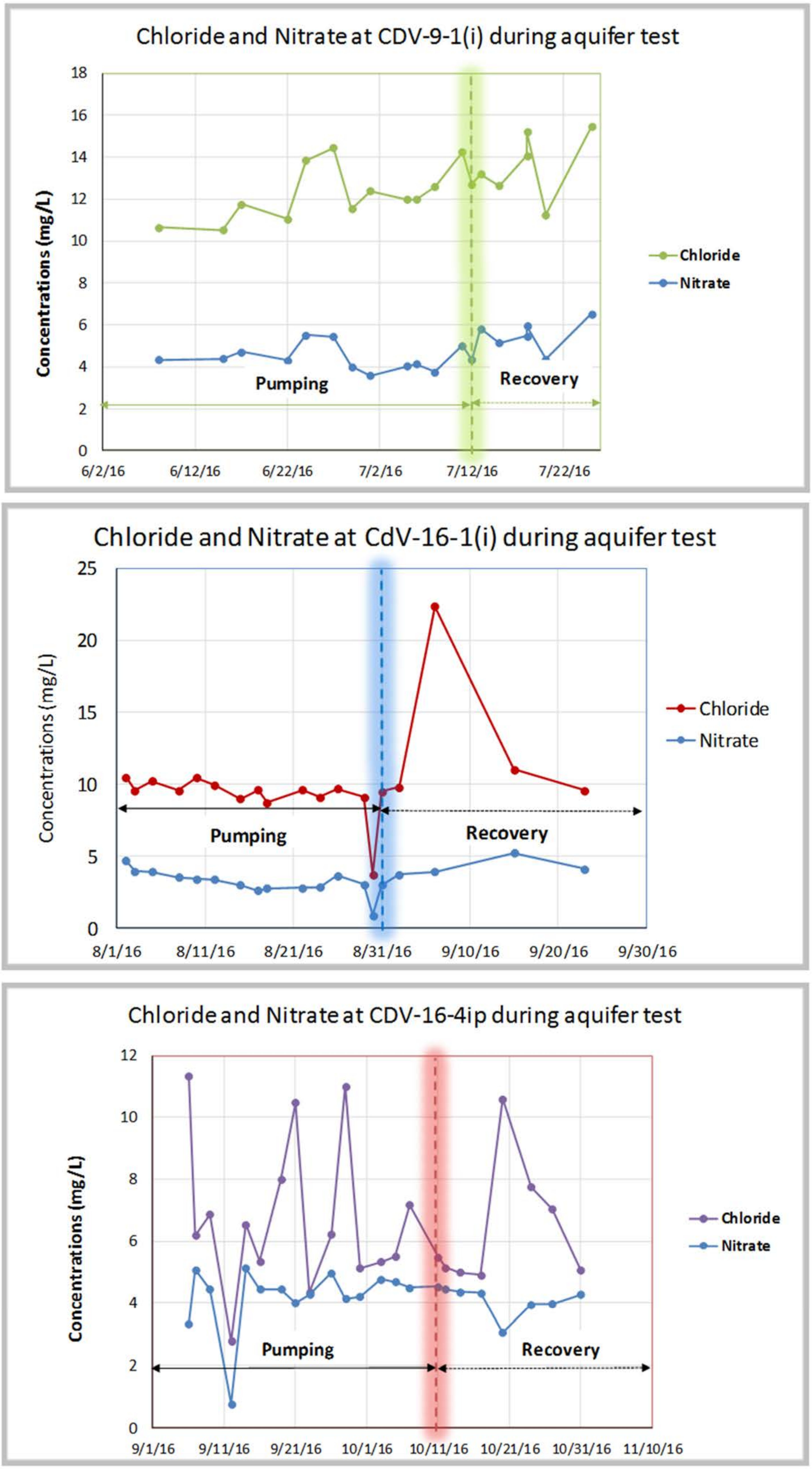

Figure H-5 **Nitrate and chloride**

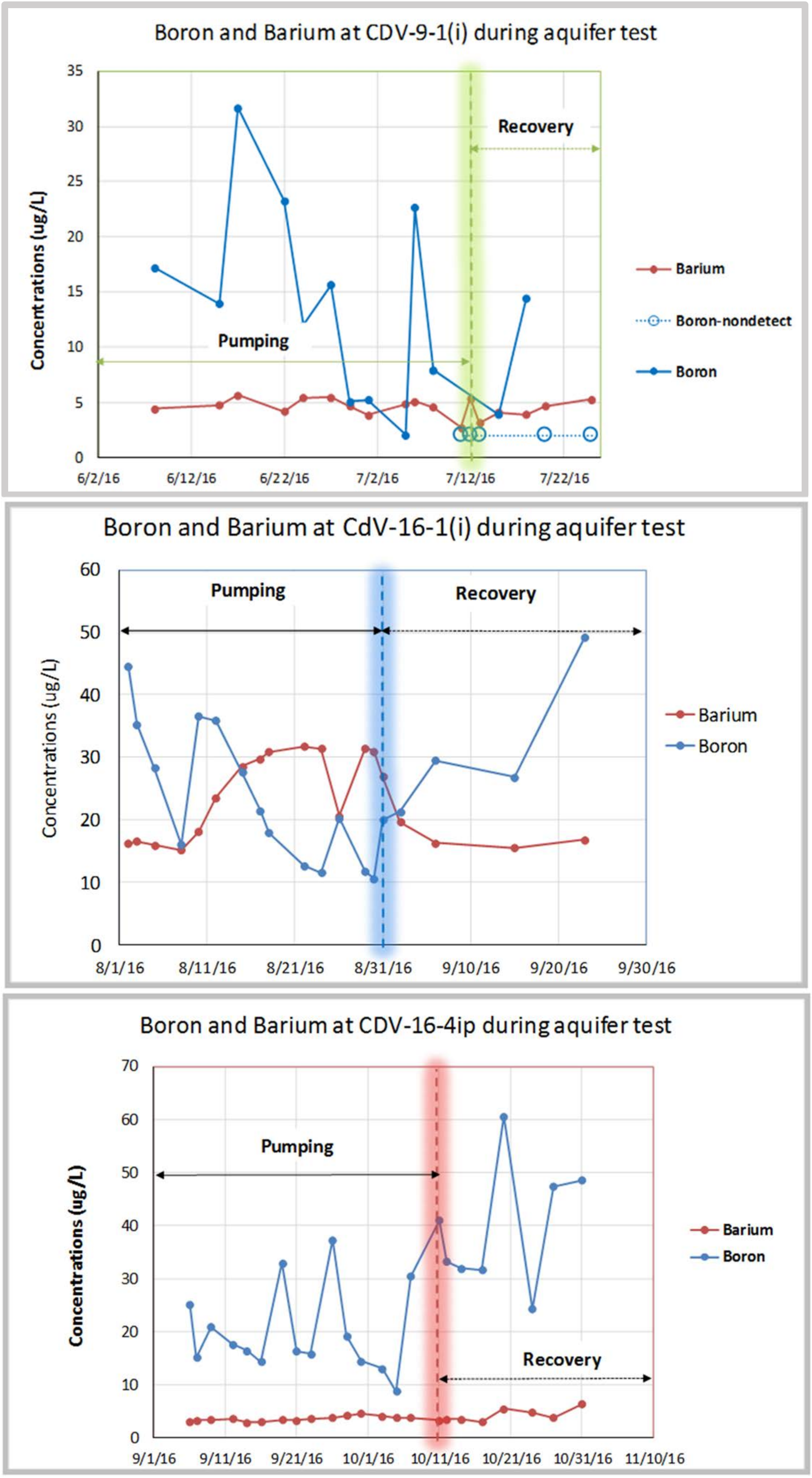

Figure H-6 **Barium and boron**